Recent Hominin Cranial Form and Function

Ricardo Miguel Alves Correia Godinho

PhD in Human Sciences

The University of Hull and The University of York

Hull York Medical School

June 2016

Abstract

This thesis aims to assess if biting mechanics drives craniofacial morphology in recent hominins. To that end, a virtual functional morphology toolkit, that includes Finite Element Analysis (FEA) and Geometric Morphometrics (GM), is used to simulate biting, measure bite force and quantify deformations arising due to simulated biting in *Homo sapiens* and its proposed ancestral species, *Homo heidelbergensis*. Moreover, the mechanical significance of the frontal sinus and of the brow-ridge is also assessed in Kabwe 1 (a *Homo heidelbergensis* specimen). The frontal sinus is examined by comparing the mechanical performance in three FE models with varying sinus morphology. A similar approach is applied to the brow-ridge study. This approach relies on the assumption that FEA approximates reality. Thus, a validation study compares the deformations experienced by a real cranium under experimental loading with those experienced by an FE model under equivalent virtual loading to verify this assumption. A sensitivity analysis examines how simplifications in segmentation impact on FEA results. Lastly, the virtual reconstruction of Kabwe 1 is described.

Results show that prediction of absolute strain magnitudes is not precise, but the distribution of regions of larger and smaller (i.e. pattern of) deformations experienced by the real cranium is reasonably approximated by FEA, despite discrepancies in the alveolus. Simplification of segmentation stiffens the model but has no impact on the pattern of deformations, with the exception of the alveolus. Comparison of the biting performance of Kabwe 1 and *H. sapiens* suggests that morphological differences between the two species are likely not driven by selection of the masticatory system. Frontal sinus morphogenesis and morphology are possibly impacted by biting mechanics in the sense that very low strains are experienced by this region. Because bone adapts to strains, the frontal sinus is possibly impacted by this mechanism. Lastly, biting mechanics has limited impact on brow-ridge morphology and does not explain fully the enormous brow-ridge of Kabwe 1. Hence, other explanations are necessary to explain this prominent feature.

Table of Contents

List of Figures

List of Tables

Acknowledgements

Beatriz, estiveste sempre comigo e este trabalho é-te dedicado.

Para o meu avô Joaquim, sempre presente e nunca esquecido.

I am very grateful and deeply indebted to Paul O'Higgins for accepting me as his student, teaching me everything from the beginning, advices and unrelenting support (academic and personal). Thank you so much Paul.

My Thesis Advisory Panel members (Paul O'Higgins, Laura Fitton, Penny Spikins and Sam Cobb) for suggestions and advises during our meetings.

Everyone at Centre of Anatomical and Human Sciences (administrative staff, academic staff, fellow students, PhDs and MScs) for making me feel welcomed throughout these years. Especially, and in alphabetic order: Andrew McIntosh, Hester Baverstock, Karen Swan, Laura Fitton, Miguel Prôa, Olivia Smith, Paul O'Higgins, Phil Cox, Phil Morris, Sam Cobb, Thomas Püschel, Viviana Toro-Ibacache. A special thanks to Miguel Prôa for his help and Vivi for her help and making available the segmentation of the *H. sapiens* cranium. Also to Laura, Sam and Paul for their valuable classes on Virtual Anatomy, Hard Tissue Biology and Geometric Morphometrics which were crucial for this thesis.

Robert Kruszynski and Chris Stringer (Natural History Museum of London) for access to the Kabwe 1 cranium CT scan. Prof. George D. Koufos (Aristotle University of Thessaloniki) for access to the Petralona cranium CT scan.

My mother, brother and grandmother who have always been present and supportive throughout the years. Also for picking and dropping me off at the airport at the most inconvenient times.

Ângela for coping with the absence and always being there.

I was funded by the Portuguese Foundation for Science and Technology (FCT; PhD funding reference: SFRH/BD/76375/2011).

Author's declaration

I confirm that this work is original and that if any passage(s) or diagram(s) have been copied from academic papers, books, the internet or any other sources these are clearly identified by the use of quotation marks and the reference(s) is fully cited. I certify that, other than where indicated, this is my own work and does not breach the regulations of HYMS, the University of Hull or the University of York regarding plagiarism or academic conduct in examinations. I have read the HYMS Code of Practice on Academic Misconduct, and state that this piece of work is my own and does not contain any unacknowledged work from any other sources'.

1 Introduction

1.1 Introduction

"*Perhaps the most powerful influence on facial morphology is the masticatory system and it is this system in particular that dominates the morphology of the upper, middle and lower face of hominoids*" (Aiello and Dean, 1990, p. 196)

Feeding has been hypothesized as one of the major influences on hominin facial morphology. This dissertation addresses this hypothesis in that it examines the linkages between facial form and masticatory system loading in recent hominins. Specifically, it compares the biting performance of *H. sapiens* to that of its hypothesized ancestral species, *H. heidelbergensis*, and considers if biting mechanics drives morphological differences between these two hominin species. It also assesses how frontal sinus and brow-ridge morphology relate to the mechanics of biting. These studies use finite element analysis (FEA) to predict deformations and bite force. Thus the thesis begins by testing the premise that FEA results approximate reality followed by an assessment of how model building and constraining approaches impact model performance. The dissertation is therefore divided into four main sections. This introduction provides a literature review of previous research relevant to the dissertation. Chapters two, three and four test FEA and describe model construction. Chapters five, six and seven address the above mentioned biologically pertinent questions. Lastly, chapter eight reviews the conclusions of this study by drawing together its findings.

The literature review of Chapter 1 begins by reviewing the mechanical functioning of bone, which impacts the ability of the cranium to generate and resist bite forces. In resisting bites the cranium deforms and these deformations are sensed by bone, triggering bone adaptation as necessary, thereby impacting on bone form. Bone mechanics and mechanical adaptation are therefore reviewed in section 1.2.

Despite the intertwining of form and function, prediction of cranial function from form is not straightforward, in part because of technological limitations, and in part because form is not necessarily related to mechanical function. Thus, selection acting on a given cranial component inevitably impacts on contiguous modules. Even, if selection is not driven by a mechanical function, the resulting anatomy might in itself

have secondary mechanical consequences. Section 1.3 thus reviews studies of hominin cranial form and function and focuses on the limitations of functional inference from form.

Next, the key morphological characteristics and contrasts between the two species examined in this dissertation, *H. sapiens* and *H. heidelbergensis*, are described (section 1.4). Lastly, section 1.5 provides a review of methods commonly used to quantitatively compare form and function, along with a detailed description of the methods that will be used throughout the dissertation (Geometric Morphometrics - GM - and FEA).

Chapter 2 presents a validation study of a voxel based FE model in which the strains experienced by a real cadaveric modern human cranium are compared to those predicted by an FE model of the same cranium under equivalent loading conditions. To that end, the cadaveric human cranium is physically loaded and the deformations experienced are recorded using digital speckle pattern interferometry (DSPI). A finite element model of that same cranium is then virtually loaded and the experienced strains are compared to those of the real cranium. This study is relevant because FEA is used extensively throughout this dissertation to predict deformations and reaction forces (used as proxy for bite force). FEA is grounded on the premise that it approximates reality and thus it has been suggested that every FEA should include a validation study. Furthermore, this study is used to guide the construction of the model of Kabwe 1. This is because validation studies are not possible with the fossil, and so best practice learned from an extant related taxon is all that is available to guide the process of segmentation.

The accuracy and precision of FEA is impacted by modelling decisions of input variables such anatomy and material properties of the model. Because fossils are usually incomplete, fragmented and invaded by sedimentary matrix they often require simplifications of internal anatomy, such as modelling of cancellous bone as a bulk material or even not distinguishing between cortical and cancellous bone. These simplifications impact on the accuracy and precision of FEA predictions. Hence, it is important to assess the impact of varying modelling decisions and simplifications of anatomy and material properties on FEA based predictions of deformation under biting loads. Chapter 3 therefore consists of a sensitivity study that assesses the impact of

model simplification. It compares the strains experienced by a detailed model comprising distinct cortical bone, cancellous bone and teeth with models of decreasing material complexity; a model with material properties of only cortical bone and teeth, and a model with properties of cortical bone applied to all structures.

Chapter 4 describes the virtual reconstruction of Kabwe 1, a representative of *H. heidelbergensis* used in chapter five and as a reference specimen in chapters six and seven. Despite being extremely well preserved, this fossil presents some missing anatomical regions that required reconstruction. Because reconstructions, physical and virtual, involve some degree of subjectivity it is relevant to describe the full reconstruction process applied to this model.

Chapter 5 compares biting performance between *H. sapiens* and *H. heidelbergensis* assessing the extent to which differences in performance are consistent with selection for changes in masticatory apparatus functioning. To this end, the biting performance in a modern human is compared to that of Kabwe 1. Biting performance is assessed in terms of the ability to generate and resist bite forces. The ability to generate bite forces is predicted through the application of principles of lever mechanics and through bite forces produced by the FEA model (measured as reaction forces at bite points). Ability to resist biting is assessed by comparing local (predicted strains, using FEA) and global deformations (how crania deform as a whole, using GM).

Chapter 6 addresses frontal sinus morphogenesis and function, which has been hypothesized to be impacted by biting mechanics. Kabwe 1 has an extremely large frontal sinus traversed by bony struts and thus is a privileged individual to test this hypothesis. Chapter 6 therefore compares three FE models of this fossil among which only the representation of frontal sinus morphology differs. The performance of the model with original sinus morphology is compared to that of another with a completely hollow sinus and to that with an infilled sinus. Performance is assessed based on local (strains from FEA) and global (changes in size and shape assessed using GM) modes of deformation.

Chapter 7 explores the mechanical relevance of the massive brow-ridge in Kabwe 1. The brow-ridge has been hypothesized to perform as a stabilizing element of

the cranium during biting. Thus, its morphology has been said to be impacted by biting. To test this hypothesis the morphology of the brow-ridge is manipulated while maintaining the remaining anatomy constant. One model presents the original morphology of the brow-ridge, another a brow-ridge reduced to a minimum and the other a post-orbital sulcus to approximate the morphology of other species that present this structure. Local and global deformations are then compared to assess if changing the morphology of the brow-ridge impacts on the deformations experienced, if form may be explained purely by mechanics or if other factors have to be considered.

Chapter 8 concludes the thesis by drawing together and summarizing its findings and by looking forward to future advances in the field.

1.2 Bone biomechanical function and adaptation

Bones provide protection for the internal organs and a lever system that enables movement (Marieb, 1992; Lindsay, 1996; Larsen, 2002; Cael, 2010; Kerr, 2010). When loaded, bone experiences forces that stress and deform (strain) it in multiple ways, and as a living, dynamic and mechanosensitive tissue it adapts to the mechanical environment (Currey, 2006). Mechanical adaptation impacts on the material properties of bone, which are related to its micro and gross morphology (Cowin and Doty, 2007; Ethier and Simmons, 2007; Katz, 2008). As such, this section includes a brief description of bone structure, bone mechanical properties and bone mechanical adaptation.

1.2.1 Bone structure

Bone is a connective tissue with an extracellular matrix composed of an organic phase (20%), mineral phase (70%) and water (10%) (Ethier and Simmons, 2007). The organic component, or osteoid, is secreted by osteoblasts in the first stage of ossification. Osteoid mainly comprises collagen, which is laid down in the form of fibrils that aggregate and form collagen fibres. In the second stage, the organic material mineralizes, by hydroxyapatite crystallization within the osteoid, thus forming the mineral component of bone (Lindsay, 1996; Junqueira and Carneiro, 2003). When the ossification process is rapid with haphazard secretion of collagen fibres, woven bone is

formed. In contrast, lamellar bone is deposited slowly and formed by parallel arrays of collagen fibres arranged in layers (lamellae). Orientation of the collagen fibres is consistent within each lamella but different among layers, thus presenting a plywood-like organization (Giraud-Guille, 1988; Lieberman, 2011).

Ossification gives rise to two macrostructurally different types of bone, compact (also referred to as cortical) and trabecular (or cancellous) (Lindsay, 1996; Junqueira and Carneiro, 2003; White and Folkens, 2005). Compact bone forms most of the external surface, or cortex, of bones and is covered by the *periosteum* on the outer surface, the *endosteum* on the inner surface and cartilage on the articular surfaces (White and Folkens, 2005). The most external layer of cortical bone is formed by the external circumferential lamellae, which are thin (+/- 5 μm thick) sheets of lamellar bone that cover the internal osteons. Osteons are cylindrical structures organized around a central (Haversian) canal and are made up of several concentric lamellae that have a maximum diameter of about 200 μm, a length of approximately 1 cm and are generally aligned parallel to the long axis of the bone (Cowin and Doty, 2007; Dechow et al., 2008). Osteons are populated by osteocytes, bone cells located in the lacunae among the lamellae. These bone cells are interconnected among themselves and with bone lining cells (located on bone surfaces) by processes that extend through canals known as *canaliculi*, forming a network throughout the bone (Lindsay, 1996; Cowin and Doty, 2007). The Haversian canals communicate with each other, the *periosteum* and the marrow cavity through the Volkmann's canals (Junqueira and Carneiro, 2003). Despite all these microstructures, on average cortical bone presents a level of porosity below 10%, although it is defined as bone with a porosity below 30% (Ethier and Simmons, 2007).

Cancellous bone is mainly found in the extremities of long bones and vertebral bodies (Parkinson and Fazzalari, 2013). Like compact bone it has a lamellar structure in which the lamellae are generally, but not always, oriented parallel to the trabeculae (Ethier and Simmons, 2007), but usually lacks the osteonal structure (Guo, 2001). It is defined as bone that presents a porosity that ranges from 30% to 90% (Cowin and Doty, 2007), with bony rod-like (trabeculae) and plate-like structures enclosing three dimensional interconnected open spaces, thus forming a cellular solid (Keaveny et al., 2001). Trabecular bone is highly heterogeneous within and between bones and the proportions of plate-like structures and rod like trabeculae vary considerably. The most delicate architectures of trabecular bone, such as are found in deep parts of long bones,

mainly present thin trabeculae that appear randomly oriented. At the other extreme, the most robust arrangements of cancellous bone are mainly found under articular surfaces, such as the head of the femur, and are made up of thick fenestrated plates (Singh, 1978) that are oriented according to the direction of habitually experienced loads (Currey, 2006).

1.2.2 Bone mechanical properties

Studies of bone material properties most commonly assess the ability of bone to resist deformation and failure due to applied forces at the micro and macrostructural levels. While extensive and thorough studies describe multiple material properties (for reviews see e.g. Cowin, 2001 and Currey, 2006) this section only presents a brief overview of some of those properties.

Bone is a linearly elastic, inhomogeneous, anisotropic, ductile material (Cowin, 2001; Humphrey and Delange, 2004; Currey, 2006). This complexity in material properties arises because bone is a highly intricate structure with several levels of organization (Katz, 2008). The organization of tropocollagen molecules in collagen and associated hydroxyapatite is denoted as the molecular level. The ultrastructural level is related to the assemblage of the collagen fibrils and hydroxyapatite into fibres. The microstructural level is associated with bone tissue, i.e., how collagen and hydroxyapatite are arranged into woven or lamellar bone. The macrostructural level is concerned with the whole bone and its material properties, which are impacted by all levels of organization (Katz, 2008). Currey (2006) denotes bone material as the solid that forms bone (i.e. material that makes the trabeculae in cancellous bone) and bone tissue as the whole structure (i.e. bone material plus hollow spaces). This scheme is used throughout this manuscript.

When a force is exerted, bone, like any other structure, undergoes stress (σ) and deforms (strain, ε). Deformation is "sensed" by osteocytes and may trigger mechanical adaptation (see below). Stress is defined as the ratio of force (F) to the cross sectional area (A) of the bone to which it is applied ($\sigma = \frac{F}{A}$). When the direction of the force is perpendicular (normal) to a given plane normal stresses develop (tensile when the structure is stretched, and compressive when compressed). When the force direction is parallel to the plane shear stresses develop (Bird and Ross, 2012). Strain is measured in

terms of the fractional changes in the dimensions of the bone due to loading and can be expressed as $\varepsilon = \frac{\Delta L}{L}$, where ΔL represents length after deformation and L equals the original length. Like stresses, strains can be compressive, tensile and shearing. In compressive and tensile strains there are changes in form but none in the angle between the sides of the structure analyzed. In shearing strains there are changes in form and a change in the angle between two adjacent sides (Figure 1-1; Currey, 2006; Bird and Ross, 2012).

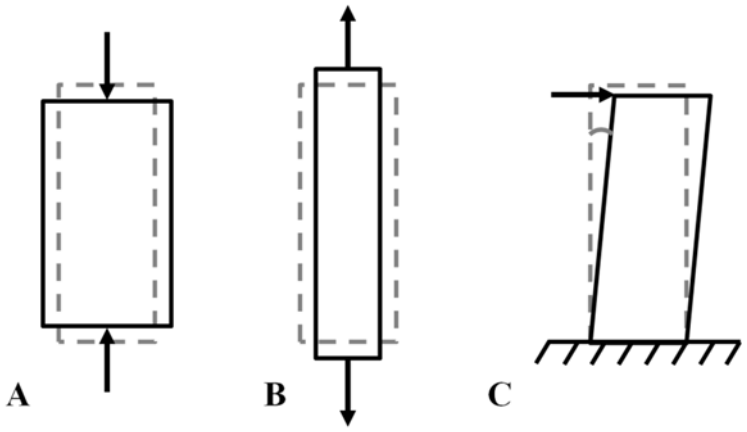

Figure 1-1: Examples of form changes due to tension (A), compression (B) and shearing (C). Black arrows represent applied forces, dashed grey = original undeformed geometry, and solid black = deformed geometry.

Most deformations experienced by bone are small and do not cause permanent deformation, i.e. once the applied force is removed, bone returns to its original form. This change in morphology is termed elastic deformation (Bird and Ross, 2012), in bone it is linearly related and proportional to the applied force within the physiological range of deformation (Currey, 2006). However, if the deformation exceeds the elastic limit, then plastic deformation occurs and bone no longer recovers its original form. In plastic deformation there is no proportionality between applied force and deformation (Bird and Ross, 2012). Thus, bone is ductile in contrast to brittle materials, which present no plastic or post-yield deformation and so, fracture (Figure 1-2; Currey, 2006; Bird and Ross, 2012). The yield point (Figure 1-2) marks the limit of elastic deformation, at which plastic deformation begins. Before this point on the stress-strain curve it is linear. Its slope in this linear region is the modulus of elasticity (Young's

modulus, denoted by *E*), and is expressed in Pascals (Pa), which are Newtons per square metre. The ultimate strength of a material is the highest point on the stress-strain curve, and this often does not coincide with the failure point (Bird and Ross, 2012).

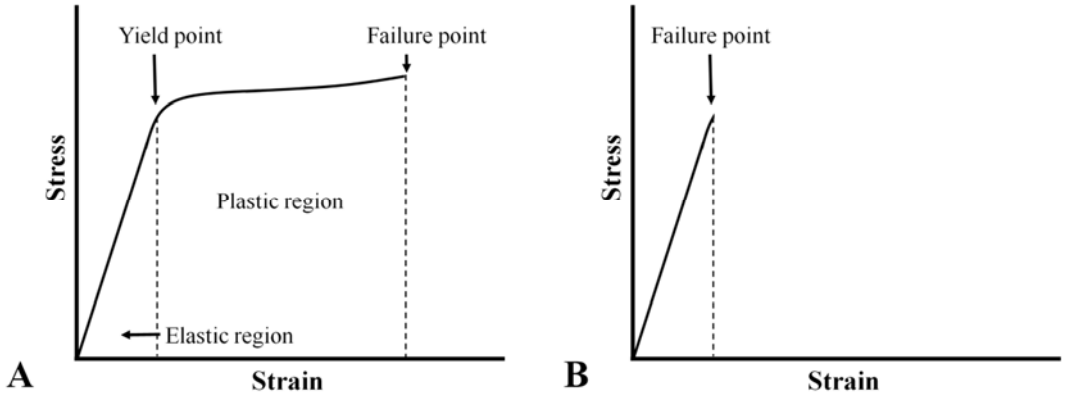

Figure 1-2: Hypothetical stress-strain curves of a ductile (A) and a brittle material (B).

Because of its complexity at the microstructural level, and due to variations in density, mineralization, cortical and trabecular bone distribution and organization, bone is an inhomogeneous structure that presents regional variation in its material properties (Currey, 2006). As such, studies have reported differences in material properties within bone tissue (e.g. interstitial lamellae and secondary osteons; Rho et al., 1999), within the same bone (e.g. mandible; Dechow et al., 1993; Dechow et al. 2008) and between bones (e.g. mandible, cranium and femur; Dechow et al., 1993; Dechow et al., 2008). Differences in material properties within and between bones have been associated with functional differences (Dechow et al., 1993; Dechow et al., 2008).

Another important material property of bone is anisotropy, thus presenting differences in strength according to the direction of the applied force (e.g. a long bone is stiffer if a force is applied along its shaft rather than perpendicular to it). Bone anisotropy is associated not only with gross morphology but also with bone microstructure, e.g., the three dimensional orientation of osteons (Currey, 2006; Dechow et al., 2008). Thus, a study using nanoindentation to measure modulus of elasticity reported values of 22.4 GPa in longitudinal loading of cortical bone tissue (average of osteons and interstitial lamellae) and of 16.6 GPa in transverse loading (Rho et al., 1999).

Lastly, bone is viscoelastic, i.e. its modulus of elasticity depends on the rate at which it is strained (strain-rate). It has been demonstrated that increases in strain rate result in increases in modulus of elasticity of bone but the increase is very small under normal physiological loading conditions (McElhaney, 1966; Currey, 2006).

It should be noted that the material properties reported for bone in different studies are not always consistent. This has been attributed to two main factors, differences in tested specimens and techniques used. Regarding the latter, two main approaches have been used, mechanical and ultrasonic. While mechanical testing directly assesses the elastic properties from resulting deformations, ultrasonic testing measures the velocity of sound waves travelling through bone and commonly reports a higher modulus of elasticity (Kim and Walsh, 1992).

Despite differences in results due to methodology and specimen choice, it is clear that the material properties of bone vary according to the scale at which it is examined. Microstructurally bone tissue, which includes trabecular and cortical tissue, has been characterized as a fibre-reinforced composite, with tensile strength and post-yield ductility provided by the collagen fibres and stiffness by the mineral component, hydroxyapatite (Guo, 2001; Ethier and Simmons, 2007). Even though both cortical and trabecular bone are lamellar, the latter is slightly less stiff than the former (e.g. the elastic modulus in cortical bone ranges from 16.6 to 25.7 GPa while in trabecular bone material it ranges from 15 to 19.4 GPa; Rho et al., 1999) due to structural and compositional differences (Guo, 2001). Trabecular bone material has lower density, higher water content and lower calcium content than cortical bone, thus making it less stiff (Guo, 2001).

Compositional differences have been associated with a higher remodelling rate in trabecular bone and the fact that freshly remodelled bone is less mineralized (Guo, 2001). Furthermore, at a larger scale cortical bone and cancellous bone (bulk) tissue (trabeculae and the spaces between them) clearly have different material properties due to the large differences in porosity and organization of the bone tissue (see above). The modulus of elasticity for bulk cortical bone is about 16GPa while that of cancellous tissue is about 1 GPa (Humphrey and Delange, 2004). These values are approximations and do not portray the complexity and regional variability that both cortical (see above) and cancellous bone tissue present. The mechanical properties of the latter, as a bulk material, are a function of the arrangement of the trabeculae and of the apparent density (mass of dry bone divided by volume of specimen) (Keaveny et al., 2001; Currey,

2006). Thus, e.g., studies have reported moduli of elasticity in human cancellous bone tissue that range from 4 to 350 MPa in the lower limb (Hodgskinson and Currey, 1992) and 3.5 to 125.6 MPa in the mandible (Misch et al., 1999).

1.2.3 Bone mechanical adaptation

Bone growth and development is influenced by epigenetic factors such as the mechanical loadings experienced during ontogeny (Moss, 1997a, 1997b; Carlson, 2005). Mechanical loading causes deformation, which is detected at the cellular level, triggering a response that ultimately results in bone mechanical adaptation (Currey, 2006; Ruff et al., 2006; Klein-Nulend and Bonewald, 2008).

Deformation detection and mechanotransduction, i.e. the process by which deformation triggers electrical and/or bio-chemical signals (Burger and Klein-Nulend, 1999; Bonucci, 2009), are not fully understood (Burger and Klein-Nulend, 1999; Skerry, 2000; Robling et al., 2006; Ethier and Simmons, 2007; Klein-Nulend and Bonewald, 2008), however it is widely accepted that the osteocyte – bone lining cells – osteoblast network is fundamental in this process (Robling et al., 2006; Klein-Nulend and Bonewald, 2008; Bonucci, 2009). Several mechanisms have been suggested by which deformation is detected at the level of osteocytes, which include direct deformation of the cells along with bone, fluid flow or hydrostatic pressure with "measurement" of bulk and shear strains, electric and magnetic transduction, oxygen tension and osteocyte hypoxia (Robling et al., 2006; Klein-Nulend and Bonewald, 2008; Bonucci, 2009). In response to deformation a cascade of biochemical processes, that may include dedifferentiation of bone lining cells into osteoblasts, ultimately results in bone (re)modelling and bone mechanical adaptation (Klein-Nulend and Bonewald, 2008; Bonucci, 2009).

Regardless of the precise mechanotransduction mechanism, bone mechanical adaptation may arise through modelling or remodelling processes. Bone modelling, in which there is independent action of osteoblasts and osteoclasts, contrasts with remodelling, where these are coordinated (Robling et al., 2006). Bone deposition or resorption may occur in the periosteal and/or endosteal surfaces and usually there is a change in bone size and/or shape (Currey, 2006). Bone modelling is age dependent and becomes much less marked once skeletal maturity is achieved (Robling et al., 2006). Bone remodelling does not affect bone size or shape and occurs through the coupled

action of osteoblasts and osteoclasts (Hall, 2005), which form the basic multicellular unit (Ortner, 2003; Robling et al., 2006). In response to deformation of the bone matrix, osteocytes produce nitric oxide, thereby regulating bone deposition via the osteoblasts and bone resorption via the osteoclasts (Bacabac et al., 2008). That bone deposition (Jones et al., 1977; Kannus et al., 1995) or bone resorption (Nordstrom et al., 1996; Goodship et al., 1998) occurs due to mechanical loading, thus changing bone mass, is clearly demonstrated. But bone adaptation may also occur via alterations in bone mineral content (Kannus et al., 1995; Valdimarsson et al., 2005) and in mineral density (Kerr et al., 1996; Valdimarsson et al., 2005). These bone mechanical adaptations occur throughout life, but the potential for adaptation to the mechanical environment decreases with age (Ruff et al., 2006). This reduction may be due to diminished capacity of adult mesenchymal cells to differentiate into osteoblasts (Nishida et al., 1999) and/or reduced sensitivity of osteoblasts and osteocytes to mechanical signals (Turner et al., 1995; Stanford et al., 2000).

Bone mechanical adaptation seems to occur when there are significant deviations from a "minimum effective strain" (Frost, 1987) or "optimum customary strain level" (Skerry, 2000). In most sites of the skeleton, this is hypothesized to be in the range of 1500 - 2500 μE (Frost, 1987) to 3000 μE (Skerry, 2000). If deformations reach that threshold deposition of bone occurs. On the other hand, if strains are lower than a certain minimum, bone resorption occurs (Turner, 1998) (Figure 1-3). However, peak strain is not the only variable that triggers bone adaptation. Other factors that have been demonstrated to cause bone adaptation include dynamic vs. static loading (Lanyon and Rubin, 1984; Turner, 1998), strain rate (Mosley and Lanyon, 1998) and strain frequency (Judex et al., 2007).

Even though most sites in the skeleton share a similar optimal strain level, this threshold is hypothesized to be site-specific, based on differences in strain experienced by different skeletal elements. Recorded strains in the cranial vault appear to be 10 times lower than those in the long bones (Hillam et al., 1995). If bone remodelling thresholds in the vault were similar to the remaining post-cranial bones this would result in severe osteoclasis. Thus, site-specific patterning information has been suggested, which would allow cells to adapt to site-specific loads (Skerry, 2000; Currey, 2006). This hypothesis is supported by studies that compared the calvarial and lower limb osteocyte morphology in rats and demonstrated differences in size, shape and orientation of these cells (Vatsa et al., 2008; Himeno-Ando et al., 2012). In the lower

limb osteocytes are larger, longer and flatter than in the vault, where they are smaller and more spherical. Furthermore, in the lower limb, osteocytes are aligned with the principal direction of loading whereas in the vault, in which loads are multidirectional due to forces exerted by intracranial pressure and masticatory function, they show no consistent orientation. Because studies using osteocytes show that rounder cells are more mechanosensitive than flat ones these results support the hypothesis of site-specific osteocyte mechanosensitivity (Bacabac et al., 2008; Vatsa et al., 2008; Himeno-Ando et al., 2012).

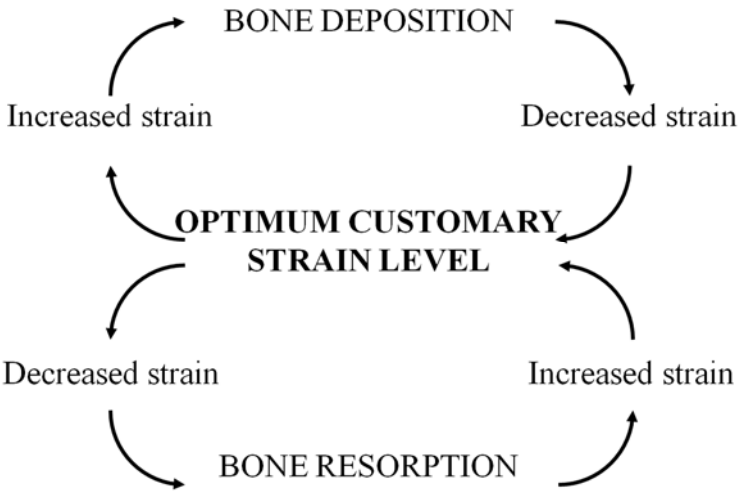

Figure 1-3: Feedback model of bone function adaptation (adapted from Lanyon, 1982).

In contrast to these findings, using Finite Element Analysis, Witzel (2011) modelled a cranium as an homogenous solid in which the only details were the eye sockets, the nose cavity, the brain cavity and the form of the dental arcade. Forces were then applied that simulated biting and the acceleration of the brain. In accordance with principles of bone mechanical adaptation regions that experienced high stresses and strains were kept and regions that experienced low stresses and strains were removed. After several iterations of this algorithm simulating adaptation, the final result was a structure that clearly resembles a Neanderthal cranium (Witzel, 2011). In this study, and another that used the same approach but with a *Diplodocus* cranium (Witzel and Preuschoft, 2005), no site specific mechanosensitivity was assumed, and bone was removed throughout the cranium based on the same stress or strain level. Thus, these results seem to support a generalized threshold model. The discordance in views with

respect to calvarial loading might be because the hypothesis of generally low strains in the calvarium has not been experimentally tested in relation to head acceleration and deceleration (which via the meninges acting on the inner table would strain the calvarium), but rather mastication.

1.3 Cranial form and function

Like any other skeletal element, crania fulfil mechanical functions, such as housing and protecting organs and providing a skeletal system that enables chewing (Lieberman, 2011). Thus, the association between cranial form and masticatory function, has principally focused on two areas, the ability to generate bite forces (Antón, 1990; O'Connor et al., 2005) and the ability to resist those forces (Rak, 1983; Rak, 1986; Demes, 1987).

1.3.1 Production of bite force

Bite force in extant species is directly measurable using force transducers while biting. This approach has been widely used to measure bite force in living humans in which large differences have been recorded (Braun et al., 1995; Sinn et al., 1996; Kikuchi et al., 1997; Paphangkorakit and Osborn, 1997). However in extinct species this is not possible and alternative approaches are necessary. Thus, researchers use skull morphology (bony proxies) to estimate muscle cross sectional areas (Demes and Creel, 1988; Antón, 1990; O'Connor et al., 2005; Eng et al., 2013), which, depending on pennation angle, are related to maximal force generation (Josephson, 1975; Weijs, 1980; Gans and de Vree, 1987). While this technique has limitations due to differences between cross sectional areas estimated via bony proxies and actual physiological muscle cross section (Eng et al., 2013; Toro-Ibacache et al., 2015b) it remains the only approach available to estimate muscle forces in extinct species. The force generated by masticatory muscles is then transferred to the teeth and converted into bite force by the masticatory lever system, which is dependent on skull morphology (i.e. the relative positions of muscle origins, muscle insertions and teeth). As such, researchers have measured the in and out-levers of the masticatory lever system to assess its efficiency (Demes and Creel, 1988; Antón, 1990; O'Connor et al., 2005; Eng et al., 2013).

1.3.2 Resisting biting

The generated bite force is transmitted to food items and the cranium experiences an equal bite reaction force. Thus, crania have to be adapted to withstand masticatory forces. In order to assess and explain how the cranium resists occlusal forces researchers have used several approaches, including simple engineering analyses of the cranium considered in terms of vertical and horizontal column-like structures that buttress the face and channel bite reaction forces (Görke, 1904; Richter, 1920; Endo, 1965; Endo, 1966), more sophisticated modelling of crania as a cylinder that is twisted during biting (Greaves, 1985; Greaves and Mucci, 1997), direct measurement of strains experienced during biting using strain gauges (Hylander et al., 1991b; Hylander et al., 1992; Ross and Hylander, 1996; Ravosa et al., 2000a; Ravosa et al., 2000b; Ross, 2001; Ross et al., 2011), and more technically complex simulation of biting and measurement of strains using finite element analysis (Gross et al., 2001; Ross et al., 2011; Janovic et al., 2015).

Traditionally dissipation of occlusal forces was explained as channelling of those loads throughout the face along vertical and horizontal pillars made of thick cortical bone, or buttresses (Cryer, 1916). Schematization of those buttressing systems led to the proposal of several frame models (Figure 1-4) to explain how crania dissipated occlusal loads (Görke, 1904; Richter, 1920; Endo, 1966). Endo compared his frame model and its predictions to experimental strain data from a series of innovative studies in which biting was simulated using dry crania and resulting strains measured using strain gauges (Endo, 1965; Endo, 1966). Due to the downward pull of temporalis and masseter muscles and the upwardly directed bite force, it was found that during incision the midline nasal element would experience axial compression in the sagittal plane while the lateral orbital elements would mainly experience bending moments and tension. In posterior biting the results are similar, but with slight tension in a small area of the inter-orbital element and slight compression in the ipsilateral lateral orbital element. Furthermore, relatively high strains on the brow-ridge were recorded during incision, leading Endo to propose that the brow-ridge was a stabilizing structure of the craniofacial skeleton during biting, while it was subjected to bending due to the downward pull of the contracting masticatory muscles and the upward biting force (Endo, 1965).

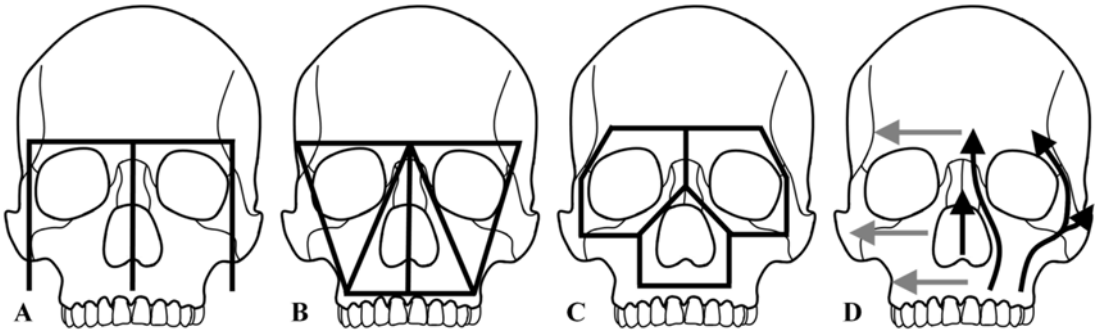

Figure 1-4: Buttressing systems proposed by different researchers. A: Görke's model (adapted from Rak, 1983); B: Richter's model (adapted from Rak, 1983); C: Endo's model (adapted from Russel, 1985); D: Seven pillar buttressing system proposed by several researchers; vertical buttresses represented by the black arrows on the right side (pterygomaxillary buttress not visible) and horizontal buttresses represented by the grey arrows on the left side (adapted from Janovic, 2015).

Assessing the mechanical relevance of the postorbital bar as a torsion resisting helical strut in ungulates and carnivores, Greaves (1985) proposed the cylindrical model of the craniofacial skeleton. He realized that during masticatory function there is asymmetric bilateral activation of the muscles. The working muscles exert a greater force than the balancing ones, thus twisting the skull towards the working side. At the same time a reaction force is generated at the biting point that twists the skull towards the opposing side. The craniofacial skeleton is, thus, subjected to torsion in which the braincase rotates counter wise to the facial skeleton, causing compression in the post-orbital bar of the working side and tension in the post-orbital bar of the balancing side (Greaves, 1985). However, in a later study it was proposed that this model does not apply to primates because masticatory muscles produce small twisting forces (Greaves and Mucci, 1997).

Despite frame and cylinder models provide theoretical grounding they do not allow direct assessment of the deformation crania undergo during biting. Thus, following Endo's approach, several studies have used strain gauges to measure strains. Although in-vivo studies in primates have only used non-human species, ranging from the strepsirrhines *Otolemur* (Ravosa et al., 2000a; Ravosa et al., 2000b; Ross, 2001) and *Aotus* (Ross and Hylander, 1996; Ross, 2001) to the cercopithecides *Macaca mulatta* (Ross, 2001; Ross et al., 2011), *Macaca fascicularis* and *Papio anubis* (Hylander et al., 1991b), they still provide relevant insights. Due to morphological and

material property differences the results vary according to the species under analysis (Ross, 2001). Despite this, it is clear that crania do not experience a simple loading regime but rather, a complex loading with modes of deformation that vary between different anatomical regions (Ross, 2001; Lieberman, 2011). For the cranium as a whole, the twisting cylinder model (Greaves, 1985) in primates is supported by the results from the *Otolemur* (Ross, 2001) and inconsistent with the results from macaques and baboons (Hylander et al., 1991b). Endo's frame model is partially supported by the results of Ross (2001) for *Aotus* and *Macaca mulatta*. Notwithstanding those differences, data consistently show a strain gradient in which the lower face experiences high strains that diminish towards the upper face (Hylander et al., 1991b; Ross and Hylander, 1996; Ravosa et al., 2000b; Ross, 2001), suggesting that occlusal loads mainly deform skeletal material close to the bite point rather than more widely in the neurocranium, with forces transmitted via the craniofacial haft. In fact, the brow-ridge has been shown to experience strains 50% lower than the mid-face (Hylander et al., 1991b; Hylander et al., 1992), thus suggesting that it is not an adaptation to biting but the result of spatial determinants (Ravosa et al., 2000c).

With increased computational power, researchers have started using finite element analysis to reexamine how occlusal forces are dissipated (Gross et al., 2001; Janovic et al., 2015). While Gross et al. (2001) do not support models proposing that occlusal force dissipation occurs via a buttressing system, Janovic et al. (2015) partially do. In a reexamination of loading regimens based on experimental strain data and a validated *Macaca fascicularis* FE model, Strait et al. (2011) caution that simple descriptions do not portray the full complexity of the deformation regime, which is a function of the complexity of the loading regime, geometry and material properties of the cranium. Nonetheless, they summarize and "*describe the global deformation of the macaque facial skeleton during mastication as 'bending in a frontal plane' caused in larger part by torsion of the zygomatic arch about its long axis and bending of the arch in sagittal planes*" (Ross et al., 2011, p.138). This deformation regime produces strains that are generally consistent with Endo's (1965, 1966) predictions of axial compression of the inter-orbital region and bending of the supra-orbital ridge (Ross et al., 2011).

Researchers have also tried to predict how fossil hominin crania resist biting. Because physical mechanical loading is not possible in fossils, two main approaches have been used, anatomical simplifications with associated predictions (Rak, 1983; Rak, 1986; Demes, 1987; Trinkaus, 1987b) and, more recently, FEA (Wroe et al., 2007;

Strait et al., 2009; Strait et al., 2010; Wroe et al., 2010). Most studies have focused *Australopithecus africanus* (Rak, 1983; Strait et al., 2009; Strait et al., 2010), *Paranthropus boisei* (Rak, 1983; Wroe et al., 2010) and *Homo neanderthalensis* (Rak, 1986; Trinkaus, 1987b), species that due to their cranial anatomy have been said to be adapted to generate and resist high occlusal loads.

1.3.3 Cranial form, function, modularity, integration and equifinality

The concept of equifinality relates to different processes that produce similar or identical outcomes (Wood, 2011) and it has recently been applied in human evolution by Churchill (2006, 2014), aiming to know if Neanderthal cranial and post-cranial anatomy is adaptated to thermoregulation or high ventilatory requirements due to intense physical activity. Equifinality applies particularly to the skull because it is composed of several modules that are, nonetheless, tightly integrated (Lieberman, 2011; Klingenberg, 2013). Thus, evolutionary changes acting on a specific module will inevitably impact on adjacent structures, making it extremely difficult to distinguish between selection, evolutionary by-products (or spandrel, *sensu* Gould and Lewontin, 1979) or genetic drift (Lieberman, 2011).

That the cranium is morphologically composed of a set of relatively independent functional components, or modules, was proposed by Van der Klaauw (1948 - 52). Modules are defined as structures that are tightly integrated internally and are relatively independent from other modules. Thus, from a GM perspective, they present levels of internal covariation that are larger than when including other structures (Klingenberg et al., 2003; Mitteroecker and Bookstein, 2008; Klingenberg, 2010; Klingenberg, 2013). This relative independence allows evolvability and mosaic evolution without compromising the functional or structural integrity of other modules and of the whole system into which they may eventually become integrated (Wagner and Altenberg, 1996; Bastir, 2008; Mitteroecker and Bookstein, 2008; Klingenberg, 2013) because evolutionary changes in one module tend to impact locally (Mitteroecker and Bookstein, 2008).

But despite their relative independence cranial modules share structures, developmental precursors, an evolutionary history and functional demands (Lieberman, 2011; Klingenberg, 2013). Moreover, these complexes are "*coordinated in their sizes*

and shapes to make up a functional whole" (Klingenberg, 2013, p.1) and changes in one module inevitably impact on nearby modules (Lieberman, 2011). Thus, clear identification of modules is hampered by covariation between such structures (or integration) and by different levels of modularity (developmental, genetic, functional and evolutionary; Klingenberg, 2010) that coexist and interact with each other (e.g. functional modularity relates to developmental modularity because function impacts on growth and development; Klingenberg, 2010).

Because of this tight integration of cranial modules it is hard to distinguish if evolutionary changes have arisen through selection acting on a given module or as an evolutionary by-product whereby the present module is modified because of selection acting elsewhere and impacting on it through integration (Gould and Lewontin, 1979; Lieberman, 2011). For example, the derived modern human chin has been associated with adaptation to mechanical demands during biting (Daegling, 1993; Dobson and Trinkaus, 2002; Groning et al., 2011b), size reduction of the dentition (Wolff, 1984), sexual dimorphism (Horowitz and Thompson, 1964; Thayer and Dobson, 2010), development of speech (Ichim et al., 2007a), and spatial factors (Holton et al., 2014; Pampush and Daegling, 2015). This profusion of possible explanations for the chin demonstrates the difficulty in distinguishing between evolutionary adaptations and by-products. Moreover, cranial morphology has also been said to be impacted by genetic drift (Ackermann and Cheverud, 2004). Thus, the concept of equifinality applies particularly to skulls in general, and to the example of the human chin in particular, which has been suggested to be the result of natural selection, genetic drift or an evolutionary by-product. Any or all of these processes might act to result in a chin.

It is, therefore, not clear how to unequivocally infer whether morphological change is due to changes in one or several aspects of function or shifts in developmental and evolutionary processes (Lieberman, 2008; Lieberman, 2011) because different processes acting on different cranial components may give rise to similar morphological outcomes (i.e. equifinality). Lieberman (2008, 2011) provides a good example regarding masticatory function, with regard to the derived orthognathic modern human face. Retraction of the facial skeleton in *H. sapiens* leads to increased mechanical advantages and therefore higher efficiency in converting muscle force into bite force, which might suggest adaptation to increased biting efficiency. However, that increase is accompanied by an hypothesized decrease in the ability to resist occlusal loads, enamel thinning and decrease in muscle force. Thus, Lieberman suggests that the

increased efficiency of modern humans in converting muscle force into bite force is a spandrel. Nevertheless, morphological changes in one module may impact on the function of other components, regardless of what originally drove those changes. Furthermore, evolutionary changes may be driven by specific agents and later be picked up by other functions (see concept of exaptation, Gould and Vrba, 1982). Thus, it is of relevance to assess the functional (masticatory, in the case of this dissertation) impact of morphological evolutionary change, even if not testing for the primary reason a form developed.

1.4 Cranial form in Homo heidelbergensis and Homo sapiens

"*It is among the truly basic and universal facts of nature that all species vary*".
Simpson (1961, p. 177) *in* Antón (2003)

This section provides a general morphological description of the species that will be analyzed in the dissertation.

1.4.1 Homo heidelbergensis

Homo heidelbergensis has a generally long and low cranial vault. The cranial base angle averages about 142.5º, the endocranial mean volume is 1263 cm^3 and the encephalization quotient ranges from 4.3 to 4.7. The frontal bone is long and low, sloping smoothly from an almost non-existent post-orbital sulcus towards the sagittal suture where, at *bregma*, the vault presents the highest point (Schwartz and Tattersall, 2003; Lieberman, 2011). The temporal squama is high and arched (Rightmire, 2008) and the parietals are also arched, presenting some bossing (Bräuer, 2008). In the slightly keeled (Schwartz and Tattersall, 2003) and coronally enlarged frontal (Bräuer, 2008), there is moderate post-orbital constriction, which is significantly reduced when compared to previous hominins. Specimens such as Petralona, Kabwe 1 and Saldanha present greatly expanded frontal sinuses (Rightmire, 2008). The massive supraorbital region is tall, double arched and confluent across the glabella. The tallest point is located at the middle of each of the arches, significantly above glabella (Schwartz and Tattersall, 2003). From that point it drops inferiorly both laterally and medially. The large brow-ridge projects above the orbital cavities, which are very large, sub-squared

and present downward and outward sloping in the inferior margins (Schwartz and Tattersall, 2003). The face is large, projecting anteriorly to the anterior cranial fossa, but less prognathic than other ancestral species. When compared to *Homo erectus* it is approximately 11% bigger (Rightmire, 2008). This difference results from increases in antero-posterior length and supero-inferior height. The zygomatics are gracile, with the root usually placed over M1/M2 (Schwartz and Tattersall, 2003; Lieberman, 2011). The margins of the nasal cavity are vertical and in some specimens the nasal walls meet the infraorbital surface at a shallow angle, forming a shallow concavity (Figure 1-5; Rightmire, 2008).

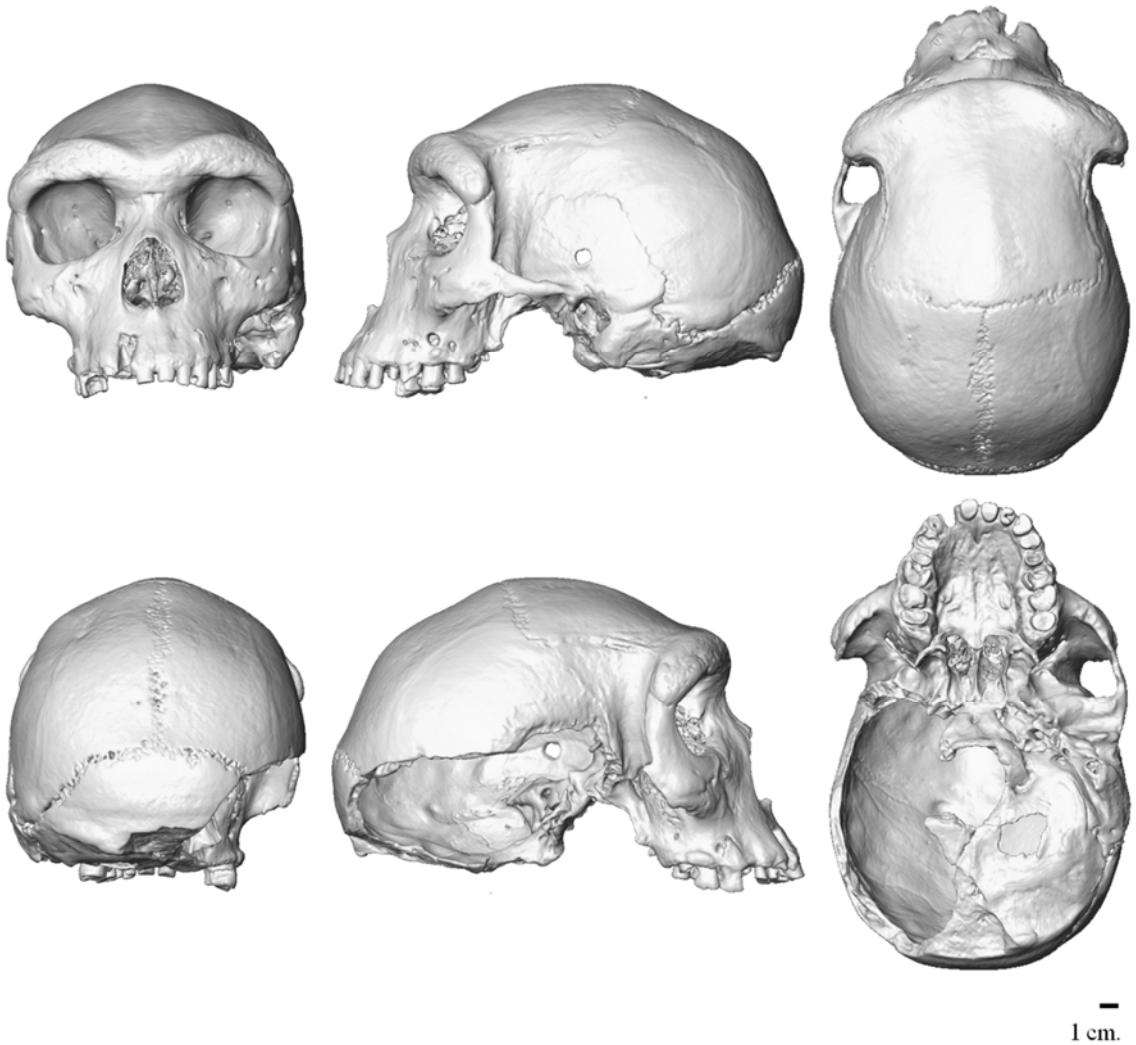

Figure 1-5: Standardized views of Kabwe 1 (*Homo heidelbergensis*). See text for description of key anatomical features.

1.4.2 Homo sapiens

Modern humans present a small, non-projecting and orthognathic face located under the anterior cranial fossa (Figure 1-6). The cranial vault is spherical, the cranial base angle particularly flexed and the oral cavity small. The brow ridges are small and gracile (Lieberman, 2011). While the endocranial volume of early modern humans averages 1495 cm^3, in recent *H. sapiens* the average is 1350 cm^3, corresponding to an encephalization quotient of 5.3 (Lieberman, 2011). This big endocranial capacity is associated with a spherical neurocranium, which has been regarded as an autapomorphy of *H. sapiens* (Lieberman et al., 2002). The tall, wide and short cranial vault presents long, wide and significantly curved parietals. The maximum breadth at the parietals matches or exceeds the width at the mastoid area. The occipital region is long and does not project significantly posteriorly. The forehead is high with a steep frontal squama, below which the brow ridge is bipartite and gracile, with clearly cut medial and lateral regions above the supra-orbital notch. There are no post-orbital sulcus and constriction (Lieberman et al., 2002; Lieberman, 2011).

The small face has been regarded as one of the major derived features in the cranium of *H. sapiens*, in which the root of the remarkably gracile and receding zygomatics is usually located above M1/M2 (Lieberman et al., 2002; Lieberman, 2011). The face is mostly retracted under the anterior cranial fossa and thus lacks the prognathism of previous species. This has been said to be the result of its small size, especially antero-posteriorly, and of the particularly flexed cranial base angle (Lieberman et al., 2002; Lieberman, 2011). This facial retraction of modern humans has been related to other anatomical specificities such as the canine fossa, a short space for the oropharynx and rectangular orbital cavities (Lieberman et al., 2002; Lieberman, 2011). Enlow and Hans (1996) proposed that morphological changes in the brain of our species explain the general morphology of our face. They suggest that enlargement of the brain (e.g., frontal and temporal lobes) causes increased flexure of the cranial base and anterior rotation of the frontal bone, resulting in a vertical forehead. This causes rotation of the orbits to a horizontal position, parallel to the ground. The enlargement of the temporal lobes causes the orbits to rotate towards the midline of the skull, thus decreasing inter-orbital area and precluding the presence of a significant nasal protrusion. Reduction in nasal projection causes reduction of the palate and, therefore, reduced prognathism. In summary "*the face has become rotated down by the expanded*

anterior cranial floor as the floor rotates downward as a result of the enlargement of the frontal lobes" (Enlow and Hans, 1996; p. 154).

Tattersall and Schwartz (2008) have suggested a list of autapomorphic cranial features in *Homo sapiens* that includes extension of the vaginal process to the lateral margin of the ectotympanic tube; approximation of the vaginal process to the mastoid process; postero-medial placement of the stylomastoid *foramen* in relation to the extremely laterally placed styloid process; high and narrow occipital plane of the occipital bone; retention of a arcuate eminence on the superior surface of the *pars petrosa*; fully segmented sutures with deep interdigitation; bipartite supraorbital area undercut at the supraorbital notch; postero-anterior thickening of the mandibular symphysis; inverted T-shaped chin; unclosed-off subarcuate fossa; back and down tilting inferior orbital plane.

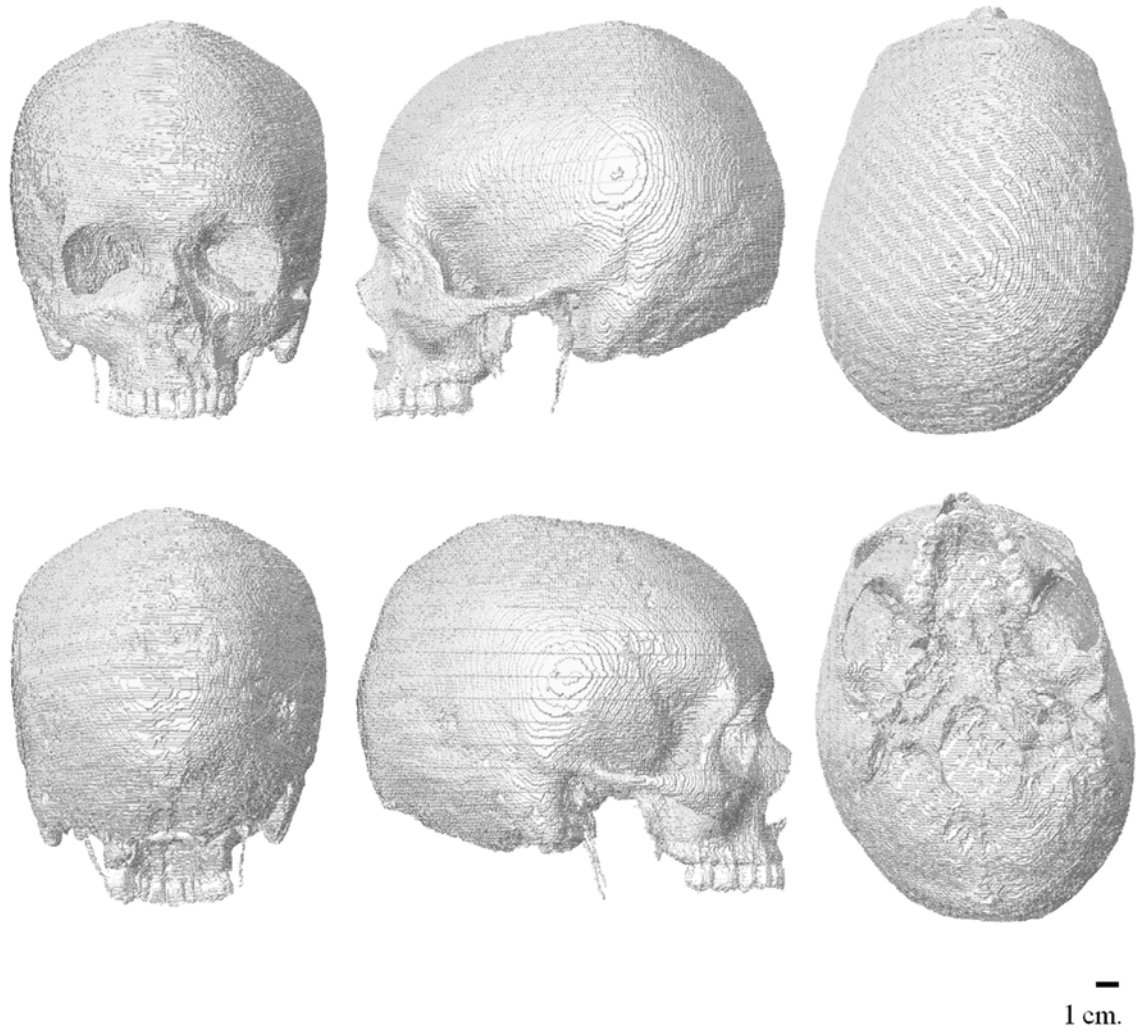

Figure 1-6: Standardized views of the cadaveric *H. sapiens* specimen used in chapters two, three and five. See text for description of key anatomical features.

1.5 Measuring cranial form and mechanical function

Hominin cranial biomechanical studies (Rak, 1983; Rak, 1986; Demes, 1987; Trinkaus, 1987b; Strait et al., 2007; Strait et al., 2009; Strait et al., 2010; Wroe et al., 2010; Benazzi et al., 2015; Smith et al., 2015b; Ledogar et al., 2016) are based on the relationship between skeletal form and function (Hildebrand, 1995), and rely on the ability to measure morphology and function. Morphometric approaches to quantify form and its covariances, including with function, have changed dramatically over the last three decades, focusing on landmark coordinates rather than measurements between landmarks and becoming increasingly reliant on computer based analysis. This section gives a brief overview of morphometric methods used to study form and how it

covaries with other interesting variables such as measures of function. It then reviews some approaches to the study and quantitative description of skeletal function. This discussion introduces methods applied later in this dissertation.

1.5.1 Morphometrics

Morphometrics, or the quantitative analysis of form (Rohlf, 1990), has typically relied on linear measurements, which are basically measures of size. Even though size and shape are intimately linked in biological processes, in statistical shape analysis form is defined as size *and* shape (Zelditch et al., 2004). This partitioning is relevant when considering, e.g., the effect of size on shape (allometry). Size is a vague term, meaning whatever the researcher declares, e.g., length or weight. Shape is defined as the geometrical information that is invariant to location, orientation and scale (Zelditch et al., 2004). As such, in order to extract information about shape, researchers have used ratios and angles in addition to lengths (Bass, 1995; Slice, 2005) and, in traditional multivariate morphometrics, these are jointly analyzed using multivariate statistical methods, including the computation of distances, ordination in e.g. principal components analysis or canonical analysis, and in studies of covariation using methods such as regression. However traditional multivariate morphometrics usually does not employ data that fully describe geometry and so do not allow visualization of morphology (Rohlf and Marcus, 1993; Adams et al., 2004; Slice, 2005). Further, ratios, and scaled measurements may describe shape but the distances underlying the resulting shape spaces do not scale linearly with linear increments of landmark displacement between specimens and statistical power is poor (Rohlf and Marcus, 1993).

In order to overcome these limitations, morphometrics underwent a revolution in the 1980s and several new techniques were created that can generally be grouped into outline (Fourier analysis), coordinate-free (Euclidian distance matrix analysis; EDMA) and superimposition based (geometric morphometrics) methods (Adams et al., 2004; Slice, 2005). Different superimposition methods were proposed, but with maturing understanding of shape theory and shape spaces geometric morphometrics (GM) it was realized that Procrustes analysis provides a uniquely well behaved shape space, a very good estimate of the mean shape and of the shape variance-covariance matrix. On the other hand Fourier analysis turns out, as expected, to be best applied to the description of cyclical phenomena such as motion or texture rather than shape

(O'Higgins, 1997). EDMA suffers most of the problems of traditional morphometrics, in that it has low statistical power and the underlying shape space is poorly behaved in terms of how distance increases with shape differences. For these reasons GM has become the standard approach for morphometric analysis of landmark data (Adams et al., 2004).

1.5.1.1 Geometric Morphometrics

GM has been defined as the statistical analysis of covariations between shape and other variables (Bookstein, 1997). In order to capture shape GM relies on landmarks, which are equivalent points between specimens that are assumed to have some biological equivalence and relevance. Landmarks have been classified according to their characteristics. Type 1 landmarks are those that are identified by discrete points at which there is juxtaposition of at least three different structures, such as bregma. Type 2 landmarks are those defined by points of minimum or maximum curvature, such as the tip of a canine. Type 3 landmarks are those that are defined relative to other structures, such as "*the point furthest away from the tip of the snout along the dorsoventral axis*" (Zelditch et al., 2004, p.31). Due to their nature, type 1 landmarks are the most reliable and least likely to induce error in landmarking and thus subsequent analysis (O'Higgins, 2000; and see Oxnard and O'Higgins (2009) for a reflection about the nature of landmarks and their appropriate selection).

A GM study has four main stages, clarification of the hypothesis which then guides acquisition of morphology (landmarking), registration (superimposition) and analysis.

The first of these, the development and statement of a hypothesis, is not unique to GM and so is not considered further here. It is a vital step, however since all the following steps are derived from this; what to measure and how, as well as what analyses to carry out (Oxnard and O'Higgins, 2009).

1.5.1.1.1 Landmarking

Landmarking corresponds to the acquisition of the geometry of specimens via a set of 2D or 3D landmark coordinates. The set of landmarks depends on the research

question (hypothesis) and on what the researcher find most appropriate. Thus, sets of landmarks often differ between studies addressing very similar questions.

Landmark coordinates can be acquired on the real specimens using digitizing arms or virtually using 2D images or 3D surfaces from surface scans, CT scans or MRI scans.

1.5.1.1.2 Registration

Once landmarking is complete for all specimens, landmark datasets are superimposed in order to deal with the effects of location, scale and orientation (Zelditch et al., 2004). Thus, sets of landmarks are translated, scaled and rotated according to registration criteria. Several superimposition methods exist and choice of method should be according to the research question because different methods lead to different shape spaces (O'Higgins, 2000). Even though, when variations are small, different superimposition methods give approximately similar results (O'Higgins, 2000). The most commonly used method is Generalized Procrustes Analysis (GPA). GPA results in landmark configurations being represented in Kendall's shape space, which has well behaved and well understood statistical properties (Dryden and Mardia, 1998). First, all specimens are translated so that their centroids (the mean of all coordinates in a configuration) overlie at the origin of the coordinate system. Second, all specimens are scaled to centroid size = 1 (the square root of the sum of squared distances of all landmarks to centroid). Lastly, rotation minimizes the squared distances between equivalent landmarks relative to a mean shape, which is calculated iteratively from all specimens (consensus). The new landmark coordinate configurations are the shape variables that are used in subsequent analyses and which quantify dissimilarity among specimens using Procrustes distances (square root of summed squared differences between shape variables).

Scaling removes centroid size differences and leads to an analysis of shape alone, but size and shape are intimately linked in biological processes. Thus, several approaches have been used in order to consider both size and shape. Procrustes form space, as defined by Mitteroecker et al. (2004), uses the natural logarithm of centroid size to augment Procrustes shape coordinates with information about centroid size. Size and shape space, as used by O'Higgins and Milne (2013), when analyzing deformation

in landmark configuration in mechanical loading simulations, reintroduces scale by multiplying the shape variables by centroid size before further analysis.

1.5.1.1.3 Analysis

Commonly used statistical methods are Principal Component Analysis (PCA), multivariate regression and Partial Least Squares (PLS).

PCA is a data reduction method that can summarize the distribution of data that exists in a high dimensional space using a lower number of independent principal components that represent morphological variance. The extent to which PCA is effective in this depends on the extent to which the original variables covary. This approach is useful in shape analysis of biological specimens because the original shape variables (landmarks after registration) are not biologically nor statistically independent, rather they are genetically, developmentally and functionally linked (Zelditch et al., 2004). By reducing dimensionality to a new set of uncorrelated principal components (PCs), the patterns of variation are easier to interpret, requiring far fewer plots of data and the reduced dimensionality facilitates understanding and exploration of morphological variation in the sample (Zelditch et al., 2004). PCs are (by convention) ranked (sorted) according to the percentage of total variance each explains. The morphological features of variation they explain can be visualized by warping the mean along PCs, thus facilitating understanding (Mitteroecker and Gunz, 2009). Nonetheless, it should be cautioned that PCs are statistical entities rather than variables designed *a priori* to express some aspect of morphology. Adding or removing specimens or landmarks can have a dramatic effect on the variance covariance matrix of a sample and so on the orientation of PCs in shape space. In consequence the biological interpretation of the aspects of shape represented by any one PC should be undertaken with caution, because these aspects are somewhat arbitrary, in being sample dependent (Mitteroecker and Gunz, 2009). PC scores may be plotted in two or three dimensions and PCA has been used to assess intra and inter-specific group differences (Delson et al., 2001; Bastir et al., 2007; Harvati et al., 2010; Baab et al., 2013) and ontogenetic trajectories (Collard and O'Higgins, 2001; Cobb and O'Higgins, 2004, 2007; Bastir et al., 2008; Freidline et al., 2012).

Like univariate regression, multivariate regression predicts the dependent variable from two or more independent ones. Thus, there is an assumption that the

independent variables impact on the dependent variable (Sokal and Rohlf, 1995; Monteiro, 1999) and the variables are therefore treated asymmetrically. Multivariate regression has been used to study the impact of size on shape (Mitteroecker et al., 2004; Franklin et al., 2007).

PLS is used to analyze patterns of covariation among previously selected 'blocks' (Rohlf and Corti, 2000) of data (e.g. face vs neurocranium). Even though it examines the association between two blocks it treats them symmetrically, thus not assuming a dependent and an independent set of variables as in regression analysis (Zelditch et al., 2004). It assumes that there is an underlying (latent) cause impacting on both blocks rather one determining the other (Zelditch et al., 2004). PLS has, therefore, been applied to studies of integration and modularity (Bastir and Rosas, 2005; Mitteroecker and Bookstein, 2008; Neaux et al., 2015), to determine the relevance of biomechanical (Noback and Harvati, 2015b, 2015a) and ecological (Monteiro et al., 2003; Noback et al., 2011) factors on form.

1.5.1.1.3.1 Visualising differences in size and shape

A highly effective way of visualizing the differences in size and shape between two configurations of landmarks (a reference and a target) is to use a transformation grid (Thompson 1917/8). A regular grid is superimposed over the reference form and it is then scaled, translated, rotated and stretched such that landmarks on the target come to lie in equivalent positions in the target grid. The most commonly used approach to drawing such grids is based on the Thin Plate Spline (Bookstein, 1989).

The transformation grids of Thompson (1942) allow assessment of how one configuration of landmarks differs relative to another (Zelditch et al., 2004). The TPS, used to draw these grids, is a mathematical interpolation that is driven by the displacements of the actual landmarks and is thus a mathematical abstraction (Zelditch et al., 2004). In consequence, while the grid describes exactly the shape differences at landmarks the differences in the spaces between landmarks are simply interpolated using a mathematical rather than a biological model (such as a simulation of cell division or bone remodelling). Notwithstanding, TPS facilitates understanding of shape changes because it provides a graphical display of those changes in an intuitively appealing way that allows registration and scaling differences to be easily ignored (Zelditch et al., 2004).

1.5.2 Quantifying masticatory system mechanical function

Studies of hominin cranial mechanical function have focused on assessments of the ability to generate bite force (Demes and Creel, 1988; Antón, 1990; O'Connor et al., 2005; Eng et al., 2013) and to resist biting (Rak, 1983; Rak, 1986; Trinkaus, 1987b; Wroe et al., 2007; Strait et al., 2009; Strait et al., 2010; Wroe et al., 2010).

The prediction of what bite force can be produced in skeletal/fossil remains has relied on the use of bony proxies to measure muscle size and infer muscle force due to the relationship between muscle size, intrinsic muscle fibre strength and muscle force (Josephson, 1975; Weijs, 1980; Gans and de Vree, 1987). Although this provides an estimate of the maximum force that can be produced by muscles it does not predict bite force because muscle force is converted into bite force through the masticatory lever arm system. Thus, researchers have tried to predict maximal bite force by estimating muscle size and measuring the mechanical advantages of the main jaw-elevator muscles (Demes and Creel, 1988; Antón, 1990; O'Connor et al., 2005; Eng et al., 2013). More recently bite force has increasingly been predicted using FEA (Wroe et al., 2010). This estimate is, of course, dependent on the input of variables, such as muscle forces, force vector directions and cranial geometry (see 1.5.2.1, Finite Element Analysis for a description of the modelling process). The resulting predicted bite force takes account of all these variables and has the potential to provide an accurate estimation.

Analysis of the ability of the craniofacial skeleton to resist biting has until recently relied on either engineering analysis of geometrically simplified crania (Rak, 1983; Rak, 1986; Demes, 1987; Trinkaus, 1987b) or direct strain measurement using strain gauges in primates (Hylander et al., 1991b; Ross and Hylander, 1996; Ravosa et al., 2000b; Ross, 2001) including hominins (Ravosa et al., 2000c). Although these approaches are informative and provide insights into how crania resist biting, they do not allow a direct assessment. Thus researchers started using FEA to predict stresses and strains experienced by crania during biting (Strait et al., 2007; Strait et al., 2009; Strait et al., 2010; Wroe et al., 2010; Benazzi et al., 2015; Smith et al., 2015b; Ledogar et al., 2016). A review of FEA and the modelling process is provided below in 1.5.2.1, Finite Element Analysis and sub-sections.

1.5.2.1 Finite Element Analysis

Finite element analysis is a numerical tool for solving engineering or mathematical physics problems (Logan, 2007). It developed in engineering but recently it has been applied to hominin biomechanics to analyze skeletal elements from a mechanical perspective and assess how they resist loading (Strait et al., 2007; Strait et al., 2009; Strait et al., 2010; Wroe et al., 2010; Benazzi et al., 2015; Smith et al., 2015b; Ledogar et al., 2016).

FEA is commonly divided in three main stages. Pre-processing deals with the discretization of the structure under investigation and allocation of boundary conditions. The solution phase consists of the mathematical solution of the applied boundary conditions and resulting stresses and strains experienced by the structure. Post-processing consists of interpretation and analysis of results. A validation phase should also be included that ensures that the solution approximates the real results (Richmond et al., 2005; Kupczik, 2008). This section presents an overview of this process.

1.5.2.1.1 Pre-processing

1.5.2.1.1.1 Model creation

Three dimensional FE models based on CT scans have been recognized as most reliable because bone is well imaged and internal architecture is captured (Marinescu et al., 2005). Nonetheless models may be also based on surface scans, MRI scans or computer-aided design (Richmond et al., 2005). CT based FE models are built through a segmentation process that uses differences in bone density, and thus grey levels and Hounsfield Units, to extract (label) the relevant structures from the scanned volume (Weber and Bookstein, 2011). This segmentation process may use global or regional thresholds, which can be calculated using a variety of approaches (Spoor et al., 1993; Coleman and Colbert, 2007). Use of global thresholds inevitably excludes bones that present low density. Thus, regional thresholds can be calculated for and applied to different anatomical areas that present significant density differences. Lastly, the manual approach consists of manually labelling the voxels one wishes to segment. This subjective approach is not completely reproducible. Notwithstanding, it is a necessary complementary approach in cases where automated global and regional approaches do not entirely segment the relevant structures. Moreover manual segmentation is often

also necessary when working with fossils that have sedimentary matrix that presents similar density to bone and so is not easily differentiated by a single threshold. Once segmentation is complete the mesh that constitutes the FE model is created. The mesh is the full set of elements into which the real structure is divided, or discretized (Richmond et al., 2005). The elements are inter-connected by nodes and may present different forms. Voxel-based models present cubic elements and can be created *via* the rapid direct conversion of the segmented volume (of CT voxels, which may themselves be cubic) into a mesh (Fagan et al., 2007). Mesh density is fundamental in FEA because the greater the number of elements in the mesh the greater the potential precision. Low mesh density was an issue in the past, but now advances in computing power allow the solution of meshes that are sufficiently dense (with hundreds of thousands to millions of elements) to yield reliable results (Richmond et al., 2005).

1.5.2.1.1.2 Material Properties

Once the mesh is created, elements are allocated material properties, which impact on the deformation they will experience (Marinescu et al., 2005; Strait et al., 2005). Bone mechanical properties that are modelled include Young's modulus of elasticity, the shear modulus and Poisson's ratio (see section 1.2.2 Bone mechanical properties for a review of these properties) and are commonly derived from mechanical or ultrasound testing (for a review see Currey, 2006).

Allocation of mechanical properties is a non-trivial process because bones in general, and crania in particular, are mechanically heterogeneous and therefore present significant regional variance in their mechanical properties (Dechow et al., 1993; Peterson and Dechow, 2003b). Thus, some researchers have modelled crania using site-specific material properties in order to reproduce that complexity (Strait et al., 2005; Strait et al., 2007). Because every element is allocated properties it is theoretically possible to represent the full material complexity of a mechanically heterogeneous structure. However, this would require knowledge of those properties in the real specimen at the same scale, which is not presently possible. Thus, allocations of material properties are inevitable simplifications of the complexity of the real specimens.

1.5.2.1.1.3 Boundary conditions

Boundary conditions represent the constraints and loads applied to the FE model (Rayfield, 2007). The constraints, also referred to as kinematic or essential boundary conditions, anchor the model in space and prevent its rigid movement when loaded (Richmond et al., 2005). The loads, also known as natural or nonessential boundary conditions, represent forces applied to the model (Richmond et al., 2005). Both loads and constraints should mimic the real boundary conditions the structure under investigation undergoes during real mechanical loading. As such, when simulating cranial masticatory function researchers usually constrain the models at the glenoid fossae and the tooth, or teeth, at which the bite is being simulated (Strait et al., 2007; Kupczik et al., 2009; Strait et al., 2009; Strait et al., 2010; Fitton et al., 2012; Fitton et al., 2015). Loads are usually simulated by modelling the main jaw-elevator muscles, i.e. temporalis, masseter and medial pterygoid (Strait et al., 2007; Kupczik et al., 2009; Strait et al., 2009; Strait et al., 2010; Fitton et al., 2012; Fitton et al., 2015), and special attention is required in the estimation of direction and magnitude of the muscle force vectors (Richmond et al., 2005). In skeletal remains, vector direction may be estimated according to bony proxies that indicate the origin and insertion, and thus line of action, of the modelled muscles (O'Connor et al., 2005). Alternatively, in cadavers it can be based on direct evidence of muscle origin and insertion (Richmond et al., 2005). Force magnitude estimation has been based on the association between physiological cross sectional areas (PCSA), intrinsic muscle strength and total muscle force (O'Connor et al., 2005). PCSAs have been obtained in dissections (van Eijden et al., 1997; Antón, 1999), CT (Weijs and Hillen, 1986; Cox and Jeffery, 2011; Toro-Ibacache et al., 2016b) and MRI scanning (Hannam and Wood, 1989). Data on muscle cross sectional areas can be used to infer maximum contractile force. EMG data reflect the degree and timing of muscle activations and can be applied to cross sectional data to estimate actual force production (Ross, 2005). When dealing with skeletal/fossil remains, force magnitudes may be based on estimates of muscle size, and thus muscle forces, using bony proxies (Antón, 1990; O'Connor et al., 2005). However this approach is limited due to low correlations between estimated cross sectional areas and physiological cross sectional areas (Toro-Ibacache et al., 2015b).

When boundary conditions approximate the real loading environment, the resulting predictions of relative cranial stresses and strains have been shown by validation studies (Bright and Rayfield, 2011; Toro-Ibacache et al., 2016a), to be

reasonable approximations to the relative stresses and strains experienced during biting in experimental simulations using real crania. Ideally such validations should be conducted with every FEA study.

1.5.2.1.2 Solution and post-processing

The solution phase corresponds to the mathematical calculation of node displacements due to applied loading and calculation of resulting stresses, strains and deformations (Richmond et al., 2005). High fidelity models require considerable computing power and are solved using high performance workstations with tens of processors or high performance clusters with hundreds of processors (Rayfield, 2007).

Once solution is achieved post-processing is undertaken according to the questions to be answered. Most studies in hominin cranial biomechanics are interested in the ability of the craniofacial skeleton to resist biting and examine the stresses and strains that the models undergo during simulated masticatory system loading (Strait et al., 2007; Kupczik et al., 2009; Strait et al., 2009; Strait et al., 2010; Fitton et al., 2012; Fitton et al., 2015). Thus, strain contour plots are generated to allow a visual and qualitative assessment of differences in performance and stress/strain magnitudes are extracted at specific sites to allow quantification of those differences (Strait et al., 2007; Kupczik et al., 2009; Strait et al., 2009; Strait et al., 2010; Fitton et al., 2012; Fitton et al., 2015).

1.5.2.1.3 Validation and sensitivity analysis

FEA predicts, with error, the stresses and strains experienced by a structure under loading. The solution is only useful if it is accurate enough to answer the question at hand (Richmond et al., 2005). Thus, it has been recommended that FEA studies should include a validation process that ensures results adequately approximate reality (Richmond et al., 2005; Ross, 2005). Most validation studies typically compare peak strains between in-vivo and/or ex-vivo data with the FEA results. Measurement of strains in the real structures has mainly relied on strain gauges (Daegling and Hylander, 2000; Vollmer et al., 2000; Richmond et al., 2005; Strait et al., 2005; Ichim et al., 2007a; Kupczik et al., 2007; Bright and Rayfield, 2011; Szwedowski et al., 2011), but recently digital speckle pattern interferometry (DSPI) has been used to measure strains

in ex-vivo skeletal structures (Groning et al., 2009; Bright and Groning, 2011; Groning et al., 2012a; Toro-Ibacache et al., 2015a) and overcome limitations inherent to strain gauge based validation studies (Richmond et al., 2005; Yang et al., 2007; Groning et al., 2009; Bright and Rayfield, 2011; Evans et al., 2012; Groning et al., 2012a).

Because boundary conditions impact decisively on the accuracy of FEA predictions, several studies have been undertaken in order to assess the sensitivity of the model to changes in those conditions (Sellers and Crompton, 2004; Ross, 2005; Ross et al., 2005; Strait et al., 2005; Kupczik et al., 2007; Cox et al., 2011; Reed et al., 2011; Fitton et al., 2012; Groning et al., 2012b; Fitton et al., 2015). These sensitivity studies have focused mainly on how variations in material properties (Strait et al., 2005; Kupczik et al., 2007; Cox et al., 2011; Reed et al., 2011; Groning et al., 2012b), constraints (Cox et al., 2011) and muscles forces, muscle vector directions and muscle activation patterns (Sellers and Crompton, 2004; Ross et al., 2005; Cox et al., 2011; Fitton et al., 2012; Groning et al., 2012b) impact on model accuracy and precision.

Most validation studies have reported a degree of success when considering relative strains (Bright and Rayfield, 2011; Ross et al., 2011; Toro-Ibacache et al., 2016a). Conversely, precise prediction of absolute strains is commonly not achieved. Despite this limitation FE models are still useful to answer broad questions that do not require accurate prediction of absolute strains.

2 Validation study of a voxel-based finite element model of a cadaveric human cranium approximating a molar bite

2.1 Introduction

The legitimacy of Finite Element Analysis (FEA) is grounded on the premise that FE Models (FEM) reflect the mechanical behaviour of the real structures they replicate, that they produce valid results. To assess validity, results from the FE model should match those obtained from the real specimen when the same loading regimen is applied (Richmond et al., 2005; Rayfield, 2007; Kupczik, 2008; Grine et al., 2010b; Bright and Rayfield, 2011). As such, validation studies have typically compared the strain magnitudes and/or vector orientations experienced by real specimens with those predicted by the virtual model (Bright and Rayfield, 2011; Szwedowski et al., 2011). While some studies have measured strains experienced by skeletal elements *in vivo* (Rubin and Lanyon, 1982; Ross, 2001), usually measurements are taken from postmortem material (Richmond et al., 2005; Strait et al., 2005; Kupczik et al., 2007; Groning et al., 2009; Bright and Rayfield, 2011; Szwedowski et al., 2011).

Until recently the most viable option to measure deformations was to affix strain gauges to bone (Daegling and Hylander, 2000; Vollmer et al., 2000; Richmond et al., 2005; Strait et al., 2005; Ichim et al., 2007a; Kupczik et al., 2007; Bright and Rayfield, 2011; Szwedowski et al., 2011). However, these present some limitations (Richmond et al., 2005), which include technical difficulties associated with fixing gauges (Groning et al., 2009) and limits to the number of gauges that can be applied and so the impossibility of dense measurement of strains over regions of interest (Yang et al., 2007; Groning et al., 2009; Bright and Rayfield, 2011; Evans et al., 2012; Groning et al., 2012a). To overcome these limitations Digital Speckle Pattern Interferometry (DSPI) has been applied to measurement of bone surface strains in validation studies (Groning et al., 2009; Bright and Groning, 2011; Groning et al., 2012a; Toro-Ibacache et al., 2016a). This is an optical full-field strain measurement technique that allows strains to be directly measured over a small area (several cm^2), determined by the field of view of the device.

In order to improve accuracy of FE strain prediction and better understand the modelling process, sensitivity analyses are carried out to assess how differences in model building approaches impact predicted strains and forces. Previous studies have examined the effects of variations in: model geometry (Strait et al., 2005), model constraints (Marinescu et al., 2005; Cox et al., 2011), material properties (Marinescu et

al., 2005; Bright and Rayfield, 2011; Szwedowski et al., 2011), muscle loading magnitudes and vector directions (Marinescu et al., 2005; Ross, 2005; Fitton et al., 2012), PDL segmentation (Groning et al., 2011a; McCormack et al., 2014), modelling of cranial sutures (Kupczik et al., 2007; Wang et al., 2008; Wang et al., 2010a; Wang et al., 2010b; Wang et al., 2011) and static vs dynamic loading (Wang et al., 2011).

Most validation studies have reported a degree of success in predicting skeletal behaviour using FEA. This said, models often fail to accurately reproduce absolute strain magnitudes while relative strains between different regions of the model are generally consistent with relative strains from experimental loadings of the real specimen (Strait et al., 2005; Kupczik et al., 2007; Bright and Rayfield, 2011; Toro-Ibacache et al., 2016a). With regard to the cranium, it has been suggested that differences between the performance of *in silico* models and actual skeletal material may be related to regional differences in material properties, to the presence of complex patterns of orthotropy and the difficulty in correctly reproducing variations in cortical bone thickness and cancellous bone architecture, given the constraints of imaging and model building (Ross, 2005; Strait et al., 2005; Bright and Rayfield, 2011; Szwedowski et al., 2011). This suggestion arises from studies that report regional differences in material properties of cortical bone in the human craniofacial skeleton (Peterson and Dechow, 2002; Peterson and Dechow, 2003a; Peterson et al., 2006; Dechow et al., 2010). On the other hand, strain orientation in validations is usually consistent between virtual and physical specimens (Bright and Rayfield, 2011; Toro-Ibacache et al., 2016a). With regard to issues with resolution and so segmentation of cortical and trabecular bone, sensitivity analyses suggest that these mainly affect strain magnitudes (overall model stiffness), but less so strain vector orientations and relative strains (Parr et al., 2012; O'Higgins and Milne, 2013; Fitton et al., 2015; Toro-Ibacache et al., 2016a).

While it would be desirable to have virtual models that exactly reproduce the performance of the real specimens, this can only be known for certain if experimental data for the full surface are available to guide model building. In most cases this is not possible, yet FE models are still useful to predict relative strains within and among models which renders FEA a useful approach with respect to many questions (Strait et al., 2005; Bright and Rayfield, 2011; Milne and O'Higgins, 2012; O'Higgins and Milne, 2013), including the comparative cranial and post-cranial biomechanics of hominoids (Richmond, 2007; Wroe et al., 2007; Wroe et al., 2010), hominins (Strait et al., 2009;

Strait et al., 2010; Wroe et al., 2010) and recent human populations (Püschel, 2013). The answer to the question "is a model valid?" is, therefore, dependent on the future application of the model and the questions to be addressed (Strait et al., 2005; Bright and Rayfield, 2011).

Thus, this study will assess if cranial FE models provide valid predictions of distributions of regions of relatively high and low strains, irrespective of overall strain magnitudes (relative strains) and/or of absolute strain magnitudes as well. To that end, strains predicted by FEA are compared to those experienced by the real cranium, based on which the FE model was created, under controlled experimental conditions. Based on previous studies that found similarities in strain pattern between experimental and FEA results, but discrepancies in overall magnitudes (Strait et al., 2005; Kupczik et al., 2007; Bright and Rayfield, 2011; Toro-Ibacache et al., 2016a), it is predicted that absolute strains will differ between the two and that strain pattern will be similar. Hence, it is hypothesized ($H_0 1$) that there are small or negligible differences in the magnitudes and orientations of strains between the actual cranium under controlled experimental loading conditions and the FE model under simulated loading. Further, it is hypothesised ($H_0 2$) that there are small or negligible differences in the distribution of regions of relatively low and high strains, irrespective of overall magnitude (here referred to as strain pattern) between predicted and experimentally measured strains. It is predicted that $H_0 1$ will be falsified and that $H_0 2$ will not be falsified.

The present validation study follows on from a previous study by Toro-Ibacache et al (2016a) that investigated the validity of predicted strains in a human cranium arising during loading and how modelling decisions impacted on model behaviour. In this study, as in that of Toro-Ibacache et al. (2016a), full field strains are measured over the infra-orbital regions using DSPI technology. Validity of model behaviour is investigated under an approximation to a molar bite whereas Toro-Ibacache et al. (2016a) approximated an incisor bite (see details of loading and constraining below). These validation studies are relevant for fossil FE studies, in which validation is not possible, because they assess if FE modelling decisions provide reliable relative strain magnitudes.

2.2 Materials and Methods

In this study the strains experienced by the infra-orbital region of a real human cranium under mechanical loading were compared to those of an FE model under equivalent virtual mechanical loading. Loading and constraining approximate a molar bite but could not replicate physiological loading (see details of loading and constraining conditions below).

The cranium is that of a 74 year old male from Hull, England, and its use for research was approved under the Human Tissues Act 2004 (available at www.hta.gov.uk) and by the relevant HYMS Ethics committee while it was cared for and handled during all experimental stages in accordance with the act and regulations. The same cadaveric head was previously used by Toro-Ibacache et al. (2016a) for validation of masticatory function in an approximation to an incisor bite. In that study the head was dissected, segmented, modelled as an FE model and mechanically loaded to approximate the simulation of an incisor bite. The cranium was extremely well preserved, with no missing skeletal elements (see Figure 2-1), and with wet bone, therefore being suitable for simulation of masticatory function in a living individual.

2.2.1 In vitro experiment

The cranium was constrained by resting it on the two mastoid processes and the meso-lingual cusp of the first left molar (see: Figure 2-1). A total compressive vertical force of 750N was applied in increments of 75N by a universal material testing machine (Lloyd's EZ50, Ametek-Lloyd Instruments Inc., UK) to the frontal bone, 15mm. anterior to bregma. The mastoids acted as a fulcrum at which the skull rotated upon the downward compressive force on the frontal bone. The tooth acted as a biting point, transferring the load onto a 5 kN load cell (Omega DP25B-S; Omega Engineering Inc., Stamford, CT, USA) previously calibrated and repeatedly checked and recalibrated between experimental runs, by applying known compressive loads with the Lloyd's testing machine described above. The cell was used to measure the reaction force at the tooth during loading and control if it scaled linearly with the compressive force applied by the testing machine.

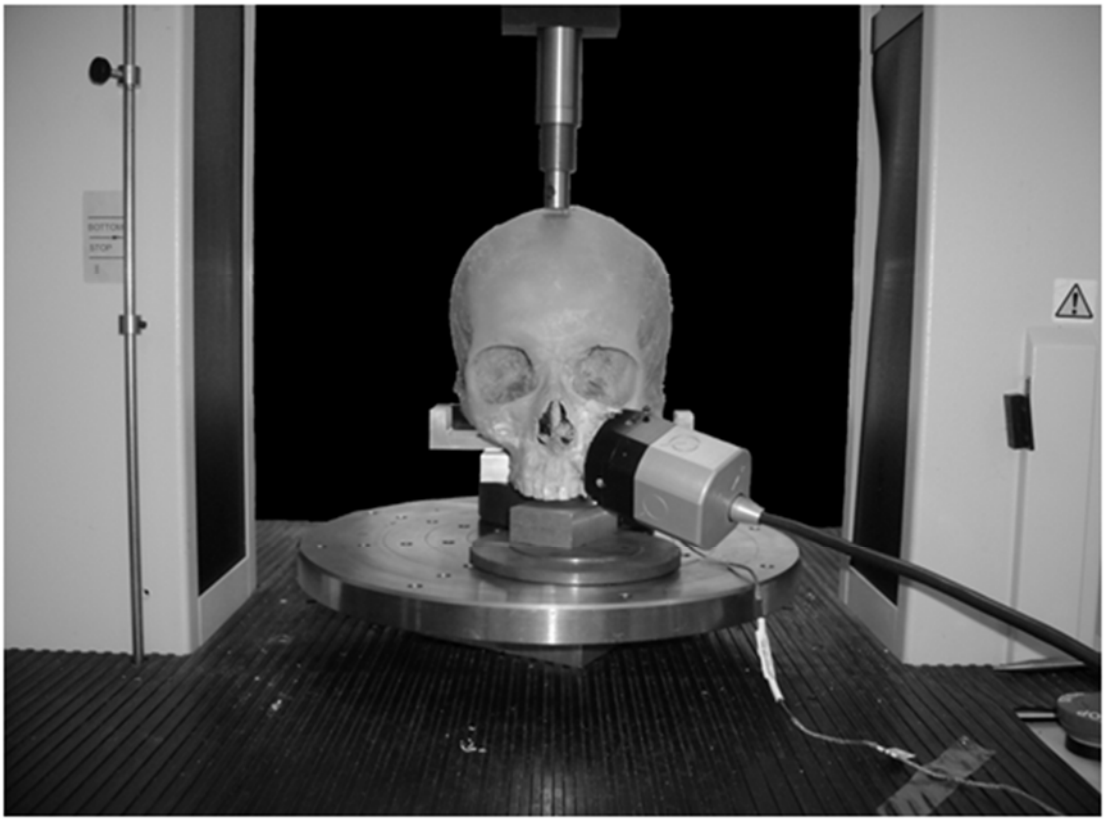

Figure 2-1: Experimental set-up of the skull used in the validation study.

A Q100 DSPI measuring system (DANTEC Dynamics GmbH, Ulm, Germany), which provides a maximum field of view of 25 X 33 mm, was used to measure the strains experienced by the infra-orbital plate during mechanical loading. That region was covered with a thin layer of white spray (DIFFU-THERM developer BAB-BCB; Technische Chemie KG, Herten, Germany) to prevent light reflection. The DSPI sensor was then attached to a tripod that was glued to the infra-orbital plate using an acrylic-based adhesive (X60; HBM Inc., Darmstadt, Germany). The software Istra Q1002.7 (DANTEC Dynamics GmbH, Ulm, Germany) was used to characterize the surface of the area of interest before loading (Figure 2-2a) and create phase maps prior to and during loading (Figure 2-2b) that were used to estimate maximum (ε1) and minimum (ε3) principal strain magnitudes and directions. The software then converts the strains into 2D (Figure 2-2c) strain contour plots. A 3D strain contour plot surface is also created that may be superimposed onto the surface of the virtual model (Figure 2-2d). Two sets of experimental rounds were run. The first set did not provide reliable data and was therefore discarded and appropriate adjustments to the setup were made to increase stability and reliability. The second, and valid, set had a total of 8 experimental

rounds. In each experimental round the cranium was loaded with a total of 750N in 10 increments of 75 N, as previously described. In between rounds the load was removed and the cranium was checked to ensure it did not move and that the load was completely removed. The second set of experimental rounds is the data presented in the results and discussion.

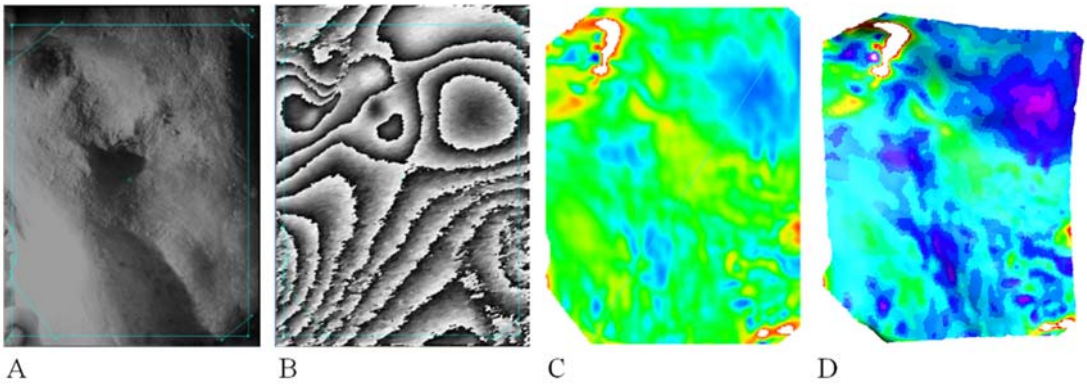

Figure 2-2: Data from DSPI. A – Camera view with border. B – Phase map with border. C – 2D strain contour plot. D – 3D strain contour plot.

Consistency of results between experimental rounds and their validity was assessed visually using 2D strain contour plots that display strain magnitudes and directions. This provides a visual assessment of differences but no quantification. Thus, strain magnitudes were extracted along two lines (Figure 2-3) that cross the field of view of the DSPI device. Strain magnitudes were used to perform a PCA (Principal Component Analysis) and to plot graphs.

2.2.2 FE experiment

The FE model was based on a CT scan of the cadaveric head, performed before dissection and mechanical testing, using a Siemens 16-channel multidetector CT scanner equipped with a STRATON tube (Siemens Somatom Sensation 16; Siemens Healthcare, Erlangen, Germany) at 120 kV and 320 mA with an H60s edge-enhancing kernel, with an original voxel size of 0.48 X 0.48 X 0.7 mm. that was later resampled to 0.349 X 0.349 X 0.349 mm. Three materials were orgininally segmented by Toro Ibacache et al. (2016a), cortical bone, trabecular bone and teeth. Further segmentation was performed by thinning cortical bone in regions that presented cancellous bone. The cortical bone segmented from the internal surface of the cortical shell was subsequently

allocated to cancellous bone, which was segmented as a bulk material. This additional segmentation was performed to make the model less stiff because preliminary FE simulations yielded strains that were lower than the ones presented in this study, thus increasing the difference in strain magnitudes between the experimental data and the FEA results. The model was later exported as a BMP image stack and directly converted into a voxel based finite element mesh using the bespoke software vox2vec. Pre and post-processing used the custom FEA program VoxFE (Fagan et al., 2007; Liu et al., 2012). Isotropic material properties were allocated to all materials. Young's modulus of cortical bone was calculated by nanoindentation (cortical bone 16.3±3.7 GPa – 21.9±2.7 GPa) as previously reported by Toro-Ibacache et al. (2016a) and within the range of previously reported values (Dechow et al., 1993; Schwartz-Dabney and Dechow, 2003). Trabecular bone was allocated an elastic modulus of 56 MPa, according to Misch et al. (1999). Teeth were modeled as single structures with a modulus of 50 GPa, within the published values for enamel (for a review see He et al. (2006), He and Swain (2008)). All materials were allocated a Poisson's ratio of 0.3.

The model was virtually positioned similarly to the real cranium so that the force vectors of the compressive loads applied matched in the real and virtual structures. Constraining of the model replicated the constraints applied to the real cranium. Thus, constraints were applied to both mastoid processes (x, y and z axes) and to the meso-lingual cusp of the first molar (z axis).

Even though these constraints match those applied to the real cranium it was theoretically possible that the cranium might have moved during loading. Hence, variations of these constraints (Table 2-1) were applied to assess the best match between measured and predicted strains. Project 1 matches the applied constraints. Project 2 varies the constraint of the left mastoid to verify there was no slipage of the mastoid constraint at that point. Projects 3 and 4 are similar to project 1 but vary position of the tooth constraint to ensure there was no movement of the cranium or of the force transducer. Project 5 is similar to project 1 but applies an extra constraint (in the horizontal x and y axes, allowing free movement inferiorly in z) to the frontal bone, at the point of compressive force application, to ensure the cranium was not constrained at that point. The 750N force was applied 15 mm anterior to bregma as in the in vitro mechanical testing.

Table 2-1: FEM projects for left molar simulation.

	Right mastoid	Left mastoid	Left first molar Location	Axes	Frontal bone
Project 1	x, y, z	x, y, z	Meso-lingual cusp	z	0
Project 2	x, y, z	z	Meso-lingual cusp	x, y, z	0
Project 3	x, y, z	x, y, z	Meso-buccal cusp	z	0
Project 4	x, y, z	x, y, z	Slope of the meso-lingual cusp	z	0
Project 5	x, y, z	x, y, z	Meso-lingual cusp	z	x, y

Strain magnitudes and directions of the different projects were qualitativelly compared by visual assessment of strain contour plots of ε1 and ε3. Differences in magnitudes were compared quantitatively by plotting graphs of extracted strain magnitudes of ε1 and ε3 along two lines equivalent to the ones traced in the in vitro simulation (see above). The lines were created in Avizo using the 3D strain contour plot surface as reference. The surface was overlaid on the appropriate infra-orbital region and landmarks placed at every millimetre along the lines. The landmarks were then exported and used to extract strain magnitudes.

2.2.3 In vitro vs. FE experiment

Comparison between real and predicted strains is only meaningful if the same loading regimen is applied because differences in force magnitude and/or direction would potentially result in different strain distributions, magnitudes and directions. Thus it was necessary to verify the force vectors had the same orientation in the real and virtual experiments. To that end reaction forces registered by the force transducer placed under the tooth were compared to the reaction forces calculated at the tooth of the FEM. Congruence of results can be interpreted as indicative of equivalent orientations of applied force vectors.

After comparison of tooth reaction forces, the deformations of the crania were compared. In vitro and predicted strain directions and magnitudes results were qualitativelly assessed by visually comparing strain contour plots of maximum and minimum principal strains and strain vector directions. Quantitative assessment of differences between measured and predicted strain magnitudes relied on plotting magnitudes extracted along the two previously described lines (see above and Figure 2-3). The different experimental rounds were arithemeticaly averaged and ± two

standard deviations were computed. This provided a range against which FEA results were compared.

Differences in strain magnitudes between FEA and experimental results are considered meaningful if there are clear visual differences between strain contour plots and if strain magnitudes of the FEA results fall outside of the ± two standard deviations interval. Strain patterns are considered meaningfully different if there are no correspondences of where high and low strains are anatomically experienced between FEA and experimental results. Differences in strain orientations are considered meaningful when visual inspection of the orientation of strain vector shows clear differences between experimentally measured strains and FEA results.

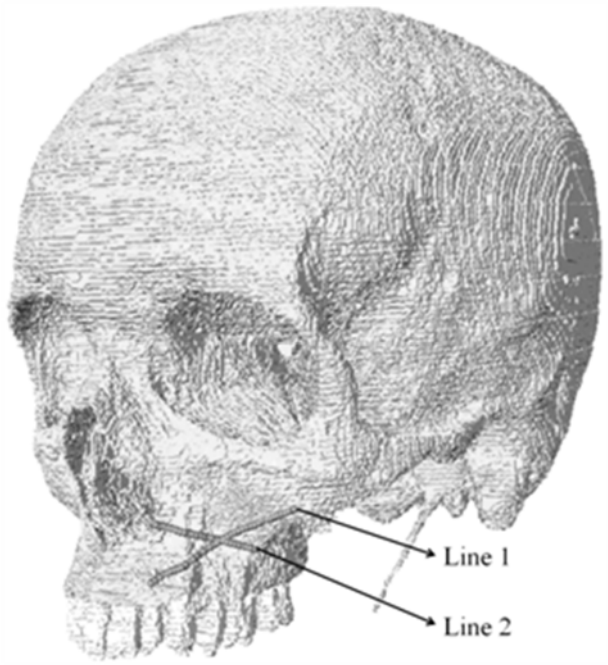

Figure 2-3: Lines used to extract strain magnitudes and compare results between measured and predicted strains.

2.3 Results

As previously described, comparison of deformations uses strain contour plots of ε1 and ε3 and scatter plots of strain magnitudes extracted from two lines located in the infra-orbital region that are equivalent between the DSPI and FEA outputs. In the comparison, directions, magnitudes and patterns are considered. Directions refer to the orientation of the strain vectors. Magnitudes in the strain contour plots are colour coded.

Thus, similar colours indicate similar magnitudes. ‘Strain pattern’ here refers to the spatial distribution of regions where high and low strains are experienced. It is compared using strain contour plots and scatter plots. In the strain contour plots strain pattern is similar if the spatial distribution of regions of relatively high and low strains is equivalent, even if magnitude differs. In the scatter plots strain pattern is similar if the line topography is similar, even if presenting different magnitudes.

2.3.1 In vitro experiment

The first step in assessing the DSPI results is to exclude outlying data from runs where error occurred. This error is not evident during the experiment and might comprise slippage of constraints, ‘locking’ of the skull between load and constraint and other causes. To identify such error requires comparison of repeated runs to exclude outliers. Results show that rounds 7 and 8 are clear outliers and these were thus discarded from further analysis. Strain magnitudes and strain patterns are clearly different from the remaining rounds presenting atypical strain peaks. This is visible on the strain contour plots (Figure 2-4) and scatter plots (Figure 2-5 and 2-6), which present different strain magnitudes, patterns and directions in ε1 and ε3. Moreover, the PCA plot shows that these rounds do not group with any others (Figure 2-7).

Even though the strain contour plots and scatter plots show similar strain patterns in rounds 1 to 6 (Figure 2-4 to 2-6), rounds 3 and 4 present higher strain magnitudes in ε1 and lower in ε3. This difference in strain magnitudes sets these two rounds apart in the PC plot. This inconsistency suggests experimental error with the DSPI and so rounds 3 and 4 were also discarded. From the remaining six rounds, 1, 2, 5 and 6 were considered reliable

The lower plots of figures 2-5 and 2-6 exclude the outlying rounds, presenting plots of rounds 1, 2, 5, 6. These are very consistent in strain magnitudes and pattern.

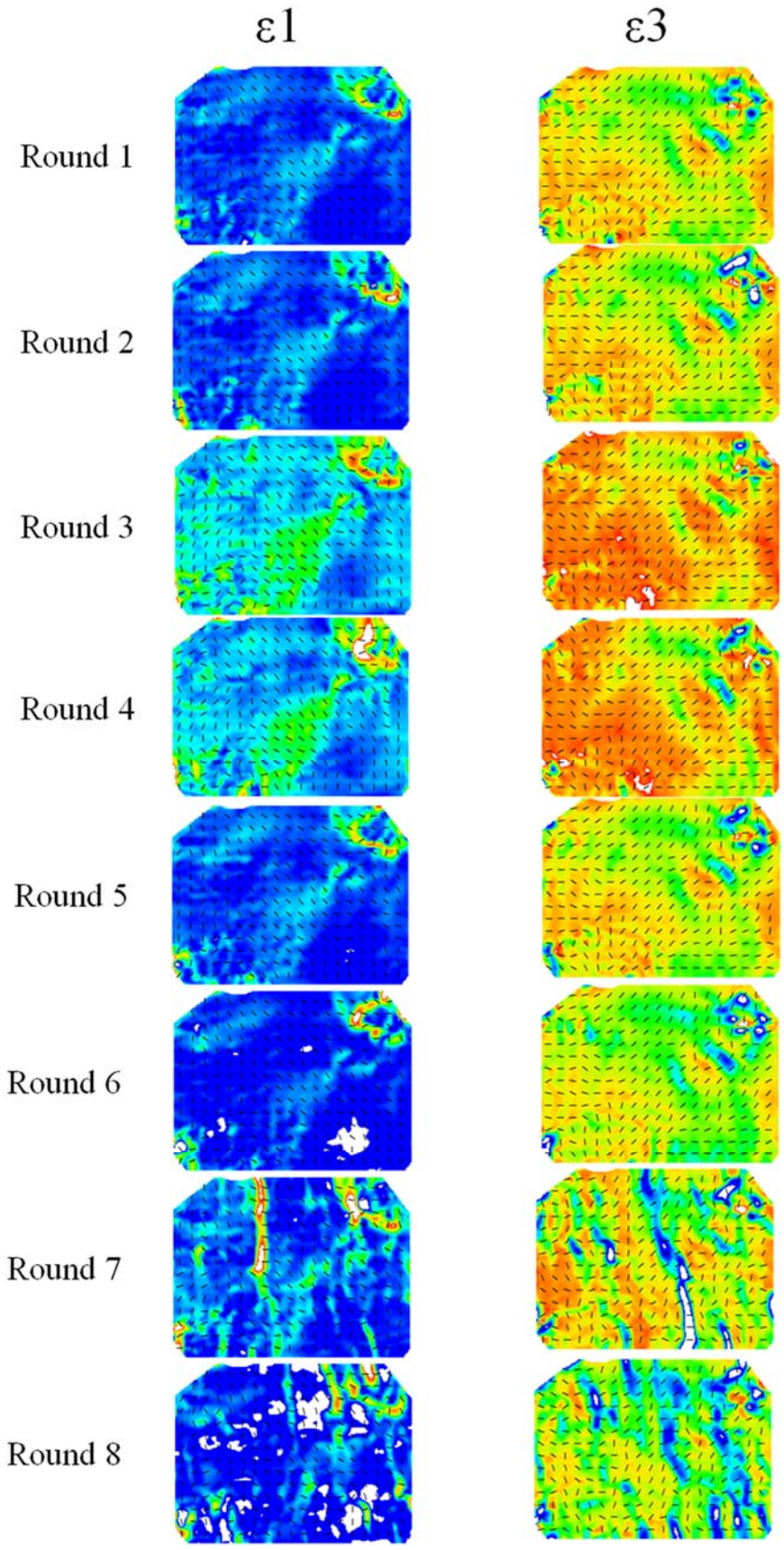

Figure 2-4: 2D strain contour plots of the DSPI output, all experimental rounds.

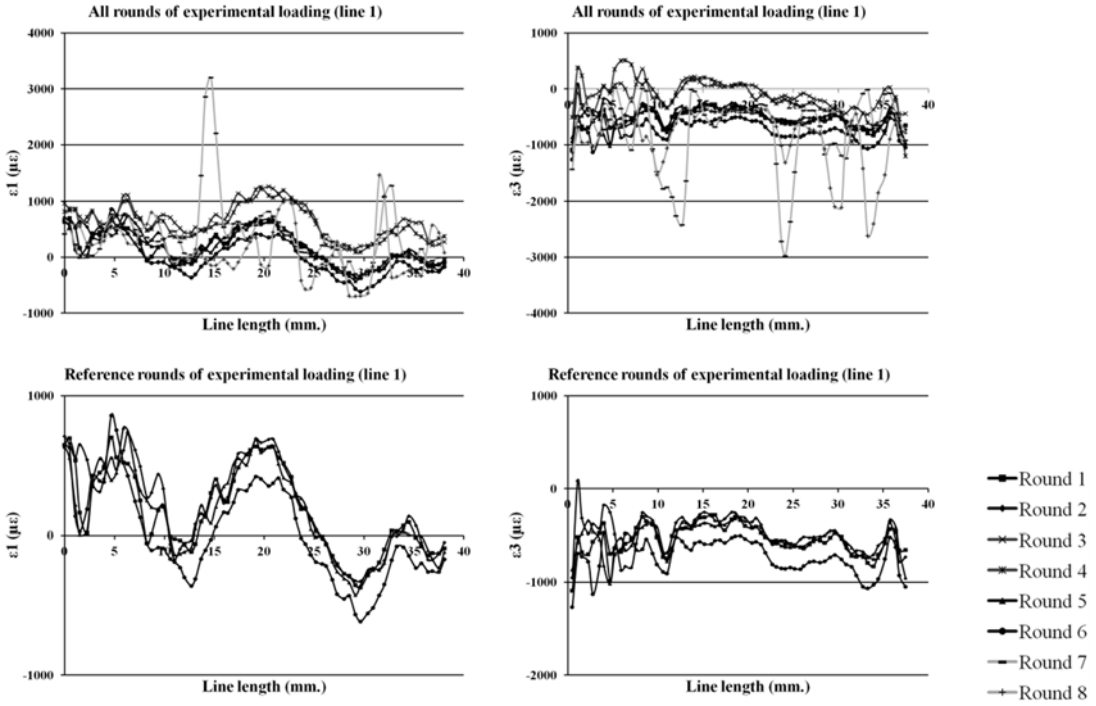

Figure 2-5: DSPI ε1 and ε3 scatter plot of line 1 including all rounds (top) and only reference rounds (1, 2, 5, 6; bottom).

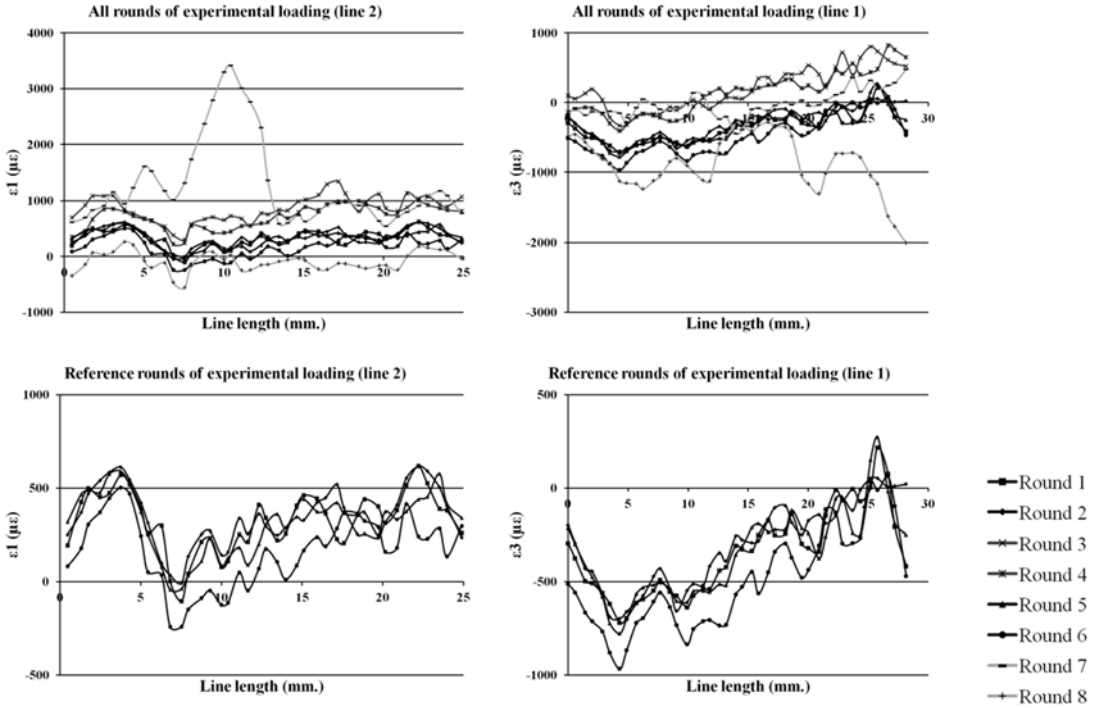

Figure 2-6: DSPI ε1 and ε3 scatter plot of line 2 including all rounds (top) and only reference rounds (1, 2, 5, 6; bottom).

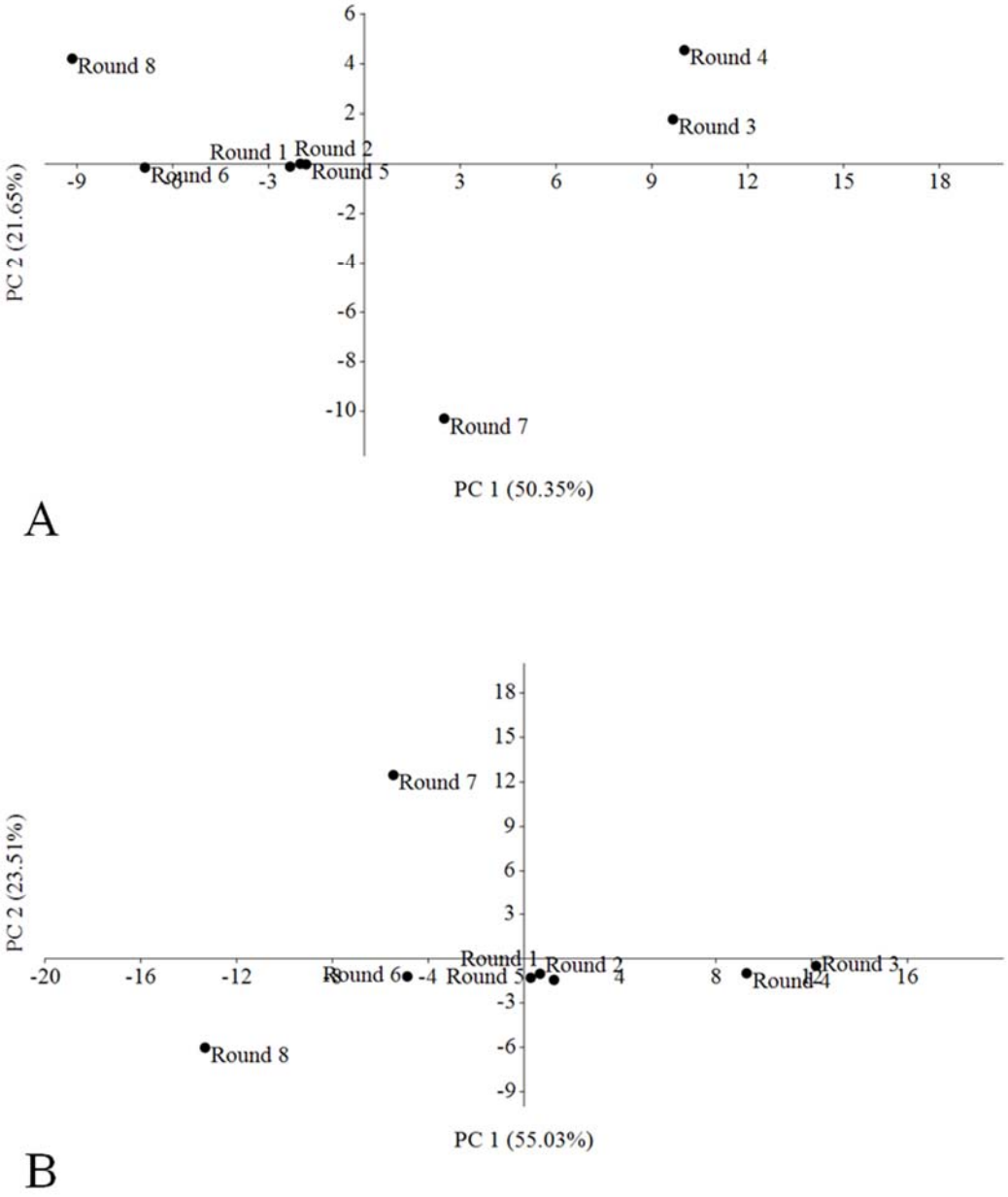

Figure 2-7: PCA of ε1 (A) and ε3 (B) of DSPI rounds 1 – 8.

Despite the differences in deformation between experimental rounds, reaction forces at M1 were very consistent during all increments of all rounds, varying between 411 N and 432 N when total force was applied (Figure 2-8).

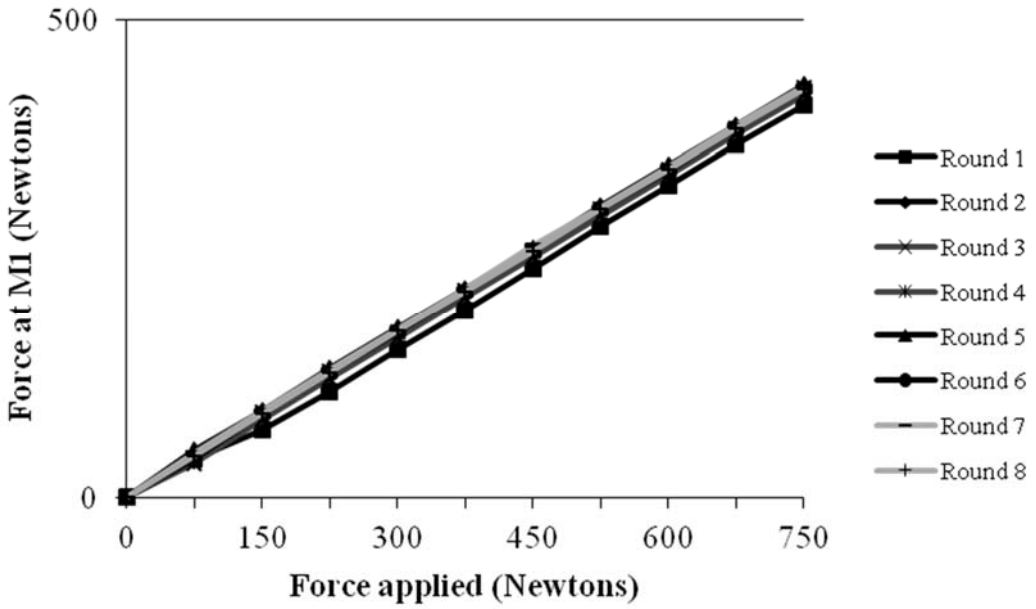

Figure 2-8: Forces measured by the load cell placed underneath the first left molar during the load increments of each experimental round.

2.3.2 Predicted strains

Qualitative assessment of the impact of varying kinematic boundary conditions was based on visual assessment of strain contour plots generated for ε1 and ε3 of all projects. Figure 2-9 shows that varying boundary conditions impact principally on strain magnitudes rather than strain pattern. Thus, all models present similar spatial distribution of high and low strains, even though with different magnitudes. When considering ε1 on the infra-orbital and alveolar region of the working side (left) of the cranium it is clear that strains are relatively high over the whole infra-orbital area, including the inter-radicular areas of the dental arcade and above the apices of teeth. Highest strains are located directly above the bite point, above and around the premolar and above and around the canine, with significant straining of the lateral area of the nasal cavity. The strain contour plot of ε3 presents a pattern generally similar to ε1, with relatively high strains in the infra-orbital region. The higher strains envelop the bite point from above the second molar to the premolar, with a discontinuity just above the first molar. Another high strain area is found above the canine and lateral to the nasal cavity (Figure 2-9). Changes in the constraints did not impact on the orientation of the strain vectors, with no evident differences found between projects (Figure 2-10).

Quantitative assessment of strain differences relied on plotting strain magnitudes experienced along the two lines that were created in the infra-orbital region (Figure 2-3). Figure 2-11 (top) shows that line one presents two strain peaks with strains dropping in-between and a wide diffuse higher strain area. Figure 2-12 and 2-13 show that these high strain areas correspond to the inter-radicular area between the lateral incisor and the left canine; the area next to/above the apex of the premolar; above the apices of the first and second molars, next to the corresponding maxillary sinus and zygomatic root. Variations in the constraints impacted mainly on strain magnitudes and not on strain pattern. Line 2 (Figure 2-11, bottom) is less irregular with two lower strain areas, that anatomically correspond to the margin of the nasal cavity and the area above the premolar and first molars' root. The higher strains are located above the left canine root and, especially, the bite point at the left first molar (Figure 2-11 to 2-13).

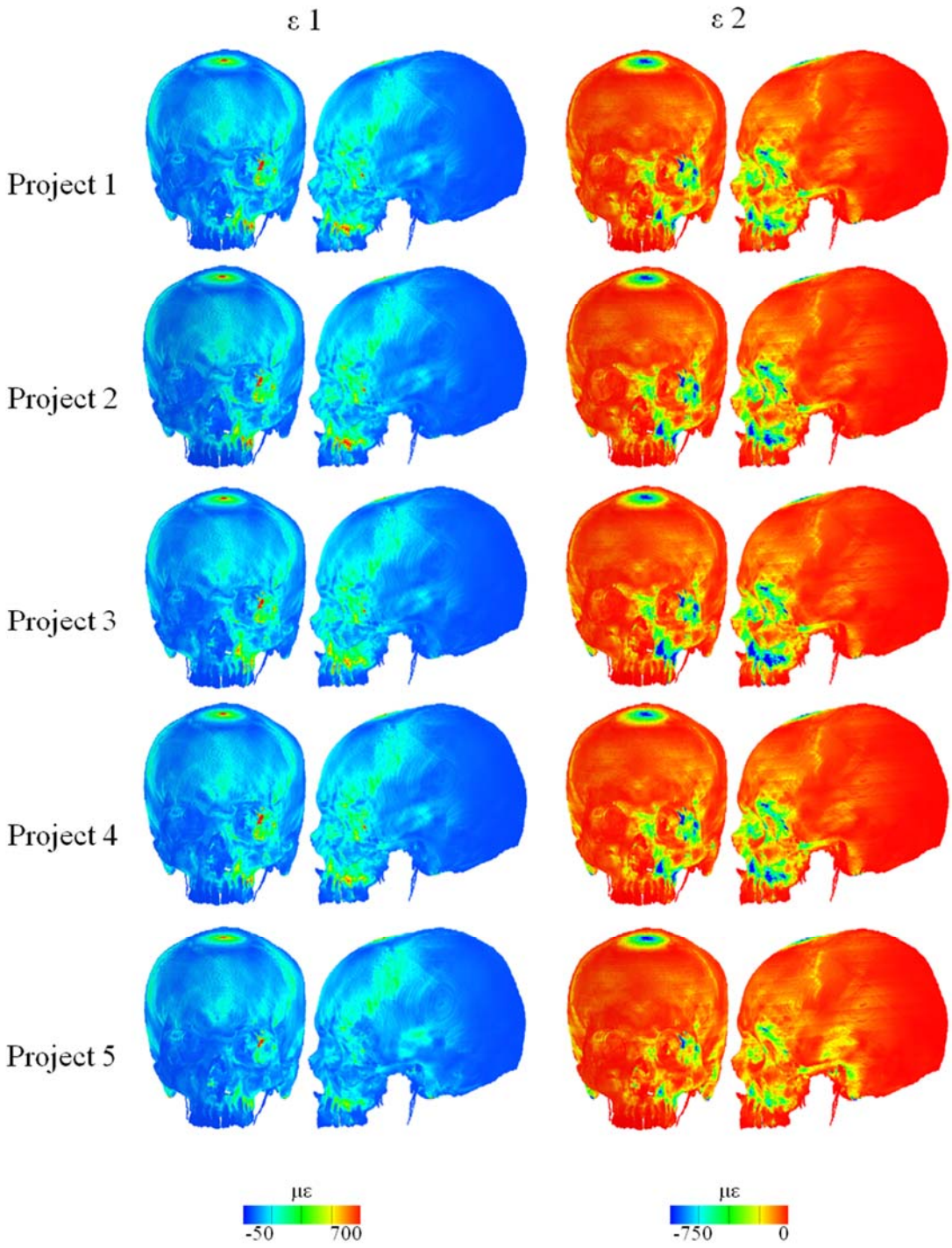

Figure 2-9: Strain contour plots of the FEA projects 1 – 5 with varying boundary conditions.

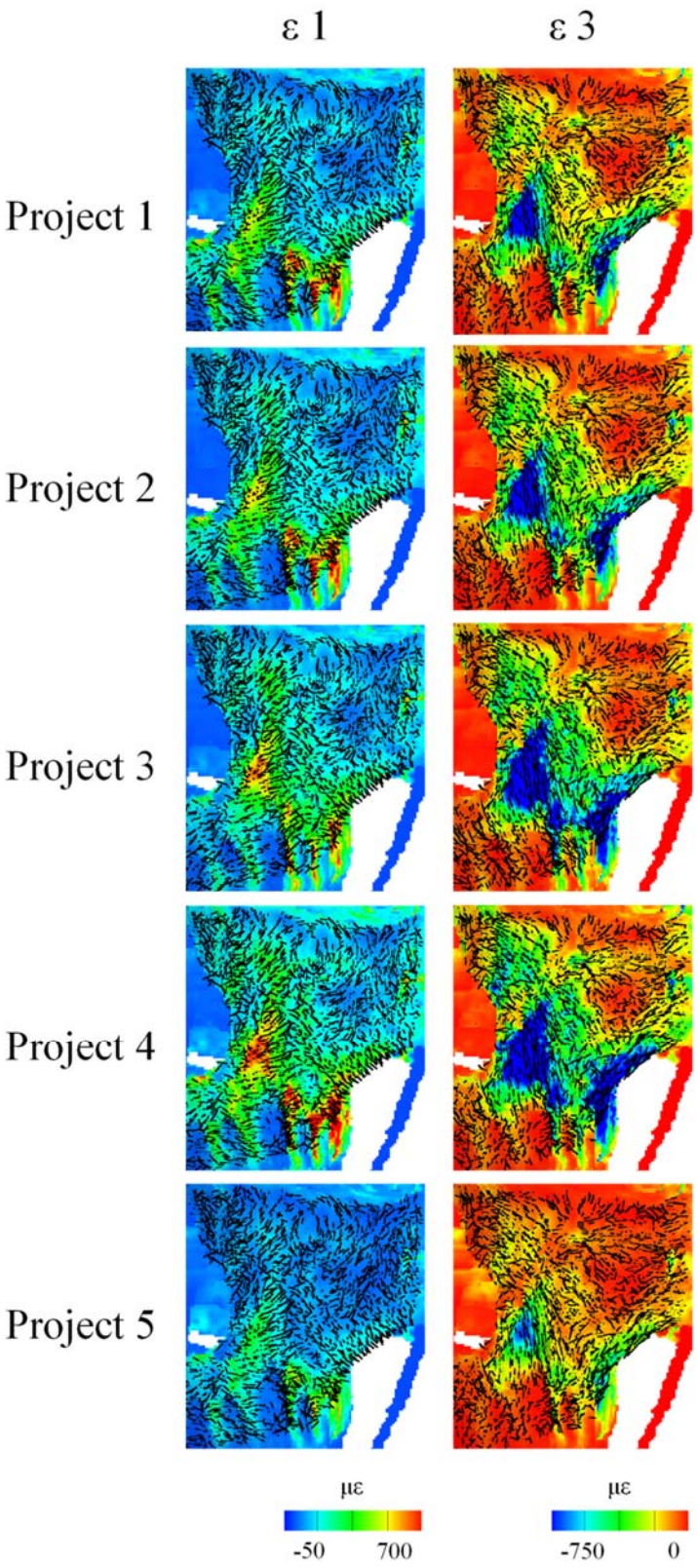

Figure 2-10: Strain contour plots, with strain vector orientations, of infra-orbital and sub-nasal region of FEA projects 1 – 5 with varying boundary conditions.

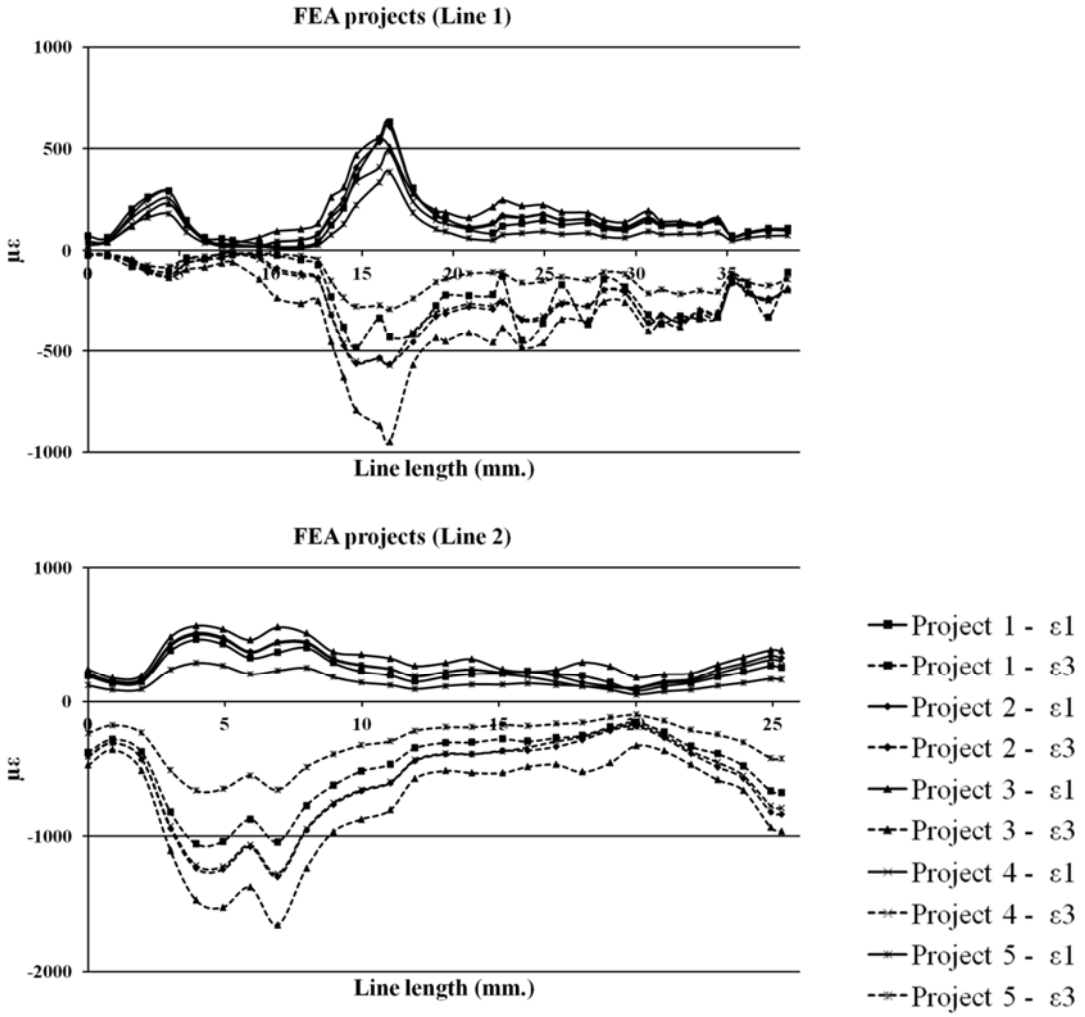

Figure 2-11: Scatter plot of projects 1 - 5 (varying boundary conditions) of the FE model of line 1 (top) and 2 (bottom), using ε1 and ε3.

2.3.3 Real vs Predicted Strains

Reaction forces measured during the consistent experimental rounds at the tooth were averaged to be used as reference for the FEA projects. The mean reaction force is 424 N and that of the reference FEA project (project 1) is 425.61 N. Thus, the difference is negligible (0.38%) and the loading regimens considered equivalent.

Table 2-2: Reaction forces registered at first left molar in the experimental rounds and in each FEA project. Reaction force of experimental rounds was averaged to serve as reference for the FEA projects.

Experimental rounds	Reaction force (N)
Round 1	411
Round 2	425
Round 5	432
Round 6	428
Mean	424

FE projects	Reaction force (N)
Project 1	425,61
Project 2	440,24
Project 3	401,27
Project 4	416,72
Project 5	265,49

When comparing the strain contour plot of the DSPI with the FE model there is a slight mismatch in the anatomical regions where the highest/lowest strains are experienced. This is visible, e.g., on the alveolar bone overlying the root of the left canine. In the 3D contour plot of the DSPI the alveolar bone experiences high strain in the mesial region and low strain in the lateral. In the FEA strain contour plot the alveolar bone over the root of the canine shows low strain and high strains are located in the inter-radicular regions. This mismatch also occurs in the scatter plots of extracted strain magnitudes (Figure 2-12 and 2-13). Despite this difference, comparison between the DSPI output within the corresponding area of the FEA results shows some similarities (Figure 2-12 and 2-13). In ε1, these consist of a region of strain peaks that generaly envelops the left canine and premolar, rising from the inter-radicular area between the lateral incisor/canine and the premolar/first molar and converging medially to the infra-orbital foramen. This high strain drops in the region overlying the roots of the premolar and, especially, of the canine. Above the first molar, at the root of the zygomatic process of the maxilla, there is a low strain area, more distinct in the real specimen, that then increases strain both laterally and medially (Figure 2-12 and 2-13). In ε3 the main difference between the DSPI output and the FE model are the lower relative strains displayed by the real specimen around the first molar and above the canine. In the remaining areas there are similarities between the models, with a relatively highly strained region that extends from the root of the zygomatic process to the inferior lateral border of the nasal aperture. In this region there are also *foci* of low strains, both in the real and virtual specimens, such as in the maxillary zygomatic process, the area next to the infra-orbital foramen and over the premolars root (Figure 2-12 and 2-13).

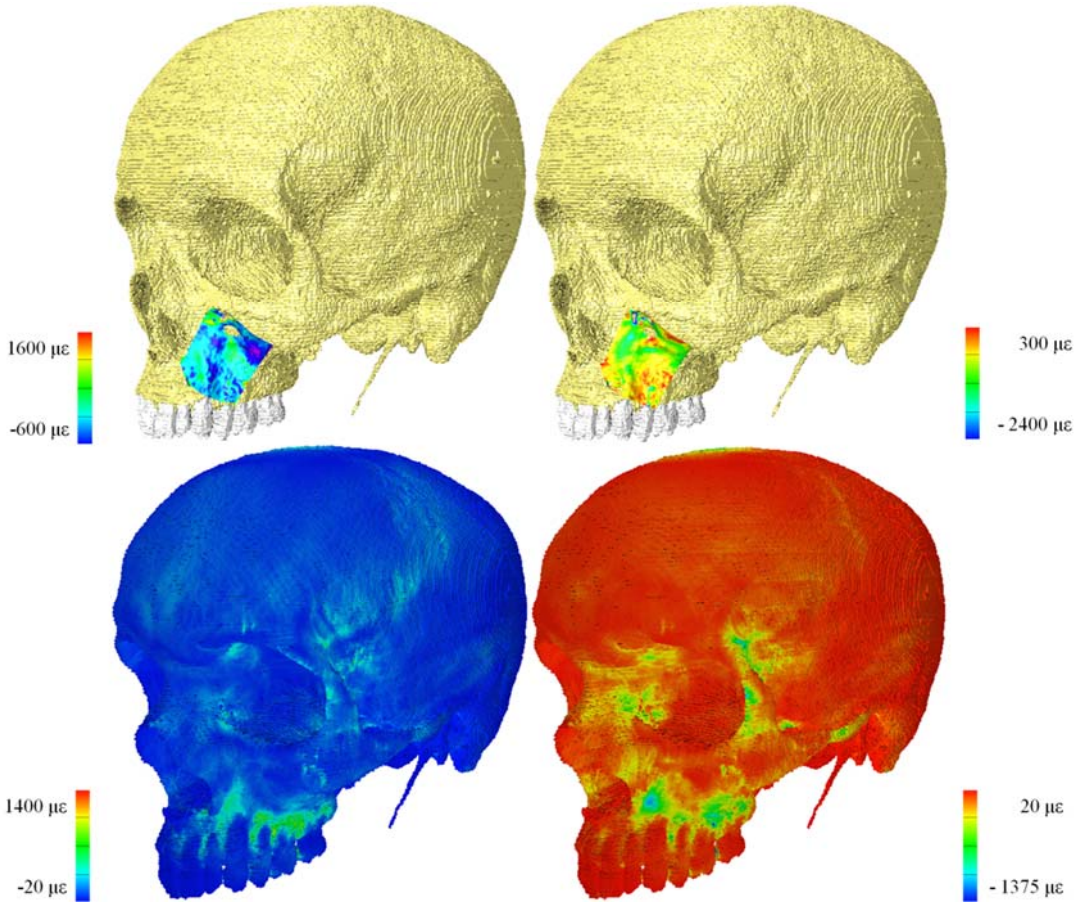

Figure 2-12: DSPI 3D strain contour plot (superimposed on cranium) and FEA strain contour plot (project 1).

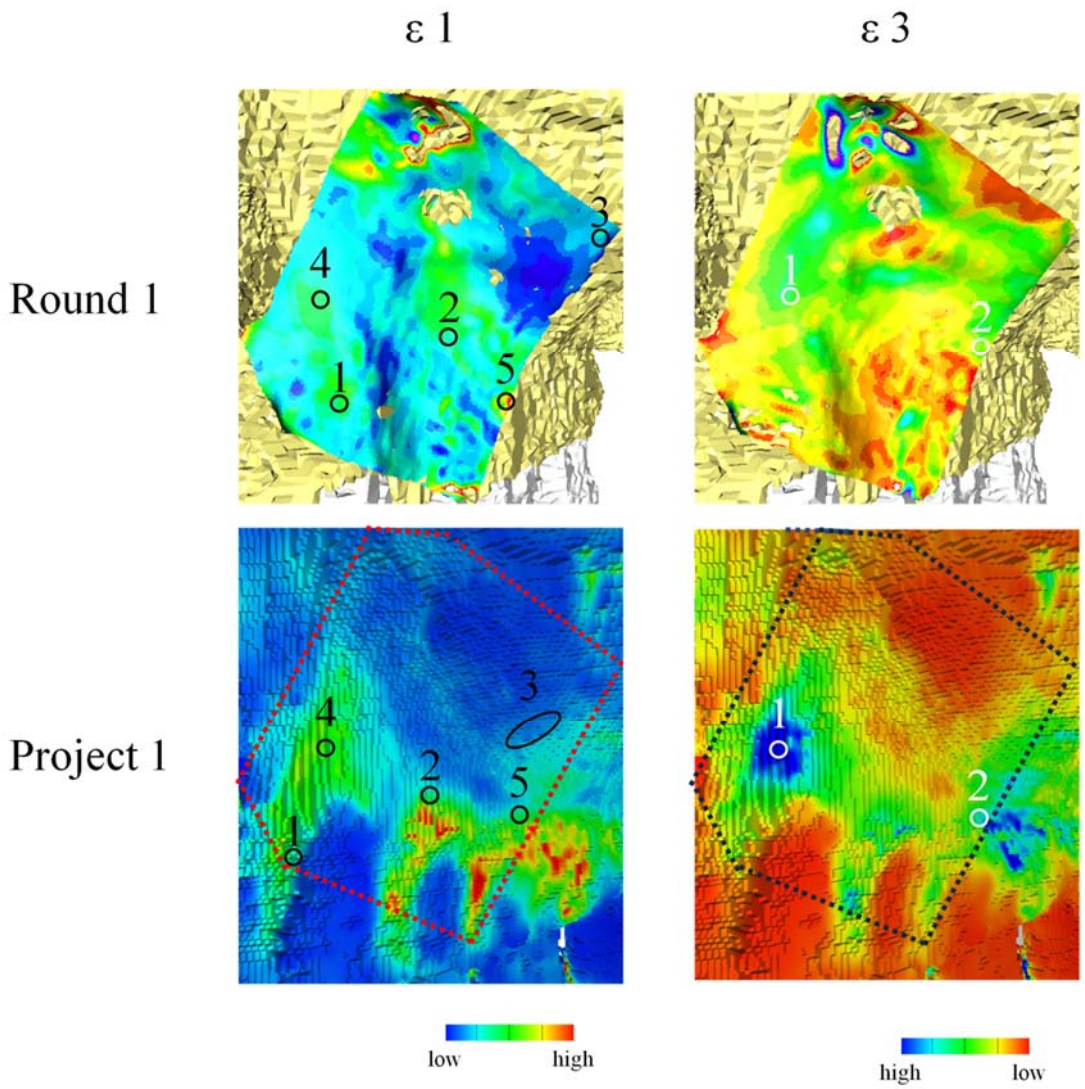

Figure 2-13: DSPI (top) and FEA (bottom) strain contour plots of ε1 (left) and ε3 (right). Numbered points correspond to matching peak strain areas between measured and predicted strains. Precise magnitudes and distributions along plotted lines are shown in Figure 2-15.

Figure 2-14 shows some similarities but not full consistency between DSPI and FEA strain vector directions (note the vectors from FEA are automatically scaled by the software according to magnitude while those from DSPI are not). Similarities in ε1 are generally found in the bottom half of the strain contour plot, with differences being more pronounced in the top half. In ε3 similarities are found in the left half of the plot, where supero-inferior compression (vectors oriented obliquely to the orientation of the contour plot) predominates. Differences in vector directions are found over the root of the canine (bottom centre).

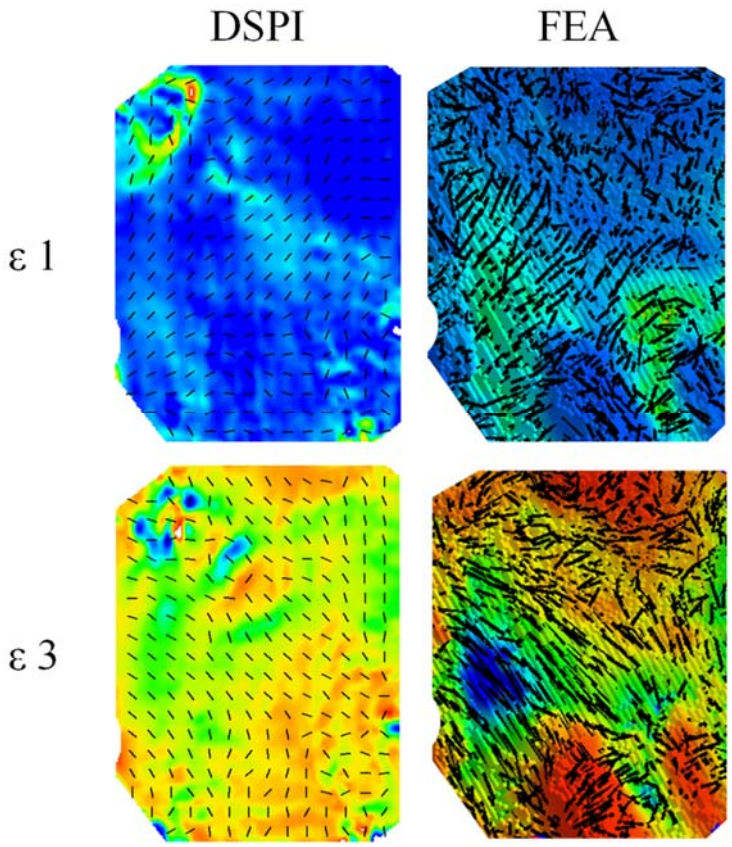

Figure 2-14: DSPI (left column) and FEA (bottom column) strain contour plots of ε1 (top row) and ε3 (bottom row), with strain vector directions.

In order to quantitatively compare real and predicted strain magnitudes these were extracted along lines 1 and 2 (Figure 2-3). In line 1 there are differences in the absolute values of ε1 between the predicted and the real strains. These differences are most significant throughout *ca.* the first third of the line. Despite these absolute differences, the general strain pattern is comparable. Thus, DSPI and FE results present the same strain peaks around the canine (first and second peaks of the line). When considering the second and third peaks both DSPI and FEM outputs almost match in absolute values, with differences consisting in the absence of a significant drop in the predicted strains in between the second and third peaks. In ε3, there are also differences in the absolute values, with predicted strains being lower than real strains. Despite these differences the overall pattern of ε3, between real and predicted strains, is similar, with a generally flat and regular line. The main differences between DSPI and VoxFE outputs are in the peak of predicted strains next to the premolar (± 15 mm), which is

absent in the DSPI output, and the flatness of the first third of the line of the predicted strains (over the canines root), which is more irregular in the real strains (Figure 2-15).

In the scatter plot of ε1 from line 2 there are two main differences between real and predicted strains. The first is the significant drop in the real strains at ± 7-8 mm, that anatomically corresponds to the area above the apex of the canine. In the FE model these low strains are directly over the tooth root, not extending upwards. The second difference is the drop in the predicted strains at about the apex of the premolar (± 20 mm). Despite these two local differences the predicted absolute strains are mostly within the range of the real ones, with a generally similar pattern between the two. In ε3, both DSPI and FE extracted strains present a remakable match. The only difference is found in the high strains experienced by the FE model just next to the bite point (± 23-25 mm, Figure 2-15, labeled as point 2).

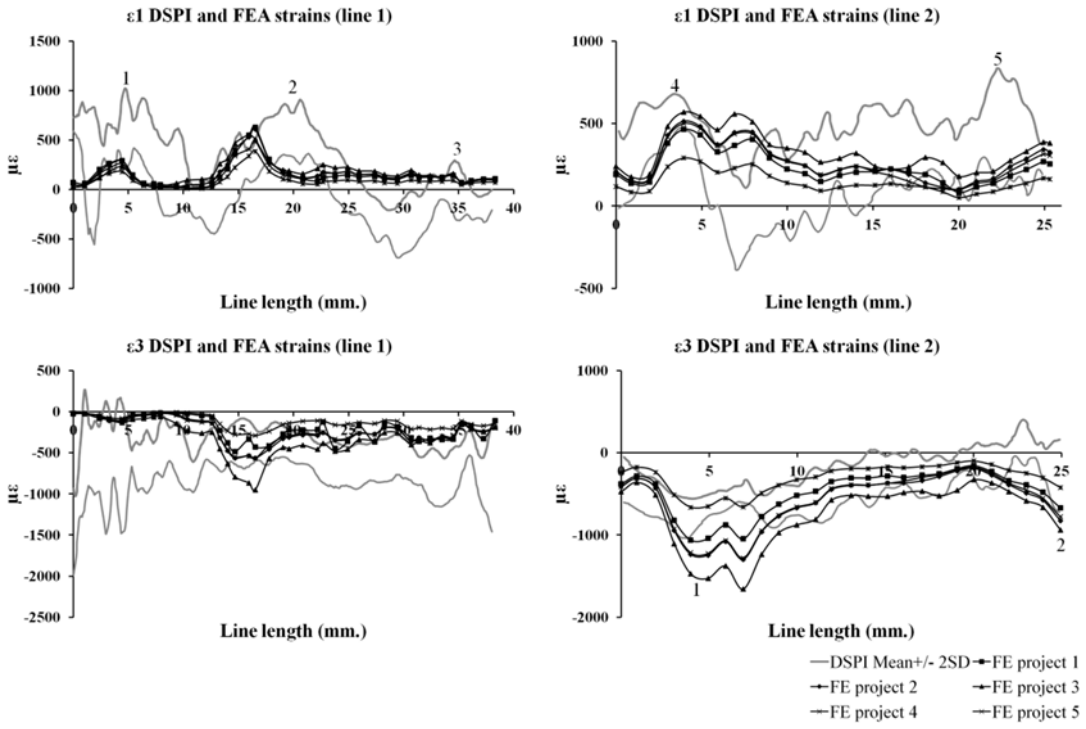

Figure 2-15: DSPI and FEA output scatter plots of line 1 (left) and 2 (right). Top scatter plots depict ε1 and bottom plots ε2. The DSPI output includes the mean of series 1, 2, 5 and 6, and ± 2 standard deviations. Numbers above and below lines represent peak strains that anatomically correspond to the number in Figure 2-13.

2.4 Discussion

This study aimed to assess the validity of an FE model of a cadaveric cranium approximating a molar bite. To this end the real specimen and the FE model were loaded with similar boundary conditions and resulting strains were compared between the two.

The real cranium was subjected to eight rounds of compressive loads and resulting strains were measured using DSPI to be used as reference for comparison with the FE model. Rounds 1, 2, 5 and 6 were consistent and used as the reference (Figure 2-4 to 2-7). The remaining four rounds (3, 4, 7, 8) were considered invalid due to inconsistency in strain magnitudes, patterns and directions (Figure 2-4 to 2-7). Rounds 3 and 4 present a similar pattern but inconsistent magnitudes relative to rounds 1, 2, 5 and 6. This inconsistency may be due to some undetected interference with the DSPI reading. Rounds 7 and 8 present atypical patterns, magnitudes and directions. It is possible that the bone in the region of the maxilla cracked due to successive loading (this cranium was used in a previous validation study by Toro-Ibacache et al. (2016a) and was subjected to over 20 experimental rounds in total), thus leading to an extremely high strain peak in round 7 and several smaller peaks in round 8 that may represent bone failure.

The FE model was loaded similarly to the real cranium. Furthermore, to verify kinematic boundary conditions applied to the FE model were the same as those experienced by the real cranium, constraints were varied to simulate possible movements of the cranium during loading. Changes in the constraints did not impact on strain distributions and directions, but rather on magnitudes, both in ε1 and ε3. This is visible in the strain contour plots (Figure 2-9 and 2-10) and in the graphs plotting strain magnitudes extracted along line 1 and 2 (Figure 2-11).

To compare results it was first important to verify if the direction of applied forces was consistent between real and virtual loads. This is relevant because differences in direction of applied force would result in different loading regimens and hence impact on strains. To that end bite forces were compared between real and virtual experiments. The mean bite force of the real valid rounds (mean of 1, 2, 5, 6 = 424 N) was similar to the bite force of the reference FE project (project 1 = 425.61 N) with a difference of 1.61 N (0.38%; Table 2-2).

When comparing the distribution of strains between the 3D DSPI output and the FE results there is a degree of mismatch between the two (Figure 2-12 and 13). This is evident, e.g., on the bone overlying the root of the canine. In the DSPI 3D plot this region presents high strains in the mesial half and low strains in the lateral half. In the FE strain contour plot there are low strains over the whole bone overlying the root of the canine. This mismatch is also found in the scatter plots of extracted strain magnitudes (Figure 2-14) and may be due to fine topographical differences of the strain contour plots and cranial morphology related to the DSPI image acquisition, generation of the DSPI 3D contour plot and FE model creation process. In particular, it is unclear if it is necessary, and if so, how, to incorporate material representing periodontal ligaments between teeth and their sockets in FE models. This would have a dramatic effect locally on strain magnitudes (Groning et al., 2011a; Wood et al., 2011).

Despite this, the 3D contour plot of the real strains presents similarities with the FEA output. In both, ε1 magnitudes peak in the region of the canine and premolar alveolar bone, rising through the facial skeleton and converging towards the nasomaxillary butress (next to the infra-orbital foramen), with strains dropping over and close to the root of the canine and less so over the premolar root. Similarly, the strains are also lower in the zygomatic root, although clearly lower in the real specimen than in the FE model. The main difference between the two is that the low strain field over/near the canine is larger, extending more superiorly in the real specimen. In ε3 both the real and virtual experiments yielded a high strain area that extends from the border of the nasal aperture to the root of the zygomatic process with “islands” of lower strains located close to the infra-orbital foramen and body of the maxillary zygomatic process. The main difference between the two lies in the higher relative strains experienced by the virtual model, particularly in the apex of the first molar, above the canines’ apex, and the inter-radicular spaces. The direction of strain vectors experienced by the real cranium and the FE model presents similarities but is not fully consistent throughout the whole infra-orbital region (Figure 2-14).

Quantification of strain differences relied on plotting the strain magnitudes extracted from two lines (Figure 2-15). In ε1, line 1 is generally flatter in the FE model than in the DSPI output. Nonetheless it presents the same general pattern with differences being mainly the absence of negative strains over the canine root and at the root of the zygoma. In ε3 the strain magnitudes are lower throughout most of the line, which is generally flatter, especially in the first third over and around the canine root.

In line 2, the absolute predicted strains lie within the interval of the real ones along most of the line, with striking similarities between them in ε3.

Hence, the $H_0$1 (magnitudes and directions of predicted strains do not differ meaningfully from the real ones) is falsified. Magnitudes in line 1 present clear differences, despite similarities in line 2. Directions present similarities but not full congruence between real and FEA results.

$H_0$2 (the pattern of predicted strains does not differ meaningfully from the pattern of real strains) is partially falsified because, despite some differences, the pattern of strain distributions in the experiment and FE simulation is generally similar.

The results presented here are therefore somewhat consistent with those of Toro-Ibacache et al. (2016a), who used the same cranium and a similar experimental setting (although the constrained tooth was the first left incisor and not the first molar) and reported successful prediction of general strain distribution but not of precise absolute magnitudes. Despite that it should be noticed that Toro-Ibacache et al. (2016a) found a better match between real and predicted strains than the present study does. Our results and those of Toro-Ibacache et al. (2016a) are consistent with those of other studies that report successful prediction of general strain patterns but not of precise absolute strain magnitudes.

The present findings and previous work of others therefore suggests that while craniofacial FEA is useful to predict general patterns of strain distribution, at present it lacks the ability to predict fine details of strain distributions and absolute strains (Strait et al., 2005; Kupczik et al., 2007; Bright and Rayfield, 2011; Toro-Ibacache et al., 2016a).

These limitations are related to the resolution of medical CT imaging (which is typically used in FE model building) and the extreme complexity of cranial material properties. Medical CTs are unable to image fine anatomical details due to voxel size. Indeed some bony structures (e.g., trabeculae in cancellous bone and bones such, ethmoidal cells, vomer) are much thinner than individual voxels. This leads to imprecision in the segmentation of details of cranial external form and loss of fine detail of the extremely complex internal anatomy of the cranium. Material properties of cranial bone are heterogeneous, with modulus of elasticity varying between individuals and dependent on the direction of applied force, hence material properties are also anisotropic, within crania and within the same bone. Teeth also present extremely

complex material properties, with clear differences between tissues (i.e., enamel, dentin, cement) and within the same tissue (see Naveh et al., 2012 for a review of the elastic modulus of different dental structures). Despite efforts to reproduce the complexity of cranial material properties (Strait et al., 2005), FE modelling still simplifies the full complexity of the real structures, and so does this validation study. Simplifications in this study include modelling of trabecular bone as a bulk material, allocation of isotropic properties to all materials and teeth modelled as single structures with Young's modulus of enamel. Moreover, absence of the periodontal ligament (PDL) also impacts on model performance and congruence of results.

Modelling of trabecular bone as a bulk material is expected to impact on strains because the cancellous spaces are infilled with material that does not replicate the directional anisotropy of stiffness of cancellous bone. Parr et al. (2012) show that infilling hollow spaces of a varanoid lizard mandible impacts on strain magnitudes, reducing them, but not on pattern. Parr et al. (2013) also reported that modelling trabecular networks, as opposed to modelling cancellous bone as a solid, impacts on the overall stiffness of the skeletal structures and, therefore, on strain magnitudes. Thus modelling of trabecular bone as a bulk material likely partially explains strain magnitude differences between the real and predicted strains.

Bone presents complex patterns of orthotropic material properties that vary within the same bony structure (Peterson and Dechow, 2003b; Peterson et al., 2006) and the use of isotropic material properties has been considered as one of the possible sources of error between *in vitro* and *in silico* experiments (Bright and Rayfield, 2011; Szwedowski et al., 2011). Studies have demonstrated that the use of orthotropic material properties yields more accurate results than isotropic (Marinescu et al., 2005; Strait et al., 2005), however the differences seem to impact on magnitudes and not on pattern of strains experienced (Strait et al., 2005). Hence, allocation of isotropic material properties to the FE model probably partially explain differences in strain magnitudes between real and predicted strains, and less so on strain patterns.

It has been suggested that teeth act as load bearing structures that also increase mandibular rigidity (Daegling et al., 1992; Marinescu et al., 2005), thereby limiting the strain magnitudes an FE mandible model experiences during loading (Marinescu et al., 2005). Segmentation and modelling of the teeth as single structures with high Young's modulus (see Naveh et al., 2012 for a review of the elastic modulus of different dental structures), as opposed to modelling them more realistically as a composite of stiff

enamel and less stiff dentine, might have stiffened the model in the region of the roots, impacting especially on the structures that overlie and surround them, such as the alveolar bone and inter/intra-radicular *septa* (with particular emphasis in the canine).

Another issue that arises in building FE models of the cranium concerns modelling of the PDL. Imaging of the PDL using medical CTs is hampered by its very small dimensions. Indeed the thickness of this ligament (0.15 - 0.38 mm.) is smaller than the typical voxel size resolution (0.50 - 1.00 mm; Weber, 2005). These imaging limitations do not allow modelling of this structure according to its correct dimensions. Furthermore, PDLs have extremely complex material properties that vary throughout the ligament due to, e.g., significant variation in the orientation of fibres (Groning et al., 2011a; Naveh et al., 2012; Hand and Frank, 2014; McCormack et al., 2014). Despite these difficulties the impact of modelling vs. not modelling the PDL as bulk material (ignoring its detailed anatomy) has been debated recently. While it has been consistently demonstrated that incorporating a cap of voxels with low Young's modulus between tooth root and socket to represent the PDL impacts in the nearby alveolar bone increasing the strains (Groning et al., 2011a; Wood et al., 2011), the effect on structures that are more distant is less clear, with some researchers demonstrating it impacts significantly (Groning et al., 2011a) and others demonstrating it does not (Wood et al., 2011). Our results show a discrepancy in strain magnitudes between real and predicted strains in structures near teeth (line 1). Notwithstanding, that discrepancy diminishes with increasing distance from the roots. Hence, our findings seem consistent with the hypothesis that modelling of the PDL has little impact on structures distant from teeth and the errors in strain prediction noted over the tooth roots may well be mitigated in future studies by using high enough resolution to incorporate a representation of the PDL.

Improvement in FEA for investigating craniofacial mechanics is therefore dependent to considerable degree on advances in scanning technology that increase resolution. Thus, higher resolution scans would enable imaging of fine anatomical details, and facilitate allocation of more precise, heterogeneous, material properties (which have been shown to be individual specific, and can be estimated from voxel grey level – Hounsfield number). Even with such advances FEA will still demand many approximations, albeit at finer levels of detail and as such validity will continue to be an important question when considering the results of FEA studies. Despite this, present FEA studies based on medical CTs are useful to address broad questions about

cranial strain distributions but lack detail that allows them to focus on finer questions and predict absolute strains.

This chapter assessed the reliability of an FE model based on a complex segmentation that is possible in well preserved crania. However, fossils are often fragmented and invaded by sedimentary matrix, precluding such complex segmentation and subsequent FE modelling. Thus, the next chapter assesses the impact of simplification of segmentation and material properties.

3 Sensitivity analysis of a voxel-based finite element model of a cadaveric human cranium

3.1 Introduction

Ideally, the geometry and material properties of Finite Element Models (FEM) should replicate reality as closely as possible. CT based models are approximations to the original geometry and presently offer the best route to accurately model geometry (Marinescu et al., 2005), but CT scans have limitations. Even though medical CTs can offer resolutions down to 200 μm, commonly resolution ranges from 0.5 to 1 mm (Brant and Helms, 2012). While this is satisfactory to model gross morphology it does not allow proper segmentation and representation of, e.g., trabecular networks and the periodontal ligament (PDL) because the width of these structures is typically narrower than the dimensions of voxels. Moreover, the material properties of bone are heterogeneous and extremely complex. Bone is anisotropic, ductile and viscoelastic, with these properties varying between individuals, and between and within bones in the same individual (Dechow et al., 1993; Peterson and Dechow, 2003b; Currey, 2006; Peterson et al., 2006). Thus, despite efforts to incorporate as much complexity as possible in models (Strait et al., 2005), they inevitably simplify real structures. In the extreme it would require *a priori* knowledge of all points in a given specimen to model full complexity. This is impossible to achieve with current 3D imaging, even at the resolution of a Synchrotron; simplification is always necessary.

Acknowledging modelling limitations, and associated uncertainty, researchers have been interested in understanding the impact of errors and simplifications in FE modelling. This can be examined via sensitivity analyses in which the impact of uncertainty in input variables is assessed on the output (Saltelli et al., 2008). Such studies consist in varying one (local sensitivity analysis), or several (global sensitivity analysis), input variable(s) and examining how those variations impact the output (results) of the model (Saltelli et al., 2008). In skeletal FEA studies, input parameters of analysis have commonly included anatomical variables that are known to vary notably and impact FEA predictions. Thus, sensitivity studies in cranial FEA have focused muscle force magnitudes, directions and activation patterns (Sellers and Crompton, 2004; Ross, 2005; Cox et al., 2011; Fitton et al., 2012; Groning et al., 2012b), variations in bone material properties (Strait et al., 2005; Kupczik et al., 2007; Cox et al., 2011; Reed et al., 2011; Groning et al., 2012b), modelling of cranial sutures

(Kupczik et al., 2007; Wang et al., 2010b; Reed et al., 2011), modelling the PDL (Wood et al., 2011; Groning et al., 2012b; Holland, 2013; McCormack et al., 2014), impact of variations in modelling of trabecular bone (Parr et al., 2013) and model constraints (Cox et al., 2011).

Such studies are of particular relevance for FEA of fossils, in which validation is not possible. FEA applied to fossils has become popular (Rayfield, 2007; Strait et al., 2009; Strait et al., 2010; Wroe et al., 2010; Cox et al., 2015; Smith et al., 2015b; Ledogar et al., 2016) and models are often based on medical CT scans. However, those specimens are often fragmented and invaded by sedimentary matrix that, due to mineralization processes, is undistinguishable from bone in scans. This often precludes, for example, segmentation of sedimentary matrix from bone and does not allow modelling of fossils with full anatomical complexity. Model simplification is therefore useful and necessary to overcome these limitations (Fitton et al., 2015). Moreover, increasing model complexity demands higher computational power to carry out FEA (Groning et al., 2012b) and this leads to a tension between degree of simplification and available computational power. Assessment of the impact of these simplifications typically relies on evaluation of differences in variables of interest resulting from FEA. Thus, researchers commonly focus on stress/strain magnitudes and directions and compare how different modelling decisions impact on those variables (Strait et al., 2005; Reed et al., 2011; Szwedowski et al., 2011; Wood et al., 2011; Groning et al., 2012b), although bite force (Sellers and Crompton, 2004) has also been used to assess model sensitivity.

While stress/strain FEA outputs are informative at a localized level (elements or nodes of elements) they do not allow assessment of how the model deforms as a whole and quantification of such large scale deformations. Geometric morphometrics (GM), on the other hand, uses configurations of landmark coordinates and multivariate statistics to assess how specimens differ, thereby quantifying morphological differences. Thus, it has been proposed that GM can be used to measure and describe global deformations (as well as local ones, if desired) of models under loading (O'Higgins et al., 2011; O'Higgins et al., 2012) and this approach has been applied in several studies (Cox et al., 2011; Groning et al., 2011a; Groning et al., 2012b; Holland, 2013; Prôa, 2013; Fitton et al., 2015; Toro-Ibacache et al., 2016a). Fitton et al. (2015) investigated the effects of simplifying details of internal anatomy (presence/absence of the maxillary sinus) and material properties of teeth in a *Macaca fascicularis* cranium, concluding

that this does not impact significantly on large scale deformations but it does have localized effects in strain distributions. Toro-Ibacache (2016a) addressed the impact of different segmentation protocols and of simplifying material properties of a cadaveric human cranium. They concluded that segmentation protocols can have a significant impact on large scale deformations but that simplifying material properties (differentiating trabecular bone from cortical bone vs. not differentiating between the two) had little impact on mode of deformation, while impacting magnitudes by decreasing them.

Hence, this study assesses how uncertainty and limitations in the creation of an FE model, and subsequent allocation of material properties, impacts its mechanical performance. This local sensitivity analysis is performed because an FE model of a fossil specimen (Kabwe 1) is used in chapters five, six and seven. Despite very well preserved, this fossil cranium has missing anatomical regions and has been invaded by sedimentary matrix, which precludes, e.g., accurate differentiation of cancellous and cortical bone is some regions. Thus, it is of relevance to assess the impact of simplification of the segmentation process and subsequent allocation of material properties. To that end the cadaveric *Homo sapiens* cranium that was used in the previous chapter will be simplified and strains magnitudes will be compared among models, along with modes of deformation. Furthermore, how varying kinematic boundary conditions (constraints) impacts on strain magnitudes and modes of deformation is also investigated. Based on previous research that found that simplification of material properties has limited effect on modes of deformation, but larger impact on overall strain magnitudes (Fitton et al., 2015; Toro-Ibacache et al., 2016a), it is predicted that model simplification will have a meaningful impact on strain magnitudes but limited to negligible impact on mode of deformation. Similarly, it is also predicted that alterations in constraints will have negligible impact on modes of deformation but a more relevant impact on magnitudes of deformation. Thus, it is hypothesized that ($H_0$1) variations in model segmentation have a limited or negligible impact on strain magnitudes, ($H_0$2) variations in model segmentation have limited or negligible impact on the spatial distribution of regions of relatively high and low strains (strain pattern), ($H_0$3) variations in constraints have limited or negligible impact on strain magnitudes, ($H_0$4) variations in constraints have limited or negligible impact on strain patterns. It is predicted that $H_0$1 and 3 will be falsified, and that $H_0$2 and $H_0$4 will not be falsified. Because FE models are used later in this thesis to predict deformations

during simulated masticatory function, this study should address impacts that are relevant at a biological level (i.e. deformations that relate to bone biology and bone deposition and/or resorption). However, this is difficult to define precisely because the exact magnitudes that trigger bone deposition or resorption are not known (Skerry, 2000; Currey, 2006). Thus, relevant and/or negligible changes are considered within the range of deformations of this study. Changes in strain magnitudes are considered meaningful if they are large enough to change the anatomical distribution of where high and low strains are experienced, and negligible if not. Changes in mode of deformation are considered meaningful if they are large enough to preclude identification of specific "bites" (see materials and methods).

3.2 Materials and Methods

In order to test the influence of segmentation on deformations resulting from FEA, three models were created. The reference specimen (model 3) is based on the previously validated human cranium in an approximation to an incisor bite (Toro-Ibacache et al., 2016a), loaded in this study to simulate a molar bite approximation (chapter 2). This model presents three materials (trabecular bone, cortical bone and teeth) with specific material properties. Descriptions of model building protocols can be found in chapter 2 and in Toro-Ibacache et al. (2016a). Simplifications of this reference model were then created by reducing the number of materials and hence the complexity of material properties. A two materials model (model 2) was created with only cortical bone and teeth, by adding trabecular bone to cortical bone. A one material model (model 1) was created by adding trabecular bone and teeth to cortical bone (Table 3-1).

Table 3-1: Description of FE models used in the sensitivity study. Material properties are in GPa.

Model	Voxel size	Elements	Cortical bone	Teeth	Trabecular bone
1 material	0.350	9255609	17	No	No
2 material	0.350	9255609	17	50	No
3 material	0.350	9255609	17	50	0.056

The boundary conditions were adapted from the previous validation study approximating a molar bite (chapter 2) with the model being constrained at the two mastoid processes and the first left molar to simulate the bite point. This is a non-physiological loading, chosen to allow the results of this sensitivity analysis to be compared with those of the validation study. The force was applied as a 750N load to the frontal bone (15 mm anterior to *bregma*). The constraints were originally varied in the validation study to control for possible movement of the cranium during loading. Here the same variations were applied to assess how they interact with segmentation to impact on strain magnitudes and modes of deformation. Thus, the constraints of the reference project (project 1) were varied by changing the constrained axis of one mastoid (project 2) and the position of the bite point (projects 3 and 4; Table 3-2). Project 5 of the validation chapter (one additional constraint at the point of force application) was discarded because it resulted in clearly different strain magnitudes. In total, 12 projects were created (4 different boundary conditions in each of 3 models).

Table 3-2: VoxFE projects for LM1 bite.

	Right mastoid	**Left mastoid**	**Left first molar**	
			Location	**Axes**
Project 1	x, y, z	x, y, z	Meso-lingual cusp	z
Project 2	x, y, z	z	Meso-lingual cusp	x, y, z
Project 3	x, y, z	x, y, z	Meso-buccal cusp	z
Project 4	x, y, z	x, y, z	Slope of the meso-lingual cusp	z

The impacts of varying segmentations (material properties) of models and boundary conditions were first assessed by visual inspection of the strain contour plots. Quantitative assessment is based on maximum (ε1) and minimum (ε3) principal strain magnitudes at thirty two points over the face (Figure 3-1). These magnitudes are compared to quantify the impacts of simplifying material properties and varying boundary conditions on principal strains.

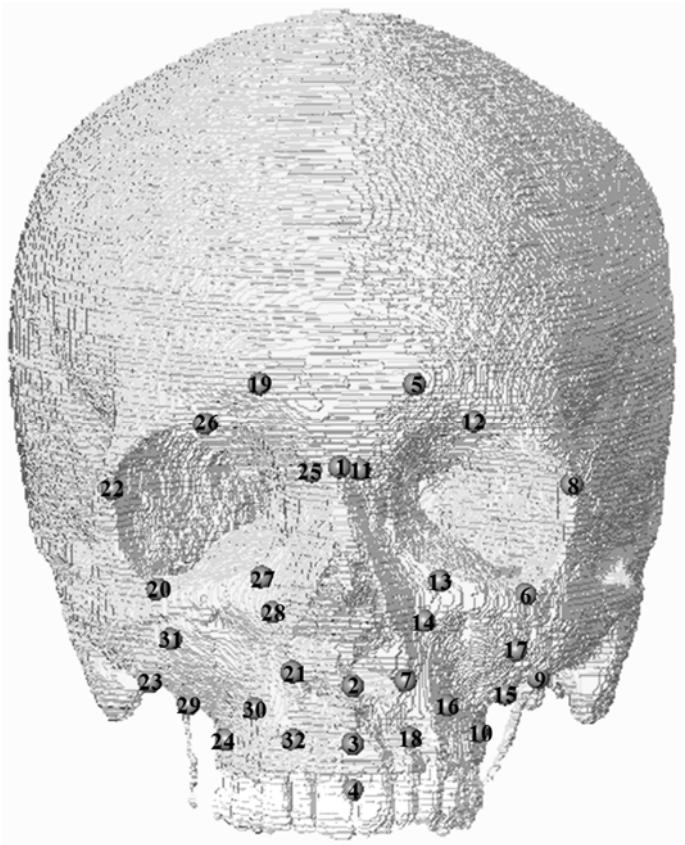

Figure 3-1: Landmarks for extraction of strain magnitudes.

To assess the sensitivity of global modes of deformation to these varying parameters, a principal component analysis (PCA) of changes in model sizes and shapes due to loading was performed using 51 landmarks (Figure 3-2). An additional "incisor bite" was simulated to allow the magnitudes of ‘error’ due to varying modelling parameters to be calibrated in relation to the magnitude of differences resulting from application of a different bite point. The "incisor bite" used the reference model 3 and project 1 and differs only in that the constraint at the molar was replaced by a similar constraint at the left central incisor.

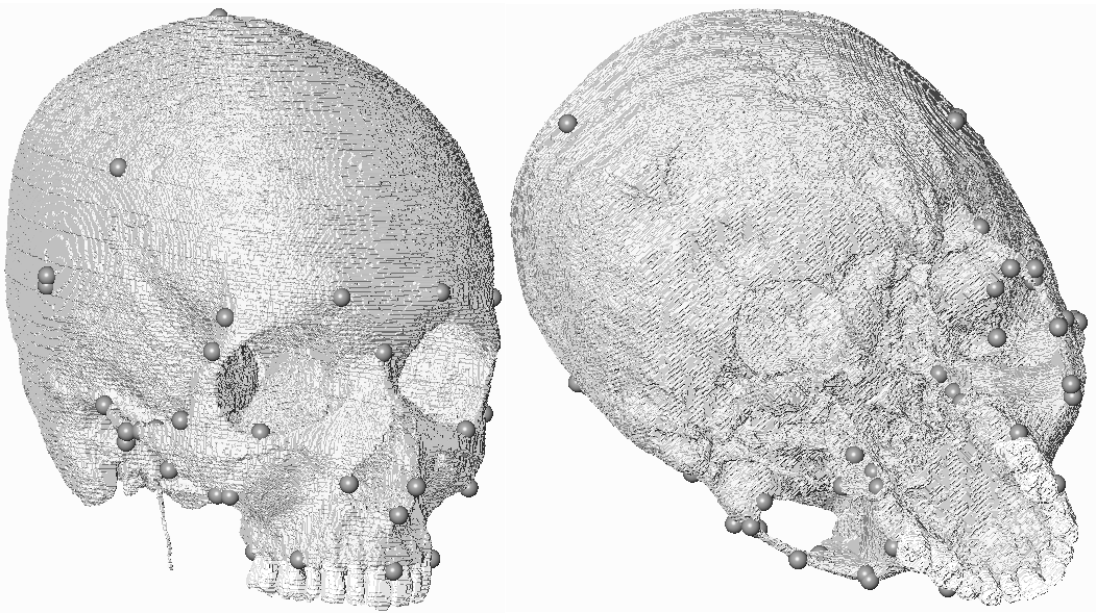

Figure 3-2: 51 landmarks used for size and shape analysis of global deformations.

3.3 Results

Visual inspection of the strain contour plots from the 12 projects shows that simplification of material properties and changes in the boundary conditions impact on strain magnitudes, but not markedly on the distribution of regions of high and low strains (strain pattern), experienced by the models. The higher strain areas are invariably located in the same anatomical regions. Thus, in all models in the neurocranium there is a clear region of high strain along the coronal suture that extends towards the anterior area of the temporal fossa and with a region of high strain at the orbital rim. There are also relatively high strains in the glabellar region that extend downwards along the naso-maxillary buttress. The infra-orbital region also presents generally high strains, with higher strains located above and next to the bite point and above the root of the canine (Figure 3-3).

Plotting the strain magnitudes extracted from the 32 points in the face shows overlap among the three models in the four projects. Despite this it should be noted that the alveolar region (points three, eighteen and especially ten) shows strain differences, with model 3 presenting higher strains than the remaining models at a few loci (Figure 3-4).

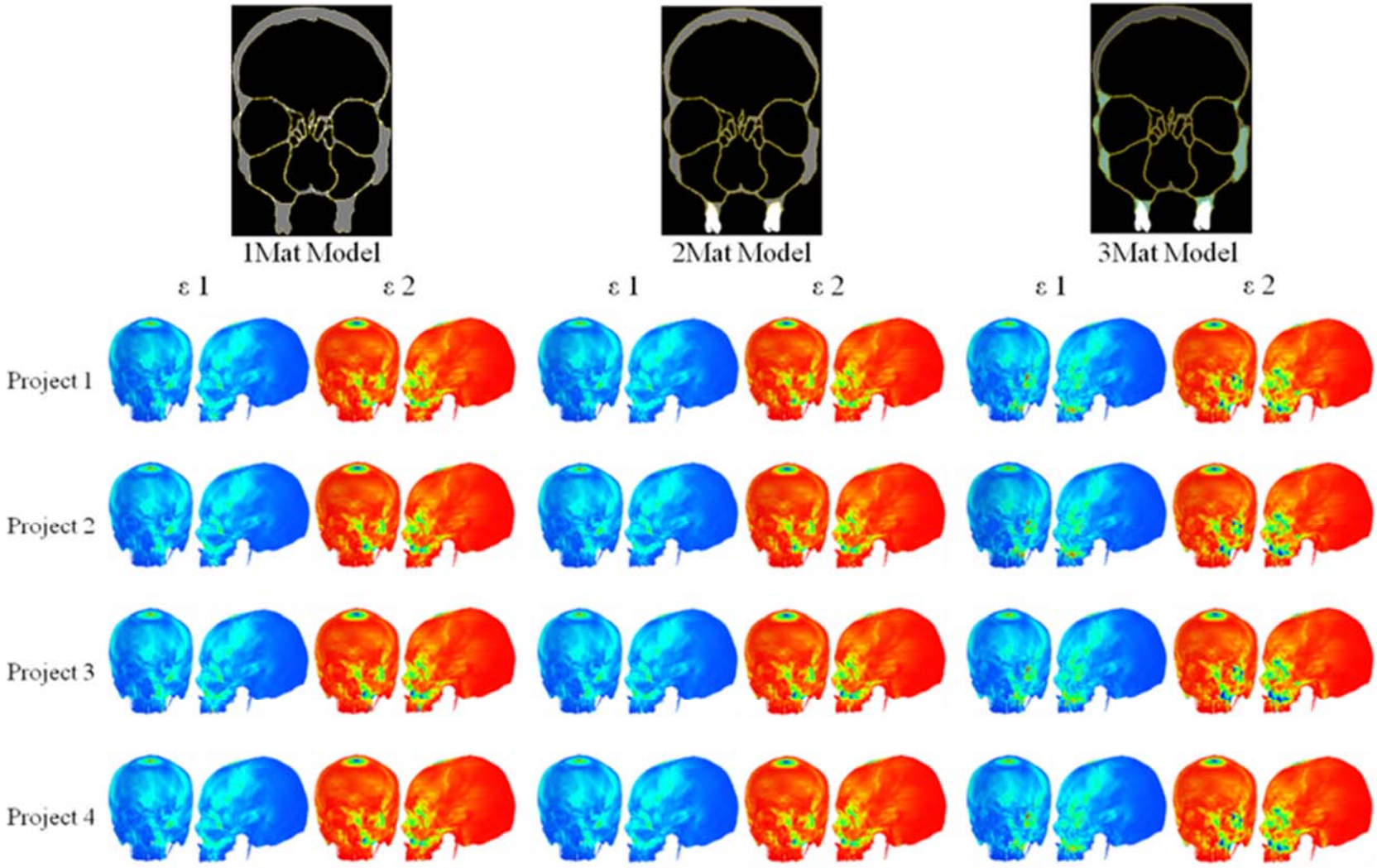

Figure 3-3: ε1 and ε3 contour plots arising from three different segmentations (pairs of columns) and projects 1-4 (rows), with varying constraints.

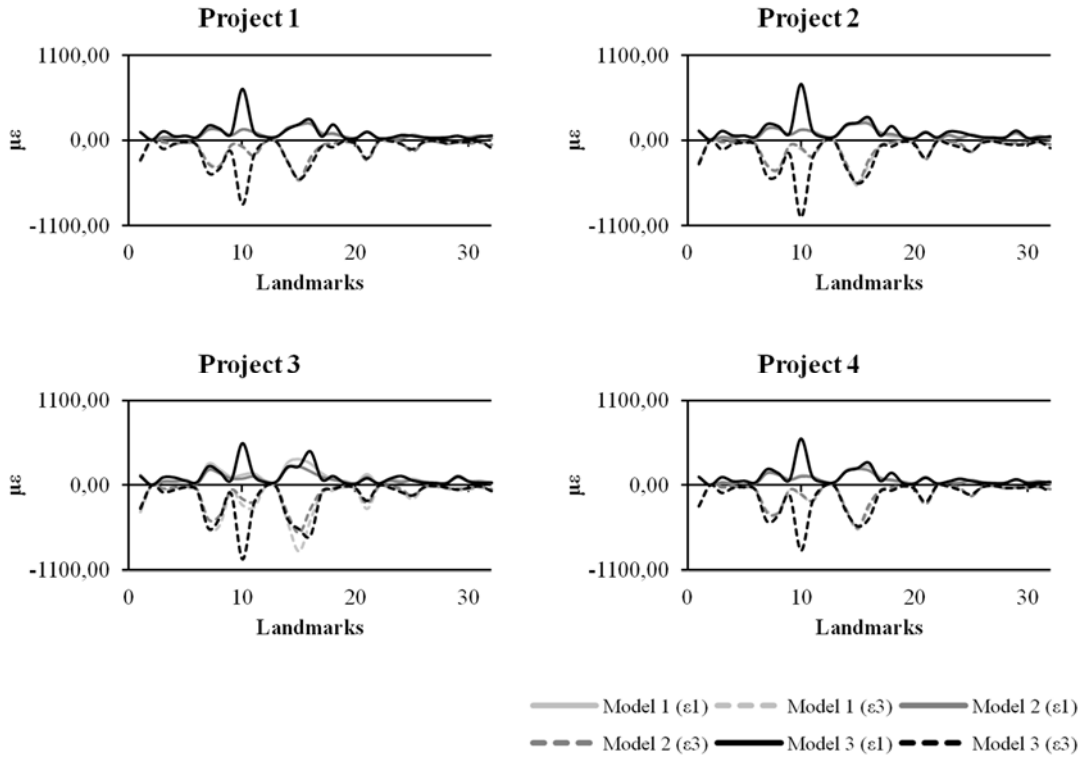

Figure 3-4: Line plots of facial ε1 and ε3 values in 4 models with different boundary conditions (projects 1-4).

Analysis of large scale deformations using the constraints defined for project 1 (the reference project) shows that simplification of model 3 (to models 2 and 1; two then one material) impacts on magnitude (distance from unloaded model) and a little less so on mode of deformation (divergence between vectors from unloaded to loaded models). The effect of reducing materials from 2 to 1 is minimal. Anatomically, the difference in mode of global deformation between model 3 and the two simplified models corresponds to a greater degree of torsion of the face towards the working side, which is seen as a relatively more superior deflection of the teeth and palate and greater supero-inferior shortening of the left orbit in model 3. These results are consistent with the graphs of facial strains (Figure 3-4) that show higher strains in model 3 and greater differences at points at or near the alveolus. The impact of model simplification on mode of deformation is small compared to the impact of varying bite point (molar to incisor) (Figure 3-5).

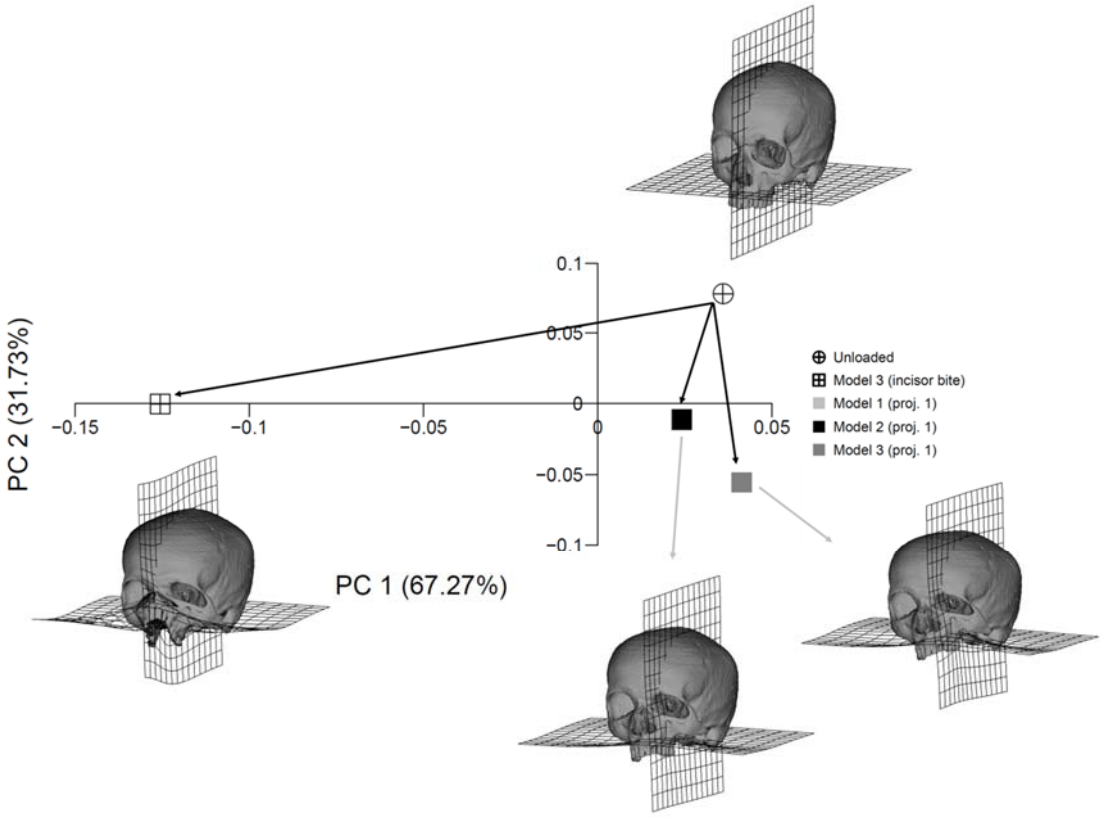

Figure 3-5: PCA of large scale deformations of project 1. Model 1 is not visible because it is in the same location in the plot as model 2. Deformations are magnified by a factor of 500 to facilitate visualization.

Figure 3-6 plots PCs 1 and 2 of the joint size and shape analysis of all projects and models. Scatters of models (segmentation varied) are similar to those in figure 3-5, however the differences among projects (constraints varied) are small compared to those among models and these tend to differ more in mode (scatter more or less orthogonal to the vector connecting unloaded and loaded models). Thus, model simplification impacts principally on magnitude of deformation in all projects and the different constraints have a smaller impact, mainly on mode.

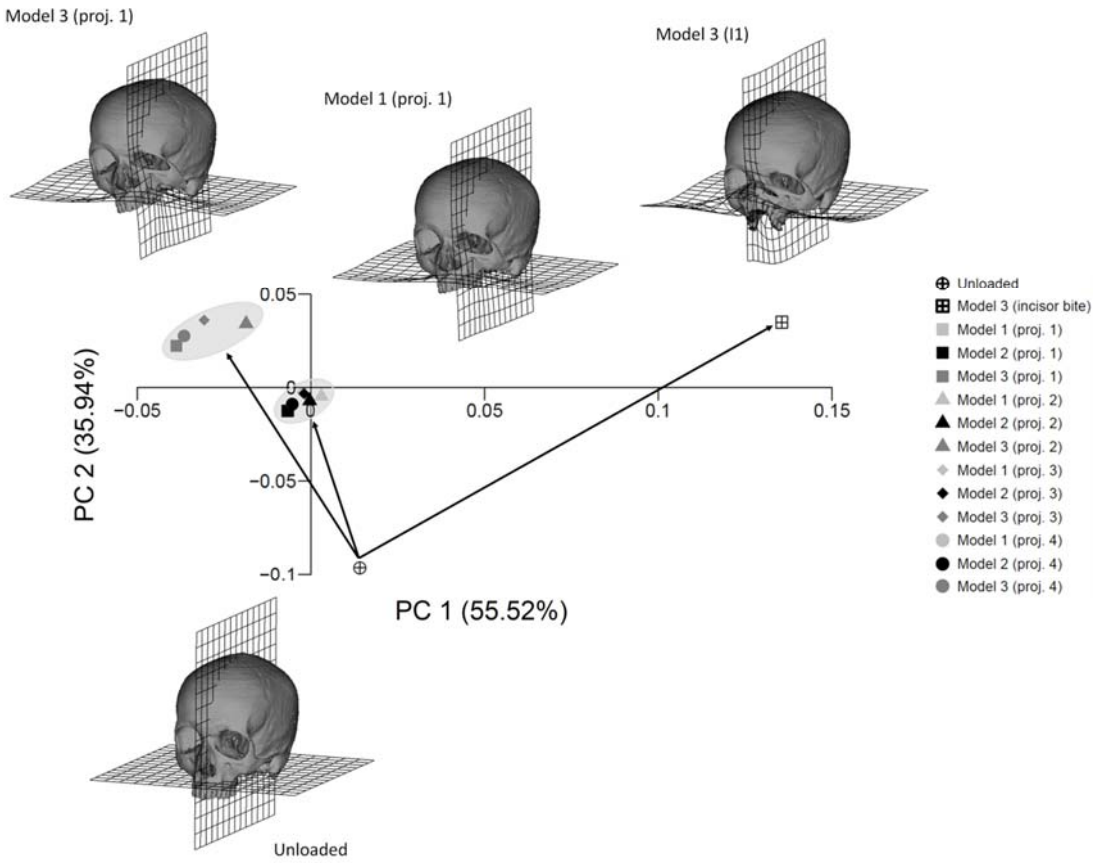

Figure 3-6: PCA of large scale deformations experienced by all models under differing kinematic boundary conditions. Deformations are magnified by a factor of 500 to facilitate visualization.

3.4 Discussion

To allow direct comparability with the results of the validation study, the loading applied in this sensitivity analysis is identical to that adopted from the validation chapter (chapter 2). This means that the results of the sensitivity analysis are not directly applicable to physiological loading scenarios but this is unlikely to be the case since the resulting modes of deformation in the face differ little from those resulting from physiological loading of the same model as assessed by comparing the strain maps for single material model (Figure 3-3) with those of the physiologically loaded model (chapter 5, Figure 5). The major differences are over the zygomatic arch, which is not loaded via masseter in this chapter, and so shows lower strains and in the calvarium which is not physiologically loaded in the sensitivity study. The face itself, in being distant from the loads and constraints in both models behaves similarly and so the results of this study are likely highly applicable.

When considering strain contour plots, variations in model segmentation and boundary conditions impact deformation. Segmentation has a clear effect on degree of deformation while the impact on mode is less evident. Thus, the spatial distribution and anatomical locations of regions of relatively high and low strains (see results for detailed description) varies little, despite differences in magnitudes.

These results are quantitatively confirmed by plotting the strains extracted at 32 points on the face, in which a significant overlap is found between strain magnitudes in the different models in each project. However, point ten displays a significant reduction in strain in models 1 and 2 relative to model 3, showing that these are considerably more stiff near the bite point. This results in a different pattern of strain distribution in that region, where they become relatively low compared to the reference three materials model. The validation study of Chapter 2 revealed that the strains in the model near the bite point do not accurately predict experimentally derived strains. Thus, validity of predicted strains in the region of the bite point and surrounding alveolus is poor and in simplified models these regions are best ignored because predictions are very unlikely to be accurate. In contrast, when considering the remaining facial skeleton strains sampled at the remaining 31 points are not markedly different among segmentations.

As expected, $H_0$1 (variations in model segmentation will have little to negligible impact on strain magnitudes) and $H_0$3 (variations in constraints will have little to negligible impact on strain magnitudes) were falsified and so, rejected. $H_0$4 (variations in kinematic boundary conditions will not impact meaningfully on the strain patterns) was largely unfalsified. On the other hand, $H_0$2 (variations in model segmentation will not impact meaningfully on the strain pattern) was falsified, particularly because of strain magnitudes predicted at point 10 in models 1 and 2. If point 10 is ignored, the hypothesis is not falsified.

These results suggest that if models are to be used to analyze structures near teeth then simplifications have clear impact. If, on the other hand, one wishes to use models to address general and broad questions then the simplifications applied in this study have low impact. This sensitivity of alveolar strains near the bite point is consistent with the findings of other researchers who have investigated, e.g., the relevance of modelling the PDL. Despite a significant dispute in the literature, several studies show that modelling the PDL has a marked local effect but less so in distant structures (Groning et al., 2011a; Groning et al., 2012b; Holland, 2013). Thus, it is possible that modelling the PDL might have given better local results, despite probably

having low impact in distant structures and on large scale deformations. However, resolution of scanning limits the anatomical accuracy with which a PDL could be represented and the consequent necessary simplifications, themselves require further sensitivity analyses before an attempt is made to incorporate a representation of the PDL.

Another factor that might have affected the results near the biting tooth is the stiffening effect of dental roots (Daegling and Hylander, 1998; Marinescu et al., 2005) and which was briefly addressed in chapter 2. As mentioned, teeth were modelled as single structures with the material properties of enamel. This is far from the real complexity of teeth, and over estimates their rigidity (for a review of material properties of teeth see Naveh et al.(2012)).To improve local prediction of strain magnitudes over the alveolar processes highly detailed modelling of the PDL and different dental tissues will be required (McCormack et al., 2014)

The results of this study are consistent with previous studies showing that altering the stiffness of the model (by changing the modulus of elasticity of specific materials) has greater impact in magnitudes of deformation than altering kinematic boundary conditions, which impact mainly mode of deformation (Cox et al., 2011; Fitton et al., 2015). In this study, the more compliant model three experiences maximum principal strains up to 391% higher, and 38% higher on average, than the stiffer model two (in which cancellous bone was allocated the modulus of elasticity of cortical bone). The minimum principal strains are 56% higher on average, and up to 919% higher, in model two than in model three. The GM analysis of global modes of deformation show a consistent result in which model three deforms more than models one and two. In the sensitivity analysis performed by Cox et al. (2011) magnitude of global deformation was found to be more affected by changes in the modulus of elasticity than changing bite point or angle of bite, which mainly impacted mode of deformation. In the study of Fitton et al. (2015), an anatomically detailed *Macaca fascicularis* model was progressively simplified by infilling trabecular spaces, foramina and maxillary sinuses. Such alterations caused an average decrease of approximately 4 to 10% in principal strain magnitudes experienced by the most solid model, and thus have a lower impact than the one found in this study. In the study of Fitton et al. (2015) global modes of deformation were impacted more by changes in bite point than by the aforementioned changes, FEA studies also consistently note that element size and mesh density impacts significantly FEA outputs, reporting errors of up to over 80% in Von

Mises stress when element size increases by 20 times (More and Bindu, 2015). While size and number of elements has significant impact on FEA outputs, results converge as mesh density increases with differences becoming increasingly smaller and negligible. This is consistent with the results of Toro Ibacache et al.(2016a), who report similar principal strain magnitudes in two models of the same human cranium which differ in element size (0.48 and 0.35) and number (3504595 and 9241525).

This and previous chapter examined the impact of modelling on the reliability of FEA results, allowing an assessment of the resolution of the data provided. The next chapter describes the reconstruction of the other FE model used in this dissertation, Kabwe 1.

4 Virtual reconstruction of Kabwe 1

4.1 Introduction

Fossil specimens are usually fragmented, distorted and invaded by sedimentary matrix, thus limiting subsequent research on morphological evolution and disparity (Neeser et al., 2009; Arbour and Brown, 2014). This has led researchers to physically reconstruct fragmented hominin crania, such as OH 5 (Leakey, 1959; Tobias, 1967) or Zhoukoudian (Weidenreich, 1937; Tattersall and Sawyer, 1996). However, physical reconstruction is heavily based on anatomical expertise and involves multiple assumptions, making it a subjective process with limited reproducibility (Benazzi et al., 2009c). Moreover, the Le Moustier Neanderthal cranium is an unfortunate example showing that physical reconstruction using original specimens may be detrimental to the long term preservation of fossils (Weber and Bookstein, 2011).

To overcome such limitations, with the advent of ready access to computing power and new specialist software, researchers started reconstructing specimens using computer based approaches. Virtual reconstruction is now a common procedure that has been applied not only to hominin fossils (Kalvin et al., 1995; Zollikofer et al., 1995; Ponce De León and Zollikofer, 1999; Neubauer et al., 2004; Zollikofer et al., 2005; Gunz et al., 2009; Grine et al., 2010a; Benazzi et al., 2011a; Kranioti et al., 2011; Watson et al., 2011; Benazzi et al., 2014), but also in the context of biological and forensic anthropology (Benazzi et al., 2009a; Benazzi et al., 2009b; Benazzi et al., 2009c) and cranial surgery (Benazzi et al., 2011b; Benazzi and Senck, 2011). Such reconstructions are commonly based on CT scans, which provide detailed imaging of bone and capture external and internal anatomy. This is potentially fundamental for finite element analysis (FEA) because model geometry is a decisive aspect in the reliability of results (Strait et al., 2005).

CT scan based reconstructions start with segmentation, during which the relevant structures are identified and labeled within the scanned volume based on differences in density, and thus on grey level Hounsfield Units (Weber and Bookstein, 2011; Weber, 2015). Segmentation choices depend on the intended further use of the model. If used only for visualization purposes in which detailed internal anatomical reconstruction is of no concern, single thresholds (set values of Hounsfield Units) that segment most of the structure can be used. Such thresholds may be set manually or calculated using a variety of approaches (Spoor et al., 1993; Coleman and Colbert,

2007), but will either exclude bones that are too thin to be selected or overestimate bone thickness. Thus, if detailed anatomy is important complex approaches that combine global, regional and manual thresholding are necessary (Weber and Bookstein, 2011). In such cases one may set a global threshold and then subsequently apply thresholds to specific anatomical regions that were not selected by previous thresholding. Finally, manual segmentation is usually necessary for fine details that were not picked up by the previous approaches.

Once the segmentation process is finished, reconstruction of missing anatomical regions begins. This process usually combines imaging software (e.g. Avizo/Amira) and geometric morphometrics (GM) to approximately restore the original geometry of an incomplete/distorted specimen (Weber and Bookstein, 2011; Weber, 2015). In specimens that preserve one side intact the most straightforward approach is to use bilateral symmetry (Gunz et al., 2009). In such cases it is possible to reflect the preserved regions onto the incomplete side and use them to replace the missing areas (Gunz et al., 2009). However, no skeletal structures are completely symmetric and present different magnitudes of asymmetry (Quinto-Sánchez et al., 2015). Thus, reflected regions will not fit perfectly the remaining preserved anatomy. To overcome this mismatch, and account for asymmetry, it is possible to use the thin plate spline (TPS) function to warp the reflected structure onto the remaining preserved anatomy (Gunz et al., 2009). Even though this is a desirable approach, fossils often lack preserved structures on both sides or along the midline, thus precluding reflection. In these cases reference based reconstruction (Gunz et al., 2004; Gunz et al., 2009) should be used. The choice of reference specimen should be considered carefully so as to not bias the reconstruction and it has been suggested that references should be species specific (Zollikofer and Ponce de León, 2005; Gunz et al., 2009; Senck et al., 2015). Such reconstructions may be statistical or geometric (Gunz et al., 2004; Gunz et al., 2009; Neeser et al., 2009). Statistical reconstruction uses patterns of covariance in a given sample to predict the location of missing landmarks via multivariate regression (Gunz et al., 2009; Neeser et al., 2009). Geometric reconstruction uses the TPS function to estimate the position of the missing landmarks based on known ones (Gunz et al., 2004; Gunz et al., 2009). The latter has the advantage of requiring one single specimen, which may be a particular individual or a mean specimen calculated from a given sample using GM (Gunz et al., 2009) but omits information on intra-specific covariations. However, Senck and Coquerelle (2015) show that using mean specimens

yields good results when reconstructing large portions of incomplete specimens. Further where sample sizes are limited to one or a few specimens, as with fossils, TPS based warping can be applied, whereas statistical approaches cannot.

Reconstruction choices impact on the final result and hence have to be considered carefully (Gunz et al., 2009; Senck et al., 2015). One option is to exclude fragmentary or damaged specimens from analysis, however when dealing with fossil remains the number of specimens is commonly very low and their exclusion may be detrimental for the study. In fact, in a study that examines the impact of different reconstruction approaches and of exclusion of incomplete specimens on morphological analysis, Arbour and Brown (2014) show that it is better to estimate missing landmarks, and thus reconstruct missing anatomy, than to exclude incomplete specimens.

In this chapter the steps are presented that were used to make a full reconstruction of Kabwe 1, a middle Pleistocene hominin cranium (dating from 150 - 250 thousand years before present) that has been classified as *Homo heidelbergensis* (Stringer, 2012). Despite missing some parts of the right side of the cranium and other localized bony structures (e.g., ethmoidal cells, orbital region of the maxilla and ethmoid) it is one of the best preserved crania in the hominin fossil record, presenting no distortion (Schwartz and Tattersall, 2003). The reconstruction is used in subsequent chapters to carry out finite element analyses (FEA) where detailed anatomical reconstruction is of concern. Thus internal and external anatomy was carefully reconstructed.

4.2 Materials and Methods

The cranium of Kabwe 1 is remarkably well preserved but presents some missing anatomy due to taphonomic and pathological processes (Schwartz and Tattersall, 2003). Such missing areas include a large portion of the right side of the cranial vault and base (parts of the right temporal, right parietal and occipital), right zygomatic, maxilla, teeth and small portions of the orbital cavities (Figure 4-1). Reconstruction was based on a CT scan (courtesy of Robert Kruszynski, *Natural History Museum, London*) performed with a Siemens Somatom Plus 4 CT scanner, with voxel size of 0.47 x 0.47 x 0.50 mm and 140 kVp, and was divided in four main phases (Figure 4-2). In the first phase the existing anatomy was segmented from the scanned volume. This was followed by reconstruction of the left side of the vault,

which was then used to reconstruct the large missing region on the right side of the cranium. Lastly, all remaining missing features were reconstructed.

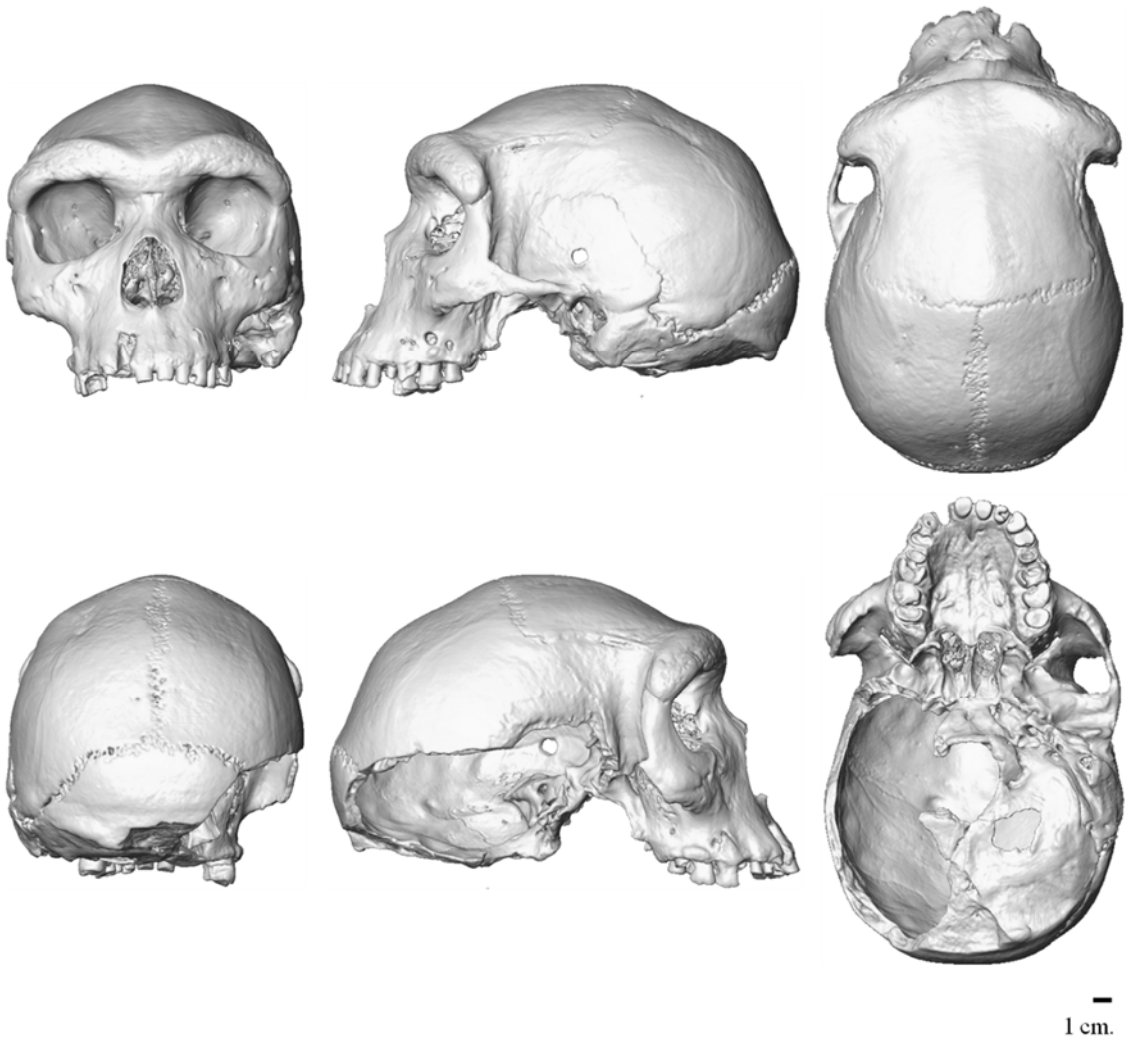

Figure 4-1: Standardized views showing missing bony structures of the cranium of Kabwe 1. Note that, despite some missing portions, the cranium is extremely well preserved and presents no distortion.

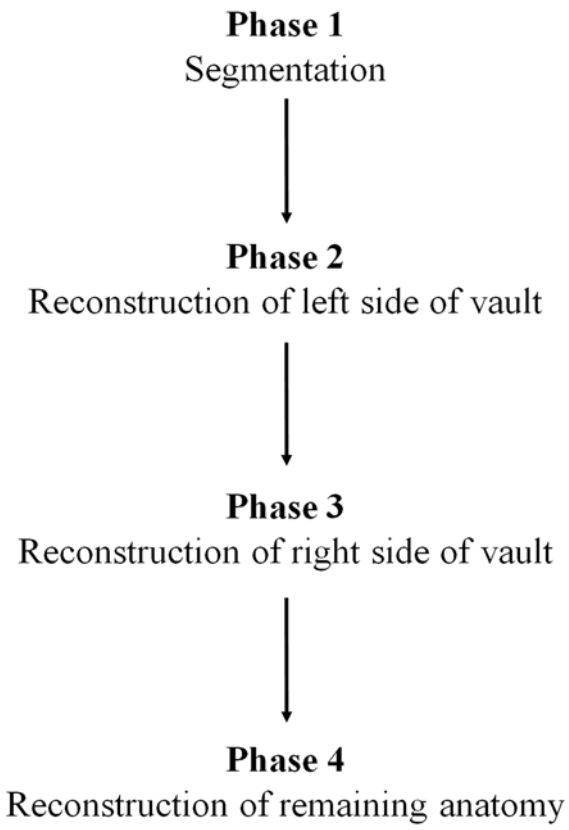

Figure 4-2: Workflow of the reconstruction of Kabwe 1.

Segmentation was performed in Avizo 7.0 and used a combination of approaches. First, the half maximum height value (HMHV; Spoor et al., 1993) was calculated and applied to the whole volume to threshold segment it. This inevitably excluded thin bones, requiring the use of regional thresholds as a second step, applied to specific anatomical regions, such as regions of the ethmoid bone. This allowed semi-automated segmentation of more, but not all, of the bony anatomy without overestimating bone thickness. Thus, manual segmentation was required for fine details of thin bones. Teeth were segmented separately, which required calculation of specific thresholds to avoid overestimating their dimensions. Last, it was necessary to remove sedimentary matrix that had invaded the cranium. This required a manual approach due to overlap of grey values between matrix and bone.

Once segmentation was complete, the left half of the cranium was mirrored to reconstruct the missing large right portion of the cranium that includes parts of the parietal, temporal, occipital and zygomatic bone. Because of asymmetry the reflected region did not fit the remaining preserved anatomy perfectly. Thus it was necessary to warp it to the preserved structures using the TPS function. This allowed an almost

perfect fit between reconstructed and preserved anatomy that required minimal manual editing. After warping only the reconstructed regions were preserved and the remaining reflected hemi-cranium was discarded. The alveolar process of the right hemi-maxilla was also restored by reflecting the preserved contra-lateral region. Regions that presented gaps (orbital surfaces of the maxilla and ethmoid, periapical regions of the maxilla, left temporal bone, occipital bone, nasal cavity walls, ethmoid bone and vomer) were reconstructed using a combination of manual editing and the software Geomagic 2011 (courtesy of Dr W Sellers, University of Manchester) to interpolate between existing bone edges. The missing portion of the occipital bone, affecting the superior nuchal line, was reconstructed using the occipital of a modern human cranium, manually editing it to adjust its morphology. Editing was performed in Geomagic 2011. Teeth were restored by reflecting existing antimeres. When this was not possible portions of teeth from a modern human were used to reconstruct incomplete teeth.

4.3 Results and discussion

The reconstruction of Kabwe 1 allowed restoration of missing anatomical regions (Figure 4-3 and 4-4) and creation of a model for further use in FEA. While it was carried out as objectively as possible, any reconstruction, physical or virtual, requires assumptions and a certain degree of subjectivity (Gunz et al., 2009). Thus other reconstructions will likely yield different results, but disparities are likely very small in most regions because segmentation was mainly based on global and regional HMHVs and restoration was highly constrained by existing structures and the use of GM based approaches.

The segmentation process relied mainly on global and regional thresholds that were selected using HMHVs. This provides a generally objective approach but depends on the sites at which the values are measured and it does not segment the whole cranium without further manual segmentation if bone thickness is not to be overestimated. Thus, while it is generally reproducible, minor differences relative to other possible segmentations are to be expected due to differences in sites where grey levels are measured and in manual segmentation decisions.

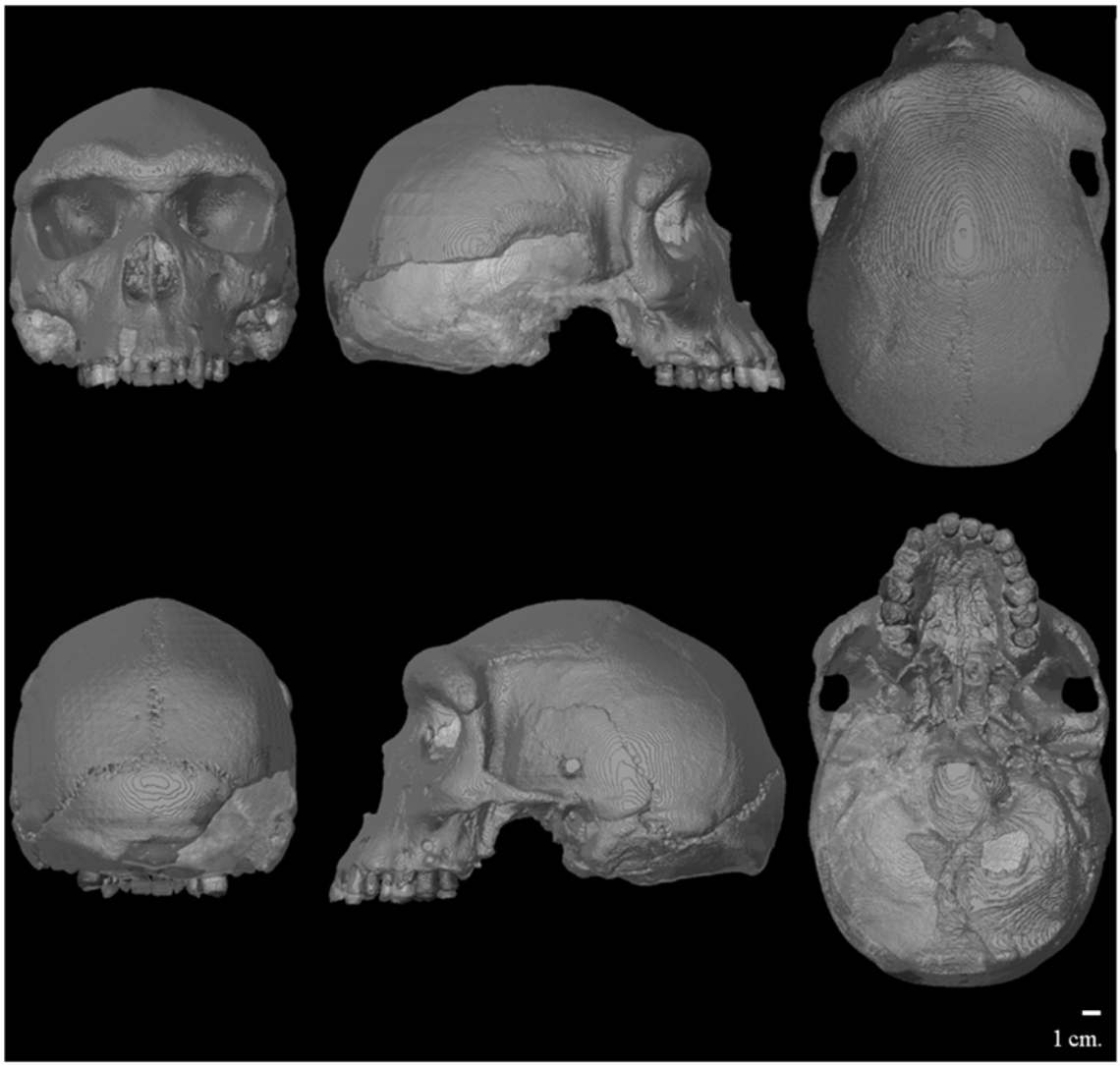

Figure 4-3: Standardized views showing the original (dark grey) and the reconstructed (translucent grey) crania of Kabwe 1.

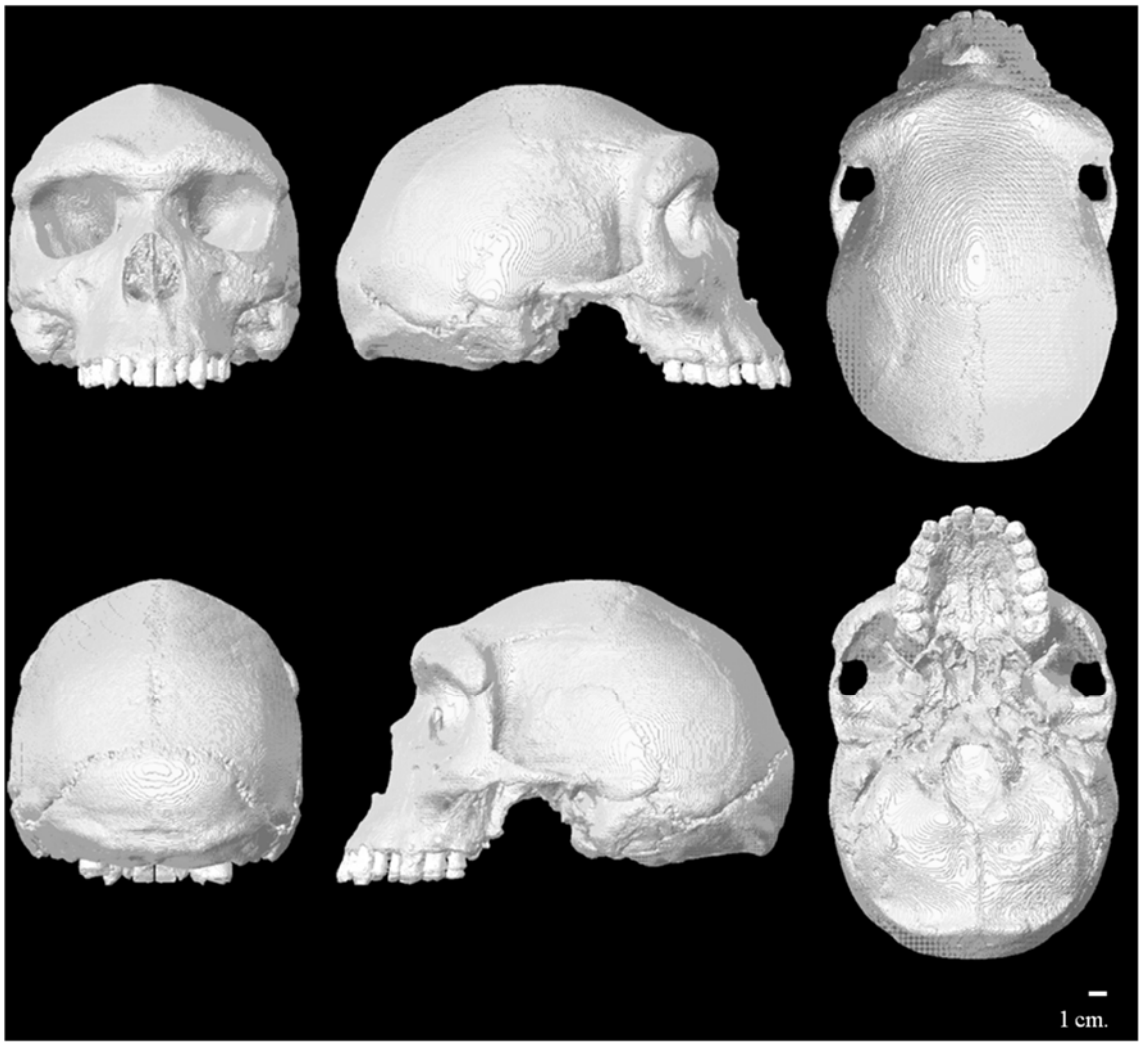

Figure 4-4: Standardized views showing the reconstructed cranium of Kabwe 1.

Reconstruction of the large missing portion on the right side of the vault and base used the reflected left side, which was then warped based on the TPS function to account for asymmetry. This procedure is expected to yield good results and outperform statistical reconstruction based on multivariate regression because it used the same individual *and* the reflected region was warped to the existing anatomy. The TPS warping used classical landmarks and no sliding semi-landmarks. While these potentially improve warping results, only minor differences are to be expected because the reference is individual specific (reflected left hemi-cranium), TPS warping used several landmarks in the vicinity of the restored region and the reflected warped portion fitted the target region almost perfectly.

While it would be preferable to use species specific homologous structures to restore teeth and the occipital we did not have access to other *Homo heidelbergensis* specimens (the Petralona cranium would have been the best specimen for this

procedure, despite not preserving anterior teeth, but the available CT scan is low resolution). In the absence of such specimens a modern human was used and its morphology was manually edited after warping to account for morphological differences in the nuchal line region of the occipital. Furthermore, reconstruction was only performed to approximately the midline and the contra-lateral side was reconstructed with the reflection/TPS based warping procedure. Visual assessment of the smoothness of the reconstruction provides confidence that the original morphology is likely closely approximated and that the results of using other approaches may differ only slightly. Likewise, the reconstruction of teeth is susceptible to error, one major source of which is the selection of reference specimens.

The use of Geomagic to fill small gaps (in the occipital bone, alveolar region of the maxilla, orbital cavities and temporal bone), proved very efficient and visual assessment shows smooth reconstructions. The region in which reconstruction was most subjective was in defining the cells of the ethmoid bone, this was performed manually. An alternative approach would have been to use the ethmoid bone of a modern human (to the best of our knowledge no other closely related fossil hominin has this bone fully preserved), warping its ethmoid to replace the existing incomplete bone. While this would have been more objective the bone forming the ethmoid sinus is extremely thin and has limited load bearing significance during biting (Ross, 2001). Moreover, because it is so thin warping would likely have required further manual editing. Thus, while results would have been different they would probably have had minor, if any, impact on subsequent FEA.

As mentioned above, any reconstruction is subjective (Gunz et al., 2009). Thus, several studies have assessed the impact of reconstruction approaches and compared the impact of using TPS based estimation of missing landmarks vs. multivariate regression vs. mean specimen (Gunz et al., 2009; Neeser et al., 2009; Arbour and Brown, 2014), reference specimen selection (Gunz et al., 2009; Neeser et al., 2009), sample size of reference sample (Neeser et al., 2009) and number of missing landmarks (Arbour and Brown, 2014). Based on these studies we believe that the present reconstruction reasonably approximates the original morphology. Nonetheless, a comparative study assessing the impact of reconstruction choices is desirable and this has not yet been done in the context of FEA. This is likely because finite element model creation is complex and highly time-consuming, which is why this was not done in the present reconstruction. However, the impact of morphological reconstruction

choices on resulting stresses and strains (commonly used parameters in comparing FEA results) will be a function of the morphological differences among reconstructions, if all other parameters (i.e., material properties, constraints, muscles forces and directions) are kept constant. Thus, differences in stresses and strains between reconstructions will increase as morphological differences increase. Despite this prediction, future work should include sensitivity studies assessing the impact of reconstruction choices.

These first three chapters focused on methodological questions related to the reliability of FEA results and modelling protocols. The next three chapters will focus on biologically pertinent questions related to cranial form and function in recent hominins. The next chapter compares the functional performance of *H. sapiens* with that of its hypothesized ancestral species, *H. heidelbergensis*, to examine if cranial morphological differences in these species are driven by biting mechanics.

5 The biting performance of *H. heidelbergensis* and *H. sapiens*

5.1 Introduction

Homo heidelbergensis is a middle Pleistocene fossil hominin that has been proposed as the ancestral species of *Homo sapiens* and *Homo neanderthalensis* (Rightmire, 1998; Stringer, 2002; Rightmire, 2008; Rightmire, 2009; Stringer, 2012) but see (Bräuer, 2001, 2008, 2012)). It has a long but low cranial vault with a mean cranial capacity of 1263 cm^3 (Schwartz and Tattersall, 2003; Lieberman, 2011), a very large face (Rightmire, 1998; Freidline et al., 2012) and presents an extremely enlarged double-arched brow-ridge that overhangs 'square' orbits that slope inferiorly and laterally at the inferior margins (Schwartz and Tattersall, 2003). The sub-nasal region is prognathic and significantly taller than that of *H. sapiens*. The maxillary root of the zygomatic arch is usually located above the first or second molar (Schwartz and Tattersall, 2003; Lieberman, 2011) and the relatively convex infraorbital region lacks the concave canine fossa found in *H. sapiens* (Freidline et al., 2012). Structurally, these anatomical features of *H. heidelbergensis* are not significantly different from those found in Neanderthals (Lieberman, 2011). This has resulted in Kabwe 1 having been classified as a Neanderthal in the past (Tappen, 1978).

The more gracile modern human cranium differs from crania of *H. heidelbergensis* and *H. neanderthalensis* in several ways. When compared to these species, *H. sapiens* has an enlarged (relative to *H. heidelbergensis*, not Neanderthals), more globular cranial vault, with a mean cranial capacity of 1350 cm^3, and a small gracile and orthognathic face, with reduced interorbital space, that is retracted under the anterior cranial fossa. This facial reduction in *H. sapiens* is associated with the presence of a canine fossa, a short oropharynx and more rectangular orbital cavities (Enlow and McNamara, 1973; Enlow and Hans, 1996; Lieberman et al., 2002; Trinkaus, 2003; Lieberman, 2011). Additionally, recent *H. sapiens* is said to have generally reduced masticatory muscle cross-sectional areas, relative to *H. neanderthalensis*, based on assessment of bony proxies (Antón, 1990; O'Connor et al., 2005). Conversely, O'Connor et al. (2005) estimate generally comparable muscle cross-sectional areas in Pleistocene and recent robust modern humans relative to Neanderthals. When compared to *H. heildelbergensis*, Eng et al. (2013) estimate slightly larger mean temporalis and masseter muscles, but smaller medial pterygoid, in *H. sapiens*.

This general gracilization of the craniofacial complex led to the view that modern humans produce lower bite forces and are less able to withstand masticatory strains than other hominins (Wroe et al., 2010; Lieberman, 2011). Few studies have compared the biting performance of *H. heidelbergensis* and *H. sapiens*, but *H. heidelbergensis* has been proposed to generate slightly higher bite forces at the first molar than recent modern humans, absolutely and relative to crown area, and slightly lower at the first incisor, despite having a less mechanically advantageous masticatory system (Lieberman, 2011). Conversely, Eng et al. (2013) estimate clearly higher bite forces at the second molar in Pleistocene and recent modern humans than in *H. heidelbergensis*, absolutely and relative to occlusal area. There is, on the other hand, significant research on the masticatory biomechanics of *H. neanderthalensis* (Rak, 1986; Demes, 1987; Trinkaus, 1987b; Demes and Creel, 1988; Antón, 1990; Spencer and Demes, 1993; Antón, 1996; O'Connor et al., 2005; Clement et al., 2012). It has been proposed that Neanderthals were adapted to generate and withstand high and/or repetitive occlusal loads at the anterior dentition (the anterior dental loading hypothesis (Rak, 1986; Demes and Creel, 1988; Clement et al., 2012)). This has supported the notion that *H. sapiens* is less adapted to generate and withstand high anterior bite forces (Lieberman, 2011). However, several studies have found that *H. sapiens* is relatively more efficient at generating bite forces than Neanderthals (Antón, 1990; O'Connor et al., 2005; Lieberman, 2011). This is because even though *H. sapiens* has been estimated to present generally smaller (in recent gracile specimens; Antón, 1990; O'Connor et al., 2005) or comparable (in Pleistocene and recent robust specimens; O'Connor et al., 2005; Eng et al., 2013) masticatory muscles, and therefore muscle forces than Neanderthals, it displays more effective muscle mechanical advantages due to its retracted and shorter face and the more anteriorly positioned masticatory muscles (Trinkaus, 1987b; Antón, 1990; O'Connor et al., 2005; Lieberman, 2011; Eng et al., 2013). As such, bite forces calculated for modern humans are comparable (in Pleistocene and recent robust specimens; O'Connor et al., 2005; Eng et al., 2013) or higher (in recent specimens; Antón, 1990; Eng et al., 2013) than those calculated for Neanderthals.

While there is some debate about the bite force production capability of these species, it seems that *H. sapiens* is not well adapted to withstand masticatory stresses and strains. Even though this has only been briefly addressed in *H. heidelbergensis*, it has been proposed that it resists masticatory stresses and strains better than *H. sapiens*

due to the larger face (Lieberman, 2011). Likewise, Neanderthals have been said to be better adapted for resisting biting loads than *H. sapiens*, especially anterior dental loading. This is because Neanderthals present a taller, more inflated and more parasagitally orientated infraorbital region that lacks a canine fossa and large anterior teeth, while modern humans have shorter facial height, a coronally orientated infraorbital region, a canine fossa and small anterior teeth (Rak, 1986; Demes, 1987; Lieberman, 2011).

The above studies analyzed biting performance using lever arm mechanics and simplifications of skeletal facial anatomy, with which it is difficult to fully consider the three dimensional anatomical complexity of the masticatory system. More recently craniofacial biomechanical studies of hominins have used Finite Element Analysis (FEA) (Strait et al., 2007; Strait et al., 2009; Strait et al., 2010; O'Higgins et al., 2011; Witzel, 2011; O'Higgins et al., 2012). This approach involves the creation of 3D models of the cranium that are then allocated bone material properties and loaded to simulate muscle attachments, lines of action and forces, with constraints applied at biting points and to fix the cranium in space (O'Higgins et al., 2011; O'Higgins et al., 2012). Functional simulations using this approach lead to predictions of bite forces and the stresses and strains experienced by the craniofacial complex. FEA has been used in cranial biomechanical analyses of fossil hominins, such as *Australopithecus africanus* (Strait et al., 2009; Strait et al., 2010) and *H. neanderthalensis* (Witzel, 2011). However, there has only been one FEA study comparing the biting performance of different hominin species (Wroe et al., 2010). In that study the ability to generate bite forces and to resist them was compared among extant hominoids, fossil hominins (*Australopithecus africanus* and *Paranthropus boisei*) and modern humans. As such, the biting performance of *H. sapiens* has not yet been compared to that of its proposed ancestor, *H. heidelbergensis* using FEA.

Thus, the present study assesses the biting mechanical impact of the morphological differences found between modern humans and its putative ancestor by comparing the biting performance of *H. sapiens* and *H. heidelbergensis*. Based on prior work (O'Connor et al., 2005; Lieberman, 2011; Eng et al., 2013) it is expected that differences will be found in: (i) bite force efficiency and possibly capability; (ii) the ability to resist masticatory loading; (iii) the magnitudes and modes of deformation experienced by the craniofacial complex. The study proceeds by testing the null hypotheses that these do not differ.

5.2 Materials and Methods

The crania of *H. heidelbergensis* and *H. sapiens* were compared based on the following mechanical performance parameters in relation to biting: (1) the mechanical advantages of the main jaw adductor muscles (temporalis, masseter and medial pterygoid), (2) the bite forces generated and the bite force production efficiency (the proportion of muscle force converted into bite force and into joint reaction forces), (3) the magnitudes and modes of deformation of each cranium assessed locally using strains and globally using geometric morphometrics.

The (1) mechanical advantages were calculated for the jaw adductor muscles (temporalis, masseter and medial pterygoid) based on 3D landmarks on two *H. heidelbergensis* (Kabwe 1 and Petralona) and one cadaveric *H. sapiens* (Figure 5-1). Because masseter and, especially, temporalis are muscles with wide origins, their mechanical advantages were calculated for their most anterior and posterior lines of action to bracket the range in each. For temporalis a third line of action was also defined, approximately in the centre line of the muscle, where it bulges and reaches its most superior point. The mechanical advantages of a lateral incisor bite were also calculated for *H. sapiens* and the results were averaged to render them comparable with those of O'Connor et al. (2005) where the mechanical advantages were calculated for the lateral incisor. Even though the *H. heidelbergensis* sample is small, Kabwe 1 and Petralona are the best preserved skulls of this species, providing complete data. The mechanical advantages were measured in only one *H. sapiens* specimen, but the results for temporalis and masseter were consistent with those from other studies and only slightly higher for medial pterygoid (O'Connor et al., 2005, and see results section).

The methodology for creating and loading the FE models is described below. The (2) bite forces were calculated from the reaction forces at the bite points of one *H. heidelbergensis* (Kabwe 1) and one *H. sapiens* (cadaveric specimen). The bite force production efficiency reflects the proportion of net applied muscle force converted into bite force and the proportion that contributes to reaction forces at the fulcrum at the glenoid fossa. These are calculated as the ratio of the bite force and net muscle force applied (Fb/Fm) and the ratio of the summed reaction forces at the glenoid fossae and net muscle force applied (Fc/Fm) (Antón, 1990; O'Connor et al., 2005). The net muscle force is calculated as the sum of the reaction forces at the constrained nodes and differs

from the total muscle force due to the orientation of the muscle force vectors. The (3) the magnitudes, directions and modes of deformation were calculated from the displacements arising from the FEA.

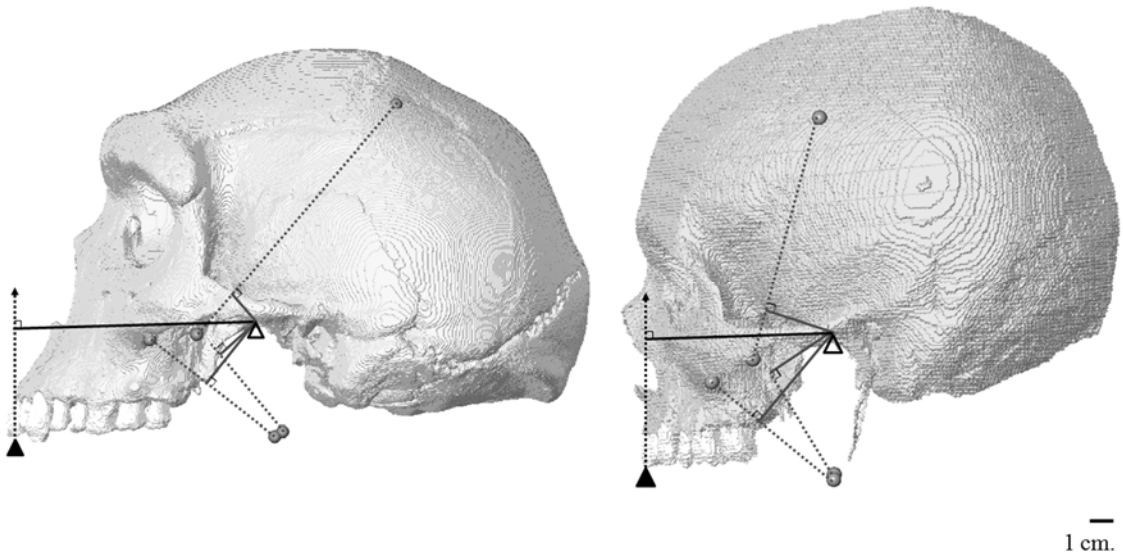

Figure 5-1: Measurement of muscle moment arms (grey solid lines) and bite lever arm (black solid line). The muscle moment arms were calculated as the perpendicular distance from the fulcrum (glenoid fossa) to the respective muscle line of action (grey dotted lines). The bite lever arm was calculated according to O'Connor et al. (2005), as the perpendicular distance from the fulcrum to the vector of the bite force applied (black dotted line). The hollow triangle indicates the constraint at the glenoid fossae, where the joint reaction forces (Fc) were calculated; the solid triangle represents the constraint at one of the three different bite points (left central incisor) where the bite force (Fb) was calculated.

5.2.1 Finite Element Models

The virtual models of Kabwe 1and the cadaveric *H. sapiens* were created from CT scans (see chapters 2 and 3 for a detailed description of model creation of the *H. sapiens* specimen and chapter 4 for the reconstruction of Kabwe 1). After segmentation and reconstruction both models were converted into voxel-based finite element models and were used to simulate three different bites. Because the human cranium lacks one of the pre-molars in the left and right hemi-arcades, tooth and bite point correspondence is established in terms of position along the dental arcade rather than

by tooth type. This decision was based on a sensitivity analysis in which the left first molar of the *H. sapiens* was replaced by the left pre-molar. The results show that facial strains are not significantly affected by this change, thus correspondence of position along the dental arcade is more important than correspondence in tooth morphology. The simulated bites used the first left tooth (left central incisor in both models), the fourth left tooth (first left pre-molar in both models) and the fifth tooth (left first molar in *H. sapiens* and second left premolar in Kabwe 1).

5.2.1.1 Skull reconstruction and model creation

5.2.1.1.1 Kabwe 1

This section provides a summary of the reconstruction of Kabwe 1. For a full description see chapter 4.

The cranium was reconstructed from a CT scan (courtesy of Robert Kruszynski, Natural History Museum), with an original anisometric voxel size (0.4687501 x 0.4687501 x 0.50 mm), that was resampled to an isometric voxel size of 0.35 mm. Automated, semi-automated and manual segmentation to refine fine details were performed using Avizo® (version 7.0). This was followed by reconstruction of the missing anatomical regions of the cranium, such as the right temporal, parts of the right parietal, occipital, maxillae, ethmoid and teeth. Where possible, this was achieved by mirroring present contralateral anatomical areas and warping them to the existing structures. Geomagic® (Studio 2011) was used to fill small gaps using the surface of surrounding structures as a reference for interpolation. When no contralateral structures were present portions of the *H. sapiens* cranium were also used for reconstruction, by warping them to fit. The cancellous bone spaces were infilled with material to form a bulk material (see below, 5.2.1.1.2, *Homo sapiens*, for justification of infilling cancellous spaces). The cranium was then directly converted into a voxel-based finite element model using a bespoke software tool, vox2vec.

5.2.1.1.2 Homo sapiens

The *H. sapiens* cranium was originally segmented by Toro-Ibacache et al. (2016a) based on a CT scan of a cadaveric human head with an original isometric voxel size of 0.484 mm and that was later resampled to an isometric voxel size of 0.350 mm. Automated, semi-automated and manual segmentation of the skeletal structures was performed and cortical bone, trabecular bone (as a bulk material) and teeth were originally segmented as separate materials. The cranium was then directly converted into a voxel-based finite element model using a bespoke software tool, vox2vec. It was submitted to validation studies that approximate the simulation of incisor (Toro-Ibacache et al., 2016a) and molar bites (Chapter 2) as well as a sensitivity study assessing the impact of model simplification on performance (Toro-Ibacache et al., 2016a;Chapter 3).

On the basis of these sensitivity studies, which showed a marked effect on magnitude but a very small effect on mode of deformation, both models were simplified by filling cancellous bone regions with material that has the same material properties as cortical bone and allocating the same cortical bone properties to teeth (see 5.2.1.3, Material properties). This allowed comparability with the Kabwe 1 FE model which is simplified because the CT scan lacks detail of cancellous bone architecture and distribution.

5.2.1.2 Constraints

Similar constraints were applied to Kabwe 1 and the *H. sapiens* models using the finite element analysis software tool, VoxFE (Fagan et al., 2007). Both temporo-mandibular joints were constrained at 24 nodes (x, y and z axis) and a third constraint (21 nodes, fixed in the z axis) was applied at the simulated bite point in each of the masticatory simulations.

5.2.1.3 Material properties

A sensitivity study conducted using the *H. sapiens* cranium (Chapter 3) shows that simplifying the model from the original three materials (cortical bone, trabecular bone and teeth) with distinct material properties, to a model with one material with properties of cortical bone has a major effect in reducing the magnitude of strains and of global deformation with a much more limited effect on mode of deformation

(relative strain magnitudes between regions and mode of global changes in size and shape). Allocating to teeth the material properties of cortical bone rather than enamel has a very localized effect in the alveolar region, altering mode and magnitude of deformation (Chapter 3). These results are consistent with other studies using non-human primates (Fitton et al., 2015) and show that using a one material model should not yield unreliable results in terms of mode of deformation, but magnitude is likely diminished to an unknown degree. Further this simplification resulted in only a 0.1% increase in the estimated bite force. This is useful in the current (see chapter 4 for full description of missing anatomy) and other contexts because fossils often lack anatomical regions because of post mortem damage and are filled with sedimentary matrix, precluding reliable reconstructions of anatomical details, such as the distribution and architecture of trabecular bone (Fitton et al., 2015). By building a one material model, reconstruction is facilitated, yet useful information can still be obtained regarding mode but not the magnitude of deformation. Such models were created for both *H. sapiens* and Kabwe 1, to which cortical bone material properties were allocated, with a Young's modulus of 17 GPa and Poisson's ratio of 0.3. The modulus of elasticity was derived from nanoindentation studies of cortical bone from the *H. sapiens* skull (Toro-Ibacache et al., 2016a), following the protocol of Kupczik et al. (2007) and it is within the range of previous studies (Dechow et al., 1993; Schwartz-Dabney and Dechow, 2003).

5.2.1.4 Muscle loads

Loads were applied to the model to represent the actions of six muscles active during biting: right and left temporalis, right and left masseter, right and left medial pterygoid.

The *H. sapiens* cadaveric head had all the masticatory muscles preserved, as well as the mandible. As such it was possible to accurately represent the specimen specific muscle vectors and muscle forces as calculated from the actual muscle areas and not from bony proxies (Toro-Ibacache et al., 2016a; Table 5-1).

Table 5-1: Applied Muscle Forces (in Newtons).

Muscle	Side	
	Left	Right
Temporalis	168.02	170.67
Masseter	134.06	124.01
Medial pterygoid	124.01	117.49

Kabwe 1 does not have a mandible, which precludes direct estimation of the lines of action and anatomical cross sectional areas (and so maximum forces) of muscles that attach to the mandible (masseter and medial pterygoid). As such we adopted the muscle forces estimated for the *H. sapiens* specimen, which renders muscle loadings identical in terms of force magnitude between crania. The directions of muscle force vectors were estimated by scaling a *H. neanderthalensis* mandible (Tabun 1 specimen) to the Kabwe 1 skull and using it to guide estimation.

5.2.1.5 Model solution, analysis and scaling

The FE models were solved using VoxFE (Fagan et al., 2007). The resulting deformations of the two models were then compared by: (1) visual assessment of contour plots of the two surface principal strain (ε1 and ε3) magnitudes over the whole cranium and of strain vector directions over the infraorbital plate; (2) quantitative comparisons of the surface strain magnitudes experienced at 41 homologous points in the crania (see Table 5-2); (3) comparisons among the loaded models, of modes of global deformation (changes in size and shape) relative to the mean (of the modern human and Kabwe I) unloaded specimen using geometric morphometric (GM) analysis of a set of 67 cranial landmarks (Table 5-2).

Because the ability to generate bite forces and to resist those bites is being assessed in crania with different sizes and shapes, it is necessary to understand and control for the effects of these differences by scaling the results as appropriate for each analysis.

To compare absolute bite force generation capacity between the modern human and Kabwe 1 is difficult because no data are available on the cross sectional areas of masticatory muscles in the latter. For this reason the same muscle forces were applied to the modern human and Kabwe 1 crania in all FEA biting simulations. To estimate

actual performance in Kabwe 1 it was therefore necessary to scale the results of FEA according to our best estimates of masticatory muscle cross sectional areas. This was performed according to the cross sectional area of the left temporal fossa in each specimen, a bony surrogate for temporalis cross sectional area and the only bony proxy available for the masticatory muscles. This scaling is crude, being limited by the assumptions that the temporal fossa area predicts muscle cross sectional area (which it likely does not see Toro-Ibacache et al., 2015b) and that there exists a similar relationship among the cross sectional areas of the different masticatory muscles in the two individuals.

Table 5-2: Landmarks used for extraction and plotting of strains (landmarks 1 - 41) and for GM analysis of magnitudes and modes of deformation (landmarks 1 - 67).

Number	Landmark
1	Bregma
2	Lambda
3	Inion
4; 42	Asterion
5; 43	Porion
6; 44	Pterion
7; 45	Frontomalare orbitale
8; 46	Frontomalare temporale
9; 47	Jugale
10; 48	Zygotemporale superior
11; 49	Zygotemporale inferior
12; 50	Maxillofrontale
13; 51	Zygoorbitale
14; 52	Zygomaxillare
15; 53	Superior rim of orbit
16; 54	Infraorbital foramen
17	Nasion
18	Rhinion
19; 55	Lateral Nasal Suture
20	Nasospinale
21; 56	Alare
22	Alveolare
23; 57	External Alveolar Incisor 2
24; 58	External Alveolar Canine

25; 59	External Alveolar Premolar4
26; 60	Zygomatic take-off
27; 61	Inferior Distal Alveolar
28	Incisive Foramen
29	Palate maximum
30	Staphylion
31; 62	Infratemporal crest
32	Basion
33	Opisthion
34; 63	Lateral Edge of Foramen Magnum
35	Hormion
36	Glabela
37	Supraglabela
38; 64	Inferolateral choanal corner
39; 65	Anterior edge of anterior ethmoid foramen
40; 66	Posterior edge of posterior ethmoid foramen
41; 67	Inferiormost margin of nasal aperture

The FEA results present information on absolute performance in each model, which is a useful comparison, allowing the assessment of how identical muscle forces translate into bite and joint reaction forces and cranial deformation. However, the crania differ in size, and in reality experience different muscle forces and so achieve bite forces that differ because of differences in form and applied muscle forces. To compare relative performance it is therefore necessary to take differences in size and applied muscle forces into account.

Stress is the result of a force applied over an area ($\sigma = \frac{F}{A}$) and strain ($\varepsilon = \frac{\Delta l}{l}$) scales with stress, through Hooks law (Bird and Ross, 2012). As such, lower bite forces result in lower stresses and strains at the bite point, and nearby structures. Likewise, if the bite force is lower, or even the same, but the size of the face is bigger, the stresses and strains in the face will be lower. As such, to compare relative performance, the strains experienced by the cranium, as assessed by strain contour plots and strains extracted at the landmarks, need to be scaled according to bite force and size differences. Scalings can be applied singly or in combination in explorations of the interactions between cranial size and applied muscle and resulting bite and joint reaction forces.

Although scaling of stresses and strains to account for size differences is well understood (Dumont et al., 2009), the scaling of size and shape distances in GM analysis due to size differences is not. Because both models present clear differences in size, it is important to determine how such differences impact on the magnitude of deformation as assessed by size and shape distances. Appendix A demonstrates that the size and shape distances between loaded and unloaded models scale with length (such as centroid size). It is worth noting that differences in magnitudes of deformation arise when size is varied but differences in modes of deformation arise when shape is varied. As such, scaling is only accurate when there are no shape differences between models. As shape becomes more different, modes vary more and comparison becomes less meaningful. This means that scalings for differences in size and applied muscle forces between *H. heidelbergensis* and *H. sapiens* are inevitably approximations whose validity is a function of the degree of difference in shape between them.

5.3 Results

5.3.1 Mechanical advantages

The estimated mechanical advantages are presented in table 5–3. Petralona and Kabwe 1 present similar mechanical advantages that increase, as expected, from anterior to posterior bites due to shortening of the lever arm while the muscle moment arm is kept constant. The mechanical advantages of the cadaveric *H. sapiens* are within the range of, or in the case of medial pterygoid, slightly greater than in the male sample presented by O'Connor et al. (2005) for incisor 2 biting (the only bite point calculated in that study); thus the maximum value for temporalis in O'Connor et al. (2005) is 0.307 and the mean value in this individual is 0.281; for masseter, maximum value in O'Connor et al. (2005) = 0.484, mean value in this individual = 0.4836; medial pterygoid, maximum value in O'Connor et al. (2005) = 0.469, value in this individual = 0.533. In the remaining bite points used in this study the mechanical advantages increase from anterior to posterior bites, with *H. sapiens* always presenting greater mechanical advantages than Kabwe 1 and Petralona. This indicates that it is more efficient in converting muscle forces into bite forces (Table 5-3). Table 5-4 presents the ratios of the mechanical advantages of Kabwe 1/*Homo sapiens* and Petralona/*Homo*

sapiens and confirms that this *H. sapiens* cranium consistently presents greater mechanical advantages for all muscles and bite points than either *H. heidelbergensis* crania.

5.3.2 Bite forces and force production efficiency

The bite forces predicted for Kabwe 1 are 0.51 – 0.55 of those predicted for *H. sapiens* (Table 5-5) when the same muscle forces are applied. Scaling for possible differences in muscle areas, and therefore muscle forces, using the surface area of the temporal fossa as a proxy results in a decrease in the discrepancy, but Kabwe 1 still generates lower bite forces than *H. sapiens* (0.59 – 0.65). Thus, as expected, force production efficiency is lower in Kabwe 1 than in the *H. sapiens* model, with 0.35 to 0.45 of the net applied muscle force being converted into bite force in Kabwe 1, while 0.46 – 0.65 of the muscle force is converted into bite force in *H. sapiens*. Thus, the ratio of the joint reaction forces and muscle force is larger in Kabwe 1 (0.55 - 0.65) than in *H. sapiens* (0.35 - 0.54; Table 5-6).

Table 5-3: Mechanical advantages of the main masticatory muscles in Kabwe 1, Petralona and *Homo sapiens*.

	TOOTH	TEMPORALIS (ANTERIOR)	TEMPORALIS (MIDDLE)	TEMPORALIS (POSTERIOR)	MASSETER (ANTERIOR)	MASSETER (POSTERIOR)	MEDIAL PTERYGOID
Kabwe 1	Incisor 1	0.31	0.19	0.06	0.37	0.22	0.37
	Pre-molar 1	0.39	0.24	0.08	0.47	0.28	0.47
	Pre-molar 2/Molar 1	0.42	0.26	0.09	0.51	0.31	0.52
Petralona	Incisor 1	0.28	0.20	0.07	0.35	0.25	0.36
	Pre-molar 1	0.35	0.25	0.08	0.43	0.31	0.45
	Pre-molar 2/Molar 1	0.38	0.27	0.09	0.47	0.33	0.49
Homo sapiens	Incisor 1	0.34	0.33	0.12	0.56	0.34	0.50
	Pre-molar 1	0.43	0.43	0.15	0.73	0.44	0.64
	Pre-molar 2/Molar 1	0.50	0.49	0.18	0.84	0.51	0.74

Table 5-4: Ratios of the mechanical advantages of the main masticatory muscles in Kabwe 1, Petralona and *Homo sapiens*.

	TOOTH	TEMPORALIS (ANTERIOR)	TEMPORALIS (MIDDLE)	TEMPORALIS (POSTERIOR)	MASSETER (ANTERIOR)	MASSETER (POSTERIOR)	MEDIAL PTERYGOID
Kabwe 1 / H. sapiens	Incisor 1	0.91	0.57	0.52	0.66	0.64	0.75
	Pre-molar 1	0.89	0.56	0.51	0.65	0.63	0.74
	Pre-molar 2/Molar 1	0.85	0.53	0.48	0.62	0.60	0.70
Petralona/ H. sapiens	Incisor 1	0.84	0.61	0.56	0.62	0.72	0.73
	Pre-molar 1	0.80	0.58	0.54	0.59	0.69	0.70
	Pre-molar 2/Molar 1	0.76	0.55	0.51	0.56	0.66	0.66

Table 5-5: Bite reaction forces generated by *H. heidelbergensis* (Kabwe 1) and *Homo sapiens* FE models. Unscaled, assuming identical muscle cross sectional areas and scaled using larger cross sectional areas to account for the larger area of the temporal fossa in Kabwe 1 (see text). The last row presents the ratio of bite forces between the unscaled Kabwe 1 model and that of *H. sapiens.*

Specimen	**Bite point**		
	Incisor 1	Premolar 1	Premolar 2/molar 1
Kabwe 1 (unscaled)	184.29	219.59	241.37
Kabwe 1 (scaled for surface area of temporal fossa)	217.24	258.86	284.53
Homo sapiens(unscaled)	332.60	404.29	477.23
Ratio (Kabwe1 unscaled/ *H. sapiens*)	0.55	0.54	0.51

Table 5-6: Force production efficiency calculated from the FE models of Kabwe 1 and *Homo sapiens*.

Specimen (bite point)	**Force production efficiency**	
	Fb/Fm	Fc/Fm
Homo sapiens (21)	0.46	0.54
Homo sapiens (24)	0.56	0.44
Homo sapiens (25)	0.65	0.35
Kabwe (21)	0.35	0.65
Kabwe (24)	0.41	0.59
Kabwe (25)	0.45	0.55

Fb = bite force; Fc = joint reaction forces; Fm = Total muscle force.

5.3.3 Strains

Again, as expected, visual assessment of the principal strain contour plots for the two models (Figure 5-2) shows that *H. sapiens* experiences significantly higher strains than those that arise in Kabwe 1 when the same muscle forces are applied. The difference is reduced after scaling principal strains for differences in the surface area of the face and bite force, however the scaled Kabwe 1 strains are still generally lower than in *H. sapiens*. The strain contour plots show that in both *H. heidelbergensis* and *H. sapiens* the largest strains are found in generally similar anatomical areas, such as directly above the bite points, the zygoma, the post-orbital bar and the pterygoid *fossae*. Despite these similarities, the interorbital and brow-ridge region of *H. sapiens* appears considerably more strained than that of Kabwe 1 (Figure 5-2).

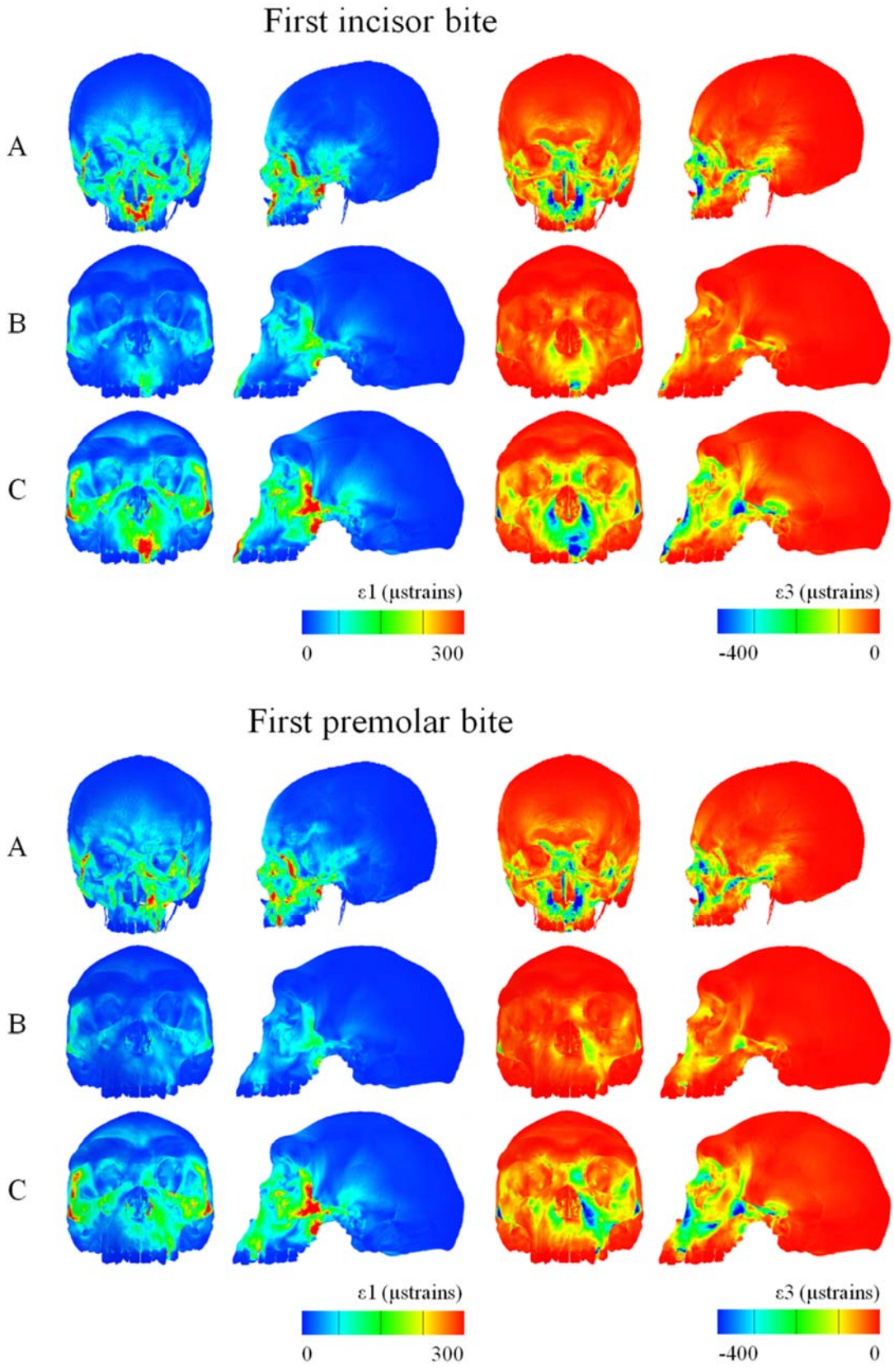
First incisor bite
A
B
C
ε1 (μstrains)
0
300
ε3 (μstrains)
-400
0
First premolar bite
A
B
C
ε1 (μstrains)
0
300
ε3 (μstrains)
-400
0

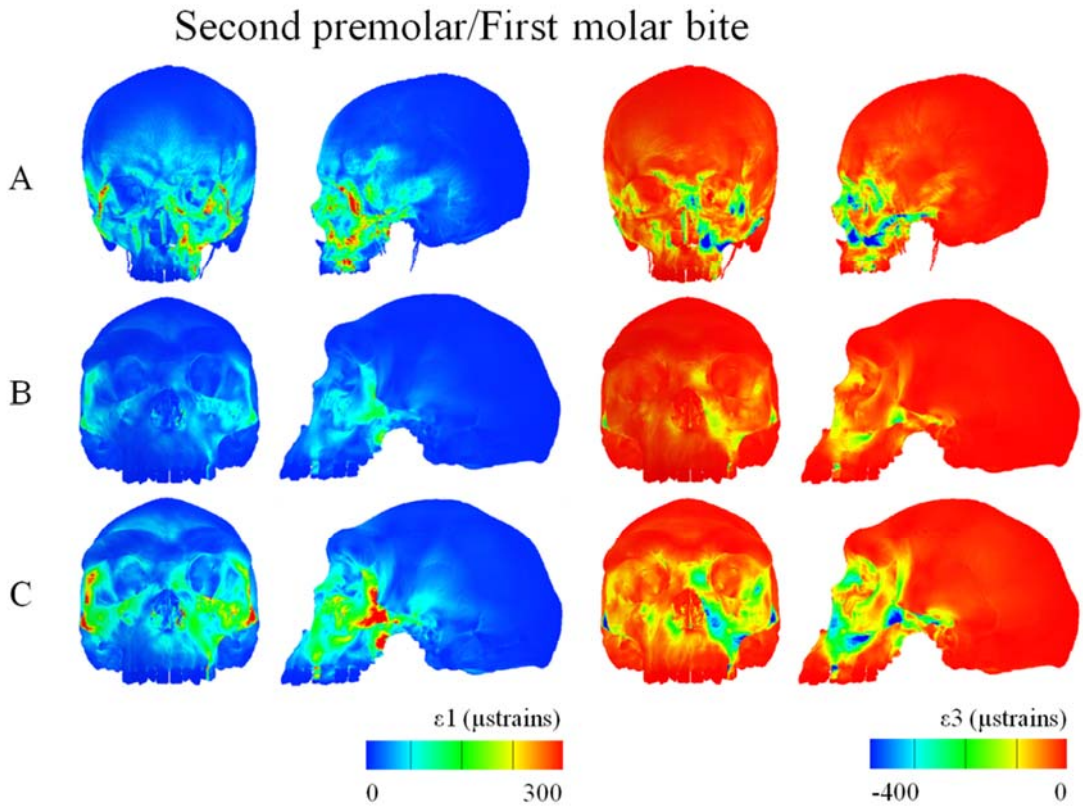

Figure 5-2: Strain contour plots of the solved FE models Kabwe 1 and *Homo sapiens*. (A) *H. sapiens*; (B) Kabwe 1 with strains unscaled; (C) Kabwe 1 with strains scaled according to bite force and size (facial surface area) differences.

As expected when the same muscle forces are applied, Kabwe 1 experiences lower strains than the *H. sapiens* model as measured at the 41 landmarked points (Figure 5-3). After scaling for facial size and bite force, differences between the models decrease markedly, but overall, Kabwe 1 still experiences lower strains than the cadaveric human model in most anatomical regions. In ε1 the exceptions are located in the nasal region (landmarks 18, 20), alveolar region (landmarks 24, 25), the palate (landmarks 28, 30) and the base of the skull (landmarks 32 – 35). In ε3 Kabwe 1 experiences higher strains mainly in the nasal region (landmarks 18, 20, 21) and the root of the zygomatic (landmark 26). The pattern of variation among landmarks in strain magnitudes is generally similar between the two models, however, as described above, some regions experience relatively higher strains in one model than in the other. These differences in relative straining between the models show that Kabwe 1 and *H. sapiens* experience, to some extent, different patterns of straining. Nonetheless, the

strains are somewhat greater overall in the human model both before and after scaling according to the ratios of facial areas and bite forces (Figure 5-2).

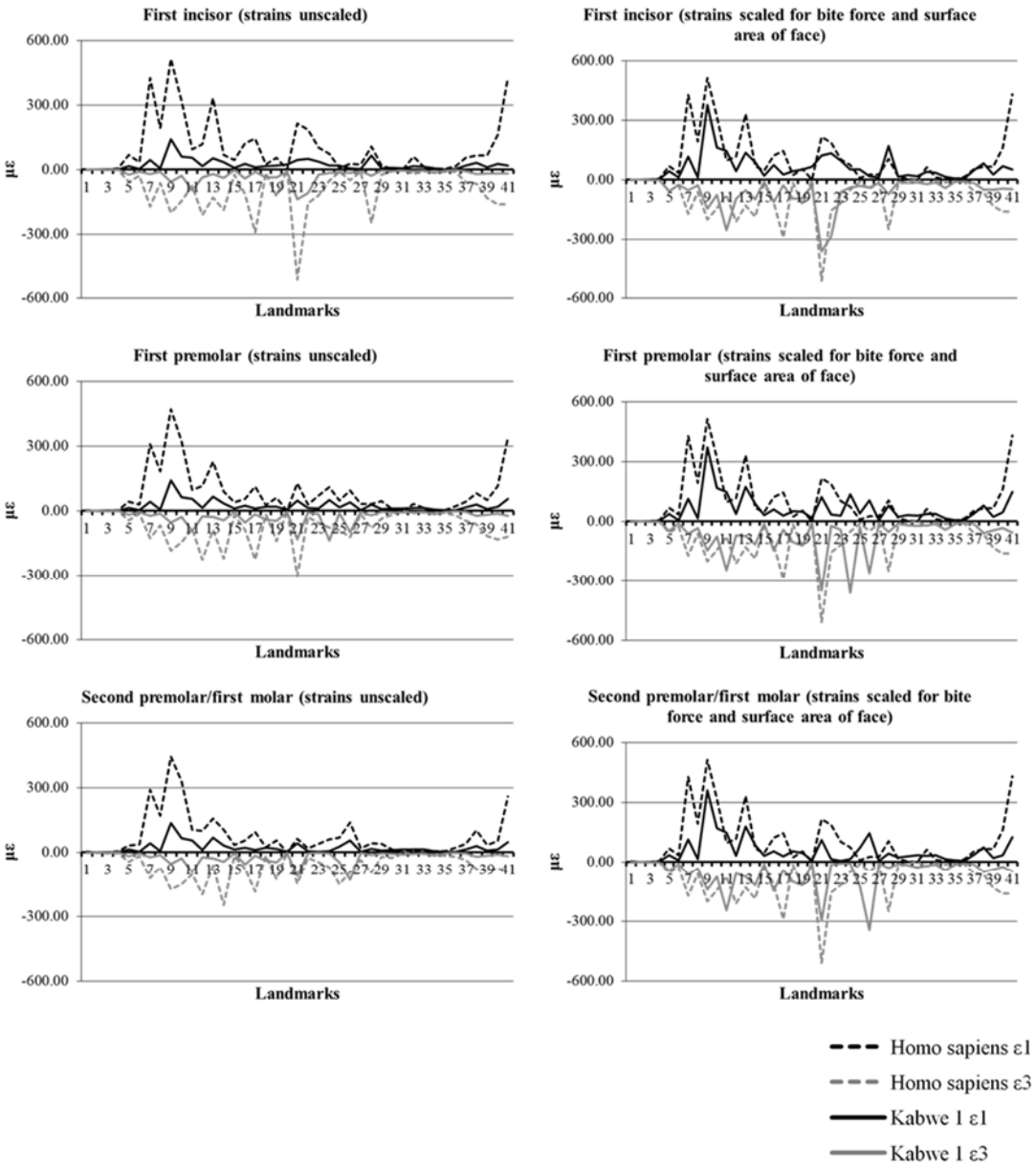

Figure 5-3: Strains experienced by the FE models at the 41 points sampled by landmarks. The strains of Kabwe 1 were scaled in the graph plots in the second column to account for differences in bite force produced and surface area of the face.

Figure 5-4 shows that, despite some similarities, the directions of the maximum (ε1) and minimum (ε3) principal strain vectors differ between the models in the different bites simulated over the infra-orbital plate, with vector directions being more

regular in Kabwe 1 than in the modern human, probably due to its more inflated and less irregular morphology.

In ε1 Kabwe 1 shows strain vectors mainly oriented along or diagonally to the transverse plane and antero-posteriorly. In the modern human there is a significantly larger proportion of vectors oriented vertically, especially in the incisor bite and over the more irregular surface regions such as the canine jugum, the canine fossa, the more angulated zygomatic root and in the supero-lateral border of the nasal cavity. In ε3 Kabwe 1 shows vectors mainly oriented vertically and diagonally with respect to the sagittal plane. In the modern human there is a significantly larger proportion of vectors oriented horizontally, once again especially in the incisor bite, with a marked transition over the more irregular areas such as the canine jugum, the canine fossa, the more angulated zygomatic root and the upper lateral border of the nasal cavity.

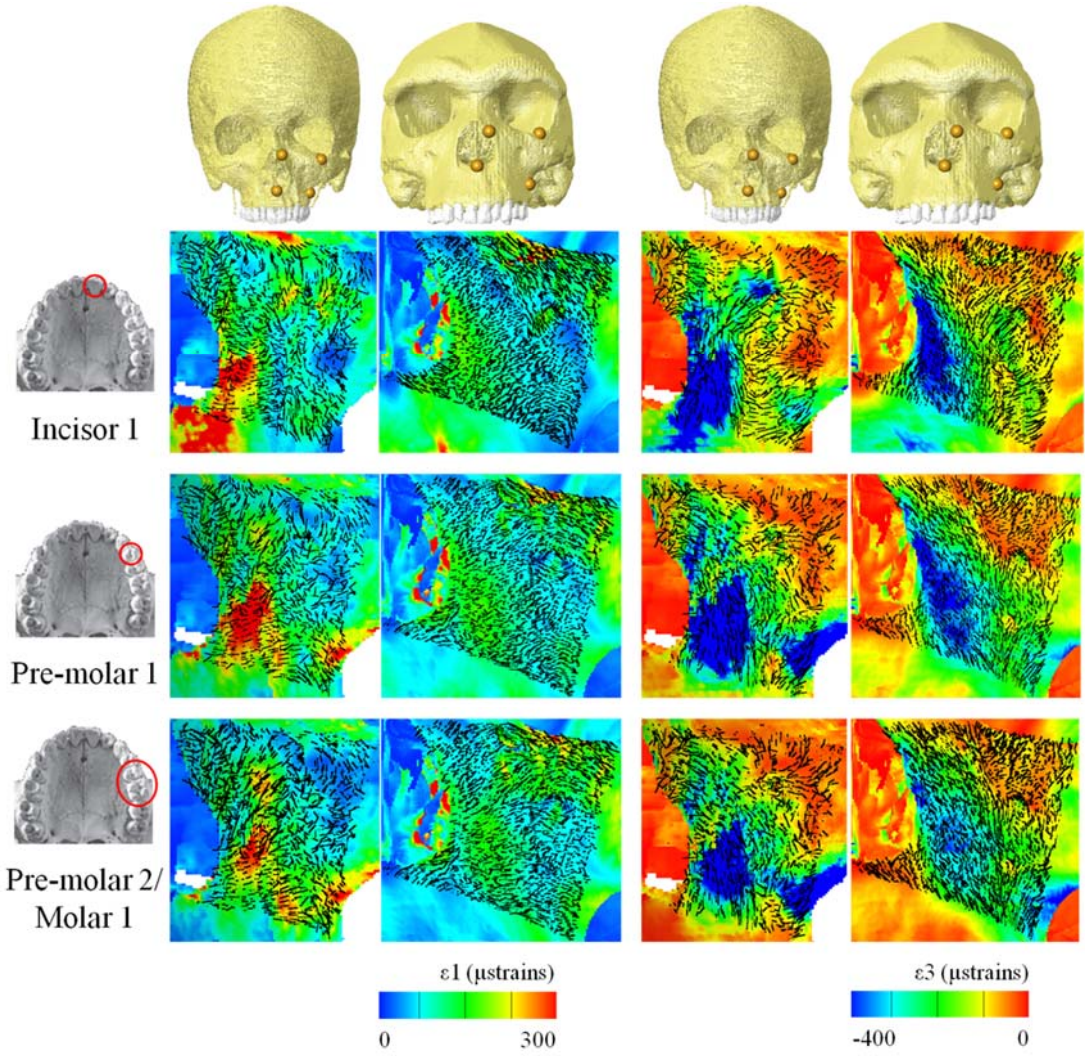

Figure 5-4: Principal strain magnitudes and directions at the infra-orbital plate in *H. sapiens* and Kabwe 1 under different simulated bites.

5.3.4 Magnitudes and modes of global deformation

In the size and shape analysis of global deformations (Figure 5-5) *H. sapiens* and *H. heidelbergensis* present different magnitudes and modes of deformation, with *H. sapiens* generally deforming more than *H. heidelbergensis* (larger distance from the mean unloaded cranium). The modern human cranium consistently presents lower PC 1 (69% of variance) values and higher PC 2 (19% of variance) and PC 3 (10% of variance) values in the same bite than Kabwe, with no overlap between the two specimens (Figure 5-5A). Warping from the unloaded cranium to the loaded crania shows that loading the central incisor causes the anterior palate to displace superiorly, resulting in shortening and widening of the nose and orbits, as well as infero-medial

deflection of the zygomatic arches. The first pre-molar bite causes infero-medial deflection of the zygomatic arches and rotation of the palate, together with the lateral margin of the nose, towards the working side (left). This results in an asymmetry between the working and balancing sides of the cranium visible in the shorter and wider left orbit. The second pre-molar bite results in deformations similar to those in the first pre-molar bite, with a more posterior location of the point where the rotation is caused in the palate (note the more posterior deflection of the palate and dental arcade in this bite than in the PM 1 bite in Figure 5-5A). Figure 5-5B shows differences in deformation during the same simulated bites in Kabwe 1 (reference) and the modern human (target). Since these diagrams show differences in deformation they should be read as follows: relative to Kabwe 1, the modern human presents more inferior deflection of the zygomatic arches in posterior biting and greater deformation of the external aspect of the nasal cavity (less so in anterior bites). In the first incisor bite, *H. sapiens* develops less anterior displacement of the subnasal region (seen as a relative infero-posterior displacement of the grid). In P^1 and P^2/M^1 bites the *H. sapiens* cranium also shows more rotation/deformation of the palate about the antero-posterior axis, i.e. more vertical displacement of the working side (seen in the higher position of the canines and in the superior deflection of the transformation grid in this region).

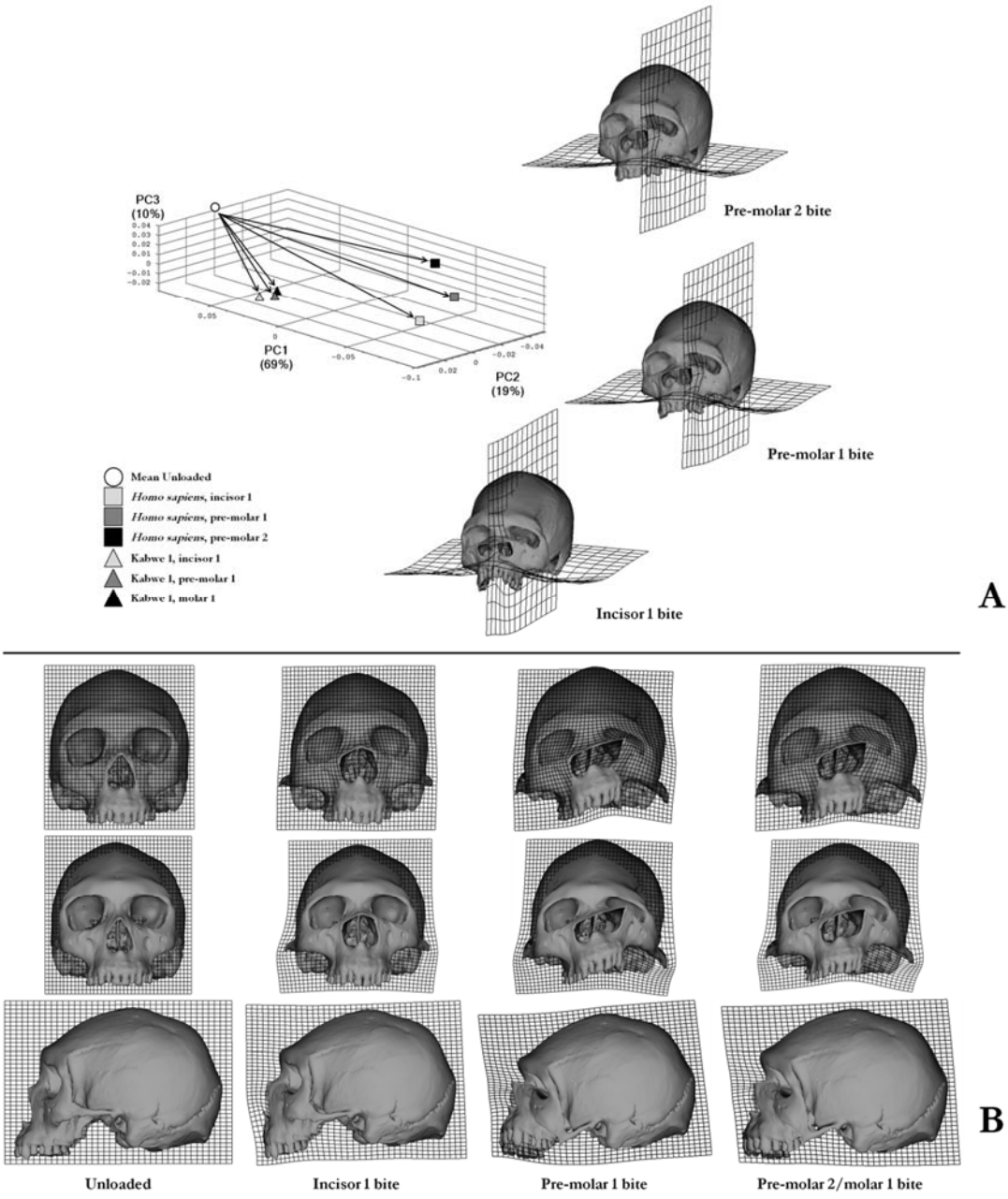

Figure 5-5: Size and shape analysis of modes and magnitudes of deformation of the models with the magnitudes of deformation of Kabwe 1 scaled according to the ratios of bite forces and facial centroid sizes. Reference cranium used for warpings is the mean unloaded cranium calculated from the unloaded Kabwe 1 and *H. sapiens* crania; (A) Size and shape PCA plot with warpings of different load cases of *H. sapiens* relative to the mean unloaded model; (B) Surface warpings with transformation grids located at the nasal cavity (first row), zygomatic arches (second row) and midline (third row) illustrating the differences in deformation due to biting between Kabwe 1 (reference) and *H. sapiens* (target). Warpings in 5-6A magnified by a factor of 500 and 5-7B by a factor of 1000 to facilitate visualization.

5.4 Discussion

The present comparisons of mechanical advantages and force production efficiencies show that *H. sapiens* is more efficient at converting muscle force into bite force than *H. heidelbergensis*. This is because the retracted and orthognathic face of *H. sapiens* shortens the bite out-lever relative to the muscle in-lever arms of *H. heidelbergensis*, as has previously been found by Eng et al. (2013). This is similar to the findings of previous studies comparing *H. sapiens* and *H. neanderthalensis* (Antón, 1990; O'Connor et al., 2005). Consistently, it was found that a greater proportion of muscle force is converted into bite reaction forces and less into reaction forces at the glenoid fossa in *H. sapiens* than in Kabwe 1. Also consistent with what was found by Eng et al, (2013), the predicted bite forces of *H. sapiens* are considerably higher than those for *H. heidelbergensis*. When the same muscle forces are applied, bite forces estimated for Kabwe 1 range from 184.29 N to 241.37 N, whereas those estimated for *H. sapiens* range from 332.60 N to 477.23 N, and so 80% - 98% greater than in Kabwe 1. These comparisons do not take into account differences in muscle forces that may have existed between *H. heidelbergensis* and *H. sapiens*. To do so the forces in Kabwe 1 need to be estimated. However, as noted earlier, this can only be done crudely based on scaling of the forces in *H. sapiens*, with the assumptions that temporal fossa area predicts muscle cross sectional area (which it likely does not, see Toro-Ibacache et al., 2015b) and that a similar relationship is present among the cross sectional areas of the different masticatory muscles in the two individuals. This noted, the surface area of the temporal fossa is only 18% bigger in Kabwe 1 than in *H. sapiens*, suggesting that the temporalis in Kabwe 1 has the potential to generate bite forces about 18% higher than modelled. Error in this estimate of the temporalis anatomical cross sectional area, together with the larger than average medial pterygoid mechanical advantage in the modern human, likely impact on the estimates derived here for the differences in predicted bite forces between *H. heidelbergensis* and *H. sapiens*. However, even when considering these differences, our simulation of Kabwe 1 biting still generates bite forces that are lower or, at best, nearly as high as those of *H. sapiens*.

Hence, the results show that Kabwe 1 was unable to generate higher bite forces than modern humans. Because Kabwe 1 produces lower (or equivalent, at best) bite forces than the modern human and because it has larger molars (approximately 20%

larger molar occlusal area, based on measurements of the two first molars), it presents a lower ratio of bite force/molar occlusal area. Demes and Creel (1988) show that occlusal molar area correlates with bite force, thus, according to this association, it would be expectable to find that modern humans would produce lower bite forces than *H. heidelbergensis*. In contrast, Lucas demonstrates an association between food items material properties and occlusal area. Thus, these results might reflect technological differences in food preparation prior to ingestion, consistently with Eng et al. (2013) and Zink and Lieberman (2016).

The predicted lower strain magnitudes in the face of Kabwe 1 arise not only because of lower bite forces but also because of size differences. As previously reported (Freidline et al., 2012), the face of Kabwe 1 is significantly bigger (about 40%, in surface area) than the face of *H. sapiens*. When strains were scaled according to the ratio of facial surface areas and predicted bite forces the discrepancies between Kabwe 1 and *H. sapiens* were markedly reduced but the predicted principal strain magnitudes were still generally greater in *H. sapiens*, with localized exceptions. This suggests that Kabwe 1 was better able to resist biting forces than *H. sapiens*. This is likely due to the generally robust skeleton of Kabwe 1 and to architectural differences similar to those reported between *H. sapiens* and Neanderthals as being linked to resisting dental loading (Rak, 1986; Demes, 1987). Those anatomical differences include the taller sub-nasal and infra-orbital regions found in Kabwe 1, and the more sagittally orientated and convex infra-orbital plate. These morphological differences may well also be related to the differences found in strain directions.

The GM size and shape analysis of global magnitudes and modes of deformation (Figure 5-5) shows that *H. sapiens* deforms differently and to a greater degree than Kabwe 1. This is consistent with the strain contour plots and graphs (Figure 5-2, Figure 5-3) which show differences in which regions experience high and low strains as well as the generally larger strain magnitudes in *H. sapiens* than in Kabwe 1, even when differences in size and bite forces are accounted for.

It should be noted that this study compares two individuals, and does not consider how variation in each species impacts on biting performance. However, the clear morphological differences between *H. heidelbergensis* and *H. sapiens* make it likely that within species variations do not account for what is observed. The present findings are consistent with previous studies that have compared *H. sapiens* with *H. heidelbergensis* and Neanderthals, in that modern humans appear more efficient at

converting muscle forces into bite forces due to a retracted and orthognathic face (Antón, 1990; O'Connor et al., 2005; Lieberman, 2008; Lieberman, 2011; Eng et al., 2013). Antón (1990) and Eng et al. (2013) find that *H. sapiens* is able to produce higher absolute bite forces than Neanderthals, while O'Connor et al. (2005) estimate that Neanderthals generate higher absolute bite forces than recent gracile modern humans and comparable to early and recent robust *H. sapiens* because of increased muscle forces. Somewhat counter intuitively facial reduction in *H. sapiens* which increases mechanical efficiency in bite force generation is accompanied by our face being less able to resist masticatory, or para-masticatory, functional loading (Rak, 1986; Demes, 1987; Lieberman, 2008; Lieberman, 2011). This, together with a decrease in the proportion of fast twitch muscle fibres (Stedman et al., 2004) relative to apes and size reduction of masticatory muscles (Demes and Creel, 1988; Antón, 1990; O'Connor et al., 2005) led Lieberman (2008) to propose that the increased mechanical advantages in *H. sapiens* are likely a spandrel (*sensu* Gould and Lewontin, 1979) rather than an adaptation.

Despite being modular, the human head is also a highly complex and integrated structure that performs multiple functions (Bastir and Rosas, 2005; Lieberman, 2008; Lieberman, 2011). This implies that evolutionary and adaptive changes in one component of the cranium impact on other components (Lieberman, 2008; Lieberman, 2011). As such, changes in facial morphology throughout hominin evolution have been related to multiple factors, including expansion of the brain and an increased cranial base angle (Enlow and Hans, 1996; Lieberman et al., 2002; Lieberman, 2008; Lieberman, 2011), thermoregulation and air conditioning (Coon, 1962; Wolpoff, 1968; Carey and Steegmann, 1981; Franciscus and Trinkaus, 1988), pre-processing of food (Carlson, 1976; Carlson and Van Gerven, 1977), stabilization of the head during running (Lieberman, 2008; Lieberman, 2011) and size reduction of the dentition (Brace, 1967; Brace and Mahler, 1971; Brace et al., 1987). Distinguishing the possibilities that facial reduction, retraction and orthognathy are the outcomes of positive selection and adaptation from the alternative that they are an evolutionary by-product (Gould and Lewontin, 1979; Lieberman, 2008; Lieberman, 2011) is therefore extremely difficult. In addition, genetic drift has also been suggested to impact on the overall cranial morphology of early *Homo* (Ackermann and Cheverud, 2004) and in modern humans, albeit less so in specific anatomical regions such as the nose (Roseman and Weaver, 2004) which fulfil functions related to metabolic aerobic demands (Lindsay, 1996;

Bastir and Rosas, 2013), olfaction (Lindsay, 1996; Bastir and Rosas, 2013), thermoregulation (Trinkaus, 1987a; Dean, 1988; Franciscus and Trinkaus, 1988) and conditioning of respired air (Franciscus and Long, 1991; Yokley, 2009; Lieberman, 2011; Noback et al., 2011).

Reduction of the size of the nasal cavity in *H. sapiens* inevitably impacts on mid-facial morphology and therefore in biting performance. This reduction may have arisen through selection, although it is not clear what the selective pressure might have been. Alternatively a large mid-face and tall, deep nasal cavity may have been positively selected for in archaic *Homo* and a large nasal cavity required either for air conditioning or to accommodate the metabolic demands of a possibly larger body in archaic taxa relative to *H. sapiens* (Yokley et al., 2009; Lieberman, 2011; Churchill, 2014; but see Elliot et al., 2014 and Heyes and MacDonald, 2015 for limitations of body mass estimation from skeletal elements) might have constrained (Reif et al., 1985) the functioning of the masticatory system. Thus a larger mid-face leads to mechanical advantages of the masticatory muscles in *H. heidelbergensis* that are less than those in subsequent *H. sapiens*, where this constraint is released. If the morphology of the nose was indeed constrained in *H. heidelbergensis* and the constraint was released in *H. sapiens*, enabling mid-facial retraction, then the increased biting force production efficiency of modern humans would be a by-product of changes in mid facial morphology.

Another possible anatomical consequence of mid-facial reduction in *H. sapiens* is the development of the chin. The morphology of the mandibular symphysis and the appearance of the chin have been associated with multiple factors, such as size reduction of the dentition (Wolff, 1984), sexual dimorphism (Horowitz and Thompson, 1964; Thayer and Dobson, 2010), and the development of speech (Ichim et al., 2007b). A compelling idea is that the chin and the morphology of the human mandibular symphysis are related to mechanical demands that arise during biting and mastication (Daegling, 1993; Dobson and Trinkaus, 2002; Groning et al., 2011b). However, recent studies suggest that the human symphysis and chin are not optimized to resist masticatory system loads (Holton et al., 2014; Holton et al., 2015; Pampush and Daegling, 2015). These studies raise the question of if the modern human chin and symphysis do indeed represent adaptations, or are a by-product of facial reduction (with or without secondary mechanical consequences) or the result of genetic drift. In a recent study Pampush (2015) excluded the effect of genetic drift as cause for

appearance of the chin in *Homo*, but was unable to differentiate between an adaptation or an evolutionary by-product (spandrel).

Regardless of whether facial retraction in *H. sapiens* is an adaptation to increase efficiency in generating bite forces, a by-product of other adaptation(s) or the product of genetic drift, it is clear that the masticatory system more efficiently converts muscle into bite forces, yet is less well able to resist these forces.

The next chapter assesses the mechanical significance of the frontal sinus and how the mechanics of biting impacts on its morphogenesis.

6 The biomechanical significance of the frontal sinus in Kabwe 1

6.1 Introduction

The human skull presents four sets of sinuses (maxillary, ethmoidal, sphenoidal and frontal), that are defined according to the position of the *ostium* in the nasal cavity and named by the bones they pneumatise (Rae and Koppe, 2004). These hollow spaces in the skull start primary pneumatization by expanding into the cartilage walls of the nasal *fossae* as early as 10 weeks post conception but develop at different times, by a two stage process (Sperber, 2001; Rae and Koppe, 2004; Smith et al., 2005; Rossie, 2006). Primary pneumatization occurs pre-natally and gives rise to nasal recesses that later develop into proper sinuses via secondary pneumatisation (Smith et al., 2005; Rossie, 2006). The former consists of interstitial growth in the cartilaginous nasal capsule with no expansion to contiguous structures. Secondary pneumatisation occurs via invasion of adjoining bones by osteoclasts and subsequent resorption (Smith et al., 2005; Rossie, 2006).

The frontal sinus begins its primary pneumatization at 3 - 4 months post-conception by developing mucosal epithelial invaginations in the frontal recess of the middle meatus of the nasal fossa (Sperber, 2001). Secondary pneumatization occurs between 6 months and 2 years through invasion of the frontal bone by populations of osteoclasts derived from the anterior and middle groups of the ethmoidal sinuses (Scheuer and Black, 2000; Sperber, 2001; Lieberman, 2011) and its subsequent growth results from resorption on the inner and deposition on the outer surfaces of the frontal bone tables, resulting in cortical drift (Tillier, 1977; Lieberman, 2011). The inner table integrates the functional matrix of the brain, adapting to it as it grows (Moss and Young, 1960). As such, by about 6 years of age the internal table of the frontal bone presents approximately 95% of its total growth (Lieberman, 2011). On the other hand, the external table, at the level of the brow-ridge and frontal sinus, presents a somatic growth pattern (Lieberman, 2011). As frontal sinus development is thought to be secondary to drift of the external table of the frontal bone (Lieberman, 2011) it completes development after puberty, at the end of which the external table of the frontal presents approximately 95% of its total growth (Tillier, 1977; Lieberman, 2011).

Among catarrhines, the frontal sinus is only present in African apes (Cave and Haines, 1940) and it has, therefore, been interpreted as a synapomorphy of the group (Rae and Koppe, 2004). In humans it presents significant intra and inter population

form variation (Buckland-Wright, 1970; Tillier, 1977) and may present high frequencies of absence in specific populations (Koertvelyessy, 1972; Greene and Scott, 1973). Fossil hominins also present significant form variation, with some individuals presenting small frontal sinuses that are restricted to the region immediately behind the glabella. Other individuals show extremely enlarged sinuses that extend laterally beyond the supraorbital arch and supero-posteriorly invading the fontal squama, such as Steinheim and Petralona (Seidler et al., 1997; Prossinger et al., 2003; Zollikofer et al., 2008).

Despite multiple studies, sinuses are still poorly understood (Seidler et al., 1997; Laitman, 2008; Márquez, 2008). Some researchers state that they serve no particular function and are biological spandrels arising as a structural consequence of changes in other bones and/or structures (Enlow, 1968; O'Higgins et al., 2006; Zollikofer et al., 2008; Zollikofer and Weissmann, 2008) rather than because of a specific mechanism acting to create them. Irrespective of how formed, others have suggested that sinuses have one or more functions, such as olfaction, respiration, thermoregulation, nitric oxide production, voice resonance, reduction of skull weight and craniofacial biomechanics (Tillier, 1977; Blaney, 1990; Bookstein et al., 1999; Rae and Koppe, 2004; Laitman, 2008; Lundberg, 2008; Márquez, 2008). These views are not necessarily opposed since a ‘spandrel’ might subsequently take on a function.

As with most biological structures (Lesne and Bourgine, 2011), the morphogenesis of the frontal sinus is likely impacted by multiple factors. One such factor, that has been suggested to determine the morphology of the upper face, and so the morphogenesis of the brow-ridge and frontal sinus, is the spatial relationship between the eyes and the brain. This spatial hypothesis predicts that if the eyes are significantly anteriorly positioned relative to the brain then big brow-ridges develop to fill the ‘gap’ and frontal sinuses develop within them (Moss and Young, 1960). Even though this hypothesis is widely accepted, other studies have examined the extent to which paranasal sinus morphology is also impacted by environmental conditions and air conditioning by investigating possible associations in humans, other primates and non-primates, between sinus size and environmental conditions. It was found that human individuals from latitudes with colder temperatures present smaller frontal (Koertvelyessy, 1972) and maxillary sinuses (Shea, 1977). Macaques (Rae et al., 2003) and rats (Rae et al., 2006) from cold climates also present smaller maxillary sinuses, but this decrease in size is associated with increased nasal cavity size. Thus, maxillary

sinus size appears to vary secondarily to nasal size, leading researchers to conclude that sinuses are not directly involved in air conditioning (Shea, 1977; Rae et al., 2003; O'Higgins et al., 2006; Rae et al., 2006).

Several studies suggest that masticatory mechanics impacts on sinus morphology, and thus on its morphogenesis. Witzel and Preuschoft (2002) and Witzel (2011) used FEA and modelled the cranium as a block to investigate how the mechanics of the masticatory system impact on skull morphology. They found that the infilled regions where the sinuses are located experience low stresses and strains when compared to other regions of the craniofacial complex. Because bone adapts to the mechanical environment (Currey, 2006) these hollow spaces might be the consequence of biomechanical bone adaption to these low stresses, enabling the cranium to resist mechanical loading with minimum bone material (Witzel and Preuschoft, 2002; Witzel, 2011). The idea that sinuses occupy regions of low stress and so have no specific mechanical role is supported by the work of Fitton et al. (2015) who noted minimal effects on facial strains during FEA simulated biting in a macaque when the maxillary sinus is infilled. Bookstein et al. (1999) and Prossinger et al. (2000) proposed that the morphology of the frontal sinus in the Petralona skull, the thin internal and external tables of the frontal bone in the brow-ridge area and the presence of a lamella honeycomb-like structure in the sinus, are evidence that bone adapted to masticatory function by reducing bone material and increasing stiffness (Bookstein et al., 1999; Prossinger et al., 2000). In contrast, Greene and Scott (1973) suggest that the 95% frequency of frontal sinus absence in the Wadi Halfa Mesolithic population is the result of high masticatory mechanical demands.

However, several researchers refute an association between sinus morphology and biomechanical loading. One of the main arguments has been that circumorbital structures, such as the brow ridge and frontal sinus, experience very low magnitude stresses and/or strains during masticatory system loading, thus precluding mechanical bone adaptation to masticatory loading (Picq and Hylander, 1989; Hylander et al., 1991b; Ravosa et al., 2000c; Hylander and Johnson, 2002). Rae and Koppe (2008) demonstrated that maxillary sinus volume is not significantly different between the frugivore *Cebus albifrons* and the hard object feeder *Cebus apella* which are closely phylogenetically related. Thus, sinus size appears to be independent of different diets that lead to different masticatory system loads.

Irrespective of the putative functions of sinuses, the present study addresses the biomechanical significance of the frontal sinus in Kabwe 1, and if masticatory system mechanical loading might impact on its morphogenesis based on the principle of bone adaptation to loads. This cranium displays a very prominent brow ridge and a very well developed frontal sinus which presents a honeycomb-like structure within it. This is similar to the Petralona skull in which the honeycombing is said to reflect loading history (Seidler et al., 1997; Bookstein et al., 1999; Prossinger et al., 2000). Finite Element Analysis (FEA) is used in order to test the following hypotheses: (1) removing the honeycomb-like structure has limited to negligible impact on strain magnitudes and directions experienced by the cranium during simulated biting; (2) infilling the frontal sinus has limited to negligible impact on strain magnitudes and directions experienced by the cranium. Based on the previous research of Witzel and Preuschoft (2002) and Witzel (2011) it is predicted that infilling the sinus will not have a meaningfull impact on the deformations experienced by the cranium. Conversely, based on previous research that hypothesize the honeycomb-like structure found within the frontal sinus of the Petralona cranium relates to loading history (Seidler et al., 1997; Bookstein et al., 1999; Prossinger et al., 2000), it is predicted that hollowing the sinus will have a meaningful impact on the deformations experienced by the cranium. Because the exact magnitudes of deformation that trigger bone deposition or resorption are not clear (Skerry, 2000; Currey, 2006), and because the FE model likely underestimates the absolute magnitudes experienced by the cranium during masticatory loading to varying degrees (see chapter 2), it is not possible to define exactly what negligible or meaningful impacts are on strain magnitudes experienced by the models (i.e. what increase or decrease in strain magnitudes would be necessary to trigger bone deposition or resorption). Thus, meaningful or negligible impacts are considered within the strain magnitudes experienced by this model. An impact is considered meaningful if strains in the relevant region (material infilling the frontal sinus, walls of the sinus and surrounding structures, such as the frontal bone) increase to a magnitude that approximates the highest strains experienced by the model (e.g. near the bite point or muscle origins). An impact is considered small or negligible if strains do not increase considerably and remain noticeably below the maximum strains experienced by the model.

6.2 Materials and Methods

The Kabwe 1 skull was virtually reconstructed based on a CT scan of the fossil that was provided by the NHM, London (courtesy of Robert Kruszynski). A brief description of the reconstruction follows below, but the detailed description is presented on chapter 4. After reconstruction the anatomy of the frontal sinus was modified. The unmodified and modified reconstructions were then directly converted into voxel based finite element models. These were used to simulate three different bites (left central incisor, left second premolar, left second molar) to assess the biomechanical performance of the facial skeleton with and without an infilled frontal sinus during biting.

6.2.1 Skull reconstruction and model creation

A medical CT stack with originally anisometric voxel size (0.4687501 x 0.4687501 x 1 mm) was resampled to produce isometric voxels (0.35 mm.). Automated, semi-automated and manual segmentation of the cranium was then performed using Avizo® (version 7.0). Manual segmentation was required to exclude from the model sedimentary matrix present in the maxillary and sphenoidal sinuses. Despite outstanding preservation, several anatomical regions of the cranium required reconstruction to repair damage from taphonomic and pathological processes. These include the alveolar regions of the maxilla, the right and left temporal bones, the occipital, the right parietal, the sphenoid, the orbital region of both *maxillae* and several teeth. Where possible, reconstruction was performed by mirroring preserved contralateral elements and warping them to existing structures. When small gaps were present, Geomagic® (Studio 2011) was used to fill them using the surface of the surrounding present structures as the reference for interpolation. Portions of a cadaveric *Homo sapiens* skull were used to reconstruct part of the occipital and missing tooth crowns where no antimeres were present.

Once the reconstruction was complete (model 2), the honeycomb-like structure of the frontal sinus was removed (model 1) and the sinus was completely infilled (model 3) (Figure 6-1). Voxel based finite element models were then generated by direct conversion using the bespoke vox2vec software tool and imported into VoxFE to be loaded and constrained (Fagan et al., 2007).

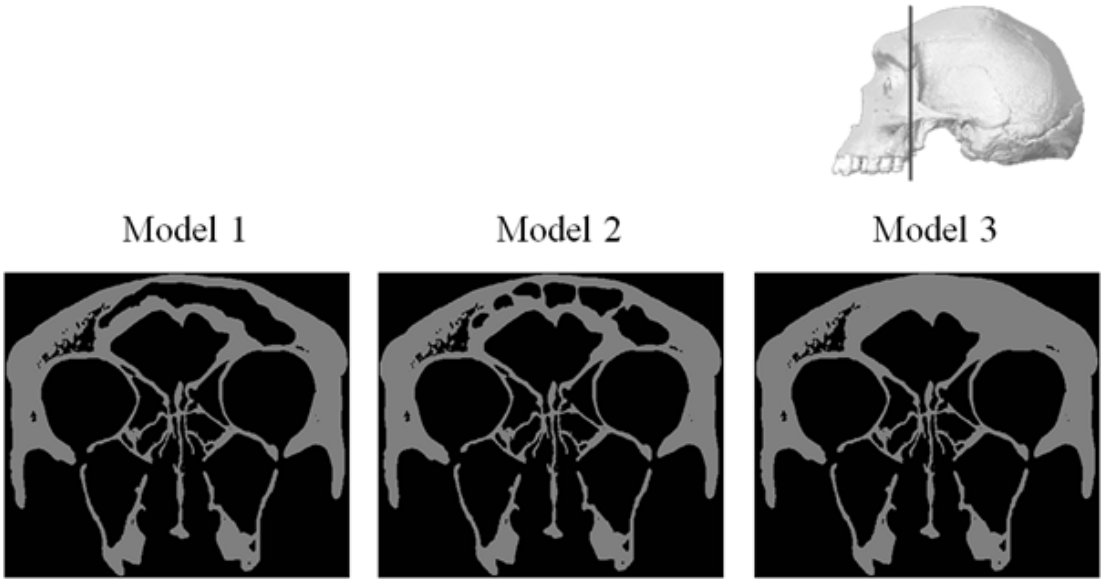

Figure 6-1: Coronal cross-section of models 1 - 3 used in biting simulations. Model 1 presents a hollow frontal sinus in which the original bony struts were removed; Model 2 presents the original frontal sinus with bony struts as captured by the CT scanner; Model 3 presents an infilled frontal sinus.

6.2.2 Constraints

Identical constraints were applied to all models using the finite element analysis software VoxFE (Fagan et al., 2007). They were constrained at each temporo-mandibular joint (24 nodes in the x, y and z axis) and a third constraint was applied successively at each of the bite points (left central incisor, left second pre-molar, left second molar; 21 nodes in the z axis). These are used to fix the cranium in space and to reflect the loading of the temporo-mandibular joints and teeth during biting.

6.2.3 Material properties

Prior sensitivity studies on a cadaveric human head (chapter 3) and in the cranium of *Macaca fascicularis* (Fitton et al., 2015) have shown only minor and localised effects when the same material properties (of cortical bone) are equally applied to cortical bone, trabecular bone and teeth, rather than their own specific material properties. These studies show that, with the exception of the alveolar bone, model simplification results in similar spatial distributions of regions experiencing high

and low strain magnitudes but, strain magnitudes are reduced on average. Simplification results in a 'stiffer' model that deforms less but in a similar way (mode of deformation) to a more complex model that distinguishes the material properties of cortical bone, trabecular bone and teeth. This is relevant to the present study because trabecular bone is neither well preserved nor imaged at sufficient resolution in the fossil to accurately distinguish it from cortical bone in a finite element model. Thus in the present study, teeth and trabecular bone were assigned the same material properties as cortical bone in all the models. Cortical bone, trabecular bone and the teeth were allocated isotropic properties, with a Young's modulus of 17 GPa and a Poisson's ration of 0.3. The modulus of elasticity was derived from nanoindentation studies of cortical bone in a cadaveric *Homo sapiens* skull (Toro-Ibacache et al., 2016a) following the protocol of Kupczik et al. (2007). The resulting value of 17 GPa is within the range of values found in previous studies (Dechow et al., 1993; Schwartz-Dabney and Dechow, 2003).

6.2.4 Muscle loads

Loads were applied to the model to simulate the actions of six muscles active during biting: right and left temporalis, right and left masseters, right and left medial pterygoids. Lack of the mandible precludes direct estimation of the direction of muscle force vectors and the use of bony proxies to estimate anatomical cross sectional areas (and so maximum forces) of muscles that attach to the mandible (masseter and medial pterygoid). However, given that three versions of the same model are to be compared, it matters little that applied muscle force vectors approximate rather than replicate physiological loadings. Much more important is that these forces are identical between models and so do not, in themselves, produce differences in strains (modes and magnitudes of deformation) between models. As such the maximum estimated muscle forces from a *Homo sapiens* cadaveric head were applied identically to each model (Toro-Ibacache, 2016a; Table 6-1). The directions of muscle force vectors applied to all models were estimated by scaling a *Homo neanderthalensis* mandible (Tabun 1 specimen) to the Kabwe 1 skull to provide estimates of the locations of muscle attachments on the mandible.

Table 6-1: Forces applied by each muscle (in Newtons).

Muscle	Side	
	Left	Right
Temporalis	168.02	170.67
Masseter	134.06	124.01
Medial pterygoid	124.01	117.49

6.2.5 Model solution and data analysis

The finite element models were solved using VoxFE. Analysis and comparison of the results employed three different approaches. (1) qualitative assessment of: (1a) maximum (ε1) and minimum (ε3) principal strain magnitudes throughout the cranium surface; (1b) maximum (ε1), medium (ε2) and minimum (ε3) principal strain magnitudes through a mid-sagittal cross section; (1c) directions of ε1 and ε3 over the external surface of the frontal squama. (2) quantitative comparison of ε1 and ε3 magnitudes at 42 points located on the surface of the frontal bone and 30 on the surface of the facial skeleton that are common to all models (Figure 6-2). (3) analysis of global modes of deformation of the cranium was assessed by Geometric Morphometrics (GM), using 67 landmarks on the craniofacial skeleton (Table 6-2). Method 1 relies on visual assessment of changes in the strain contour plots and of the directions of the vectors. Method 2 quantitatively compares strain magnitudes by plotting magnitudes arising from each simulated bite. Method 3 employs geometric morphometrics to compare changes in size and shape between the unloaded and loaded models. This consists of an initial generalized Procrustes analysis, followed by rescaling by centroid size. This is followed by a PCA of the resulting size and shape coordinates (O'Higgins, 2000; Zelditch et al., 2004). This analysis leads to a quantitative appraisal of differences in global model deformations (changes in size and shape) in terms of modes and magnitudes of deformation arising from loading.

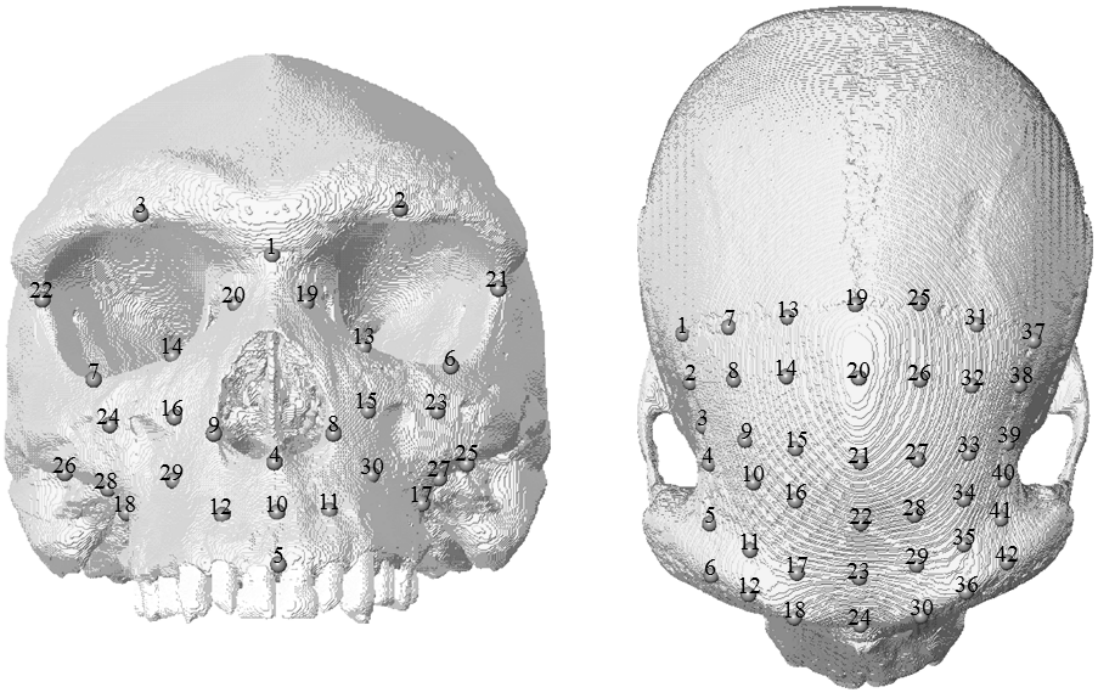

Figure 6-2: 30 facial points (left) and 42 points in the frontal bone (right) used for extraction of ε1 and ε3 and biomechanical performance comparison among models.

Table 6-2: Landmarks used in the GM analysis of modes of deformation.

Number	Landmark
1	Bregma
2	Lambda
3	Inion
4; 42	Asterion
5; 43	Porion
6; 44	Pterion
7; 45	Frontomalare orbitale
8; 46	Frontomalare temporale
9; 47	Jugale
10; 48	Zygotemporale superior
11; 49	Zygotemporale inferior
12; 50	Maxillofrontale
13; 51	Zygoorbitale
14; 52	Zygomaxillare
15; 53	Superior rim of orbit
16; 54	Infraorbital foramen
17	Nasion
18	Rhinion

19; 55	Lateral Nasal Suture
20	Nasospinale
21; 56	Alare
22	Alveolare
23; 57	External Alveolar Incisor 2
24; 58	External Alveolar Canine
25; 59	External Alveolar Premolar4
26; 60	Zygomatic take-off
27; 61	Inferior Distal Alveolar
28	Incisive Foramen
29	Palate maximum
30	Staphylion
31; 62	Infratemporal crest
32	Basion
33	Opisthion
34; 63	Lateral Edge of Foramen Magnum
35	Hormion
36	Glabela
37	Supraglabela
38; 64	Inferolateral choanal corner
39; 65	Anterior edge of anterior ethmoid foramen
40; 66	Posterior edge of posterior ethmoid foramen
41; 67	Inferiormost margin of nasal aperture

6.3 Results

The strain contour plots (Figure 6-3 and 6-5), the contour plots with overlain strain vector directions (Figure 6-4) and the strain magnitudes extracted from the 42 points in the frontal bone and the 30 points in the face (Figure 6-6) consistently show that hollowing out or infilling the frontal sinus impacts little or not at all on strain magnitudes and has little or no impact on the strain directions experienced by the cranium when simulating each of the three different bites.

Thus, the strain contour plots are very similar for each of the bites, with no marked differences, both in ε1 and ε3, between the models with a completely hollow frontal sinus (model 1) and a frontal sinus with trabeculae forming a honeycomb-like structure (model 2). Slight, localized decreases in strain magnitude are observed between the hollow and honeycomb models and the infilled sinus model. This is

apparent in the outer table of the frontal bone for ε1 (Figure 6-4). It should also be noted that in the infilled sinus model strain magnitudes are consistently low within the material infilling the sinus during all simulated bites (Figure 6-5). These results are consistent with the plots of strain magnitudes extracted from the frontal bone, with models 1 and 2 almost completely overlapping both in ε1 and ε3. Again as in the strain contour plots, model 3 shows a decrease in the strain magnitudes experienced along, and close to, the midline of the frontal bone (Figure 6-6), however when considering the full range of strain magnitudes experienced by the cranium this decrease is proportionately very small. Changes in the frontal sinus have even less, indeed almost no, impact on the strain magnitudes extracted from the face (Figure 6-6).

Figure 6-4 shows that hollowing or infilling the sinus has little or no impact on vector directions in ε1 in all bites, with vectors being mainly oriented in the coronal plane with an increasingly larger proportion of vectors oriented diagonally to the coronal plane in posterior biting. In ε3 changing the sinus has little effect, with vectors predominantly oriented along the sagittal plane in anterior biting and diagonally to it in posterior bites.

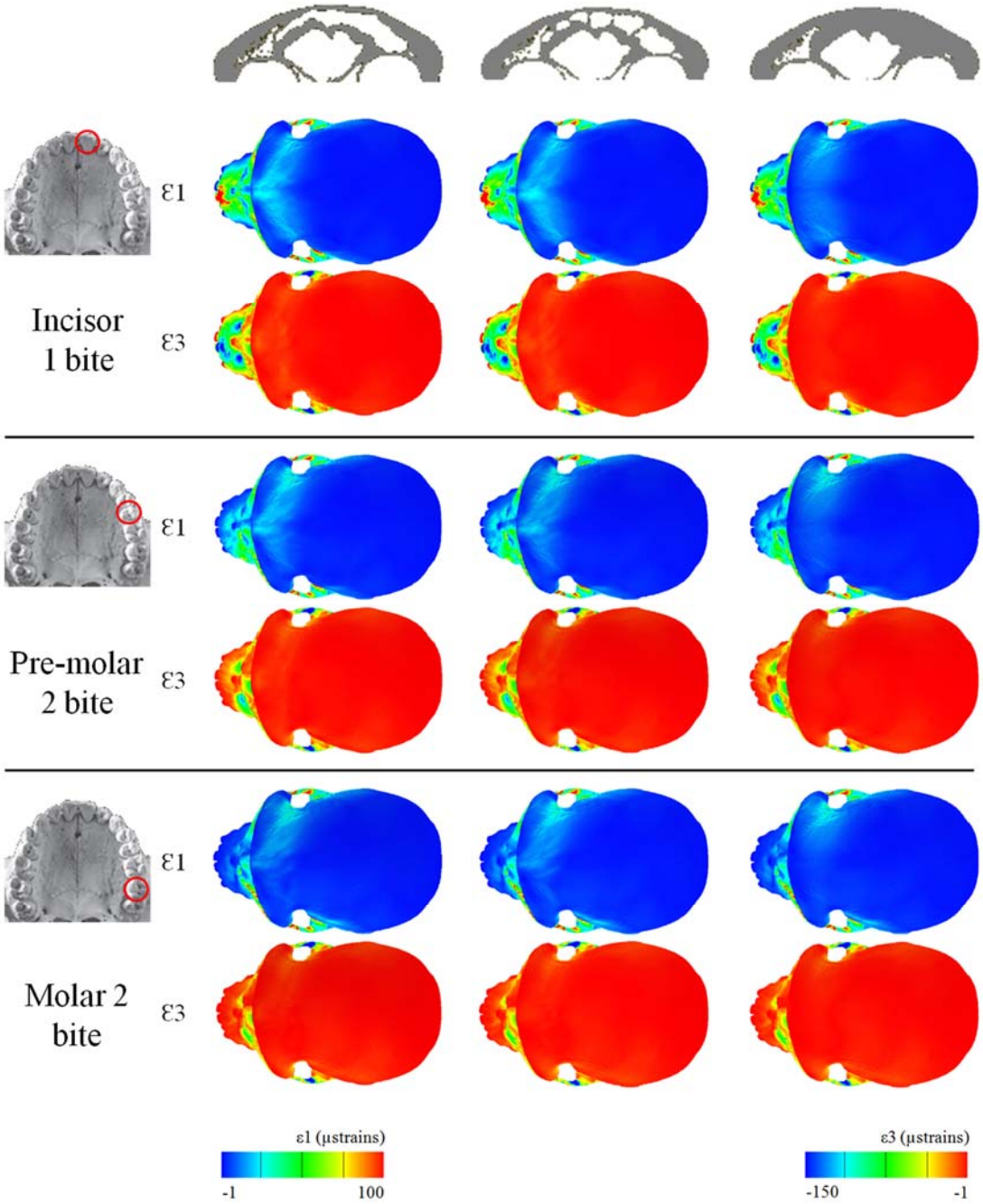

Figure 6-3: Principal strain 1 and 3 contour plots showing the strain magnitudes experienced over the cranium (*norma superioris*) under the three simulated bites (rows 1 and 2 show the incisor bite; rows 3 and 4 show the second pre-molar bite; rows 5 and 6 show the second pre-molar bite; left column shows the hollow sinus model; central column shows the honeycomb model; right column shows the infilled sinus model).

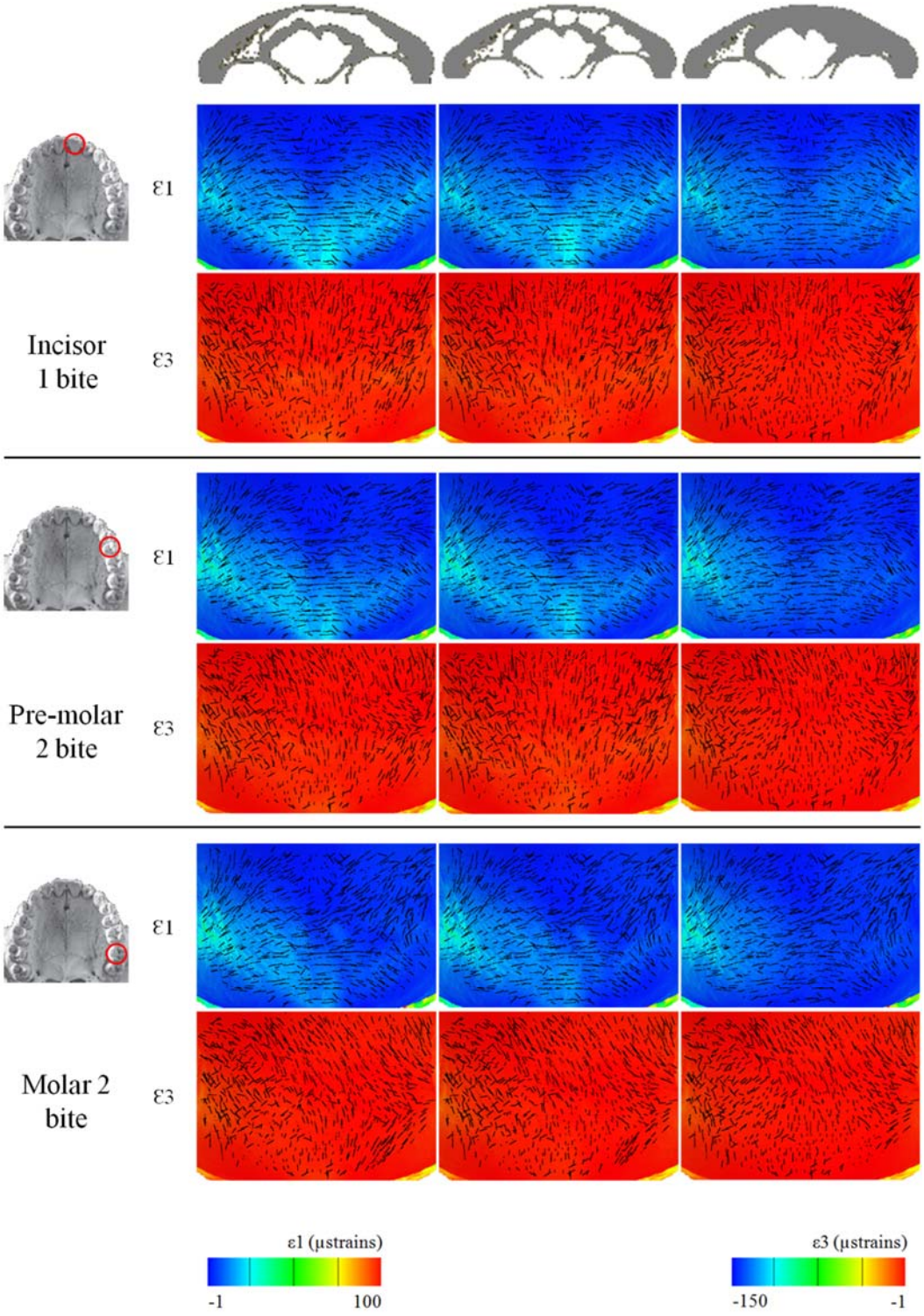

Figure 6-4: Principal strain 1 and 3 vector directions over the frontal sinus, on the external surface of the frontal bone (*norma superioris*) under the three simulated bites (rows 1 and 2 show the incisor bite; rows 3 and 4 show the second pre-molar bite; rows 5 and 6 show the second pre-molar bite; left column shows the hollow sinus model; central column shows the honeycomb model; right column shows the infilled sinus model).

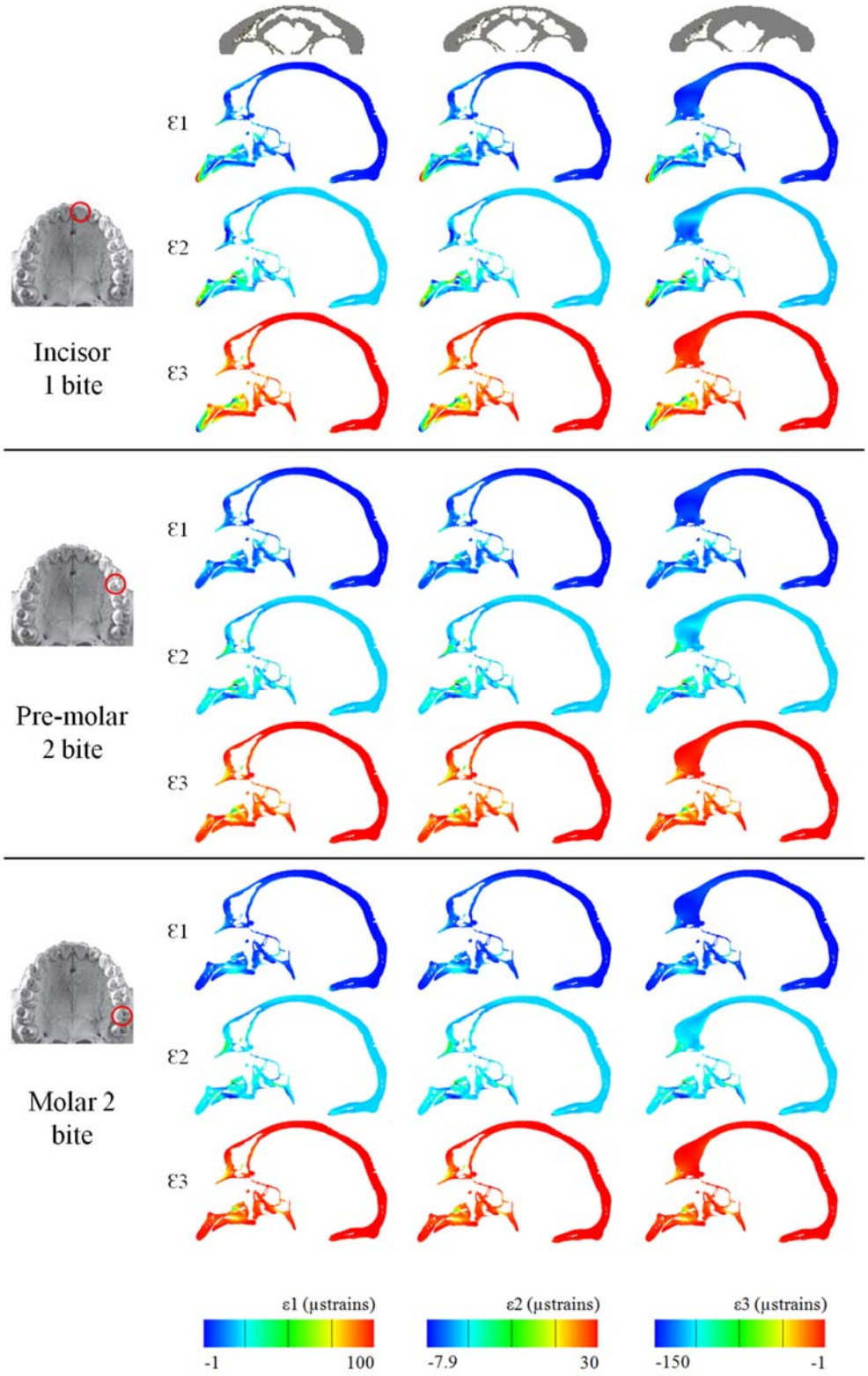

Figure 6-5: Principal strain contour plots from the three simulated bites in the three models (rows 1, 2 and 3 show the incisor bite; rows 4, 5 and 6 show the second pre-molar bite; rows 7, 8 and 9 show the second pre-molar bite; left column shows the hollow sinus model; central column shows the honeycomb model; right column shows the infilled sinus model).

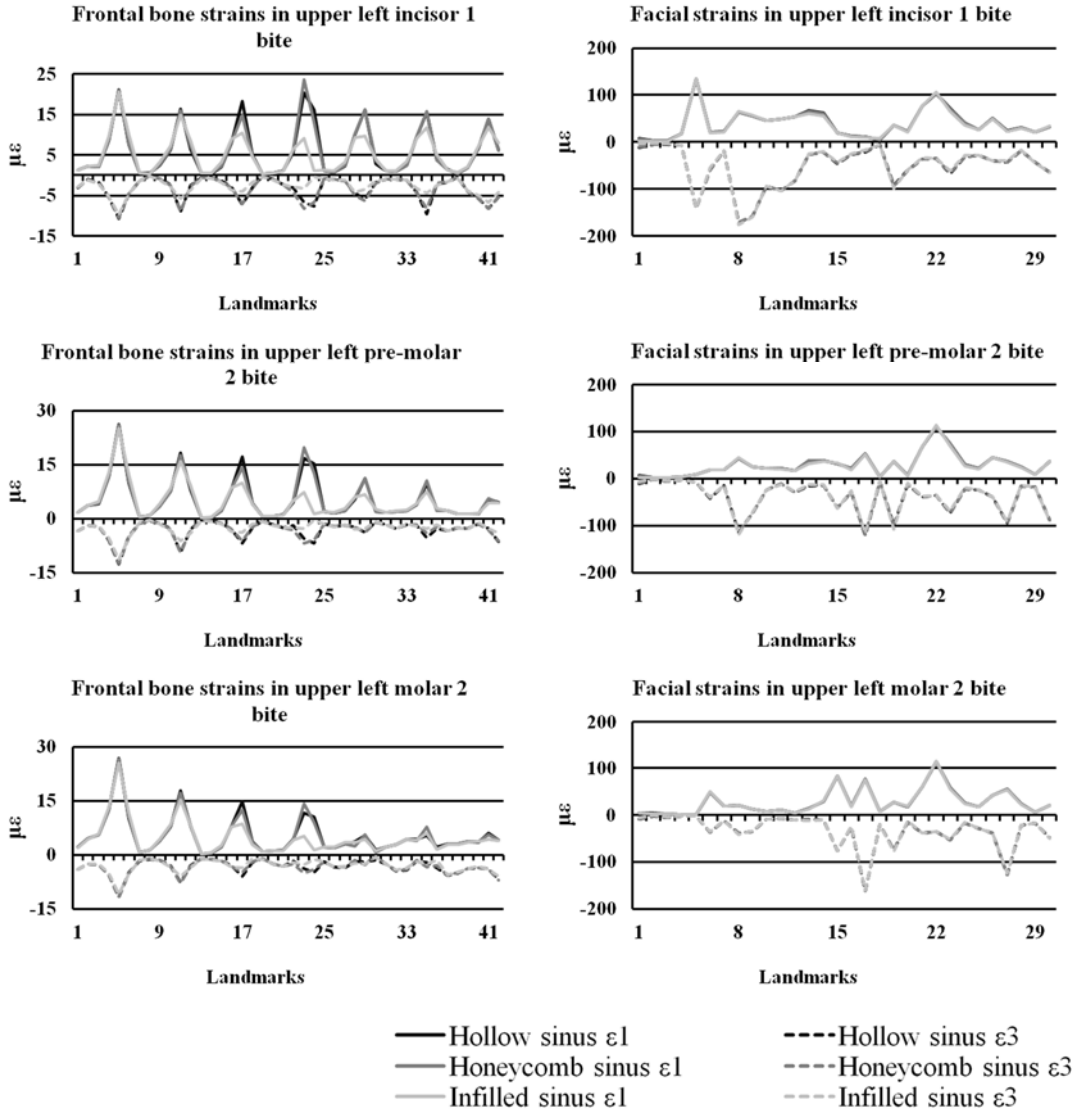

Figure 6-6: Maximum (ε1) and minimum (ε3) principal strain magnitudes experienced by the frontal bone, at 42 points (left column; see Fig 3), and over the face, at 30 points (right column; see Fig 3). The first row shows the results from simulation of the incisor bite; the second, of the second pre-molar; and the third, of the second molar bite.

The results of the GM analysis of global modes and magnitudes of deformation are, again, consistent with the pattern of differences in strain magnitudes predicted in the different models during the three simulated bites. Figure 6-7 shows that changes in bite point clearly impact much more than changes in the sinus, with models tightly clustering by bite point rather than by type of sinus. The model that invariably deforms

less in all bites is that with the infilled sinus, and the remaining two are very close to each other (indeed the markers in the plot overlap). These findings reflect those from the analyses of strains in indicating only local effects of experimental manipulation of sinus anatomy.

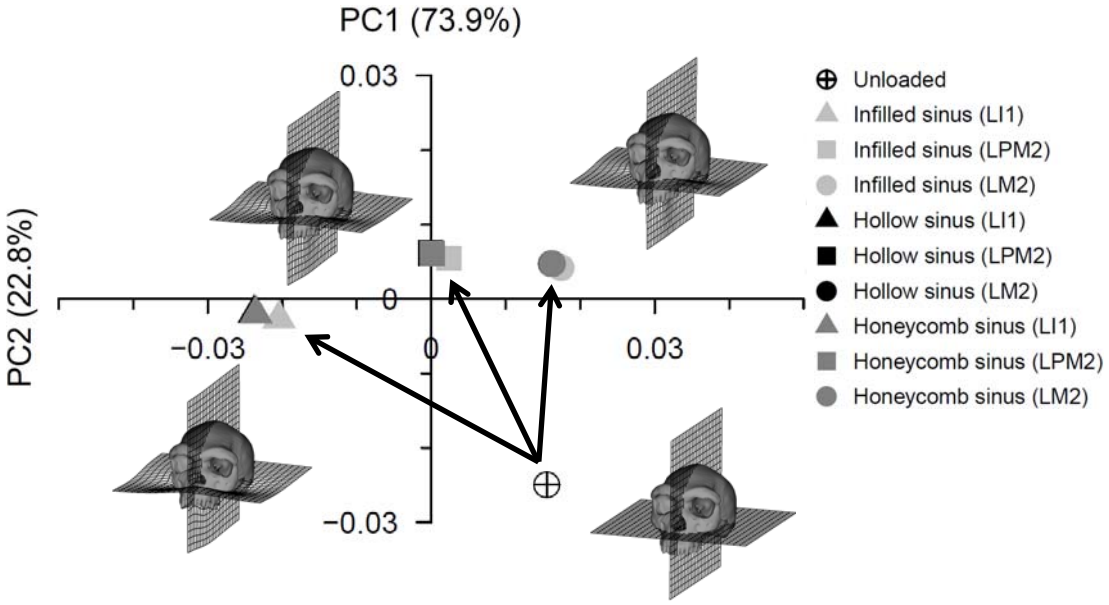

Figure 6-7: Principal components analyisis of the modes of deformation (changes in size and shape when loaded) of the different models in all bite simulations. Deformations magnified by a factor of 1000 to facilitate visualization.

6.4 Discussion

The results show that experimentally manipulating frontal sinus anatomy, by hollowing or infilling, does not impact significantly on the strain magnitudes and directions, nor on the modes of deformation of the cranium in general. The strain magnitudes experienced by the frontal bone are consistently low, especially in the infilled sinus of model 3. Hollowing the frontal sinus does not cause strain magnitudes to rise significantly and changes are restricted to the bone overlying the sinus.

These findings do not falsify the hypotheses that the manipulations of sinus morphology would have limited to negligible effect with respect to much of the cranial skeleton. There are small effects over regions of the frontal bone immediately overlying the sinus. Thus, (1) strain magnitudes experienced by the cranium during simulated biting are affected minimally and locally by removing the honeycomb-like structure

and (2) strain magnitudes are affected minimally and locally by infilling the frontal sinus.

Similar findings were made with respect to infilling cancellous bone spaces and the maxillary sinus in a study of macaques (Fitton et al., 2015) and cavities in a varanoid lizard mandible (Parr et al., 2012). The present results are consistent with other studies that found low strain magnitudes in the frontal bone and/or circumorbital structures due to masticatory system loading (Picq and Hylander, 1989; Hylander et al., 1991b; Ravosa et al., 2000c; Hylander and Johnson, 2002; Kupczik et al., 2009). However, this does not preclude mechanical adaptation of the frontal bone to loads experienced during biting. Thus, the negative feedback loop, mechanostat model predicts that bone remodels according to strain magnitudes experienced relative to specific thresholds. If bone strains exceed a certain threshold bone deposition occurs, thus increasing bone mass. If bone strains are below another threshold then bone resorption occurs, thus decreasing bone mass (Frost, 1987, 1996; Turner, 1998; Frost, 2003). Even though it is not clear what that threshold is, and if it is generalized or site specific (Hillam et al., 1995; Skerry, 2000; Currey, 2006), it has been widely demonstrated that bone adapts to changes in mechanical loading via changes in mass (Jones et al., 1977; Kannus et al., 1995; Nordstrom et al., 1996; Goodship et al., 1998) and in mineral density (Kerr et al., 1996; Valdimarsson et al., 2005). As such, it is possible to hypothesize that the low strains experienced by this region may trigger an osteoclastic response and bone resorption, thereby impacting on the morphogenesis of the frontal sinus. This hypothesis is consistent with the studies of Preuschoft and Witzel (2002) and Witzel (2011), who modelled crania as block materials with no hollow spaces, other than the brain cavity, and that found low strains in the regions where sinuses arise. This led them to suggest that these hollow spaces might arise via bone adaptation to low strains.

This possible adaptation of bony anatomy in relation to the frontal sinus is, nonetheless, compatible with the structural/spatial models that state that sinuses arise as a result of the spatial relationships of different components of the cranium (Enlow, 1968; Zollikofer et al., 2008; Zollikofer and Weissmann, 2008). The primacy of spatial relationships is crystallized in the functional matrix hypothesis, which posits that the morphology of the upper face results from the spatial relationships between the eyes and the brain (Moss and Young, 1960). Given the consequences of these spatial relationships on brow-ridge formation, it is possible that the low strain magnitudes

subsequently experienced within the brow-ridge drive biomechanical bone adaptation *via* bone resorption, thereby sculpting the frontal sinus. As with the spatial hypothesis, this biomechanical interpretation of frontal sinus morphogenesis does not preclude, but rather may work in concert with, other mechanisms that also underlie the initiation, presence, shape and size of this structure, such as olfaction, respiration, thermoregulation, nitric oxide production and role in facial ontogeny (Tillier, 1977; Blaney, 1990; Bookstein et al., 1999; Rae and Koppe, 2004; Laitman, 2008; Lundberg, 2008; Márquez, 2008).

It should be noted that because infilling the sinus did not impact significantly on the strains experienced by nearby regions, and in the cranium as a whole, there are important consequences in relation to FE model simplification, which is always necessary. Particular issues arise with fossils, which are often imaged at resolutions that do not allow very detailed modelling of their internal anatomy and may be invaded by mineralized sedimentary matrix that is not distinguishable from bone in CTs. This study supports the application of simplifications, in particular infilling of the region of the frontal sinus in such circumstances when building finite element models. This study also supports the conclusions of a previous study in which simplifications of models by infilling hollow trabecular bone and sinus spaces (Fitton et al., 2015) had little impact on mode, but greater impact on the magnitude of model deformation.

These results also are important in relation to the validity of the strategy of warping a base specimen to different target morphologies to speed up the model building process (Sigal et al., 2008; Stayton, 2009; Sigal et al., 2010; O'Higgins et al., 2011; O'Higgins et al., 2012). Warping of cranial models will inevitably result in warped spaces within the bone that are very unlikely to represent the spaces that would arise as a result of mechanical adaptation and as such models cannot be assured of reliably predicting deformations when submitted to FEA. By infilling then warping, the issue might be circumvented, albeit predicted strain magnitudes will inevitably be lower than they should be, but modes of deformation can be expected to be approximately the same (Fitton et al., 2015). This potential strategy requires detailed sensitivity analyses before it can be adopted, but the evidence of this and previous studies (Fitton et al., 2015) leads us to be optimistic.

In addition to informing about how masticatory mechanics impacts on the morphogenesis of the frontal sinus, this chapter also shows that infilling the frontal

sinus does not impact significantly on the deformations experienced by the cranium. This is relevant for the next chapter, which examines the mechanical significance of the brow-ridge, because manipulation of the morphology of the brow-ridge required infilling of the sinus.

7 The biomechanical significance of the brow-ridge in Kabwe 1

7.1 Introduction

The brow ridge is conventionally divided into three components: the glabellar region (in the midline of the skull, approximately between the two eye sockets); the supraciliary arches (above the medial part of the orbit); the supraorbital region (above the lateral part of the orbit) (Lieberman, 2000). It has been considered to be an anatomical trait of phylogenetic relevance and has been used in hominin phylogenetic analyses. In such studies *Homo sapiens* is repeatedly noted as the only hominin species that lacks a strongly developed browridge (Smith and Rayard, 1980; Russell, 1985; Lieberman, 2000). All remaining hominin species present well developed brow ridges often with associated post-orbital *sulci* and constriction. Despite this there is significant variation in its morphology among diverse hominin species. For example, variation has been noted in the antero-posterior and supero-inferior dimensions of the browridge, supero-inferior positioning of the glabellar region and dimensions of the post-orbital sulcus (Lieberman, 2000).

The growth and development of the brow ridge region differs from the remaining cranial vault because it is below the circumcranial reversal line. Above this line, the cranial vault grows by depositing bone at the sutures and the internal and external tables as the brain grows. However, below this line, which includes the brow-ridge on the external aspect of the frontal bone, the endocranium is mainly resorptive and bone adapts to the growing brain via resorption of the internal tables and deposition at the external tables (Enlow and Hans, 1996; Lieberman, 2011). Because the internal table follows a neural growth trajectory it reachs approximately 95% of adult size by the time of eruption of the first molar. On the other hand, externally, in the region of the brow-ridge, the outer table of the frontal bone follows a somatic growth trajectory, reaching approximately 95% of adult size by the end of the adolescent growth spurt. This difference in growth trajectories is effected by differential drift between the internal and external tables of the brow-ridge (Enlow and Hans, 1996; Lieberman, 2000; Scheuer and Black, 2000; Lieberman, 2011).

Different hypotheses that are not mutually exclusive have been proposed to explain the differences in brow-ridge form among different species. The most widely accepted is the spatial hypothesis which, in its most strict version, states that "*the*

presence or absence of supraorbital ridges is only a reflection of the spatial relationship between two functionally unrelated cephalic components, the orbit and the brain case" (Moss and Young, 1960; p. 281). The increased distance between these functional matrices, due to their different growth trajectories, results in increases in the size of brow-ridges (Moss and Young, 1960; Ravosa, 1988). The orientation of the *splanchnocranium* in relation to the neurocranium also influences brow-ridge morphology. More ventrally oriented faces are associated with bigger brow-ridges (*e.g. Gorilla*) and more dorsally oriented with smaller brow-ridges (*e.g. Pongo*) (Moss and Young, 1960; Biegert, 1963; Shea, 1985; Shea, 1986). Subsequent research has supported this interpretation (Ravosa, 1988) and also shows that brow-ridges scale allometrically, with individuals of bigger species growing proportionally bigger brow-ridges (Ravosa, 1988; Ravosa, 1991; Freidline et al., 2012). Other proponents of the spatial hypothesis add that the mechanical action of the masticatory system also impacts on the morphology of the brow-ridge and state that it, along with other structures, is part of the skull's buttressing system (Weidenreich, 1941; Shea, 1986; Ravosa, 1988).

The, 'alternative', mechanical hypothesis emphasizes the potential role of mechanical loading in brow-ridge morphogenesis. It posits that the mechanical loadings experienced by the skull during masticatory system loading impact decisively on the morphology of the brow-ridge (Russell, 1985). This notion was deeply influenced by the pioneering work of Endo in the 1960's (Endo, 1965; Endo, 1966) who simulated biting in dry human skulls and measured, using strain gauges, the stresses and strains experienced by the face. He found that during incision the brow-ridge experienced relatively high stresses and strains when compared to other anatomical regions of the face. In consequence he proposed that the brow-ridge acted as a beam subjected to bending due to the downward force applied by masticatory muscles and upward forced applied at the incisors during anterior dental action. This finding gave rise to other studies in humans (Endo, 1970; Russell, 1985; Hilloowala and Trent, 1988b) and, in a study using native Australian skulls, Russell (1985) suggested that anterior masticatory loading is central in the development of the brow-ridge. Further studies that support the mechanical hypothesis also focused on fossil hominin species (Oyen et al., 1979; Smith and Rayard, 1980), galagos (Ravosa et al., 2000a), *Macaca fascicularis* (Hylander et al., 1991b; Kupczik et al., 2009), *Papio anubis* (Hylander et al., 1991b), *Pongo pygmaeus* (Hilloowala and Trent, 1988a), *Gorilla gorilla* (Hilloowala and Trent, 1988a) and *Pan*

troglodytes (Hilloowala and Trent, 1988a). While proving influential, the mechanical hypothesis was later disputed on the basis of *in vivo* studies of galagos, macaques and papionins that failed to record elevated strains in the brow-ridge during masticatory system loading (Picq and Hylander, 1989; Hylander et al., 1991b; Ravosa et al., 2000b; Hylander and Johnson, 2002). More recently, *in silico* studies using an ontogenetic sample of Finite Element Models (FEM) of *Macaca fascicularis* also predicted relatively low strains in the brow-ridge of individuals of different ages (Kupczik et al., 2009).

Despite the finding that strains are low over the brow-ridge, this structure could still arise through bone biomechanical adaptation and play a role in stiffening the face. This is because if it were adapted to loads it would be expected to show low strains during physiological loading of the jaws. Thus after more than 40 years of research, conflicting views exist with regard to the mechanisms that give rise to the brow-ridges and their function. On the one hand, it has been suggested that the morphology of the supraorbital region is highly conditioned by masticatory mechanical loading (Endo, 1966; Oyen et al., 1979; Russell, 1985; Hilloowala and Trent, 1988b, 1988a). On the other, researchers who have recorded low strains in this area suggest that it does not play a relevant biomechanical role and that its growth and development is mainly related to mechanisms other than the response to masticatory stresses and strains (Picq and Hylander, 1989; Hylander et al., 1991a, 1991b; Hylander and Johnson, 2002; Kupczik et al., 2009).

In addition to the spatial, allometric and mechanical hypotheses, other hypotheses have been proposed to explain large brow-ridges. These are less well accepted but include protection from blows to the head (Tappen, 1973, 1978), protection of the eyes in aquatic environments (Verhaegen, 2013), provision of sunshade (Barton, 1895 *in* Clark and Willermet (1997)) and prevention of hair from obscuring vision (Krantz, 1973).

Research into the mechanical role of the brow-ridge is hampered by the impossibility of carrying out *in vivo* experimental manipulations such as excision of this structure. However, recent advances in virtual functional simulation offer a way forward. Thus using Finite Element Analysis (FEA) it is feasible to virtually manipulate the morphology of the brow-ridge while simulating masticatory system loadings to assess the impact of variations in form on functional performance. This approach, already used by Strait et al. (2007) in a study about the mechanical

consequences of variations in palatal thickness and suggested by Kupczik et al. (2009) regarding the brow-ridge, would allow the mechanical relevance of this structure to be assessed. This approach offers the possibility of assessing how variations in brow-ridge morphology impact on the strains experienced by the remaining craniofacial skeleton.

Kabwe 1, a male *Homo heidelbergensis* dated 150 - 300 kya b.p. (Schwartz and Tattersall, 2003), presents an extremely well developed brow-ridge that appears to be significantly larger than is needed to fulfil spatial demands. As such, it is an especially suitable specimen to experimentally manipulate, by progressively reducing the size of the brow-ridge to the minimum required to bridge the gap between the face and neurocranium. The present study manipulates brow-ridge morphology in this way to assess the impact of different brow-ridge morphologies on the biomechanical performance of the facial skeleton of Kabwe 1. The null hypothesis is that changes in the morphology of the brow-ridge do not impact meaningfully the functional performance of the facial skeleton of Kabwe 1. To test this hypothesis three FE models were created and their functional performance when simulating biting was compared. Model 1 presents the original brow-ridge of Kabwe 1, model 2 a reduced brow-ridge and model 3 a post-orbital sulcus (Figure 7-1). Considering previous research stating that brow-ridge morphology does not relate to masticatory function (Picq and Hylander, 1989; Hylander et al., 1991a, 1991b; Hylander and Johnson, 2002; Kupczik et al., 2009), it is predicted that manipulating this structure will have no meaningful impact on the deformations experienced by the cranium. As in the previous chapter, meaningful or negligible impacts are considered within the magnitudes experienced by this model. Thus, in this context, an impact is meaningful if strains experienced by the face, brow-ridge and surrounding structures increase to a magnitude that approximates the highest strains experienced by the model. An impact is considered small or negligible if strains do not increase considerably and remain well below the maximum strains experienced by the model. This approach is adopted because the exact magnitudes of deformation that trigger bone deposition or resorption are not clear (Skerry, 2000; Currey, 2006), and because the FE model likely underestimates the absolute magnitudes experienced by the cranium during simulated masticatory loading to varying degrees (see chapter 2).

7.2 Materials and Methods

A virtual reconstruction of the Kabwe 1 skull was made from a CT scan of the fossil provided by the NHM, London (courtesy of Robert Kruszynski). A brief description of the reconstruction process is presented below, but the complete description of the reconstruction is available in chapter 4. After reconstruction, the models were directly converted into voxel based finite element models, which were used to simulate three different bites (left central incisor, left second premolar, left second molar) to assess the biomechanical performance of the facial skeleton during these bites.

7.2.1 Skull reconstruction and model creation

A medical CT stack of Kabwe I with anisometric voxel size (0.4687501 x 0.4687501 x 1 mm) was resampled to an isometric voxel size of 0.35 mm. Automated, semi-automated and manual segmentation of the cranium was performed using Avizo® (version 8.0). Manual segmentation was also required to remove sedimentary matrix present in the maxillary and sphenoidal sinuses. Despite being outstandingly well preserved, taphonomic and pathological processes caused the destruction of several anatomical regions of the cranium that required reconstruction. These include the alveolar regions of the maxilla, right and left temporal bones, the occipital, the right parietal, the sphenoid, the ethmoid, the orbital part of both maxillae and multiple teeth. When possible, reconstruction of missing parts was performed by mirroring preserved contralateral elements and warping them to the existing structures. When small gaps were present, Geomagic® (Studio 2011) was used to fill them using the surface of surrounding structures as the reference for interpolation. Portions of a CT reconstruction of a cadaveric *Homo sapiens* skull were used to reconstruct part of the occipital and missing tooth crowns for which there were no antimeres preserved.

Once the reconstruction was complete (model 1; Figure 7-1), the frontal sinuses were infilled to allow later excavation of this region to produce variant morphologies. Analysis of the impact of infilling the sinus in model 1 showed that the surface strains over the brow-ridge and elsewhere in the cranium did not differ significantly between the models with hollow and filled frontal sinus (chapter 6). The morphology of the brow-ridge was manipulated, using Geomagic®, by decreasing its size (model 2) and

creating a post orbital sulcus in model 2 (model 3; Figure 7-1). Voxel based finite element models were then generated by direct conversion using the vox2vec software.

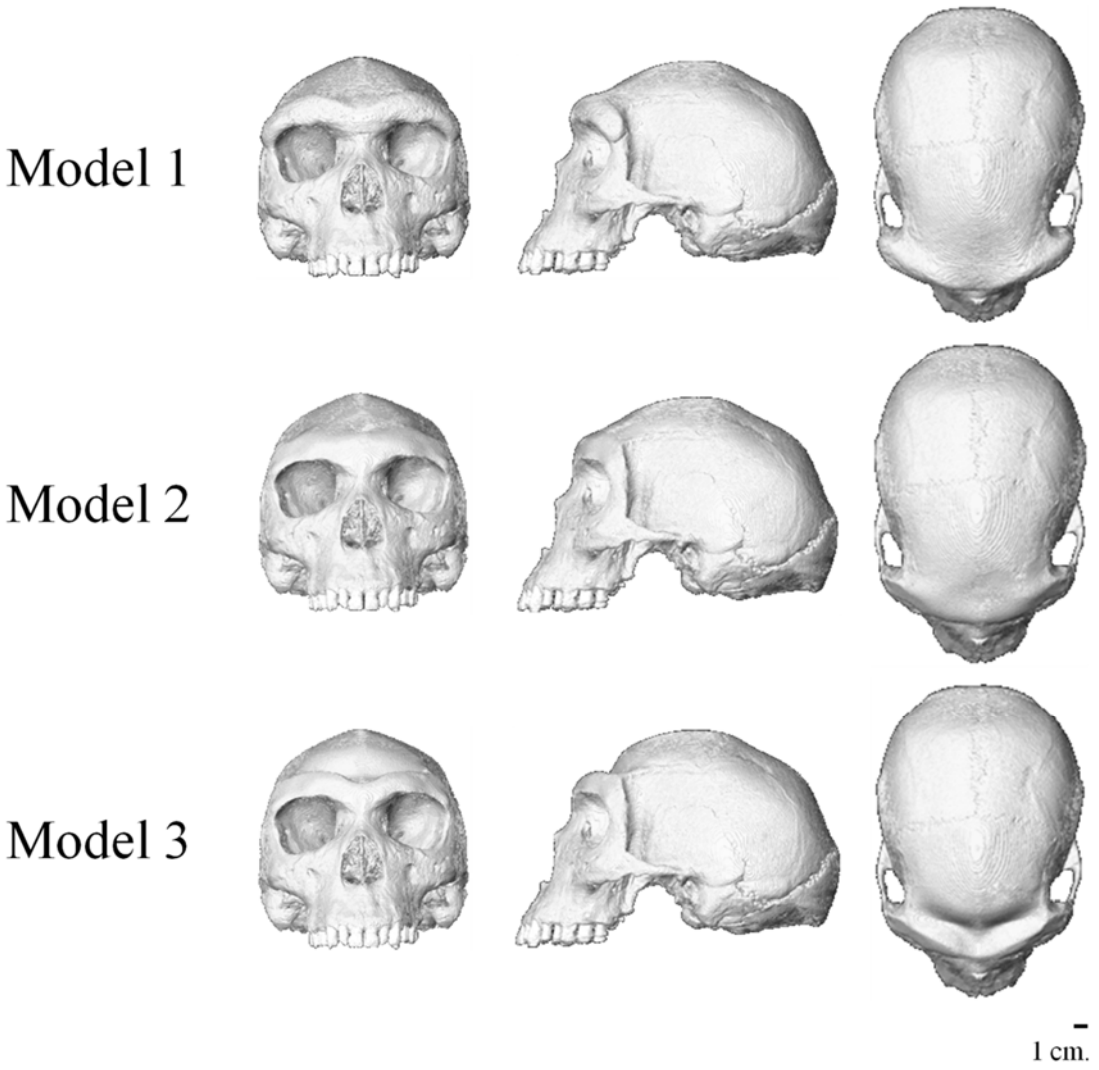

Figure 7-1: Models 1 - 3. Model 1 represents the original reconstruction. Model 2 is the reduced brow-ridge model. Model 3 is the *post-orbital* sulcus model.

7.2.2 Constraints

Identical constraints were applied to all the models using the bespoke finite element analysis software tool, VoxFE (Fagan et al., 2007). The models were constrained at the tempo-mandibular joints (24 nodes in the x, y and z axis) and a third constraint was applied at the simulated bite point in each of the masticatory simulations (left central incisor, left second pre-molar, left second molar (21 nodes constrained in the vertical axis alone).

7.2.3 Material properties

Following prior sensitivity studies that showed only local effects of differentiating the material properties of teeth and the surrounding bone these were assigned the same material properties in all the models used in this study. Further, sensitivity analyses assessing the effect of model simplifications in a human cadaveric cranium (chapter 3; Toro Ibacache et al., 2016a) and in a cranium of *Macaca fascicularis* (Fitton et al., 2015) show that infilling of trabecular bone stiffens the skull and so reduces strain magnitudes but that the distribution of regions of high and low strain and of global modes (rather than magnitudes) of deformation are not affected. Allocating teeth the same material properties as bone has the effect of locally reducing strain gradients in the alveolar region, with little effect elsewhere. This is relevant to the present study because trabecular bone is neither well enough preserved nor imaged at sufficient resolution to accurately represent it in a finite element model and the dentition was incomplete and required reconstruction. As such, in all models, trabecular bone and teeth were not separately represented and were allocated the same material properties as cortical bone. Based on the sensitivity analyses we expect this to have little impact on the mode of deformation of the loaded cranium, but to reduce the degree to which it deforms.

Cortical bone, trabecular bone and the teeth were allocated isotropic properties, with a Young's modulus of 17 GPa and a Poisson's ration of 0.3. The modulus of elasticity was derived from nanoindentation studies of cortical bone in a cadaveric *Homo sapiens* skull (Toro Ibacache et al., 2016a) following the protocol of Kupczik et al. (2007). The resulting value of 17 GPa is within the range of values found in previous studies (Dechow et al., 1993; Schwartz-Dabney and Dechow, 2003).

7.2.4 Muscle loads

Loads were applied to the model to represent the actions of six muscles active during biting: right and left temporalis, right and left masseter, right and left medial pterygoid. Absence of the mandible precludes direct estimation of the direction of muscle force vectors and estimation using bony proxies of anatomical cross sectional areas (and so maximum forces) of muscles that attach to the mandible (masseter and

medial pterygoid). However, given that three versions of the same model with identical loads and constraints are to be compared, it matters little that applied muscle force vectors approximate rather than replicate physiological loadings. Clearly more important is that these forces are identical between models and so do not, in themselves, produce differences in strains (modes of deformation) between models. As such, the maximum estimated muscle forces from a *Homo sapiens* cadaveric head were applied identically to each model (Table 7-1; Toro Ibacache et al., 2016a). The directions of muscle force vectors were estimated by scaling a *Homo neanderthalensis* mandible (Tabun 1 specimen) to the Kabwe 1 skull. These directions were also identical between models.

Table 7-1: Applied Muscle Forces (in Newtons).

Muscle	**Side**	
	Left	Right
Temporalis	168.02	170.67
Masseter	134.06	124.01
Medial pterygoid	124.01	117.49

7.2.5 Model solution and analysis

The finite element models 1-3 were solved using VoxFE (Fagan et al., 2007). The resulting deformations of the finite element models were compared through: (1) qualitative assessment of strain magnitudes and directions of maximum (ε1) and minimum (ε3) principal strains; (2) quantitative comparisons of ε1 and ε3 at 30 nodes (points) located in the facial skeleton, common to all models (Figure 7-2); (3) through an analysis of changes in size and shape between loaded and unloaded models of a configuration of 33 landmarks (points) from the whole cranium (Figure 7-3 and Table 7-2). Method 1 relies on visual assessment of the strain contour plots over the whole cranium and directions of the strain vectors in the infra-orbital region. Method 2 quantitatively compares strains by plotting magnitudes arising from each simulated bite (this approach is not applied to the brow-ridge because manipulation of this structure precludes direct correspondence between compared nodes). Method 3 employs geometric morphometrics to compare changes in size and shape between the unloaded

and loaded models. This consists of an initial registration step comprising scaling to unit size and then translation of landmark configurations to their centroids, with subsequent rotation to minimise the sum of squared distances between each scaled, translated configuration and the mean configuration. This is followed by rescaling of each configuration to its original centroid size and with a PCA of the resulting size and shape coordinates (O'Higgins, 2000; Zelditch et al., 2012). This analysis leads to a quantitative comparison of global model deformations (changes in size and shape) in terms of the directions (modes) and magnitudes (degree or extent) of deformation arising from loading.

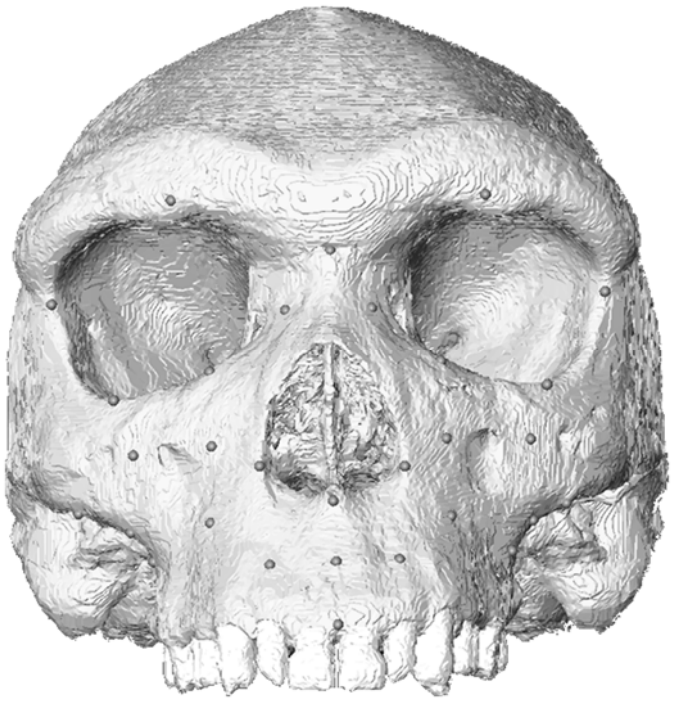

Figure 7-2: Depiction of the 30 points placed on the facial skeleton to extract ε1 and ε3.

Figure 7-3: 33 cranial landmarks used to perform the global analysis of deformation. See Table 7-2 for landmark identification and description.

Table 7-2: Landmarks used in the analysis of global deformation.

No.	Name
1	Vertex
2	Nasion
3	Anterior Nasal Spine
4	Prosthion
5	Opisthocranium
6; 7	Supraorbital torus
8; 9	Infraorbitale
10; 11	Nasal notch
12; 13	Ext. Alv. P4
14; 15	Last molar
16; 17	Zygo-maxillar
18; 19	Fronto-zygomatic
20; 21	Jugale
22; 23	Zygomatic Arch lateral
24; 25	Zygomatic Root posterior
26; 27	Zygomatic Root anterior
28; 29	Zygomatic Arch medial
30; 31	Infratemporal Crest
32; 33	Euryon

It is important to note that there are two different definitions of ‘deformation’. In material science and in morphometrics, ‘deformation’ refers to changes in size and shape of an object. This is the definition followed here since it reflects the quantities measured by strains and size and shape distances. This differs from the definition of ‘deformation’ used in mechanics (see Truesdell and Noll (2004), p. 48) where it refers to the displacement of nodes of the FE model between unloaded and loaded states and so includes rigid body motions with no size or shape change.

7.3 Results

Visual assessment of the strain contour plots (Figure 7-4) and of the strains vectors (Figure 7-5) of ε1 and ε3 shows no significant intra-bite differences among models 1, 2 and 3. When considering different bites, as expected, differences are found in the strain contour plots and vectors. For each biting simulation, large strain magnitudes are experienced directly above the bite point and nearby regions. The left central incisor bite results in large strains over the sub-nasal region and nasal borders, the second left premolar bite results in large strains over the infra-orbital region and left nasal border, and the second left molar bite produces large strains over the infra-orbital region, zygomatic root and left nasal border. Large strains are developed at the origins of the masseter (masseteric line of the zygomatic) and medial pterygoid (pterygoid fossa) muscles in all simulated bites (Figure 7-4). The direction of the strain vectors mainly show transverse tension and general superior-inferior compression, with some inter-bite differences (Figure 7-5).

The brow-ridges and frontal regions of the models differ so it is not possible to directly compare strains at equivalent sampling points. However, visual comparison of models indicates that there is a slight increase in the strain magnitudes experienced by the lateral margins of the ridges and at supraglabella with decreasing brow-ridge size (from model 1 to models 2 and then 3). This increase in strain magnitudes is most marked in the post-orbital sulcus of model 3 (Figure 7-4).

Plotting of the extracted strains experienced by the face shows an almost complete overlap among the three different models under each bite (Figure 7-6).

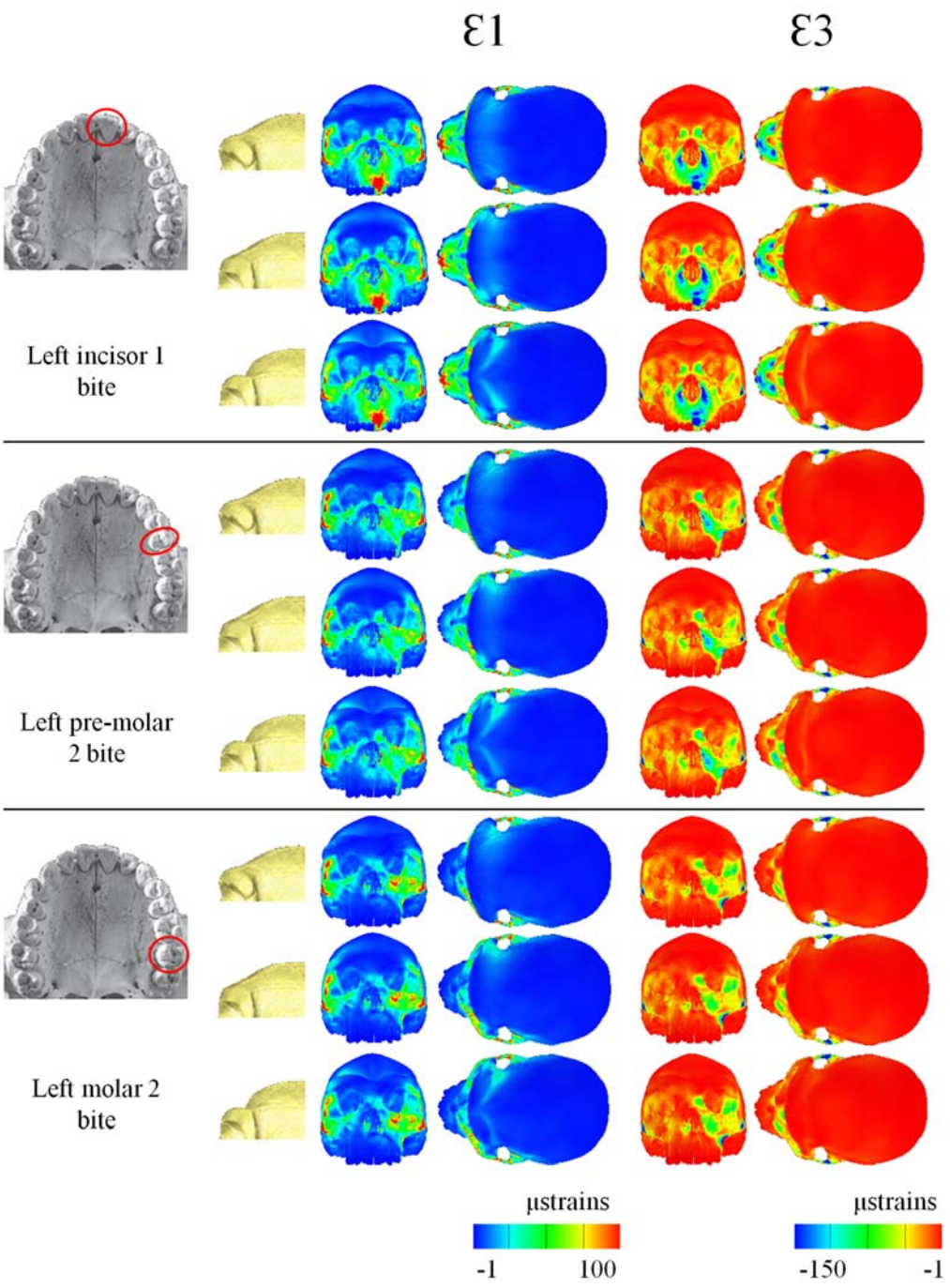

Figure 7-4: Strain contour plots of ε1 and ε3 of models 1 - 3 under the different bites simulated.

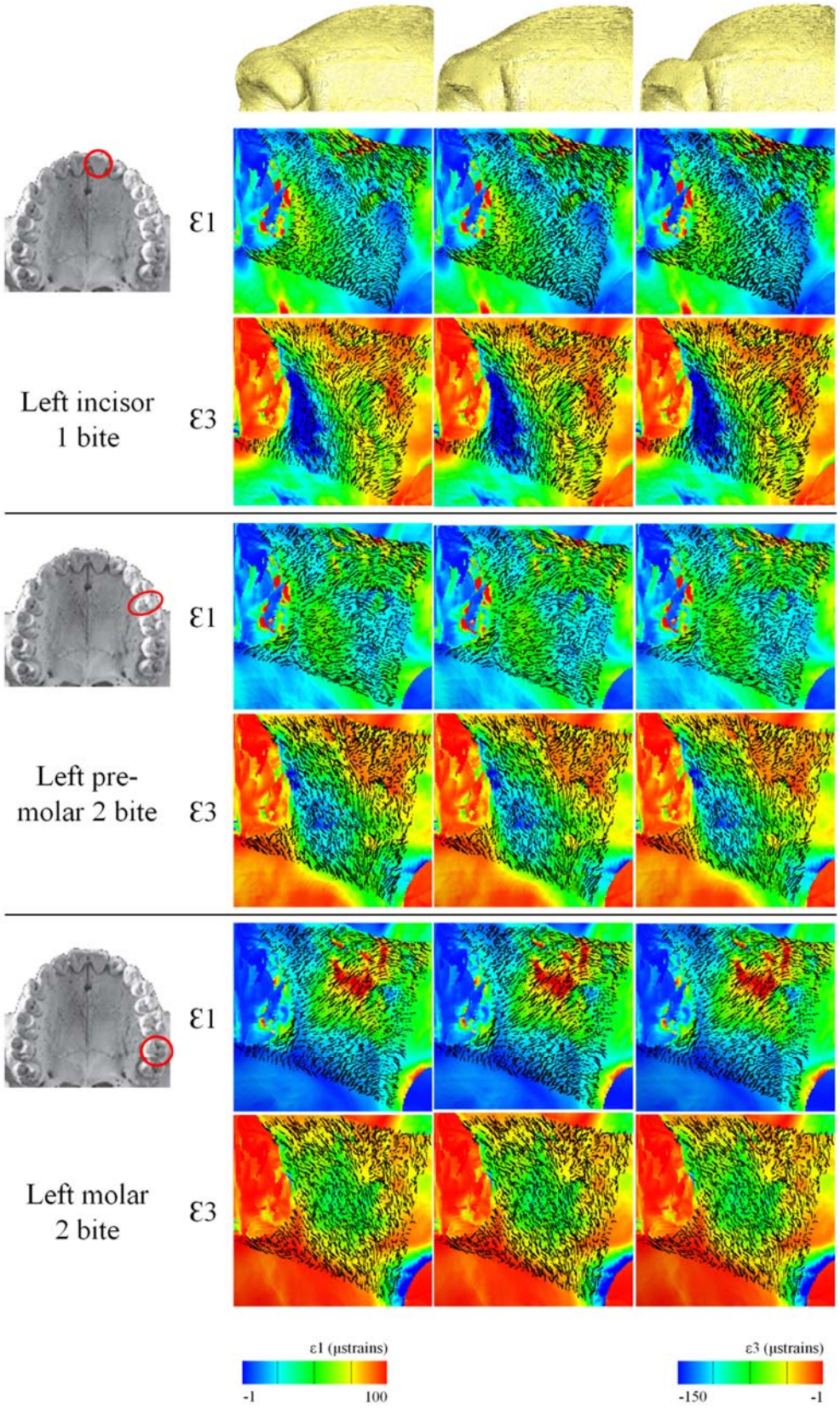

Figure 7-5: Strain contour plots and strain directions of ε1 and ε3 of the infra-orbital plate of the different models under the different bites simulated.

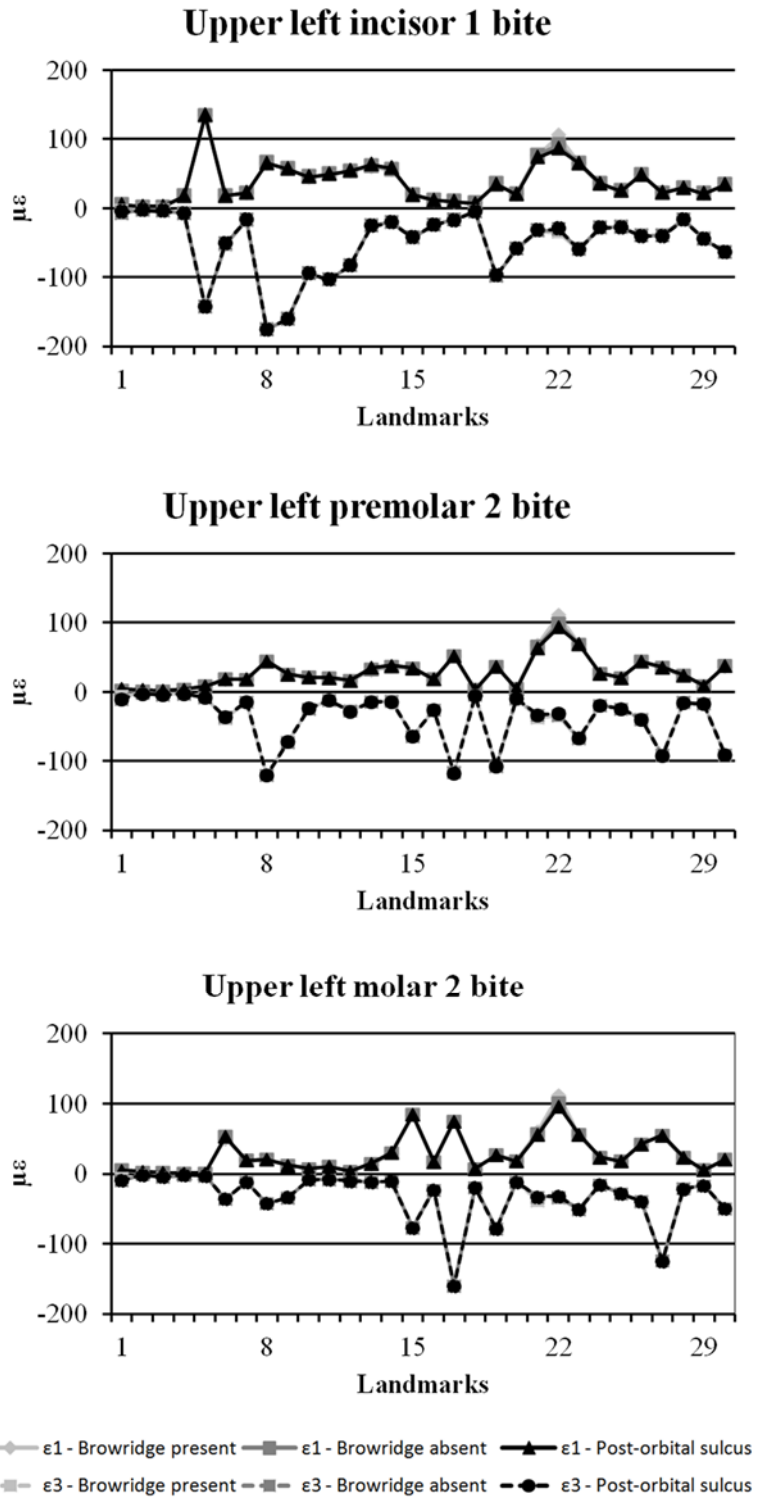

Figure 7-6: Plots of facial strains experienced by the models at 30 equivalent anatomical points.

The size and shape PCA of the configuration of 33 landmarks results in the plot of PCs 1 (70.9% of variance) and 2 (26.0% of variance; Figure 7-7). The loaded models cluster tightly by bite point and so the vector of deformation (changes in size and shape) connecting the unloaded and loaded models reflects almost identical modes and magnitudes of deformation irrespective of brow-ridge morphology. This said, within each cluster model 1 is closest to the unloaded model, and model 3 is furthest. This indicates that the magnitude of deformation (and so overall model stiffness during biting) differs a little with model 1 deforming least and model 3 the most (Figure 7-7). This effect is very small when compared to the differences between bites and the total degree of deformation from the unloaded model.

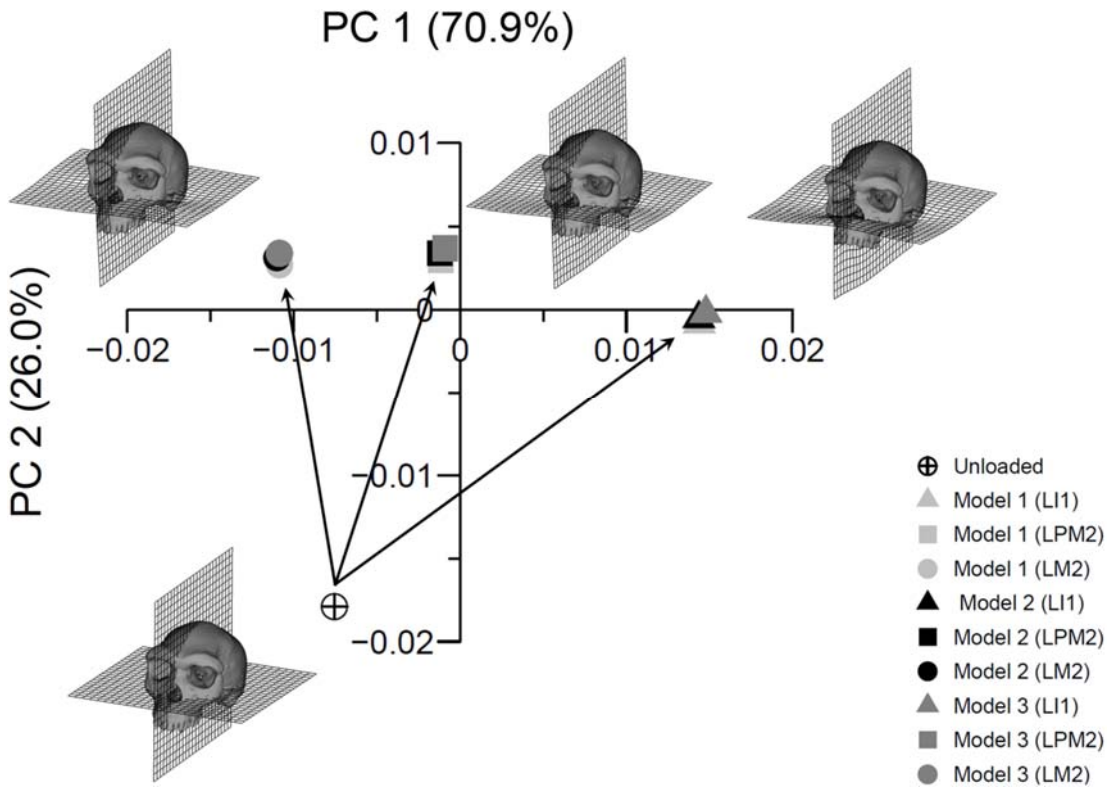

Figure 7-7: PCA, in size-shape space, of the unloaded and loaded models in the three different simulated bites. Deformations magnified by a factor of 1000 to facilitate visualization.

7.4 Discussion

As expected the different simulated bites result in different modes of deformation which are reflected in strain magnitudes, strain directions and global

changes in size and shape in all models. The differences in modes and magnitudes of deformation among models that arise during simulated bites are, however, very small compared to the differences among bites. This demonstrates that changing the morphology of the brow-ridge does not impact significantly on the mode of deformation experienced by the face, thus failing to falsify the null hypothesis, that changing the morphology of the brow-ridge does not impact meaningfully the functional performance of the facial skeleton.

On the other hand, the models do show differences in the mode and magnitude of deformation of the manipulated region of the skull; there are slight increases in strain magnitudes at the lateral margins of the brow-ridges and in the frontal *squama*. This is relevant because these strain magnitude differences might be sufficient for biomechanical adaptation, as predicted by the mechanostat model, to occur. The latter predicts that bone remodels according to the strains experienced relative to an optimum customary strain level (Frost, 1987, 1996; Turner, 1998; Skerry, 2000; Frost, 2003). As such, if strains reach a certain threshold bone deposits due to osteoblastic action, if strains are lower than another threshold then bone resorbs due to osteoclastic action. Even though it is not clear what that threshold is nor if it is generalized or site specific (Hillam et al., 1995; Skerry, 2000; Currey, 2006) it is clear that bone adapts to changes in mechanical loading by changing mineral density (Kerr et al., 1996; Valdimarsson et al., 2005) or mass (Jones et al., 1977; Kannus et al., 1995; Nordstrom et al., 1996; Goodship et al., 1998). It is, therefore, possible that, to some extent, the growth and development of the brow ridge may be mechanically driven. However the increases in strain magnitudes observed when the brow-ridge is progressively reduced are slight and so are unlikely to completely explain the massive brow-ridges of Kabwe 1. Other factors might therefore underlie this peculiar morphology.

The spatial relationship between the eyes and the brain might explain (according to the spatial hypothesis, Moss and Young, 1960) the morphology of the brow-ridge. However model 3, with ridges reduced to a minimum to bridge the gap between frontal and orbits, rather than model 1 (original brow-ridge), reflects the spatial requirement and so the spatial hypothesis does not seem to fully explain the massive ridges. This interpretation is supported by the fact that species that present a large disjunction between the orbits and the braincase often manifest post-orbital *sulci* and post-orbital constrictions that are not found in this specimen.

It has also been suggested that the brow-ridges grow allometrically in cercopithecines and that bigger skulls present relatively bigger ridges (Ravosa, 1988). Freidline et al. (2013) also identified a correlation between facial and brow-ridge size in Pleistocene and upper Palaeolithic fossil hominins, including *Homo heidelbergensis*. As such, scaling of the face relative to the frontal might partially explain the morphology of the brow-ridge in Kabwe 1.

Even though the spatial, mechanical and allometric models have been shown to explain the morphology of ridges other mechanisms may also be considered. Hylander and Johnson (2002) have demonstrated that facial bony structures, such as the paranasal swellings in *Mandrillus sphinx*, form due to factors that are neither spatial nor mechanical. Rather they reflect social behaviour and structure. Thus, these structures underlie the vibrant soft tissue colourings of the muzzle of male mandrills, which bear a significant function in social signalling and display. Growth and development of the swellings in *Mandrillus leucophaeus* has been related to androgen production (Elton and Morgan, 2006). In humans the brow-ridge is a sexually dimorphic anatomical trait (Buikstra and Ubelaker, 1994) that has been identified as relevant in the perception of an individual by others (Cieri et al., 2014) and its growth and development has also been related to androgen production, along with general facial sexual dimorphism (Cieri et al., 2014). It is, therefore, plausible that the morphology of the brow-ridges of Kabwe 1 might also be related to factors such as display and social signalling and that endocrinological mechanisms might partially explain its morphology, along with spatial, mechanical and allometric factors. This hypothesis remains to be tested in the context of sexual dimorphism among fossils and living primates.

The next chapter concludes the thesis, providing a summary of the key findings and suggesting future research.

8 Conclusion

The general aim of the thesis was to understand how biting mechanics impact on the facial morphology of *H. sapiens* and its hypothesized ancestral species, *H. heidelbergensis*. To that end a virtual functional morphology toolkit, that includes GM and FEA, was used to improve conventional methodological approaches and provide new insights on this topic. Because the analyses rely heavily on FEA, it was first necessary to clarify the reliability of the results before addressing the biologically pertinent questions about recent hominin cranial form and function. Thus, the dissertation is divided in four main sections. The first section (chapter 1) provides a literature review of the core topics approached in the dissertation. The second section (chapters 2 - 4) tests the reliability of FEA results, how modelling simplifications impact on those results and provides a thorough description of the virtual reconstruction of Kabwe 1. Section 3 (chapters 5 - 6) address how biting mechanics impacts on recent hominin cranial morphology. Lastly, this conclusion summarizes the key findings.

8.1 Summary of key findings

Chapter 2 presents a validation study in which the resulting ε1 and ε3 magnitudes and directions of an experimentally loaded real cranium are compared to those of an FE model under equivalent virtual loading. To that end a first molar bite was approximated by placing the real cranium in a mechanical testing machine, constraining the two mastoid processes and first left molar and applying a vertical compressive force to the frontal bone. Resulting ε1 and ε3 magnitudes and directions were registered in the infra-orbital plate using DSPI. An equivalent virtual loading scenario was applied to the FE model and resulting strain magnitudes and directions were extracted from the equivalent region. The FE model was previously segmented by a fellow PhD student (Dr. Viviana Toro-Ibacache) and was further segmented in the current study. Our results show that absolute strain magnitudes are not adequately predicted but the distribution of regions of high and low (pattern of) strains is reasonably approximated despite some differences mainly in the alveolar region. Predicted strain vector orientations present similarities to the ones found in the real cranium but not full consistency. Thus, these results, which are generally consistent with previous validation studies, indicate that FEA is useful for prediction of general

patterns of deformation but currently lacks the resolution to predict precise absolute strain magnitudes and directions. This mismatch between real and predicted strains is related to limitations in CT imaging and full understanding of cranial material properties. Future developments in these two fields will likely improved FE model creation and allocation of material properties and improve the precision of FEA results.

Chapter 3 tests the impact of simplifications in segmentation and in the material properties of an FE model by analyzing magnitudes and modes of deformation among models with varying complexity. Hence, an FE model with three materials (model 3; cortical bone, cancellous bone and teeth) with tissue-specific material properties was simplified into two materials (model 2; cortical bone and teeth) by adding cancellous bone into cortical bone. Lastly, a one material (model 1; cortical bone) model was created by adding cancellous bone and teeth into cortical bone. Results show a general decrease in strain magnitudes when simplifying model 3 into model 2, but no significant differences between models 1 and 2. Despite this difference in magnitude the only change in pattern of strains is found in the alveolar region, with no other changes found in the remaining facial skeleton. These results are consistent with those of mode of deformation using GM. It was found that simplification from model 3 to model 2 impacts on magnitude and mode of deformation, but no differences were found between models 2 and 1. The differences in mode of deformation correspond to a larger degree of torsion of the face about an antero-posterior axis towards the working side of the facial skeleton. However, these differences in mode of deformation are small when compared to differences due to changing "bite point" from the first molar to the central incisor. Thus, these results, which are consistent with other previous studies, show that model simplification impacts mainly on magnitudes of deformation and less so on mode. This is useful when working with fossils (which is the case in this thesis) because specimens are often fragmented and invaded by sedimentary matrix, hence requiring simplifications.

The full process of reconstruction of Kabwe 1 is presented in chapter 4. Segmentation used global and regional thresholding, which was then complemented with manual segmentation to pick up regions that were not included when using the previous two approaches. Once segmentation of existing anatomy was complete, restoration of missing anatomical regions used a combination of reflection and warping of existing contra-lateral elements, use of small portions of skeletal regions of a cadaveric *H. sapiens* that were warped to the existing anatomy, surface editing using

the software Geomagic to fill in gaps in bone and manual reconstruction. The final result is highly reproducible because segmentation and reconstruction were mainly based on automated or semi-automated approaches, with minimum manual editing. Nonetheless, all reconstructions are, to a certain degree, subjective. Hence differences to other potential reconstructions are expectable, but small because the manual component of the reconstruction (segmentation and restoration of missing elements) was reduced to a minimum.

Chapter 5 compares the biting performance of *H. sapiens* to that of its hypothesized ancestral species, *H. heidelbergensis*, in order to understand if biting mechanics explains the cranial morphological differences found between these two recent hominin species. Hence, the comparison was based on an integrated approach that tests the ability to produce and resist bite force. The ability to produce bite force was tested by comparing the mechanical advantages of the jaw elevator muscles, bite forces predicted by FEA, proportion of muscle force converted into bite force and into glenoid fossa joint reaction forces. The ability to resist bite forces was tested by comparing magnitudes and modes of deformation using surface principal strain magnitudes and directions, and GM analysis of the deformations experienced by specific anatomical points. The results show that *H. sapiens* is more efficient at converting muscle force into bite force and that it produces higher absolute bite forces than the *H. heidelbergensis* representative (Kabwe 1). Despite that, it is generally less able to resist the produced bite forces, thus presenting generally higher strain magnitudes, despite localized differences. Moreover, it deforms differently when compared to Kabwe 1. These differences in magnitude and mode of deformation are due to well known anatomical differences in size and shape. This inconsistency in ability to produce and resist bite forces makes it likely that differences in biting mechanics are a biological spandrel rather than an adaptation, as previously suggested by other studies, or the result of genetic drift. One possibility is that changes in the nasal cavity, either due to selection or release of constraint, impact on the morphology of the lower face, thus changing the ability to generate and resist bite force.

The impact of biting mechanics on frontal sinus morphology is examined in chapter 6. This is tested by comparing the mechanical performance of three models of Kabwe 1 under simulated biting in which only frontal sinus morphology changes, while the remaining anatomy is kept constant. The original sinus is very large and has bony struts traversing it. This morphology (model 2) was changed by removing the bony

struts and making the sinus completely hollow (model 1) and by infilling it and making it completely solid (model 3). Three different bite points were simulated and magnitudes and modes of deformation were assessed. Results show that changes in sinus morphology have little impact and that these are negligible when compared to differences due to changes in bite point. However it should be noted that strains are consistently low in the region of the frontal sinus and in the material infilling it in model 3. Thus, it is plausible that sinus morphogenesis and therefore morphology, is impacted by biting and mechanical function via bone adaptation to low strains while the sinus fulfils one or several of the functions suggested in the literature.

Lastly, in chapter 7 the mechanical significance of the brow-ridge in examined in Kabwe 1, a privileged individual to test this because of its remarkably large brow-ridge. Three models were created with different brow-ridge morphologies. Model 1 presents the original morphology, model 2 a reduced brow-ridge and model 3 a post-orbital sulcus. Biting was simulated in three different teeth and resulting magnitudes and modes of deformation examined. It was found that changes in brow-ridge morphology had minor impact and induce changes in deformation that are significantly smaller than varying bite point. Thus, it is concluded that biting mechanics has limited impact on brow-ridge morphology and that it is influenced by multiple factors. One possible factor may be communication and social signalling, but this hypothesis requires further research.

In summary, regarding the biologically pertinent questions, it is concluded that differences in facial morphology between modern humans and their putative ancestral species, *H. heidelbergensis*, have clear mechanical impact, but it is unlikely that biting mechanics drives those differences. Rather, such differences are likely a by-product of selection acting on other cranial systems or of genetic drift. Likewise, biting mechanics has limited impact on brow-ridge morphology and other factors are needed to explain external upper face morphology. Biting also causes little deformation in the bones delimiting the frontal sinus and in the material filling the sinus when it is infilled. Whether, these low strains impact on sinus morphogenesis via bone adaptation, in this case by removal of material, which is known to occur when a low strain threshold is reached is unclear but the evidence is that the strains in this region are very low compared to elsewhere in the face and so this is a distinct possibility.

8.2 Implications for future research

The resolution of FEA studies allows prediction of general patterns of deformation but not of precise magnitudes of deformation (chapter 2). This mismatch between real and predicted deformation is the result of limitations in scanning resolution and understanding of the material properties of cranial hard and soft tissues. Thus, FEA studies will benefit greatly if crania are imaged at μCT scanning resolutions instead of that of medical CT scanning. Such level of resolution will allow proper segmentation of structures such as trabecular networks, the PDL, the temporal fascia and different dental tissues. Moreover, further research on cranial hard and soft tissue material properties that may be incorporated in FE modelling will also improve FEA prediction of deformations.

Despite these limitations, simplified FE models are still able to predict general patterns of deformation (chapters 2 and 3) and provide new insights into recent hominin cranial form and function that can guide future research. Chapter 5 brought new insights into recent hominin cranial form and function. However it did not consider the effects of intra-specific form variation in *H. heidelbergensis* and *H. sapiens* and how that impacts on the cranial biomechanical function of these species. This was not examined is this dissertation because it would require creation of other FE models, which is very time-consuming, and because of the clear morphological differences between these two species. One way of examining this topic is to perform a GM analysis of intra-specific morphological variance and create specimens that represent this variance by warping an existing specimen (e.g. Kabwe 1 in *H. heidelbergensis* and the cadaveric human cranium for *H. sapiens*) along the first principal components. This approach, already used by Smith et al (2015a), would allow assessment of the impact of the main components of morphological variation on the biomechanical performance of these species and bracket the effects of intra-specific variation.

Another question that arises from chapter 5 is if differences in biting performance are a by-product of selection acting on other cranial systems or the release of constraints acting on contiguous structures. One such structure is the internal nasal cavity. Thus, it is of interest in the future to examine how the morphology of this structure evolved from the hypothesized ancestor *H. heidelbergensis* to the descendant modern humans. This study is limited by the poor preservation of this structure in fossil hominins and by the small sample size available for *H. heidelbergensis*. Despite that

new insights may be achieved by using GM methods to estimate missing anatomical points (i.e. use of the TPS function to estimate missing landmarks) and to analyze internal nasal cavity morphology in these two species.

Literature cited

Ackermann RR, Cheverud JM. 2004. Detecting genetic drift versus selection in human evolution. Proceedings of the National Academy of Sciences of the United States of America 101:17946-17951.

Adams DC, Rohlf FJ, Slice DE. 2004. Geometric morphometrics: ten years of progress following the 'revolution'. Italian Journal of Zoology 71:5-16.

Aiello L, Dean C. 1990. Human Evolutionary Anatomy. London: Academic Press Limited.

Antón SC. 1990. Neandertals and the anterior dental loading hypothesis: a biomechanical evaluation of bite force production. Kroeber Anthropological Society Papers 71-72:67-76.

Antón SC. 1996. Tendon-associated bone features of the masticatory system in Neandertals. Journal of Human Evolution 31:391-408.

Antón SC. 1999. Macaque masseter muscle: Internal architecture, fiber length and cross-sectional area. International Journal of Primatology 20:441-462.

Antón SC. 2003. Natural history of Homo erectus. Yearbook of Physical Anthropology: Vol 46 46:126-169.

Arbour JH, Brown CM. 2014. Incomplete specimens in geometric morphometric analyses. Methods in Ecology and Evolution 5:16-26.

Baab KL, McNulty KP, Harvati K. 2013. Homo floresiensis Contextualized: A Geometric Morphometric Comparative Analysis of Fossil and Pathological Human Samples. Plos One 8:e69119.

Bacabac RG, Mizuno D, Schmidt CF, MacKintosh FC, Van Loon JJWA, Klein-Nulend J, Smit TH. 2008. Round versus flat: Bone cell morphology, elasticity, and mechanosensing. Journal of Biomechanics 41:1590-1598.

Bass WM. 1995. Human Osteology: a laboratory and field guide. Missouri: Missouri Archaeological Society.

Bastir M. 2008. A systems-model for the morphological analysis of integration and modularity in human craniofacial evolution. Journal of Anthropological Sciences 86:37-58.

Bastir M, O'Higgins P, Rosas A. 2007. Facial ontogeny in Neanderthals and modern humans. Proceedings of the Royal Society B-Biological Sciences 274:1125-1132.

Bastir M, Rosas A. 2005. Hierarchical nature of morphological integration and modularity in the human posterior face. American Journal of Physical Anthropology 128:26-34.

Bastir M, Rosas A. 2013. Cranial Airways and the Integration Between the Inner and Outer Facial Skeleton in Humans. American Journal of Physical Anthropology 152:287-293.

Bastir M, Rosas A, Lieberman DE, O'Higgins P. 2008. Middle cranial fossa anatomy and the origin of modern humans. Anatomical Record-Advances in Integrative Anatomy and Evolutionary Biology 291:130-140.

Benazzi S, Bookstein FL, Strait DS, Weber GW. 2011a. A new OH5 reconstruction with an assessment of its uncertainty. Journal of Human Evolution 61:75-88.

Benazzi S, Fantini M, De Crescenzio F, Mallegni G, Mallegni F, Persiani F, Gruppioni G. 2009a. The face of the poet Dante Alighieri reconstructed by virtual modelling and forensic anthropology techniques. Journal of Archaeological Science 36:278-283.

Benazzi S, Fiorenza L, Kozakowski S, Kullmer O. 2011b. Comparing 3D Virtual Methods for Hemimandibular Body Reconstruction. The Anatomical Record: Advances in Integrative Anatomy and Evolutionary Biology 294:1116-1125.

Benazzi S, Gruppioni G, Strait DS, Hublin J-J. 2014. Technical Note: Virtual reconstruction of KNM-ER 1813 Homo habilis cranium. American Journal of Physical Anthropology 153:154-160.

Benazzi S, Nguyen HN, Kullmer O, Hublin J-J. 2015. Exploring the biomechanics of taurodontism. Journal of Anatomy 226:180-188.

Benazzi S, Senck S. 2011. Comparing 3-Dimensional Virtual Methods for Reconstruction in Craniomaxillofacial Surgery. Journal of Oral and Maxillofacial Surgery 69:1184-1194.

Benazzi S, Stansfield E, Kullmer O, Fiorenza L, Gruppioni G. 2009b. Geometric Morphometric Methods for Bone Reconstruction: The Mandibular Condylar Process of Pico della Mirandola. The Anatomical Record: Advances in Integrative Anatomy and Evolutionary Biology 292:1088-1097.

Benazzi S, Stansfield E, Milani C, Gruppioni G. 2009c. Geometric morphometric methods for three-dimensional virtual reconstruction of a fragmented cranium: the case of Angelo Poliziano. International Journal of Legal Medicine 123:333-344.

Biegert J. 1963. The evaluation of the skull, hands, and feet for primate taxonomy. In: Washburn SL, editor. Classification and Human Evolution: Routledge. p 116-145.

Bird J, Ross C. 2012. Mechanical Engineering Principles. New York: Routledge.

Blaney SPA. 1990. Why paranasal sinuses? The Journal of Laryngology & Otology 104:690-693.

Bonucci E. 2009. The osteocyte: the underestimated conductor of the bone orchestra. RENDICONTI LINCEI 20:237-254.

Bookstein F, Schafer K, Prossinger H, Seidler H, Fieder M, Stringer C, Weber GW, Arsuaga JL, Slice DE, Rohlf FJ, Recheis W, Mariam AJ, Marcus LF. 1999. Comparing frontal cranial profiles in archaic and modern *Homo* by morphometric analysis. Anatomical Record 257:217-224.

Bookstein FL. 1997. Morphometric tools for landmark data: geometry and biology. New York: Cambridge University Press.

Brace CL. 1967. Environment, Tooth Form, and Size in the Pleistocene. Journal of Dental Research 46:809-816.

Brace CL, Mahler PE. 1971. Post-Pleistocene changes in the human dentition. American Journal of Physical Anthropology 34:191-203.

Brace CL, Rosenberg KR, Hunt KD. 1987. Gradual Change in Human Tooth Size in the Late Pleistocene and Post- Pleistocene. Evolution 41:705-720.

Brant WE, Helms CA. 2012. Fundamentals of diagnostic radiology: Lippincott Williams & Wilkins.

Bräuer G. 2001. The 'Out-of-Africa' Model and the Question of Regional Continuity. In: Tobias PV, editor. Humanity from African naissance to coming millennia. Firenze: Firenze University Press. p 183-189.

Bräuer G. 2008. The origin of modern anatomy: By speciation or intraspecific evolution? Evolutionary Anthropology 17:22-37.

Bräuer G. 2012. Middle Pleistocene Diversity in Africa and the Origin of Modern Humans. In: Hublin J-J, McPherron SP, editors. Modern Origins: Springer Netherlands. p 221-240.

Braun S, Bantleon H-P, Hnat WP, Freudenthaler JW, Marcotte MR, Johnson BE. 1995. A study of bite force, part 1: Relationship to various physical characteristics. The Angle Orthodontist 65:367-372.

Bright JA, Groning F. 2011. Strain Accommodation in the Zygomatic Arch of the Pig: A Validation Study Using Digital Speckle Pattern Interferometry and Finite Element Analysis. Journal of Morphology 272:1388-1398.

Bright JA, Rayfield EJ. 2011. Sensitivity and ex vivo validation of finite element models of the domestic pig cranium. Journal of Anatomy 219:456-471.

Buckland-Wright JC. 1970. A Radiographic Examination of Frontal Sinuses in Early British Populations. Man 5:512-517.

Buikstra J, Ubelaker D. 1994. Standards for Data Collection from Human Skeletal Remains: Proceedings of a Seminar at the Field Museum of Natural History. Arkansas: Arkansas Archeological Survey.

Burger EH, Klein-Nulend J. 1999. Mechanotransduction in bone—role of the lacuno-canalicular network. The FASEB Journal 13:101-112.

Cael C. 2010. Functional anatomy: musculoskeletal anatomy, kinesiology, and palpation for manual therapists. Baltimore: Lippincott Williams and Wilkins.

Carey JW, Steegmann AT. 1981. Human Nasal Protrusion, Latitude, and Climate. American Journal of Physical Anthropology 56:313-319.

Carlson DS. 1976. Temporal variation in prehistoric Nubian crania. American Journal of Physical Anthropology 45:467-484.

Carlson DS. 2005. Theories of Craniofacial Growth in the Postgenomic Era. Seminars in Orthodontics 11:172-183.

Carlson DS, Van Gerven DP. 1977. Masticatory function and post-pleistocene evolution in Nubia. American Journal of Physical Anthropology 46:495-506.

Cave A, Haines R. 1940. The paranasal sinuses of the anthropoid apes. Journal of Anatomy 74:493-523.

Churchill SE. 2006. Bioenergetic perspectives on Neanderthal thermoregulatory and activity budgets. In: Harvati K, Harrison T, editors. Neanderthals Revisited: New Approaches and Perspectives. Dordrecht: Springer. p 113-134.

Churchill SE. 2014. Thin on the ground [electronic resource] : Neandertal biology, archeology and ecology. Hoboken, NJ: Wiley-Blackwell.

Cieri RL, Churchill SE, Franciscus RG, Tan J, Hare B. 2014. Craniofacial Feminization, Social Tolerance, and the Origins of Behavioral Modernity. Current Anthropology 55:419-443.

Clark GA, Willermet CM. 1997. Conceptual Issues in Modern Human Origins Research (Evolutionary Foundations For Human Behavior). New York: Walter de Gruyter & Co.

Clement AF, Hillson SW, Aiello LC. 2012. Tooth wear, Neanderthal facial morphology and the anterior dental loading hypothesis. Journal of Human Evolution 62:367-376.

Cobb SN, O'Higgins P. 2004. Hominins do not share a common postnatal facial ontogenetic shape trajectory. Journal of Experimental Zoology Part B-Molecular and Developmental Evolution 302B:302-321.

Cobb SN, O'Higgins P. 2007. The ontogeny of sexual dimorphism in the facial skeleton of the African apes. Journal of Human Evolution 53:176-190.

Coleman MN, Colbert MW. 2007. Technical note: CT thresholding protocols for taking measurements on three-dimensional models. American Journal of Physical Anthropology 133:723-725.

Collard M, O'Higgins PO. 2001. Ontogeny and homoplasy in the papionin monkey face. Evolution & Development 3:322-331.

Coon CS. 1962. The origin of Races. New York: Knopf.

Cowin S, Doty S. 2007. Tissue Mechanics. New York: Springer.

Cowin SC. 2001. Bone mechanics handbook.

Cox PG, Fagan MJ, Rayfield EJ, Jeffery N. 2011. Finite element modelling of squirrel, guinea pig and rat skulls: using geometric morphometrics to assess sensitivity. Journal of Anatomy 219:696-709.

Cox PG, Jeffery N. 2011. Reviewing the Morphology of the Jaw-Closing Musculature in Squirrels, Rats, and Guinea Pigs with Contrast-Enhanced MicroCt. The Anatomical Record: Advances in Integrative Anatomy and Evolutionary Biology 294:915-928.

Cox PG, Rinderknecht A, Blanco RE. 2015. Predicting bite force and cranial biomechanics in the largest fossil rodent using finite element analysis. Journal of Anatomy 226:215-223.

Cryer MH. 1916. The internal anatomy of the face: Lea & Febiger.

Currey JD. 2006. Bones, Structure and Mechanics. New Jersey: Princeton University Press.

Daegling DJ. 1993. Functional morphology of the human chin. Evolutionary Anthropology: Issues, News, and Reviews 1:170-177.

Daegling DJ, Hylander WL. 1998. Biomechanics of torsion in the human mandible. American Journal of Physical Anthropology 105:73-87.

Daegling DJ, Hylander WL. 2000. Experimental observation, theoretical models, and biomechanical inference in the study of mandibular form. American Journal of Physical Anthropology 112:541-551.

Daegling DJ, Ravosa MJ, Johnson KR, Hylander WL. 1992. Influence of Teeth, Alveoli, and Periodontal Ligaments on Torsional Rigidity in Human Mandibles. American Journal of Physical Anthropology 89:59-72.

Dean MC. 1988. Another look at the nose and the functional significance of the face and nasal mucous membrane for cooling the brain in fossil hominids. Journal of Human Evolution 17:715-718.

Dechow P, Chung D, Bolouri M. 2008. Relationship Between Three-Dimensional Microstructure and Elastic Properties of Cortical Bone in the Human Mandible and Femur. In: Vinyard C, Ravosa M, Wall C, editors. Primate Craniofacial Function and Biology. New York: Springer US. p 265-292.

Dechow PC, Nail GA, Schwartz-Dabney CL, Ashman RB. 1993. Elastic Properties of Human Supraorbital and Mandibular Bone. American Journal of Physical Anthropology 90:291-306.

Dechow PC, Wang Q, Peterson J. 2010. Edentulation Alters Material Properties of Cortical Bone in the Human Craniofacial Skeleton: Functional Implications for Craniofacial Structure in Primate Evolution. The Anatomical Record: Advances in Integrative Anatomy and Evolutionary Biology 293:618-629.

Delson E, Harvati K, Reddy D, Marcus LF, Mowbray K, Sawyer GJ, Jacob T, Marquez S. 2001. The Sambungmacan 3 Homo erectus calvaria: A comparative morphometric and morphological analysis. Anatomical Record 262:380-397.

Demes B. 1987. Another Look at an Old Face - Biomechanics of the Neandertal Facial Skeleton Reconsidered. Journal of Human Evolution 16:297-303.

Demes B, Creel N. 1988. Bite Force, Diet, and Cranial Morphology of Fossil Hominids. Journal of Human Evolution 17:657-670.

Dobson SD, Trinkaus E. 2002. Cross-sectional geometry and morphology of the mandibular symphysis in Middle and Late Pleistocene Homo. Journal of Human Evolution 43:67-87.

Dryden IL, Mardia KV. 1998. Statistical Shape Analysis: Wiley-Blackwell.

Dumont ER, Grosse IR, Slater GJ. 2009. Requirements for comparing the performance of finite element models of biological structures. Journal of Theoretical Biology 256:96-103.

Elliott M, Kurki H, Weston DA, Collard M. 2014. Estimating fossil hominin body mass from cranial variables: An assessment using CT data from modern humans of known body mass. American Journal of Physical Anthropology 154:201-214.

Elton S, Morgan B. 2006. Muzzle size, paranasal swelling size and body mass in Mandrillus leucophaeus. Primates 47:151-157.

Endo B. 1965. Distribution of Stress and Strain Produced in the Human Facial Skeleton by the Masticatory Force. The Journal of Anthropological Society of Nippon 73:123-136.

Endo B. 1966. Experimental Studies on the Mechanical Significance of the Form of the Human Facial Skeleton: University.

Endo B. 1970. Analysis of Stresses around the Orbit Due to Masseter and Temporalis Muscles Respectively. The Journal of Anthropological Society of Nippon 78:251-266.

Eng CM, Lieberman DE, Zink KD, Peters MA. 2013. Bite force and occlusal stress production in hominin evolution. American Journal of Physical Anthropology 151:544-557.

Enlow DH. 1968. The human face: an account of the postnatal growth and development of the craniofacial skeleton: Hoeber Medical Division, Harper & Row.

Enlow DH, Hans MG. 1996. Essentials of Facial Growth. Philadelphia: W. B. Saunders Company.

Enlow DH, McNamara JA. 1973. The Neurocranial Basis for Facial Form and Pattern. The Angle Orthodontist 43:256-270.

Ethier CR, Simmons CA. 2007. Introductory Biomechanics - From Cells to Organisms. New York: Cambridge University Press.

Evans SP, Parr WCH, Clausen PD, Jones A, Wroe S. 2012. Finite element analysis of a micromechanical model of bone and a new 3D approach to validation. Journal of Biomechanics 45:2702-2705.

Fagan MJ, Curtis N, Dobson CA, Karunanayake JH, Kitpczik K, Moazen M, Page L, Phillips R, O'Higgins P. 2007. Voxel-based finite element analysis - Working directly with microCT scan data. Journal of Morphology 268:1071-1071.

Fitton LC, PrôA M, Rowland C, Toro-Ibacache V, O'Higgins P. 2015. The Impact of Simplifications on the Performance of a Finite Element Model of a Macaca fascicularis Cranium. The Anatomical Record 298:107-121.

Fitton LC, Shi JF, Fagan MJ, O'Higgins P. 2012. Masticatory loadings and cranial deformation in *Macaca fascicularis*: a finite element analysis sensitivity study. Journal of Anatomy 221:55-68.

Franciscus RG, Long JC. 1991. Variation in Human Nasal Height and Breadth. American Journal of Physical Anthropology 85:419-427.

Franciscus RG, Trinkaus E. 1988. The Neandertal nose. American Journal of Physical Anthropology 75:209-210.

Franklin D, Cardini A, O'Higgins P, Oxnard CE, Dadour I. 2007. Mandibular morphology as an indicator of human subadult age: geometric morphometric approaches. Forensic Science, Medicine, and Pathology 4:91-99.

Freidline SE, Gunz P, Harvati K, Hublin J-J. 2013. Evaluating developmental shape changes in Homo antecessor subadult facial morphology. Journal of Human Evolution 65:404-423.

Freidline SE, Gunz P, Harvati K, Hublin JJ. 2012. Middle Pleistocene human facial morphology in an evolutionary and developmental context. Journal of Human Evolution 63:723-740.

Frost HM. 1987. Bone "mass" and the "mechanostat": A proposal. The Anatomical Record 219:1-9.

Frost HM. 1996. Perspectives: A proposed general model of the "mechanostat" (suggestions from a new skeletal-biologic paradigm). The Anatomical Record 244:139-147.

Frost HM. 2003. Bone's mechanostat: A 2003 update. The Anatomical Record Part A: Discoveries in Molecular, Cellular, and Evolutionary Biology 275A:1081-1101.

Gans C, de Vree F. 1987. Functional bases of fiber length and angulation in muscle. Journal of Morphology 192:63-85.

Giraud-Guille MM. 1988. Twisted plywood architecture of collagen fibrils in human compact bone osteons. Calcified Tissue International 42:167-180.

Goodship AE, Cunningham JL, Oganov V, Darling J, Miles AW, Owen GW. 1998. Bone loss during long term space flight is prevented by the application of a short term impulsive mechanical stimulus. Acta Astronautica 43:65-75.

Görke O. 1904. Beitrag zur funktionellen Gestaltung des Schädels bei den Anthropomorphen und Menschen durch Untersuchung mit Röntgenstrahlen. Arch Anthrop 1:91-108.

Gould SJ, Lewontin RC. 1979. The Spandrels of San Marco and the Panglossian Paradigm: A Critique of the Adaptationist Programme. Proceedings of the Royal Society of London. Series B, Biological Sciences 205:581-598.

Gould SJ, Vrba ES. 1982. Exaptation-A Missing Term in the Science of Form. Paleobiology 8:4-15.

Greaves W, Mucci R. 1997. Mechanical loads in the postorbital bar during mastication in artiodactyls and primates. Am J Phys Anthropol [Suppl] 23:119.

Greaves WS. 1985. The Mammalian Postorbital Bar as a Torsion-Resisting Helical Strut. Journal of Zoology 207:125-136.

Greene DL, Scott L. 1973. Congenital Frontal Sinus Absence in the Wadi Halfa Mesolithic Population. Man 8:471-474.

Grine FE, Gunz P, Betti-Nash L, Neubauer S, Morris AG. 2010a. Reconstruction of the late Pleistocene human skull from Hofmeyr, South Africa. Journal of Human Evolution 59:1-15.

Grine FE, Judex S, Daegling DJ, Ozcivici E, Ungar PS, Teaford MF, Sponheimer M, Scott J, Scott RS, Walker A. 2010b. Craniofacial biomechanics and functional and dietary inferences in hominin paleontology. Journal of Human Evolution 58:293-308.

Groning F, Bright JA, Fagan MJ, O'Higgins P. 2012a. Improving the validation of finite element models with quantitative full-field strain comparisons. Journal of Biomechanics 45:1498-1506.

Groning F, Fagan M, O'Higgins P. 2012b. Modeling the Human Mandible Under Masticatory Loads: Which Input Variables are Important? Anatomical Record-Advances in Integrative Anatomy and Evolutionary Biology 295:853-863.

Groning F, Fagan MJ, O'Higgins P. 2011a. The effects of the periodontal ligament on mandibular stiffness: a study combining finite element analysis and geometric morphometrics. Journal of Biomechanics 44:1304-1312.

Groning F, Liu J, Fagan MJ, O'Higgins P. 2009. Validating a voxel-based finite element model of a human mandible using digital speckle pattern interferometry. Journal of Biomechanics 42:1224-1229.

Groning F, Liu J, Fagan MJ, O'Higgins P. 2011b. Why Do Humans Have Chins? Testing the Mechanical Significance of Modern Human Symphyseal Morphology With Finite Element Analysis. American Journal of Physical Anthropology 144:593-606.

Gross MD, Arbel G, Hershkovitz I. 2001. Three-dimensional finite element analysis of the facial skeleton on simulated occlusal loading. Journal of Oral Rehabilitation 28:684-694.

Gunz P, Mitteroecker P, Bookstein F, Weber G. 2004. Computer-aided reconstruction of incomplete human crania using statistical and geometrical estimation methods. In: Computer Applications and Quantitative Methods in Archaeology: Archaeopress. p 92–94.

Gunz P, Mitteroecker P, Neubauer S, Weber GW, Bookstein FL. 2009. Principles for the virtual reconstruction of hominin crania. Journal of Human Evolution 57:48-62.

Guo XE. 2001. Mechanical Properties of Cortical Bone and Cancellous Bone Tissue. In: Bone Mechanics Handbook, Second Edition: CRC Press. p 10-11-10-23.

Hall BK. 2005. Bones and Cartilage: Developmental and Evolutionary Skeletal Biology. San Diego: Elsevier Academic Press.

Hand AR, Frank ME. 2014. Fundamental of Oral Histology and Physiology. Pondicherry: Wiley Blackwell.

Hannam AG, Wood WW. 1989. Relationships between the size and spatial morphology of human masseter and medial pterygoid muscles, the craniofacial skeleton, and jaw biomechanics. American Journal of Physical Anthropology 80:429-445.

Harvati K, Hublin JJ, Gunz P. 2010. Evolution of middle-late Pleistocene human cranio-facial form: A 3-D approach. Journal of Human Evolution 59:445-464.

He LH, Fujisawa N, Swain MV. 2006. Elastic modulus and stress–strain response of human enamel by nano-indentation. Biomaterials 27:4388-4398.

He LH, Swain MV. 2008. Understanding the mechanical behaviour of human enamel from its structural and compositional characteristics. Journal of the Mechanical Behavior of Biomedical Materials 1:18-29.

Heyes P, MacDonald K. 2015. Neandertal energetics: Uncertainty in body mass estimation limits comparisons with Homo sapiens. Journal of Human Evolution 85:193-197.

Hildebrand M. 1995. Analysis of vertebrate structure, 4th edition ed. New York: Wiley.

Hillam RA, Jackson M, Goodship AE, Skerry TM. 1995. Regional Differences in Human Bone Strain in-Vivo. Journal of Bone and Mineral Research 10:S443-S443.

Hilloowala RA, Trent RB. 1988a. Supraorbital ridge and masticatory apparatus I: Primates. Human Evolution 3:343-350.

Hilloowala RA, Trent RB. 1988b. Supraorbital ridge and masticatory apparatus II: Humans (Eskimos). Human Evolution 3:351-356.

Himeno-Ando A, Izumi Y, Yamaguchi A, Iimura T. 2012. Structural differences in the osteocyte network between the calvaria and long bone revealed by three-dimensional fluorescence morphometry, possibly reflecting distinct mechano-adaptations and sensitivities. Biochemical and Biophysical Research Communications 417:765-770.

Hodgskinson R, Currey JD. 1992. Young's modulus, density and material properties in cancellous bone over a large density range. Journal of Materials Science: Materials in Medicine 3:377-381.

Holland M. 2013. The effect of the inclusion of the periodontal ligament upon the stiffness of a human cranial finite element model: a validated sensitivity study. In: HYMS. York: University of York.

Holton NE, Bonner LL, Scott JE, Marshall SD, Franciscus RG, Southard TE. 2015. The ontogeny of the chin: an analysis of allometric and biomechanical scaling. Journal of Anatomy 226:549-559.

Holton NE, Franciscus RG, Ravosa MJ, Southard TE. 2014. Functional and morphological correlates of mandibular symphyseal form in a living human sample. American Journal of Physical Anthropology 153:387-396.

Horowitz SL, Thompson RH. 1964. Variations Of The Craniofacial Skeleton In Postadolescent Males And Females. The Angle Orthodontist 34:97-102.

Humphrey JD, Delange SL. 2004. An introduction to biomechanics: solids and fluids, analysis and design. New York: Springer Science & Business Media.

Hylander W, Johnson KR. 2002. Functional morphology and *In Vivo* bone strain patterrns in the craniofacial region of primates: beware of biomechanical stories about fossils. In: Plavcan JM, Kay RF, Jungers WL, Schaik CP, editors. Reconstructing Behavior in the Primate Fossil Record. New York: Kluwer Academic/Plenum Publishers. p 43-72.

Hylander W, Picq PG, Johnson KR. 1992. Bone strain and the supraorbital region of primates. In: Carlson DS, Goldstein SA, editors. Bone biodynamics in orthodontic and orthopaedic treatment. Ann Arbor, MI: Center for Human Growth and Development. p 315-349.

Hylander WL, Picq PG, Johnson KR. 1991a. Function of the Supraorbital Region of Primates. Archives of Oral Biology 36:273-281.

Hylander WL, Picq PG, Johnson KR. 1991b. Masticatory-Stress Hypotheses and the Supraorbital Region of Primates. American Journal of Physical Anthropology 86:1-36.

Ichim I, Kieser JA, Swain MV. 2007a. Functional significance of strain distribution in the human mandible under masticatory load: Numerical predictions. Archives of Oral Biology 52:465-473.

Ichim P, Kieser J, Swain M. 2007b. Tongue Contractions during speech may have led to the development of the bony geometry of the chin following the evolution of human language: a mechanobiological hypothesis for the development of the human chin. Medical Hypotheses 69:20-24.

Janovic A, Saveljic I, Vukicevic A, Nikolic D, Rakocevic Z, Jovicic G, Filipovic N, Djuric M. 2015. Occlusal load distribution through the cortical and trabecular bone of the human mid-facial skeleton in natural dentition: A three-dimensional finite element study. Annals of Anatomy - Anatomischer Anzeiger 197:16-23.

Jones HH, Priest JD, Hayes WC, Tichenor CC, Nagel DA. 1977. Humeral Hypertrophy in Response to Exercise. Journal of Bone and Joint Surgery-American Volume 59:204-208.

Josephson RK. 1975. Extensive and intensive factors determining the performance of striated muscle. Journal of Experimental Zoology 194:135-153.

Judex S, Lei X, Han D, Rubin C. 2007. Low-magnitude mechanical signals that stimulate bone formation in the ovariectomized rat are dependent on the applied frequency but not on the strain magnitude. Journal of Biomechanics 40:1333-1339.

Junqueira LC, Carneiro J. 2003. Basic Histology, 10th Edition ed. New York: McGraw-Hill.

Kalvin AD, Dean D, Hublin JJ. 1995. Reconstruction of human fossils. IEEE Computer Graphics and Applications 15:12-15.

Kannus P, Haapasalo H, Sankelo M, Sievanen H, Pasanen M, Heinonen A, Oja P, Vuori I. 1995. Effect of Starting Age of Physical-Activity on Bone Mass in the Dominant Arm of Tennis and Squash Players. Annals of Internal Medicine 123:27-31.

Katz J. 2008. Mechanics of hard tissue. In: Peterson DR, Bronzino JD, editors. Biomechanics: principles and applications: Boca Raton, Florida: CRC Press. p 1-20.

Keaveny TM, Morgan EF, Niebur GL, Yeh OC. 2001. Biomechanics of trabecular bone. Annual Review of Biomedical Engineering 3:307-333.

Kerr A. 2010. Introductory Biomechanics. Edinburgh: Churchill Livingstone Elsevier.

Kerr D, Morton A, Dick I, Prince R. 1996. Exercise effects on bone mass in postmenopausal women are site-specific and load-dependent. Journal of Bone and Mineral Research 11:218-225.

Kikuchi M, Korioth TWP, Hannam AG. 1997. The Association Among Occlusal Contacts, Clenching Effort, and Bite Force Distribution in Man. Journal of Dental Research 76:1316-1325.

Kim HD, Walsh WR. 1992. Mechanical and ultrasonic characterization of cortical bone. Biomimetics 1:293-310.

Klein-Nulend J, Bonewald L. 2008. The Osteocyte. In: Bilezikian JP, Raisz LG, Martin TJ, editors. Principles of Bone Biology. San Diego: Elsevier Inc. p 153-174.

Klingenberg CP. 2010. Evolution and development of shape: integrating quantitative approaches. Nat Rev Genet 11:623-635.

Klingenberg CP. 2013. Cranial integration and modularity: insights into evolution and development from morphometric data. Hystrix-Italian Journal of Mammalogy 24:43-58.

Klingenberg CP, Mebus K, Auffray JC. 2003. Developmental integration in a complex morphological structure: how distinct are the modules in the mouse mandible? Evolution & Development 5:522-531.

Koertvelyessy T. 1972. Relationships between the frontal sinus and climatic conditions: A skeletal approach to cold adaptation. American Journal of Physical Anthropology 37:161-172.

Kranioti EF, Holloway R, Senck S, Ciprut T, Grigorescu D, Harvati K. 2011. Virtual Assessment of the Endocranial Morphology of the Early Modern European Fossil Calvaria From Cioclovina, Romania. The Anatomical Record: Advances in Integrative Anatomy and Evolutionary Biology 294:1083-1092.

Krantz GS. 1973. Cranial Hair and Brow Ridges. Mankind 9:109-111.

Kupczik K. 2008. Virtual biomechanics: basic concepts and technical aspects of finite element analysis in vertebrate morphology. Journal of Anthropological Sciences 86:193-198.

Kupczik K, Dobson CA, Crompton RH, Phillips R, Oxnard CE, Fagan MJ, O'Higgins P. 2009. Masticatory Loading and Bone Adaptation in the Supraorbital Torus of Developing Macaques. American Journal of Physical Anthropology 139:193-203.

Kupczik K, Dobson CA, Fagan MJ, Crompton RH, Oxnard CE, O'Higgins P. 2007. Assessing mechanical function of the zygomatic region in macaques: validation and sensitivity testing of finite element models. Journal of Anatomy 210:41-53.

Laitman JT. 2008. Harnessing the Hallowed Hollows of the Head: The Mysterious World of the Paranasal Sinuses. The Anatomical Record: Advances in Integrative Anatomy and Evolutionary Biology 291:1346-1349.

Lanyon LE, Rubin CT. 1984. Static Vs Dynamic Loads as an Influence on Bone Remodeling. Journal of Biomechanics 17:897-905.

Larsen WJ. 2002. Anatomy: Development, Function, Clinical Correlations. Saint Louis: Saunders.

Leakey LS. 1959. A new fossil skull from Olduvai. Nature 184:491-493.

Ledogar JA, Smith AL, Benazzi S, Weber GW, Spencer MA, Carlson KB, McNulty KP, Dechow PC, Grosse IR, Ross CF, Richmond BG, Wright BW, Wang Q, Byron C, Carlson KJ, de Ruiter DJ, Berger LR, Tamvada K, Pryor LC, Berthaume MA, Strait DS. 2016. Mechanical evidence that Australopithecus sediba was limited in its ability to eat hard foods. Nat Commun 7.

Lesne A, Bourgine P. 2011. Introduction. In: Bourgine P, Lesne A, editors. Morphogenesis - Origins of patterns and shapes. Heidelberg: Springer-Verlag. p 1 - 13.

Lieberman D. 2000. Ontogeny, homology, and phylogeny in the hominid craniofacial skeleton: the problem of the browridge. In: O'Higgins P, Cohn M, editors. Development, Growth and Evolution - Implications for the Study of the Hominid Skeleton. London: Academic Press. p 85 - 122.

Lieberman D. 2011. The Evolution of the Human Head. Cambridge: Harvard University Press.

Lieberman DE. 2008. Speculations about the selective basis for modern human craniofacial form. Evolutionary Anthropology 17:55-68.

Lieberman DE, McBratney BM, Krovitz G. 2002. The evolution and development of cranial form in Homo sapiens. Proceedings of the National Academy of Sciences of the United States of America 99:1134-1139.

Lindsay DT. 1996. Functional Human Anatomy. St. Louis: Mosby-Year Book, Inc.

Liu J, Shi JF, Fitton LC, Phillips R, O'Higgins P, Fagan MJ. 2012. The application of muscle wrapping to voxel-based finite element models of skeletal structures. Biomechanics and Modeling in Mechanobiology 11:35-47.

Logan D. 2007. A First Course in the Finite Element Method. Delhi: Thomson.

Lundberg JO. 2008. Nitric Oxide and the Paranasal Sinuses. The Anatomical Record: Advances in Integrative Anatomy and Evolutionary Biology 291:1479-1484.

Marieb E. 1992. Human anatomy and physiology. Redwood City, California: Curnmings Publishing Company, Inc.

Marinescu R, Daegling DJ, Rapoff AJ. 2005. Finite-element modeling of the anthropoid mandible: The effects of altered boundary conditions. Anatomical Record Part a-Discoveries in Molecular Cellular and Evolutionary Biology 283A:300-309.

Márquez S. 2008. The Paranasal Sinuses: The Last Frontier in Craniofacial Biology. The Anatomical Record: Advances in Integrative Anatomy and Evolutionary Biology 291:1350-1361.

McCormack SW, Witzel U, Watson PJ, Fagan MJ, Gröning F. 2014. The Biomechanical Function of Periodontal Ligament Fibres in Orthodontic Tooth Movement. Plos One 9:e102387.

McElhaney JH. 1966. Dynamic response of bone and muscle tissue. Journal of Applied Physiology 21:1231-1236.

Milne N, O'Higgins P. 2012. Scaling of form and function in the xenarthran femur: a 100-fold increase in body mass is mitigated by repositioning of the third trochanter. Proceedings of the Royal Society B-Biological Sciences 279:3449-3456.

Misch CE, Qu ZM, Bidez MW. 1999. Mechanical properties of trabecular bone in the human mandible: Implications for dental implant treatment planning and. Surgical placement. Journal of Oral and Maxillofacial Surgery 57:700-706.

Mitteroecker P, Bookstein F. 2008. The evolutionary role of modularity and integration in the hominoid cranium. Evolution 62:943-958.

Mitteroecker P, Gunz P. 2009. Advances in Geometric Morphometrics. Evolutionary Biology 36:235-247.

Mitteroecker P, Gunz P, Bernhard M, Schaefer K, Bookstein FL. 2004. Comparison of cranial ontogenetic trajectories among great apes and humans. Journal of Human Evolution 46:679-697.

Monteiro LR. 1999. Multivariate Regression Models and Geometric Morphometrics: The Search for Causal Factors in the Analysis of Shape. Systematic Biology 48:192-199.

Monteiro LR, Duarte LC, dos Reis SF. 2003. Environmental correlates of geographical variation in skull and mandible shape of the punare rat Thrichomys apereoides (Rodentia : Echimyidae). Journal of Zoology 261:47-57.

More ST, Bindu R. 2015. Effect of Mesh Size on Finite Element Analysis of Plate Structure. International Journal of Engineering Science and Innovative Technology 4:181-185.

Mosley JR, Lanyon LE. 1998. Strain rate as a controlling influence on adaptive modeling in response to dynamic loading of the ulna in growing male rats. Bone 23:313-318.

Moss ML. 1997a. The functional matrix hypothesis revisited. 1. The role of mechanotransduction. American Journal of Orthodontics and Dentofacial Orthopedics 112:8-11.

Moss ML. 1997b. The functional matrix hypothesis revisited. 4. The epigenetic antithesis and the resolving synthesis. American Journal of Orthodontics and Dentofacial Orthopedics 112:410-417.

Moss ML, Young RW. 1960. Functional-Approach to Craniology. American Journal of Physical Anthropology 18:281-292.

Naveh GRS, Chattah NLT, Zaslansky P, Shahar R, Weiner S. 2012. Tooth-PDL-bone complex: Response to compressive loads encountered during mastication - A review. Archives of Oral Biology 57:1575-1584.

Neaux D, Gilissen E, Coudyzer W, Guy F. 2015. Integration between the face and the mandible of Pongo and the evolution of the craniofacial morphology of orangutans. American Journal of Physical Anthropology:n/a-n/a.

Neeser R, Ackermann RR, Gain J. 2009. Comparing the accuracy and precision of three techniques used for estimating missing landmarks when reconstructing fossil hominin crania. American Journal of Physical Anthropology 140:1-18.

Neubauer S, Gunz P, Mitteroecker P, Weber GW. 2004. Three-dimensional digital imaging of the partial Australopithecus africanus endocranium MLD 37/38. Canadian Association of Radiologists Journal-Journal De L Association Canadienne Des Radiologistes 55:271-278.

Nishida S, Endo N, Yamagiwa H, Tanizawa T, Takahashi EH. 1999. Number of osteoprogenitor cells in human bone marrow markedly decreases after skeletal maturation. Journal of Bone and Mineral Metabolism 17:171-177.

Noback ML, Harvati K. 2015a. The contribution of subsistence to global human cranial variation. Journal of Human Evolution 80:34-50.

Noback ML, Harvati K. 2015b. Covariation in the Human Masticatory Apparatus. The Anatomical Record 298:64-84.

Noback ML, Harvati K, Spoor F. 2011. Climate-related variation of the human nasal cavity. American Journal of Physical Anthropology 145:599-614.

Nordstrom P, Thorsen K, Bergstrom E, Lorentzon R. 1996. High bone mass and altered relationships between bone mass, muscle strength, and body constitution in adolescent boys on a high level of physical activity. Bone 19:189-195.

O'Connor CF, Franciscus RG, Holton NE. 2005. Bite force production capability and efficiency in neandertals and modern humans. American Journal of Physical Anthropology 127:129-151.

O'Higgins P. 1997. Methodological issues in the description of forms. In: Lestrel PE, editor. Fourier Descriptors and their Applications in Biology: Cambridge University Press. p 74-105.

O'Higgins P. 2000. The study of morphological variation in the hominid fossil record: biology, landmarks and geometry. Journal of Anatomy 197:103-120.

O'Higgins P, Bastir M, Kupczik K. 2006. Shaping the human face. In: Bromage TG, Vidal A, Aguirre E, A. P-O, editors. Integrative approaches to human health and evolution. Amsterdam: Elsevier.

O'Higgins P, Cobb SN, Fitton LC, Groning F, Phillips R, Liu J, Fagan MJ. 2011. Combining geometric morphometrics and functional simulation: an emerging toolkit for virtual functional analyses. Journal of Anatomy 218:3-15.

O'Higgins P, Fitton LC, Phillips R, Shi JF, Liu J, Groning F, Cobb SN, Fagan MJ. 2012. Virtual Functional Morphology: Novel Approaches to the Study of Craniofacial Form and Function. Evolutionary Biology 39:521-535.

O'Higgins P, Milne N. 2013. Applying geometric morphometrics to compare changes in size and shape arising from finite elements analyses. Hystrix, the Italian Journal of Mammalogy 24:7.

Ortner DJ. 2003. Identification of Pathological Conditions in Human Skeletal Remains. San Diego: Academic Press.

Oxnard C, O'Higgins P. 2009. Biology Clearly Needs Morphometrics. Does Morphometrics Need Biology? Biological Theory 4:84-97.

Oyen OJ, Rice RW, Cannon MS. 1979. Browridge Structure and Function in Extant Primates and Neanderthals. American Journal of Physical Anthropology 51:83-96.

Pampush JD. 2015. Selection played a role in the evolution of the human chin. Journal of Human Evolution 82:127-136.

Pampush JD, Daegling DJ. 2015. Symphyseal surface strain during in vitro human mandibular wishboning. American Journal of Physical Anthropology:n/a-n/a.

Paphangkorakit J, Osborn JW. 1997. Effect of Jaw Opening on the Direction and Magnitude of Human Incisal Bite Forces. Journal of Dental Research 76:561-567.

Parkinson IH, Fazzalari NL. 2013. Characterisation of Trabecular Bone Structure. In: Silva JM, editor. Skeletal Aging and Osteoporosis: Biomechanics and Mechanobiology. Berlin, Heidelberg: Springer Berlin Heidelberg. p 31-51.

Parr WCH, Chamoli U, Jones A, Walsh WR, Wroe S. 2013. Finite element micro-modelling of a human ankle bone reveals the importance of the trabecular network to mechanical performance: New methods for the generation and comparison of 3D models. Journal of Biomechanics 46:200-205.

Parr WCH, Wroe S, Chamoli U, Richards HS, McCurry MR, Clausen PD, McHenry C. 2012. Toward integration of geometric morphometrics and computational biomechanics: New methods for 3D virtual reconstruction and quantitative analysis of Finite Element Models. Journal of Theoretical Biology 301:1-14.

Peterson J, Dechow PC. 2002. Material properties of the inner and outer cortical tables of the human parietal bone. The Anatomical Record 268:7-15.

Peterson J, Dechow PC. 2003a. Material properties of the human cranial vault and zygoma. Anatomical Record Part a-Discoveries in Molecular Cellular and Evolutionary Biology 274A:785-797.

Peterson J, Dechow PC. 2003b. Material properties of the human cranial vault and zygoma. The Anatomical Record Part A: Discoveries in Molecular, Cellular, and Evolutionary Biology 274A:785-797.

Peterson J, Wang Q, Dechow PC. 2006. Material properties of the dentate maxilla. Anatomical Record Part a-Discoveries in Molecular Cellular and Evolutionary Biology 288A:962-972.

Picq PG, Hylander WL. 1989. Endo Stress-Analysis of the Primate Skull and the Functional-Significance of the Supraorbital Region. American Journal of Physical Anthropology 79:393-398.

Ponce De León MS, Zollikofer CPE. 1999. New evidence from Le Moustier 1: Computer-assisted reconstruction and morphometry of the skull. The Anatomical Record 254:474-489.

Preuschoft H, Witzel U. 2002. Biomechanical investigations on the skulls of reptiles and mammals. Senckenbergiana lethaea 82:207-222.

Prôa M. 2013. Cranial Form Evolution and Functional Adaptations to Diet among Papionins: A Comparative Study combining Quantitative Genetics, Geometric Morphometrics, and Finite Element Analysis. In: Hull York Medical School. York: University of York.

Prossinger H, Bookstein F, Schafer K, Seidler H. 2000. Reemerging stress: Supraorbital torus morphology in the mid-sagittal plane? Anatomical Record 261:170-172.

Prossinger H, Seidler H, Wicke L, Weaver D, Recheis W, Stringer C, Müller GB. 2003. Electronic removal of encrustations inside the Steinheim cranium reveals paranasal sinus features and deformations, and provides a revised endocranial volume estimate. The Anatomical Record Part B: The New Anatomist 273B:132-142.

Püschel T. 2013. Biomechanical Modelling of Human Femora: a comparison between agriculturalists and hunter-gatherers using FEA, GMM and beam theory. In: Hull York Medical School. York: University of York.

Quinto-Sánchez M, Adhikari K, Acuña-Alonzo V, Cintas C, Silva de Cerqueira CC, Ramallo V, Castillo L, Farrera A, Jaramillo C, Arias W, Fuentes M, Everardo P, de Avila F, Gomez-Valdés J, Hünemeier T, Gibbon S, Gallo C, Poletti G, Rosique J, Bortolini MC, Canizales-Quinteros S, Rothhammer F, Bedoya G, Ruiz-Linares A, González-José R. 2015. Facial asymmetry and genetic ancestry in Latin American admixed populations. American Journal of Physical Anthropology:n/a-n/a.

Rae TC, Hill RA, Hamada Y, Koppe T. 2003. Clinal variation of maxillary sinus volume in Japanese macaques (*Macaca fuscata*). American Journal of Primatology 59:153-158.

Rae TC, Koppe T. 2004. Holes in the head: Evolutionary interpretations of the paranasal sinuses in catarrhines. Evolutionary Anthropology: Issues, News, and Reviews 13:211-223.

Rae TC, Koppe T. 2008. Independence of Biomechanical Forces and Craniofacial Pneumatization in *Cebus*. The Anatomical Record: Advances in Integrative Anatomy and Evolutionary Biology 291:1414-1419.

Rae TC, Vioarsdottir US, Jeffery N, Steegmann AT. 2006. Developmental response to cold stress in cranial morphology of *Rattus*: implications for the interpretation of climatic adaptation in fossil hominins. Proceedings of the Royal Society B-Biological Sciences 273:2605-2610.

Rak Y. 1983. The Australopithecine Face. In: Rak Y, editor. The Australopithecine Face: Academic Press. p 1.

Rak Y. 1986. The Neanderthal - a New Look at an Old Face. Journal of Human Evolution 15:151-164.

Ravosa MJ. 1988. Browridge Development in Cercopithecidae - a Test of 2 Models. American Journal of Physical Anthropology 76:535-555.

Ravosa MJ. 1991. Ontogenetic perspective on mechanical and nonmechanical models of primate circumorbital morphology. American Journal of Physical Anthropology 85:95-112.

Ravosa MJ, Johnson KR, Hylander WL. 2000a. Strain in the galago facial skull. Journal of Morphology 245:51-66.

Ravosa MJ, Noble VE, Hylander WL, Johnson KR, Kowalski EM. 2000b. Masticatory stress, orbital orientation and the evolution of the primate postorbital bar. Journal of Human Evolution 38:667-693.

Ravosa MJ, Vinyard CJ, Hylander WL. 2000c. Stressed out: Masticatory forces and primate circumorbital form. Anatomical Record 261:173-175.

Rayfield EJ. 2007. Finite element analysis and understanding the biomechanics and evolution of living and fossil organisms. Annual Review of Earth and Planetary Sciences 35:541-576.

Reed DA, Porro LB, Iriarte-Diaz J, Lemberg JB, Holliday CM, Anapol F, Ross CF. 2011. The impact of bone and suture material properties on mandibular function in Alligator mississippiensis: testing theoretical phenotypes with finite element analysis. Journal of Anatomy 218:59-74.

Reif W-E, Thomas RK, Fischer M. 1985. Constructional morphology: The analysis of constraints in evolution dedicated to A. Seilacher in honour of his 60. birthday. Acta Biotheoretica 34:233-248.

Rho J-Y, Roy ME, Tsui TY, Pharr GM. 1999. Elastic properties of microstructural components of human bone tissue as measured by nanoindentation. Journal of Biomedical Materials Research 45:48-54.

Richmond BG. 2007. Biomechanics of phalangeal curvature. Journal of Human Evolution 53:678-690.

Richmond BG, Wright BW, Grosse L, Dechow PC, Ross CF, Spencer MA, Strait DS. 2005. Finite element analysis in functional morphology. Anatomical Record Part a-Discoveries in Molecular Cellular and Evolutionary Biology 283A:259-274.

Richter W. 1920. Der Obergesichtschädel des Menschen als Gebissturm, ein statische Kunstwerk. Dtsch Monatsschr Zahnheilkd 38:49-68.

Rightmire GP. 1998. Human evolution in the middle Pleistocene: The role of Homo heidelbergensis. Evolutionary Anthropology 6:218-227.

Rightmire GP. 2008. Homo in the middle pleistocene: Hypodigms, variation, and species recognition. Evolutionary Anthropology 17:8-21.

Rightmire GP. 2009. Middle and later Pleistocene hominins in Africa and Southwest Asia. Proceedings of the National Academy of Sciences 106:16046-16050.

Robling AG, Castillo AB, Turner CH. 2006. Biomechanical and molecular regulation of bone remodeling. Annual Review of Biomedical Engineering 8:455-498.

Rohlf FJ. 1990. Morphometrics. Annual Review of Ecology and Systematics:299-316.

Rohlf FJ, Corti M. 2000. Use of two-block partial least-squares to study covariation in shape. Systematic Biology 49:740-753.

Rohlf FJ, Marcus LF. 1993. A revolution in morphometrics. Trends in Ecology & Evolution 8:129-132.

Roseman CC, Weaver TD. 2004. Multivariate apportionment of global human craniometric diversity. American Journal of Physical Anthropology 125:257-263.

Ross CF. 2001. In vivo function of the craniofacial haft: The interorbital "pillar". American Journal of Physical Anthropology 116:108-139.

Ross CF. 2005. Finite element analysis in vertebrate biomechanics. Anatomical Record Part a-Discoveries in Molecular Cellular and Evolutionary Biology 283A:253-258.

Ross CF, Berthaume MA, Dechow PC, Iriarte-Diaz J, Porro LB, Richmond BG, Spencer M, Strait D. 2011. In vivo bone strain and finite-element modeling of the craniofacial haft in catarrhine primates. Journal of Anatomy 218:112-141.

Ross CF, Hylander WL. 1996. In vivo and in vitro bone strain in the owl monkey circumorbital region and the function of the postorbital septum. American Journal of Physical Anthropology 101:183-215.

Ross CF, Patel BA, Slice DE, Strait DS, Dechow PC, Richmond BG, Spencer MA. 2005. Modeling masticatory muscle force in finite element analysis: Sensitivity analysis using principal coordinates analysis. Anatomical Record Part a-Discoveries in Molecular Cellular and Evolutionary Biology 283A:288-299.

Rossie JB. 2006. Ontogeny and homology of the paranasal sinuses in Platyrrhini (Mammalia: Primates). Journal of Morphology 267:1-40.

Rubin CT, Lanyon LE. 1982. Limb Mechanics as a Function of Speed and Gait - a Study of Functional Strains in the Radius and Tibia of Horse and Dog. Journal of Experimental Biology 101:187-211.

Ruff C, Holt B, Trinkaus E. 2006. Who's afraid of the big bad Wolff? "Wolff's law" and bone functional adaption. American Journal of Physical Anthropology 129:484 - 498.

Russell MD. 1985. The Supraorbital Torus - a Most Remarkable Peculiarity. Current Anthropology 26:337-360.

Saltelli A, Ratto M, Andres T, Campolongo F, Cariboni J, Gatelli D, Saisana M, Tarantola S. 2008. Global sensitivity analysis: the primer. Chichester: John Wiley & Sons.

Scheuer L, Black S. 2000. Developmental Junvenile Osteology. San Diego: Elsevier Academic Press.

Schwartz-Dabney CL, Dechow PC. 2003. Variations in cortical material properties throughout the human dentate mandible. American Journal of Physical Anthropology 120:252-277.

Schwartz JH, Tattersall I. 2003. The Human Fossil Record - Craniodental Morphology of Genus Homo. USA: Wiley-Liss.

Seidler H, Falk D, Stringer C, Wilfing H, Muller GB, zur Nedden D, Weber GW, Reicheis W, Arsuaga JL. 1997. A comparative study of stereolithographically modelled skulls of Petralona and Broken Hill: Implications for future studies of middle Pleistocene hominid evolution. Journal of Human Evolution 33:691-703.

Sellers WI, Crompton RH. 2004. Using sensitivity analysis to validate the predictions of a biomechanical model of bite forces. Annals of Anatomy-Anatomischer Anzeiger 186:89-95.

Senck S, Bookstein FL, Benazzi S, Kastner J, Weber GW. 2015. Virtual Reconstruction of Modern and Fossil Hominoid Crania: Consequences of Reference Sample Choice. The Anatomical Record 298:827-841.

Senck S, Coquerelle M. 2015. Morphological Integration and Variation in Facial Orientation in Pongo pygmaeus pygmaeus: A Geometric Morphometric Approach via Partial Least Squares. International Journal of Primatology 36:489-512.

Shea BT. 1977. Eskimo craniofacial morphology, cold stress and the maxillary sinus. American Journal of Physical Anthropology 47:289-300.

Shea BT. 1985. On Aspects of Skull Form in African Apes and Orangutans, with Implications for Hominoid Evolution. American Journal of Physical Anthropology 68:329-342.

Shea BT. 1986. On Skull Form and the Supraorbital Torus in Primates. Current Anthropology 27:257-260.

Sigal IA, Hardisty MR, Whyne CM. 2008. Mesh-morphing algorithms for specimen-specific finite element modeling. Journal of Biomechanics 41:1381-1389.

Sigal IA, Yang H, Roberts MD, Downs JC. 2010. Morphing methods to parameterize specimen-specific finite element model geometries. Journal of Biomechanics 43:254-262.

Singh I. 1978. The architecture of cancellous bone. Journal of Anatomy 127:305-310.

Sinn DP, DeAssis EA, Throckmorton GS. 1996. Mandibular excursions and maximum bite forces in patients with temporomandibular joint disorders. Journal of Oral and Maxillofacial Surgery 54:671-679.

Skerry T. 2000. Biomechanical influences on skeletal growth and development. In: O'Higgins P, Cohn MJ, editors. Development, Growth and Evolution. Implications for the study of the Hominid skeleton. London: Academic Press. p 29 - 39.

Slice DE. 2005. Modern morphometrics. In: Modern morphometrics in physical anthropology: Springer. p 1-45.

Smith AL, Benazzi S, Ledogar JA, Tamvada K, Pryor Smith LC, Weber GW, Spencer MA, Dechow PC, Grosse IR, Ross CF, Richmond BG, Wright BW, Wang Q, Byron C, Slice DE, Strait DS. 2015a. Biomechanical Implications of Intraspecific Shape Variation in Chimpanzee Crania: Moving Toward

an Integration of Geometric Morphometrics and Finite Element Analysis. The Anatomical Record 298:122-144.

Smith AL, Benazzi S, Ledogar JA, Tamvada K, Pryor Smith LC, Weber GW, Spencer MA, Lucas PW, Michael S, Shekeban A, Al-Fadhalah K, Almusallam AS, Dechow PC, Grosse IR, Ross CF, Madden RH, Richmond BG, Wright BW, Wang Q, Byron C, Slice DE, Wood S, Dzialo C, Berthaume MA, van Casteren A, Strait DS. 2015b. The Feeding Biomechanics and Dietary Ecology of Paranthropus boisei. The Anatomical Record 298:145-167.

Smith F, Rayard G. 1980. Evolution of the supraorbital region in upper pleistocene fossil hominids from south-central Europe. American Journal of Physical Anthropology 53:589 - 610.

Smith TD, Rossie JB, Cooper GM, Mooney MP, Siegel MI. 2005. Secondary pneumatization of the maxillary sinus in callitrichid primates: Insights from immunohistochemistry and bone cell distribution. The Anatomical Record Part A: Discoveries in Molecular, Cellular, and Evolutionary Biology 285A:677-689.

Sokal R, Rohlf F. 1995. Biometry - The principles and practice of statistics in biological research. NY: WH Freeman.

Spencer MA, Demes B. 1993. Biomechanical Analysis of Masticatory System Configuration in Neandertals and Inuits. American Journal of Physical Anthropology 91:1-20.

Sperber GH. 2001. Craniofacial Development. Hamilton: BC Decker Inc.

Spoor CF, Zonneveld FW, Macho GA. 1993. Linear Measurements of Cortical Bone and Dental Enamel by Computed-Tomography - Applications and Problems. American Journal of Physical Anthropology 91:469-484.

Stanford CM, Welsch F, Kastner N, Thomas G, Zaharias R, Holtman K, Brand RA. 2000. Primary human bone cultures from older patients do not respond at continuum levels of in vivo strain magnitudes. Journal of Biomechanics 33:63-71.

Stayton CT. 2009. Application of thin-plate-spline transformations to finite element models, or, how to turn a bog turtle into a spotted turtle to analyze both. Evolution 63:1348-1355.

Stedman HH, Kozyak BW, Nelson A, Thesier DM, Su LT, Low DW, Bridges CR, Shrager JB, Minugh-Purvis N, Mitchell MA. 2004. Myosin gene mutation correlates with anatomical changes in the human lineage. Nature 428:415-418.

Strait DS, Grosse IR, Dechow PC, Smith AL, Wang Q, Weber GW, Neubauer S, Slice DE, Chalk J, Richmond BG, Lucas PW, Spencer MA, Schrein C, Wright BW, Byfton C, Ross CF. 2010. The Structural Rigidity of the Cranium of Australopithecus africanus: Implications for Diet, Dietary Adaptations, and the Allometry of Feeding Biomechanics. Anatomical Record-Advances in Integrative Anatomy and Evolutionary Biology 293:583-593.

Strait DS, Richmond BG, Spencer MA, Ross CF, Dechow PC, Wood BA. 2007. Masticatory biomechanics and its relevance to early hominid phylogeny: An examination of palatal thickness using finite-element analysis. Journal of Human Evolution 52:585-599.

Strait DS, Wang Q, Dechow PC, Ross CF, Richmond BG, Spencer MA, Patel BA. 2005. Modeling elastic properties in finite element analysis: How much precision is needed to produce an accurate model? Anatomical Record Part a-Discoveries in Molecular Cellular and Evolutionary Biology 283A:275-287.

Strait DS, Weber GW, Neubauer S, Chalk J, Richmond BG, Lucas PW, Spencer MA, Schrein C, Dechow PC, Ross CF, Grosse IR, Wright BW, Constantino P, Wood BA, Lawn B, Hylander WL, Wang Q, Byron C, Slice DE, Smith AL. 2009. The feeding biomechanics and dietary ecology of Australopithecus africanus. Proceedings of the National Academy of Sciences of the United States of America 106:2124-2129.

Stringer C. 2002. Modern human origins: progress and prospects. Philosophical Transactions of the Royal Society B-Biological Sciences 357:563-579.

Stringer C. 2012. The status of Homo heidelbergensis (Schoetensack 1908). Evolutionary Anthropology 21:101-107.

Szwedowski TD, Fialkov J, Whyne CM. 2011. Sensitivity analysis of a validated subject-specific finite element model of the human craniofacial skeleton. Proceedings of the Institution of Mechanical Engineers Part H-Journal of Engineering in Medicine 225:58-67.

Tappen NC. 1973. Structure of bone in the skulls of Neanderthal fossils. American Journal of Physical Anthropology 38:93-97.

Tappen NC. 1978. The vermiculate surface pattern of brow ridges in Neandertal and modern crania. American Journal of Physical Anthropology 49:1-10.

Tattersall I, Sawyer GJ. 1996. The skull of "Sinanthropus" from Zhoukoudian, China: a new reconstruction. Journal of Human Evolution 31:311-314.

Thayer ZM, Dobson SD. 2010. Sexual dimorphism in chin shape: Implications for adaptive hypotheses. American Journal of Physical Anthropology 143:417-425.

Thompson DW. 1942. On growth and form. Cambridge: Cambridge University Press.

Tillier AM. 1977. La pneumatisation du massif cranio-facial chez les hommes actuels et fossiles. Bulletins et Mémoires de la Société d'anthropologie de Paris:177-189.

Tobias PV. 1967. Olduvai Gorge Vol. 2: the Cranium and Maxillary Dentition of Australopithecus (Zinjanthropus) boisei. Cambridge: Cambridge University Press.

Toro-Ibacache V, Fitton LC, Fagan MJ, O'Higgins P. 2015a. Validity and sensitivity of a human cranial finite element model: implications for comparative studies of biting performance. Journal of Anatomy:n/a-n/a.

Toro-Ibacache V, Fitton LC, Fagan MJ, O'Higgins P. 2016a. Validity and sensitivity of a human cranial finite element model: implications for comparative studies of biting performance. Journal of Anatomy 228:70-84.

Toro-Ibacache V, Zapata MuÑoz V, O'Higgins P. 2015b. The Predictability from Skull Morphology of Temporalis and Masseter Muscle Cross-Sectional Areas in Humans. The Anatomical Record 298:1261-1270.

Toro-Ibacache V, Zapata Muñoz V, O'Higgins P. 2016b. The relationship between skull morphology, masticatory muscle force and cranial skeletal deformation during biting. Annals of Anatomy - Anatomischer Anzeiger 203:59-68.

Trinkaus E. 1987a. Bodies, Brawn, Brains and Noses: Human Ancestors and Human Predation. In: Nitecki M, Nitecki D, editors. The Evolution of Human Hunting. New York: Springer US. p 107-145.

Trinkaus E. 1987b. The Neandertal Face - Evolutionary and Functional Perspectives on a Recent Hominid Face. Journal of Human Evolution 16:429-443.

Trinkaus E. 2003. Neandertal faces were not long; modern human faces are short. Proceedings of the National Academy of Sciences 100:8142-8145.

Truesdell C, Noll W. 2004. The non-linear field theories of mechanics. Berlin: Springer.

Turner CH. 1998. Three rules for bone adaptation to mechanical stimuli. Bone 23:399-407.

Turner CH, Takano Y, Owan I. 1995. Aging Changes Mechanical Loading Thresholds for Bone-Formation in Rats. Journal of Bone and Mineral Research 10:1544-1549.

Valdimarsson O, Alborg HG, Duppe H, Nyquist F, Karlsson M. 2005. Reduced training is associated with increased loss of BMD. Journal of Bone and Mineral Research 20:906-912.

van der Klaauw C. 1948 - 52. Size and position of the functional components of the skull. Archives Neerland Zoologie 9:1 - 559.

van Eijden TMGJ, Korfage JAM, Brugman P. 1997. Architecture of the human jaw-closing and jaw-opening muscles. Anatomical Record 248:464-474.

Vatsa A, Breuls RG, Semeins CM, Salmon PL, Smit TH, Klein-Nulend J. 2008. Osteocyte morphology in fibula and calvaria — Is there a role for mechanosensing? Bone 43:452-458.

Verhaegen M. 2013. The aquatic ape evolves: common misconceptions and unproven assumptions about the so-called aquatic ape hypothesis. Human Evolution 28:237-266.

Vollmer D, Meyer U, Joos U, Vegh A, Piffko J. 2000. Experimental and finite element study of a human mandible. Journal of Cranio-Maxillofacial Surgery 28:91-96.

Wagner GP, Altenberg L. 1996. Perspective: Complex Adaptations and the Evolution of Evolvability. Evolution 50:967-976.

Wang Q, Dechow P, Wright B, Ross C, Strait D, Richmond B, Spencer M, Byron C. 2008. Surface Strain on Bone and Sutures in a Monkey Facial Skeleton: An In Vitro Approach and its Relevance to Finite Element Analysis. In: Vinyard C, Ravosa M, Wall C, editors. Primate Craniofacial Function and Biology: Springer US. p 149-172.

Wang Q, Smith AL, Strait DS, Byron CD, Grosse IR, Wright BW. 2010a. The global impact of sutures assessed in a Finite Element Model of a macaque cranium. American Journal of Physical Anthropology:239-239.

Wang QA, Smith AL, Strait DS, Wright BW, Richmond BG, Grosse IR, Byron CD, Zapata U. 2010b. The Global Impact of Sutures Assessed in a Finite Element Model of a Macaque Cranium. Anatomical Record-Advances in Integrative Anatomy and Evolutionary Biology 293:1477-1491.

Wang QA, Wood S, Grosse I, Strait D, Zapata U, Byron C, Wright B. 2011. Impact of sutures assessed in a finite element model of a macaque cranium using dynamic simulation. American Journal of Physical Anthropology 144:304-304.

Watson PJ, O'Higgins P, Fagan MJ, Dobson CA. 2011. Validation of a morphometric reconstruction technique applied to a juvenile pelvis. Proceedings of the Institution of Mechanical Engineers Part H-Journal of Engineering in Medicine 225:48-57.

Weber GW. 2015. Virtual Anthropology. American Journal of Physical Anthropology 156:22-42.

Weber GW, Bookstein FL. 2011. Virtual Anthropology - A Guide for a New Interdisciplinary Field. Wien: Springer-Verlag.

Weidenreich F. 1937. Reconstruction of the Entire Skull of an Adult Female Individual of Sinanthropus pekinensi. Nature 140:1010.

Weidenreich F. 1941. The Brain and Its Rôle in the Phylogenetic Transformation of the Human Skull. Transactions of the American Philosophical Society 31:320-442.

Weijs WA. 1980. Biomechanical Models and the Analysis of Form: A Study of the Mammalian Masticatory Apparatus. American Zoologist 20:707-719.

Weijs WA, Hillen B. 1986. Correlations between the cross-sectional area of the jaw muscles and craniofacial size and shape. American Journal of Physical Anthropology 70:423-431.

White T, Folkens P. 2005. The Human Bone Manual. San Diego: Elsevier Academic Press.

Witzel U. 2011. Virtual Synthesis of the Skull in Neanderthals by FESS. In: Condemi S, Weniger G-C, editors. Continuity and Discontinuity in the Peopling of Europe: One Hundred Fifty Years of Neanderthal Study. New York: Springer. p 203-211.

Witzel U, Preuschoft H. 2002. Function-dependent shape characteristics of the human skull. Anthropologischer Anzeiger 60:113-135.

Witzel U, Preuschoft H. 2005. Finite-element model construction for the virtual synthesis of the skulls in vertebrates: Case study of *Diplodocus*. Anatomical Record Part a-Discoveries in Molecular Cellular and Evolutionary Biology 283A:391-401.

Wolff JA. 1984. A Theoretical Approach to Solve the Chin Problem. In: Chivers D, Wood B, Bilsborough A, editors. Food Acquisition and Processing in Primates: Springer US. p 391-405.

Wolpoff MH. 1968. Climatic Influence on Skeletal Nasal Aperture. American Journal of Physical Anthropology 29:405-&.

Wood B. 2011. Wiley-Blackwell Encyclopedia of Human Evolution, 2 Volume Set: John Wiley & Sons.

Wood SA, Strait DS, Dumont ER, Ross CF, Grosse IR. 2011. The effects of modeling simplifications on craniofacial finite element models: The alveoli (tooth sockets) and periodontal ligaments. Journal of Biomechanics 44:1831-1838.

Wroe S, Ferrara TL, McHenry CR, Curnoe D, Chamoli U. 2010. The craniomandibular mechanics of being human. Proceedings of the Royal Society B-Biological Sciences 277:3579-3586.

Wroe S, Moreno K, Clausen P, Mchenry C, Curnoe D. 2007. High-resolution three-dimensional computer simulation of hominid cranial mechanics. Anatomical Record-Advances in Integrative Anatomy and Evolutionary Biology 290:1248-1255.

Yang L, Zhang P, Liu S, Samala PR, Su M, Yokota H. 2007. Measurement of strain distributions in mouse femora with 3D-digital speckle pattern interferometry. Optics and Lasers in Engineering 45:843-851.

Yokley TR. 2009. Ecogeographic Variation in Human Nasal Passages. American Journal of Physical Anthropology 138:11-22.

Zelditch ML, Swiderski DL, Sheets HD, Fink WL. 2004. Geometric Morphometrics For Biologists: A Primer. New York: Elsevier.

Zelditch ML, Swiderski DL, Sheets HD, Fink WL. 2012. Geometric Morphometrics For Biologists: A Primer. New York: Elsevier.

Zink KD, Lieberman DE. 2016. Impact of meat and Lower Palaeolithic food processing techniques on chewing in humans. Nature 531:500-503.

Zollikofer CP, Ponce de León MS. 2005. Virtual reconstruction: a primer in computer-assisted paleontology and biomedicine. New Jersey: Wiley-Interscience.

Zollikofer CPE, de Leon MSP, Lieberman DE, Guy F, Pilbeam D, Likius A, Mackaye HT, Vignaud P, Brunet M. 2005. Virtual cranial reconstruction of Sahelanthropus tchadensis. Nature 434:755-759.

Zollikofer CPE, Ponce de Leon MS, Martin RD, Stucki P. 1995. Neanderthal Computer Skulls. Nature 375:283-285.

Zollikofer CPE, Ponce De LeÓn MS, Schmitz RW, Stringer CB. 2008. New Insights Into Mid-Late Pleistocene Fossil Hominin Paranasal Sinus Morphology. The Anatomical Record: Advances in Integrative Anatomy and Evolutionary Biology 291:1506-1516.

Zollikofer CPE, Weissmann JD. 2008. A Morphogenetic Model of Cranial Pneumatization Based on the Invasive Tissue Hypothesis. Anatomical Record-Advances in Integrative Anatomy and Evolutionary Biology 291:1446-1454.

Appendix A

This appendix focuses on GM analysis and visualization of modes and magnitudes of deformation (changes in size and shape excluding rigid body rotations and translations) of objects due to loading. Since loading results in changes in both size and shape these are considered together. Here we demonstrate that size and shape distances due to loading (differences between unloaded and loaded objects) scale linearly inversely with size as defined by length (square root of surface area), and directly, with applied force, in identically shaped objects.

Here size and shape distances are calculated by multiplying the shape coordinates (from GPA) of each specimen by that specimen's original centroid size. This results in the specimens being represented by points in a (size and shape) space that can be thought of as Kendall's shape space with size as an additional dimension. The vector of centroid size (the additional dimension) at any point on the manifold can be visualised as passing radially from the centroid of the manifold of Kendall's shape space (zero size), through that point (centroid size = 1) and beyond the manifold to infinity (infinite size). When centroid size is 1, the objects lie on the manifold of Kendall's shape space.

The scaling relationships we describe here only apply to objects that are identical in shape because as shapes become more different loadings also become different and both of these differences lead to different modes and magnitudes of deformation. Further, for identically shaped models, all measures of 'size' (e.g. cube root of volume, square root of area, lengths, centroid size) scale in the same way. In contrast, for different model shapes they do not and so scaling relationships will differ according to which 'size' variable is used. When scaling models with different shapes, the extent to which the scaling relationship described here holds will depend on the degree of shape difference, and so is an approximation.

The scaling relationships also only apply for very small deformations such as arise from FEA analyses using linear elastic models, as in this study. This is because as objects deform, load vectors also inevitably change. In consequence, modes of deformation also change as deformations become large. This situation of large

deformations requires modified FEA analyses (sequentially deforming over small increments), and separate scalings to be computed for each approximately linear increment.

With these caveats noted, we show below that when the same load is applied to two objects with the same shape but different sizes, the ratio of size and shape distances from the unloaded form will equal the inverse of the ratio of 'lengths' (e.g. square root of area, length, centroid size), will give the same ratio.

This is demonstrated using two examples of 3D models, one of a simple geometric form (a cube; example 1) and the other a complex 3D form (a cranium; example 2). Each example compares magnitudes and modes of deformation among two models that have the same shape but different sizes. These were converted into FE models and in each analysis, identical material properties and boundary conditions were applied to load the models and cause deformation. After solution, landmark coordinates were extracted in each of the models and these were used to visualise and compare global modes of deformation of the models (in size and shape space) due to loading.

Example 1

Two virtual cubes were created, one with 100 mm of side length (small cube) and another with 200 mm (large cube), both with a modulus of elasticity of 17GPa and a Poisson's ratio of 0.3. Two loading regimens were applied, one of 1000N and another of 2000N. The results show that, in size and shape space, the small cube deforms (with small error due to the limits of computation) twice as much as the large cube under similar loadings (ratio of size and shape distances: 0.009764/0.004867=2.006) and that doubling the load doubles the deformation of the cubes (small cube ratio of size and shape distances: 0.019530/0.009764=2.000; large cube: 0.009748/0.004867=2.003) (Figure A1).

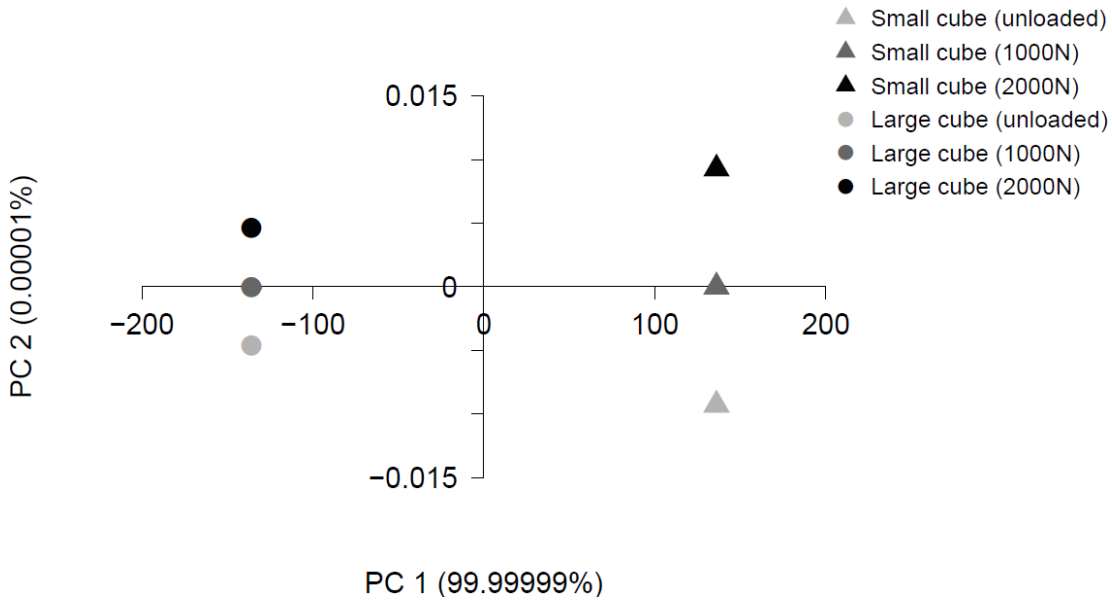

Figure A1: Size and shape space PCA of Cubes 1 and 2 before and after deformation due to loading.

Example 2

Two versions of the *Homo sapiens* cranium were created, one with a voxel side length of 0.35 mm (small cranium) and another with 0.70 mm (large cranium) with identical material properties (Modulus of elasticity of 17GPa and Poisson's ratio of 0.3). The same boundary conditions were applied, with both glenoid fossae constrained in the X, Y and Z axes and the central incisor in the Z axis. The load applied simulated the action of the temporalis, both masseters and medial pterygoids with a total force of 838.26 N (see Table 5-1). The results show that the small cranium deforms twice as much (with small error due to the limits of computation) as the large cranium under the same loading (ratio of size and shape distances: 0.179926/0.0899989=1.999) (Figure A2).

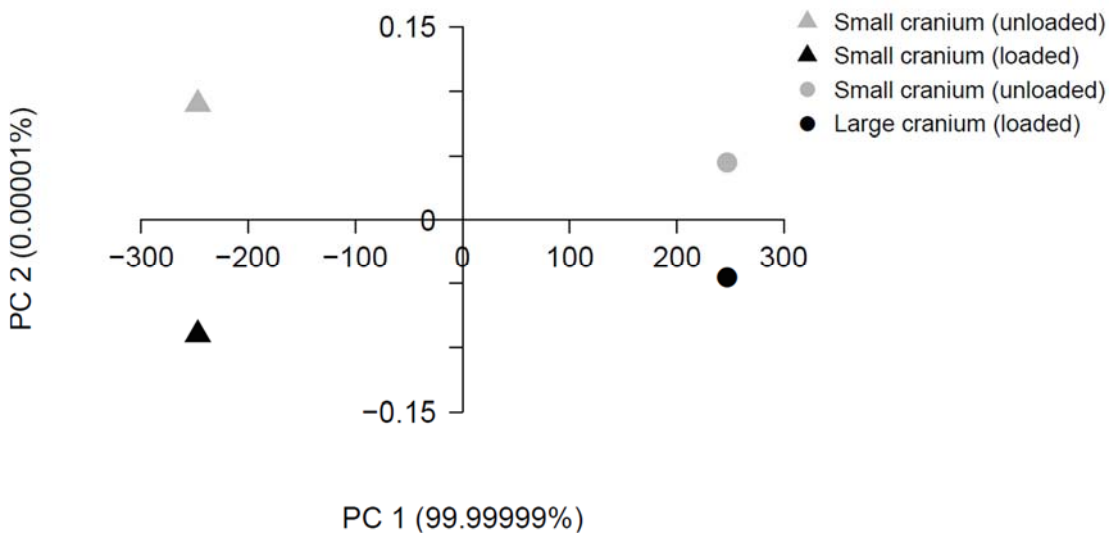

Figure A2: Size and shape space distances of cranium 1 and 2 before and after deformation due to loading.

As such, if two objects differ only in size, but not in shape, the ratio of size and shape distances scales as the inverse of the ratio of 'lengths'. This means that to account for differences in size, the differences in size and shape coordinates computed between loaded and unloaded models should be scaled according to the inverse of the ratio of centroid sizes. As noted earlier, this is accurate between identically shaped models, and an approximation when shape differs.

Finally it should be noted that, although it would be an incomplete analysis, the effects of loading on shape alone may be considered by carrying out GPA with no rescaling to compare the shape of the loaded object with that of the unloaded. In this case, the distances, computed between loaded and unloaded models scale according to the inverse of the ratio of areas or the squares of lengths (e.g. the centroid sizes squared). This is because the size vector in a size and shape analysis results in inflation of (size and shape) distances among larger unloaded and loaded models relative to that between smaller models. When models are scaled to the same centroid size (e.g. centroid size = 1 for an analysis in Kendall's shape manifold) the distances between unloaded models become zero (they are the same shape) and those between loaded and unloaded models are also scaled, but for each model the scaling is in direct proportion to its size. Thus, division by centroid size to convert size and shape coordinates to Procrustes shape coordinates has the consequence that while size and shape distances between unloaded and loaded models scale according to the inverse of the ratio of

centroid sizes between unloaded models, the resulting Procrustes distances scale with the inverse of the ratio of the squares of centroid sizes.